STORM SURGE ANALYSIS USING NUMERICAL AND STATISTICAL TECHNIQUES AND COMPARISON WITH NWS MODEL SLOSH

A Thesis

by

MANISH AGGARWAL

Submitted to the Office of Graduate Studies of
Texas A&M University
in partial fulfillment of the requirements for the degree of

MASTER OF SCIENCE

August 2004

Major Subject: Ocean Engineering

STORM SURGE ANALYSIS USING NUMERICAL AND STATISTICAL TECHNIQUES AND COMPARISON WITH NWS MODEL SLOSH

A Thesis

by

MANISH AGGARWAL

Submitted to Texas A&M University
in partial fulfillment of the requirements
for the degree of

MASTER OF SCIENCE

Approved as to style and content by:

Billy L. Edge (Chair of Committee)	Cheung. H. Kim (Member)
Douglas Sherman (Member)	Paul N. Roschke (Head of Department)

August 2004

Major Subject: Ocean Engineering

ABSTRACT

Storm Surge Analysis Using Numerical and Statistical Techniques and Comparison with NWS Model SLOSH. (August 2004)

Manish Aggarwal, B.E., Delhi College of Engineering,

Delhi, India

Chair of Advisory Committee: Dr. Billy Edge

This thesis presents a technique for storm surge forecasting. Storm surge is the water that is pushed toward the shore by the force of the winds swirling around the storm. This advancing surge combines with the normal tides to create the hurricane storm tide, which can increase the mean water level by almost 20 feet. Numerical modeling is an important tool used for storm surge forecast. Numerical model ADCIRC (Advanced Circulation model; Luettich et al, 1992) is used in this thesis for simulating hurricanes. A statistical technique, EST (Empirical Statistical Technique) is used to generate life cycle storm surge values from the simulated hurricanes. These two models have been applied to Freeport, TX. The thesis also compares the results with the model SLOSH (Sea, Lake, and Overland Surges from Hurricanes), which is currently used for evacuation and planning. The present approach of classifying hurricanes according to their maximum sustained winds is analyzed. This approach is not found to applicable in all the cases and more research needs to be done. An alternate approach is suggested for hurricane storm surge estimation.

DEDICATION

To God and my family for guiding me throughout my life

ACKNOWLEDGMENTS

This research was conducted at Texas A&M University and was supported by the Department of Civil Engineering, Texas A&M University through the Texas Engineering Experiment Station (TEEX).

I would like to thank my Chair Dr. Billy Edge for his guidance and contribution in my understanding of this research and coastal engineering as a whole. I would also like to thank my advisory committee members: Dr. C. H. Kim and Dr. Douglas Sherman for their trust and guidance throughout this research project.

I also wish to thank my fellow classmates and friends for their active help and contribution: Dr. Wahyu Pandoe, Mr. Young-Hyun Park, and Mr. Oscar Cruz Castro.

The thesis would not have been possible without the interest shown by Mr. George Kidwell and Mr. Mel McKey of the Velasco Drainage District who made substantial contributions to the completion of this modeling study.

Special thanks to my family for their constant support and motivation without which, I would have never come this far.

TABLE OF CONTENTS

Page

Page

LIST OF FIGURES

Page

Page

LIST OF TABLES

Page

1 INTRODUCTION

1.1 Motivation

Storm surge is an abnormal rise of water generated by a storm, over and above the predicted astronomical tide. In coastal areas, storm surge causes the greatest concentration of death and destruction during a hurricane, more than even the powerful winds and the tremendous amounts of rainfall. Storm surges can be caused either by tropical storms or extra-tropical storms. The focus of this study is the storm surge caused by tropical storms or hurricanes. Since hurricanes are intense form of tropical storms they are discussed in this study. For a hurricane, the surge typically has duration of several hours and affects about 100 miles of coastline from its landfall location. In the great Galveston, Texas, hurricane of 1900, an estimated 6,000 people drowned when the island was almost completely submerged by the storm surge. Hurricane storm surges of over 20 feet have been observed; hurricane Camille in 1969 produced a surge of approximately 7.4 m (24 feet) in the area of Gulfport, Mississippi. The destruction caused by such abnormally high water is truly astounding.

In the aftermath of other historic hurricane storm surges, areas of coast have been abandoned completely, as in the case of Indianola, Texas, which was deserted after a storm in 1875. More recently in July of 2003, hurricane Claudette caused severe damage in the state of Texas. The damage was estimated to be about $5 million comprising of damage to public as well as private properties and beach erosion. This damage resulted even though Claudette was not a strong Hurricane, being Category 1 on Saffir-Simpson

---

The thesis follows the style and format of *Journal of Waterway, Port, Coastal and Ocean Engineering*.

scale that is the lowest category of hurricane.

A hurricane is a severe tropical storm that forms in the southern Atlantic Ocean, Caribbean Sea, and Gulf of Mexico or in the eastern Pacific Ocean. Hurricanes are also known as typhoons in some regions. Hurricanes need warm tropical oceans, moisture and light winds above them. If the right conditions last long enough, a hurricane can produce violent winds, incredible waves, torrential rains and floods. Hurricanes rotate in a counterclockwise direction around an "eye".

Storm surges are caused by atmospheric pressure gradients and shear stresses acting on the surface of a body of water. Local water levels are affected day to day by even weak atmospheric disturbances that occur at a great distance, but the greatest impact certainly is from well-developed tropical storms and hurricanes that pass within the intermediate area. There are on average six Atlantic hurricanes each year; over a 3-year period, approximately five hurricanes strike the United States coastline from Texas to Maine (Ho 1987*)*.

Though strong winds from hurricanes and tropical storms often have the greatest influence on the level of the storm surge along a coastline, there are sometimes other factors, which contribute significantly to the total storm surge level. The total water level change experienced during a hurricane depends upon the combination of a number of complex influences. These influences include: 1) the storm surge, 2) astronomical tides, which are the normal cause of day to day water level change at the coast, 3) surface wave set-up, and 4) rainfall flooding. Storm surge is the combined effect on the water surface elevation by the reduced pressure, wind shear and wave runup. In the case of wave set-up, in some locations as much as 50% of the total surge level can be the result of wind

wave set-up (Jelesnianski and Taylor 1973).

Two general approaches have been used to forecast hurricane storm surges: statistical modeling and numerical modeling. In statistical modeling, past observations of storm surge heights are correlated statistically to observed or forecasted hurricane characteristics. However, since hurricanes are relatively uncommon and are small scale in nature (compared to meteorological phenomena), insufficient data exist to allow such statistical correlations to be derived to the extent desired.

Numerical modeling offers a viable alternative to statistical modeling for hurricane storm surge problem. In computer modeling of storm surge, a set of differential equations governing the flow of water (transport equations) are solved with relevant and pertinent boundary conditions to obtain storm surge. This approach, though effective fails to quantify storm surge value relative to the hurricane characteristics.

Hence, a better approach as used in this study would be to utilize both of the above approaches. Knowing that hurricanes in the Atlantic Ocean can be assigned a temporal cycle, a frequency relationship can be performed. For these estimates to be useful, an accurate database needs to be populated with hurricane storm surge levels and their inherent characteristics. This study aims to provide an effective approach for estimating storm surge effects on an area by utilizing both numerical and statistical approaches for storm surge estimating.

1.2 Approach

Numerical modeling using the long wave model ADCIRC (Advanced Circulation model; Luettich, Westerlink, and Scheffner, 1992) is used to model historical hurricanes

that have affected the area and some of the extreme storms are perturbed to achieve the maximum impact in the area. The numerical simulations help in the generation of a database of storm characteristics like storm surge values, maximum winds, radius of maximum winds, eye pressure etc. This database of storm characteristics is used in the statistical model EST (Empirical Simulation Technique, Scheffner et al., 1999). This procedure uses historic events to generate a large population of life-cycle databases that are post-processed to compute mean value maximum storm surge elevation frequency relationships with statistical error estimates.

This study also tries to compare the results with NWS numerical model SLOSH (Jelesnianski et al, 1992). The model SLOSH has been used extensively to delineate coastal areas susceptible to hurricane storm surge flooding.

1.3 Study Area

The region of general interest within the Gulf of Mexico for this application consists of the Freeport area as shown in the Fig. 1-1. Freeport is an important industrial center and deepwater port located on the Texas coast. The community has a diversified source of income, but is predominantly dependent on the petro-chemical industry. The principal sources of income are derived from processing petroleum and petroleum by-products. Brazoria County houses one of the world's largest chemical complexes with the Dow Chemical being the principal employer. Since this area is exposed to storm surges resulting from tropical and extra tropical events, a levee system was constructed at Freeport, TX, in 1982. The levee was constructed for providing flood damage protection to the area and has an elevation of 6.5-7m above sea level. The levee system consists of a series of levees and pumping stations that protect an area of about 68 square kilometers.

The project was completed in 1982. The levee system is vital to protection against flooding of the nation's most vital petro-chemical industry worth almost $500 billion.

Fig. 1-1: Study area

1.4 Procedure

This study first required the development of a computational grid for the study area. The ADCIRC model then used the computational grid to simulate tidal circulation and storm events. The model grid was verified by comparing model-generated tide time series with the corresponding time series reconstructed from existing harmonic analyses and on-site measurements of surface elevation. Storm event simulations were verified by comparing simulated results of water surface elevation with archived storm

measurements. Once the model was shown to be capable of reproducing historic events, all storms that significantly impacted the study area since 1886 were simulated. The beginning year 1886 is used as that is the first year in the available database maintained by the National Weather Service. In order to insure that the most severe events were included for all along the coastline, simulations included hypothetical events that could likely occur.

Following the numerical simulations for all the selected storms, the database of computed surges and tides was used as input for the statistical procedure EST. Frequency computations are made at 35 locations in the Freeport area. These stations are located at points of interest within the domain and help in establishing the extreme event storm surges along the levee system that was constructed for providing flood damage protection to the area.

1.4.1 Computational Grid

The modeling strategy has been to define the entire Gulf of Mexico as the computational domain and to refine the region of interest using the significant grid flexibility offered by the finite elements and the ADCIRC codes. Using the entire Gulf as the pertinent domain is quite convenient from a variety of perspectives. Most important, two well-defined open ocean boundaries of limited extent can be used to specify the boundary forcing functions that define the interaction between the Atlantic Ocean and the Caribbean Sea with the Gulf. The procedure for generation of the finite element grid required the following steps:

1) Obtaining coastline to serve as boundary for our domain.

2) Generation of model bathymetry.

3) Applying boundary conditions.

4) Using grid generation software (SMS: Surface Water Modeling System) to generate finite element grid.

A problem often encountered in the modeling of near-shore regions in the Gulf of Mexico is that the areas of interest are not well removed from the computational boundaries. The Gulf of Mexico being a semi-enclosed basin has numerous amphidromes that affect both the amplitude and phase of astronomical tide and storm surge. Circulation inside Gulf of Mexico is a function of wind and pressure hence computational domain for a hurricane surge model should encompass the whole gulf. If the model boundaries are placed in areas near to the coast, errors are introduced in the solution, as the large-scale effects as discussed above cannot be taken into account. Flow features such as resonant shelf edge waves, hurricane forerunners, and/or complex wind patterns associated with a hurricane driving the flow onto the shelf, make it desirable to define larger computational domains, including regions well beyond the continental shelf adjacent to the area of interest. The open boundary across the Strait of Florida was selected to run from Cape Sable in Florida to Havana, Cuba. The second open boundary stretches just south of the Yucatan Strait. The resulting finite element grid consists of 28,266 nodes, 52,624 elements and is shown in Fig. 1-2. Minimum node-to-node spacing in the study is approximately 50 m. The bathymetry for the computational domain is shown in Fig. 1-3. The increased resolution of the study area is shown in Fig. 1-4. Bathymetry in the study area is shown in Fig. 1-5. This large domain approach to specification of boundary

conditions virtually eliminates contamination of model results from poorly defined boundary conditions.

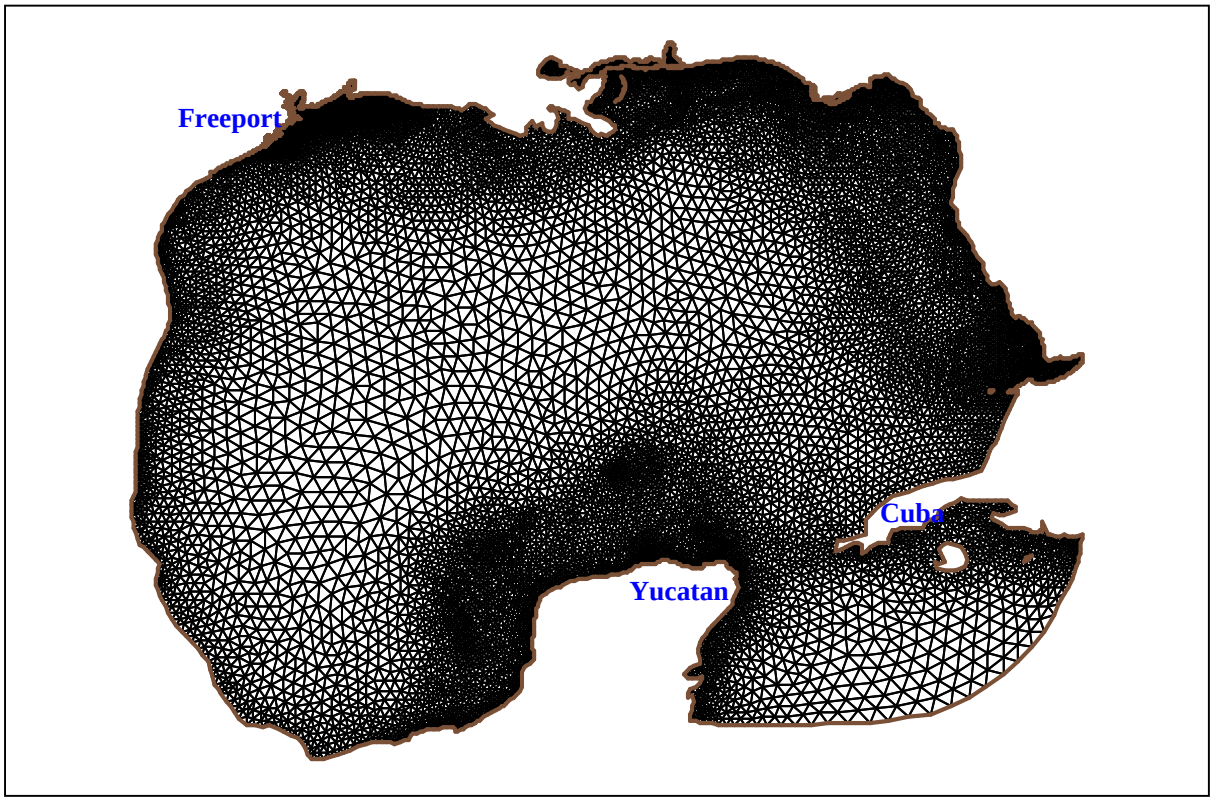

Fig. 1-2: Computational domain

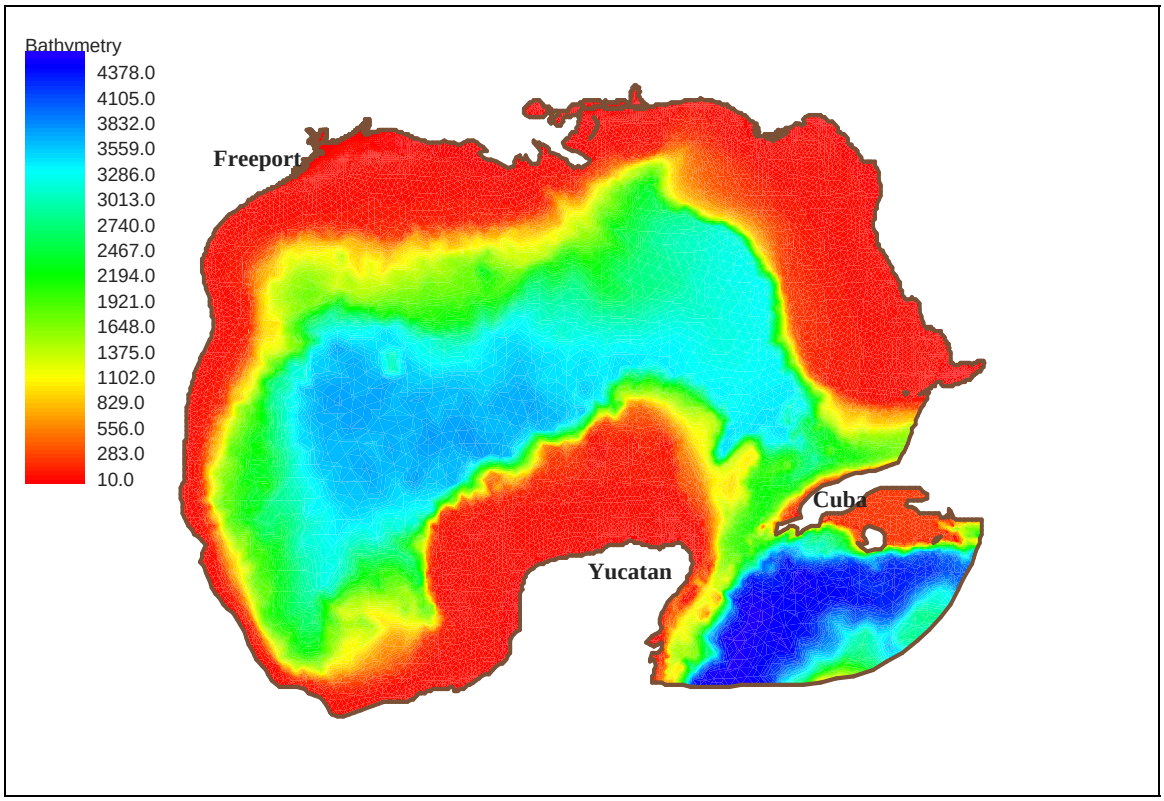

Fig. 1-3: Bathymetry in the computational domain

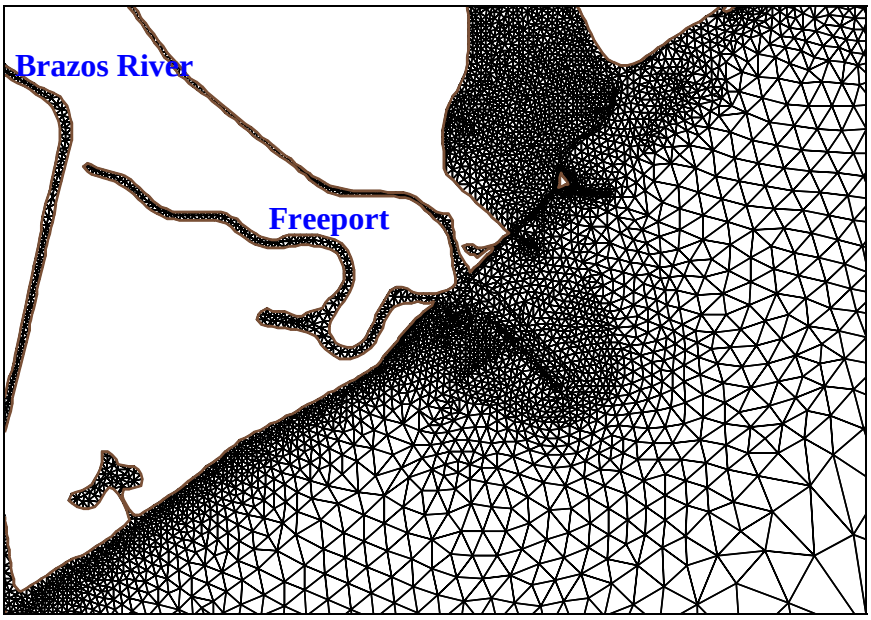

Fig. 1-4: Grid resolution in the region of interest

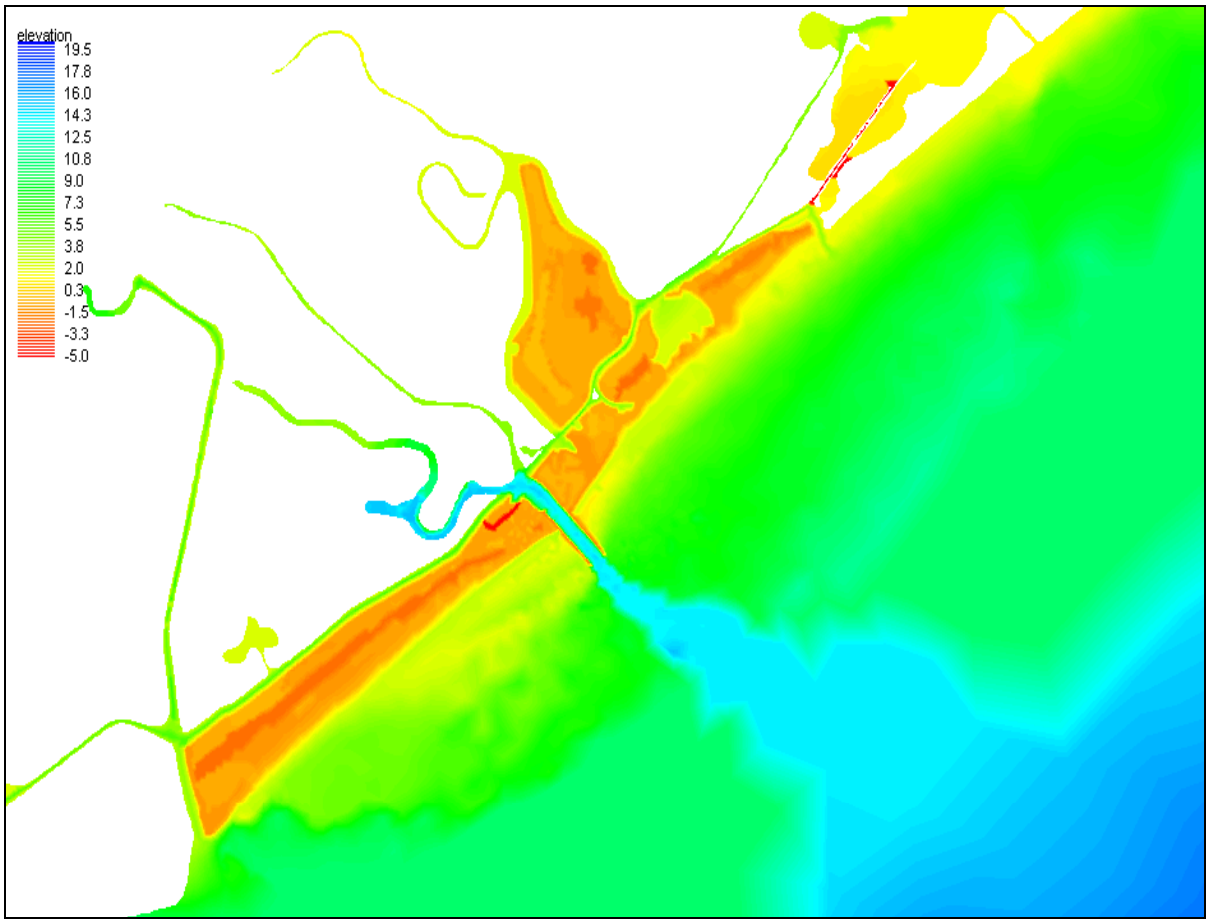

Fig. 1-5: Bathymetry in the area of interest

1.5 Outline

The thesis consists of 7 sections. Section 1 consists of motivation, approach, study area, general procedure used in the thesis and outline. ADCIRC model and its components, which are related to this thesis, constitute section 2. SLOSH model, its history and methodology are described in section 3. Section 4 gives some insight into the EST method. The implementation of ADCIRC and EST to the study area is further described in section 5. The comparisons of ADCIRC/EST results with SLOSH model are given in section 6. Section 7 consists of conclusions.

2 ADCIRC: MODEL DESCRIPTION

This section is divided into four parts. First part sheds light on ADCIRC model. The other three parts discuss components of the model relevant to this thesis like tidal forcing, bottom friction and wind forcing.

2.1 ADCIRC Model

Water-surface elevations and currents for both tides and storm events are obtained from the large-domain long wave hydrodynamic model ADCIRC (Advanced Circulation model; Luettich et al, 1992). ADCIRC is a finite element (FEM) code that makes use of the Generalized Wave Continuity Equation (GWCE) for improved stability and efficiency over other FEM hydrodynamic codes. Included within the code are features that allow the user to include tidal and atmospheric forcing in the computations. Wind can be input in a variety of different formats and could be derived from any source that the user has available. The model was developed as a family of two- and three-dimensional codes with the capability of:

a. Simulating tidal circulation and storm surge propagation over large computational domains while simultaneously providing high resolution in areas of complex shoreline and bathymetry. The targeted areas of interest include continental shelves, near shore areas, and estuaries.
b. Representing all pertinent physics of the three-dimensional equations of motion. These include tidal potential, Coriolis, baroclinic and all nonlinear terms of the governing equations.

c. Providing accurate and efficient computations over time periods ranging from months to years.

The 2-dimensional, Depth Integrated (2DDI) model formulation begins with the depth-averaged shallow-water equations for conservation of mass and momentum subject to incompressibility and hydrostatic pressure approximations. The Boussinesq approximation, where density is considered constant in all terms but the gravity term of the momentum equation, is also incorporated in the model. Using the standard quadratic parameterization for bottom stress and omitting baroclinic terms and lateral diffusion and dispersion, the following set of conservation statements in primitive, non-conservative form and expressed in a spherical coordinate system are incorporated in the model (Flather 1988; Kolar et al. 1994):

$$\frac{\partial \zeta}{\partial t} + \frac{1}{R\cos\phi}\left[\frac{\partial UH}{\partial \lambda} + \frac{\partial (UV\cos\phi}{\partial \phi}\right] = 0 \qquad (1)$$

$$\frac{\partial U}{\partial t} + \frac{1}{R\cos\phi} U \frac{\partial U}{\partial \lambda} + \frac{1}{R} V \frac{\partial U}{\partial \phi} - \left[\frac{\tan\phi}{R} \mathrm{U} + f\right]V =$$
$$-\frac{1}{R\cos\phi}\frac{\partial}{\partial \lambda}\left[\frac{P_S}{\rho_o} + g(\zeta - \eta)\right] + \frac{\tau_S{}^{\lambda}}{\rho_o H} - \tau * U \qquad (2)$$

$$\frac{\partial V}{\partial t} + \frac{1}{R\cos\phi} U \frac{\partial V}{\partial \lambda} + \frac{1}{R} V \frac{\partial V}{\partial \phi} - \left[\frac{\tan\phi}{R} U + f\right]V =$$
$$-\frac{1}{R\cos\phi}\frac{\partial}{\partial \lambda}\left[\frac{P_S}{\rho_o} + g(\zeta - \eta)\right] + \frac{\tau_S{}^{\phi}}{\rho_o H} - \tau * V \qquad (3)$$

where :

ζ = free surface elevation relative to the geoid,

$U,\ V$ = depth-averaged horizontal velocities,

$H = \zeta + h$ = total depth of water column,

h = bathymetric depth relative to the geoid,

$f = 2\Omega sin\varphi$ = Coriolis force,

Ω = angular speed of the Earth,

ϕ = latitude in degrees,

λ = longitude in degrees,

P_s = atmospheric pressure at the free surface,

g = acceleration due to gravity,

η = effective Newtonian equilibrium tide potential,

ρ_o = reference density of water,

α = effective Earth elasticity factor,

$\tau_{s\lambda}, \tau_{s\phi}$ = applied free-surface stress,

τ^* = $C_f(U^2 + V^2)^{1/2}/H$, bottom shear stress,

C_f = bottom friction coefficient,

R = radius of Earth,

t = time.

In order to overcome general stability problems encountered when finite element models depend upon the direct solution of these primitive forms of the governing equations, the ADCIRC code was developed around the Generalized Wave Continuity Equation (GWCE). Combining a time-differentiated form of the momentum equations

yields this form of the primitive equations. With the inclusion of a simple eddy viscosity model for closure (Kolar and Gray 1994), the GWCE in Spherical coordinates takes the form:

$$\frac{\delta^2\zeta}{\delta t^2} + \tau_0 \frac{\partial\zeta}{\partial t} - \frac{1}{R\cos\phi}\frac{\partial}{\partial\lambda}\left[\frac{1}{R\cos\phi}\left(\frac{\partial(HUV)}{\partial\lambda} + \frac{\partial(HUV\cos\phi)}{\partial\phi}\right) - UVH\frac{\tan\phi}{R}\right]$$

$$-\left[-2\omega\sin\phi HV + \frac{H}{R\cos\phi}\frac{\partial}{\partial\lambda}\left(g(\zeta-\alpha\eta) + \frac{P_S}{\rho_O}\right) + \tau_0 HU - \tau_0 HU - \frac{\tau_{S\lambda}}{\rho_O}\right]$$

$$-\frac{1}{R}\frac{\partial}{\partial\phi}\left[\frac{1}{R\cos\phi}\left(\frac{\partial(HVV)}{\partial\lambda} + \frac{\partial(HVV\cos\phi)}{\partial\phi}\right) + UUH\frac{\tan\phi}{R} + 2\omega\sin\phi HU\right]$$

$$-\frac{1}{R}\frac{\partial}{\partial\phi}\left[\frac{H}{R}\frac{\partial}{\partial\lambda}\left(g(\zeta-\alpha\eta) + \frac{P_S}{\rho_O}\right) + (\tau^* - \tau_0)HV - \frac{\tau_{S\phi}}{\rho_O}\right] \tag{4}$$

$$-\frac{\partial}{\partial t}\left[\frac{VH}{R}\tan\phi\right] - \tau_0\left[\frac{VH}{R}\tan\phi\right] = 0$$

The ADCIRC-2DDI model solves the GWCE (Equation (4)) in conjunction with the primitive momentum equations given in Equations (2) and (3). The equations are solved using a FEM grid, made up of linear triangular elements (only three nodes per element). The model domain can be as extensive as an entire ocean basin, or more localized, as in the case of a small bay or estuary. The numerical solution of the governing equations presented above follows a two-step procedure in ADCIRC code. First, the GWCE (Equation (4)) is solved. The linear terms in the GWCE are discretized using a Galerkin weighted residual, three time level, and implicit scheme. The non-linear terms, along with Coriolis forcing, atmospheric forcing and tidal potential are solved

explicitly (Westerink et al. 1993). The explicit formulation of these terms has the advantage that the solution depends only upon the previous time step. On the other hand, the implicit terms depend upon the solution of a system of equations, arranged in a banded matrix.

The second step in the solution of the governing equations, after solving the GWCE, is to solve the momentum equations (Eq. (2) and (3)). Most of the terms of the momentum equations are handled in a Crank-Nicholson, two-time level, and implicit discretization scheme. The explicit terms in the momentum equations are the τ_* terms, the convective terms and the eddy viscosity terms.

The available boundary conditions used in ADCIRC include:

- specified elevation (harmonic tidal constituents or time series)
- specified normal flow (harmonic tidal constituents or time series)
- zero normal flow
- slip or no slip conditions for velocity
- external barrier overflow out of the domain
- internal barrier overflow between sections of the domain
- surface stress (wind and/or wave radiation stress)
- atmospheric pressure
- outward radiation of waves (Sommerfield condition)

Those used in the model are described in section 5.4

ADCIRC can be forced with:

- elevation boundary conditions
- normal flow boundary conditions

- surface stress boundary conditions
- earth load/self attraction tide

A feature of ADCIRC that makes its application particularly useful in storm surge modeling of bays along the Texas Gulf coast is the capability of wetting and drying in the computational cells. Most of the coastal basins that make up the estuaries along the Texas Gulf coast are very shallow, with depths that are often no more than a meter. In addition to the shallow bay depths, the topography of coastal lands is that of flat coastal plains, with very gentle slopes. The barrier islands in Freeport are just a few meters above mean water level. During extreme meteorological events like hurricanes, it is possible that shallow areas may become dry from "blow down" (due to water being driven from the area by storm winds). On the other hand, the surge during a storm can cause extensive inland coastal flooding as is evident historically in all large storms affecting the Freeport area over the time period considered in this study.

An element based technique for wetting/drying was developed for implementation in ADCIRC. Conceptually, the algorithm assumes removable barriers exist along the sides of all triangular elements of the grid. Nodes of the elements are designated as "dry" nodes, "interface" nodes, and "wet" nodes. All elements connected to a dry node are assumed to have barriers in place such that there is no flow through the element, i.e. a dry element. An element connected to all wet nodes is a wet element and is included in the full flow domain. Interface nodes connect wet and dry elements. Boundaries connecting interface nodes are considered as standard land boundary nodes at which the water level rises and falls against the element barrier.

2.2 Tidal Propagation

Tidal potential forcing, which causes the normal observed periodic water level changes in large bodies of water, is included in ADCIRC. Other popular large-scale hydrodynamic models, like SLOSH and RMA2, do not include tidal potential forcing. ADCIRC determines the magnitude of the tidal potential η in equation (4) at each grid node and each model time step by the relationship:

$$\eta(\lambda,\phi,t) = \sum_{j,n} B_{jn}(t_0) L_j(\phi) \cos\left[\frac{2\pi(t-t_0)}{T_{jn}} + j\lambda + v_{jn}(t_0)\right] \qquad (5)$$

where:

j = tidal species

= 0 = declinational

= 1 = diurnal

= 2 = semidiurnal

B_{jn} = amplitude constant of the n^{th} tidal constituent of species j

F_{jn} = time dependent nodal factor

v_{jn} = time dependent astronomical argument

L_j = function for species j

$j = 0 \Rightarrow L_0 = 3\sin^2\phi - 1$

$j = 1 \Rightarrow L_1 = \sin(2\phi)$

$j = 2 \Rightarrow L_2 = \cos^2\phi$

t_0 = a reference time, usually the beginning time of simulation

T_{jn} = period of constituent *n* of species *j*

The values of f (B_{jn}) and ν for the constituents used for the tidal potential computations are determined for the specific time that a model run begins using Le Provost database (Westerink, J.J. et al, 1993). LeProvost database (Le Provost et al, 1994) is an atlas of the main components of the tides and has been produced on the basis of a finite element hydrodynamic model, with the aim of offering the scientific community, using satellite altimetric data, a prediction of the tidal contribution to sea surface height variations under the ground tracks of the satellite that is totally independent of altimetric variation. Eight constituents, M_2, S_2, N_2, K_2, $2N_2$, K_1, O_1, and Q_1 have been simulated. Five secondary constituents: Mu_2, Nu_2, L_2, T_2, and P_1, required to insure a priori correct predictions, have been deduced by admittance. The admittance is assumed to be a slowly varying function of frequency so that the admittance of the major constituents can be used for determining the response at nearby frequencies for the secondary constituents.

The accuracy and precision of these solutions have been estimated by reference to the harmonic constituents' data set available from analysis of the entire collection of the pelagic, plateau and coastal observations made to date, and archived. Over the deep oceans these solutions fit the observations to within a few centimeters for the larger components: M_2, S_2, K_1, O_1, and a few millimeters for the others. Over the continental shelves the differences are larger, because of the increase in the magnitude of the tidal waves, but the flexibility offered by the finite element technique to refine the discretization mesh of the model over the shallow seas enables detailed cotidal maps to be produced along the coasts. Note that tidal potential was not used during the simulation

of tropical storms. Tides were combined after the simulations during the frequency analysis.

2.3 Bottom Stress

Bottom stress in the 2DDI version of ADCIRC is generally expressed as:

$$\tau_{bx} = U\tau^* \quad and \quad \tau_{by} = V\tau^*$$

Depending on the form used for τ^* the result is either a linear, quadratic or hybrid function of depth-averaged velocity. For most coastal applications, quadratic friction should be used with a drag coefficient, $C_f \sim 0.0025$. In very shallow water, hybrid friction may be useful with $C_{fmin} \sim 0.0025$, particularly when wetting and drying is included since this expression becomes highly dissipative as the water depth becomes small. Linear friction is primarily useful for model testing or when a totally linear model run is desired. In this case the magnitude of τ^* should be consistent (at least in order of magnitude) with a value that would have been computed using the quadratic friction expression and not with the value of C_f that would normally be used in the quadratic expression. The description of formulation based on the form of τ^* is given here.

Linear friction: $\tau^* = C_f$

where C_f = constant in time (may vary with space), read in model as input, unit s^{-1}

Quadratic friction: $\tau^* \equiv \frac{C_f \left(U^2 + V^2\right)^{1/2}}{H}$

where C_f = constant in time (may vary with space), read in model as input

H = water depth

Hybrid friction: $\tau^* \equiv \frac{C_f \left(U^2 + V^2\right)^{1/2}}{H}$

where $C_f = C_{f\min}\left[1 + \left(\frac{H_{break}}{H}\right)^{\theta}\right]^{\gamma/\theta}$

and C_{fmin}, H_{break}, ϑ, γ are constant in time and are read in as model input

In the hybrid friction relationship C_f approaches C_{fmin} in deep water, ($H > H_{break}$), and approaches $C_{f\min}\left(\frac{H_{break}}{H}\right)^{\gamma}$ in shallow water, ($H < H_{break}$). The exponent ϑ determines how rapidly C_f approaches each asymptotic limit and γ determines how rapidly the friction coefficient increases as water depth decreases. If $C_{f\min} = \frac{g\,n^2}{H_{break}^{\gamma}}$ and $\gamma = 1/3$, where g is the gravitational constant and n is the Manning Coefficient, the hybrid friction will have a Manning equation frictional behavior for $H < H_{break}$.

2.4 Wind Forcing

In addition to the capability for tidal forcing within ADCIRC, there are provisions to input atmospheric and wind forcing information into the simulations. Several formats for the wind data are supported, including a fleet numeric and National Weather Service (NWS) wind file format. For this study, the Planetary Boundary Layer (PBL) model (Cardone et al. 1992) supplies the atmospheric forcing information. This model was developed to simulate hurricane generated wind fields using basic characteristics about a particular storm that can be easily retrieved from sources such as NWS archives of past hurricanes.

The input data to the model consists of location of the eye of the hurricane (latitude and longitude) in degrees, wind speed and pressure measured at the eye for 6-hour intervals. Such data are available for all the storms. A sample input data for Hurricane Claudette (2003) is shown in Table 2-1.

Table 2-1: Input data for Hurricane Claudette (2003)

Time (Day. Hour)	Latitude	Longitude	Maximum wind speed (knots)	Eye Pressure (mm of Hg)
15.03	27.8	-94	70	988
15.09	28	-95.1	75	982
15.15	28.5	-96.1	75	983
15.21	28.6	-97.5	65	989

There are five simple parameters to describe the strength, size, and motion of a model storm; the parameters are: (1) Latitude: Normally the latitude of the storm's landfall; if the storm does not landfall, the latitude of a point of interest on the coast. The storm surge is only mildly sensitive to this parameter and varies by less than 10 percent between latitudes 15° and 45°, all other parameters being the same. (2) Radius of maximum winds: The distance from the storm center to the maximum wind of the storm. This distance is not dependent on storm motion, and for any given time it is assumed to be the same in all directions. This parameter controls the horizontal extent of the surge on the coast. If only the value of the peak surge on the coast is desired then the accuracy of

this parameter becomes unimportant, and for most purposes a rough estimate of this distance is sufficient. (3) Central pressure of the storm: The pressure difference from the center to the periphery of the storm. For an actual storm, this could be the mean of several differences measured along rays from the storm enter to the first anticyclonically turning isobar. This is the most important storm parameter; it controls the peak surge on the coast. For constant pressure drop, the peak surge on the coast is only weakly dependent on the radius of maximum wind. The pressure drop is not used directly in the model computations; instead it is used as an argument to arrive at a more convenient measure for computations, the stationary-storm-maximum-wind. (4) Speed of storm: Rate of motion of the storm center. With all other parameters held fixed, there is a critical storm speed that gives the highest peak surge on the coast. (5) Direction of storm: Direction of motion of the storm center. With all other parameters held fixed, there is a critical direction of storm motion, which gives the highest peak surge on the coast.

This model simulates hurricane-generated wind and atmospheric pressure fields by solving the equations of horizontal motion that have been vertically averaged through the depth of the planetary boundary layer. The PBL model requires input defining both the hourly location of the eye of the storm and a set of meteorological parameters defining the storm at various stages of development. These parameters include latitude and longitude of the eye of the storm, track direction and forward speed measured at the eye, radius to maximum wind, central and peripheral atmospheric pressures, and an estimate of the geostrophic wind speed and direction. A two-step process is used to generate wind fields for use by ADCIRC from the storm data. First, a program for the PBL model is used to determine the track of the storm as one our ‘snapshots’. These

snapshot data include the radius of maximum wind, which is approximated using a nomograph that incorporates the maximum wind speed and atmospheric pressure anomaly (Jelesnianski and Taylor, 1973), which is shown in Fig. 2-1. In the second step, the PBL model computes the wind field and pressure field of the hurricane over the relevant areas of the Gulf of Mexico.

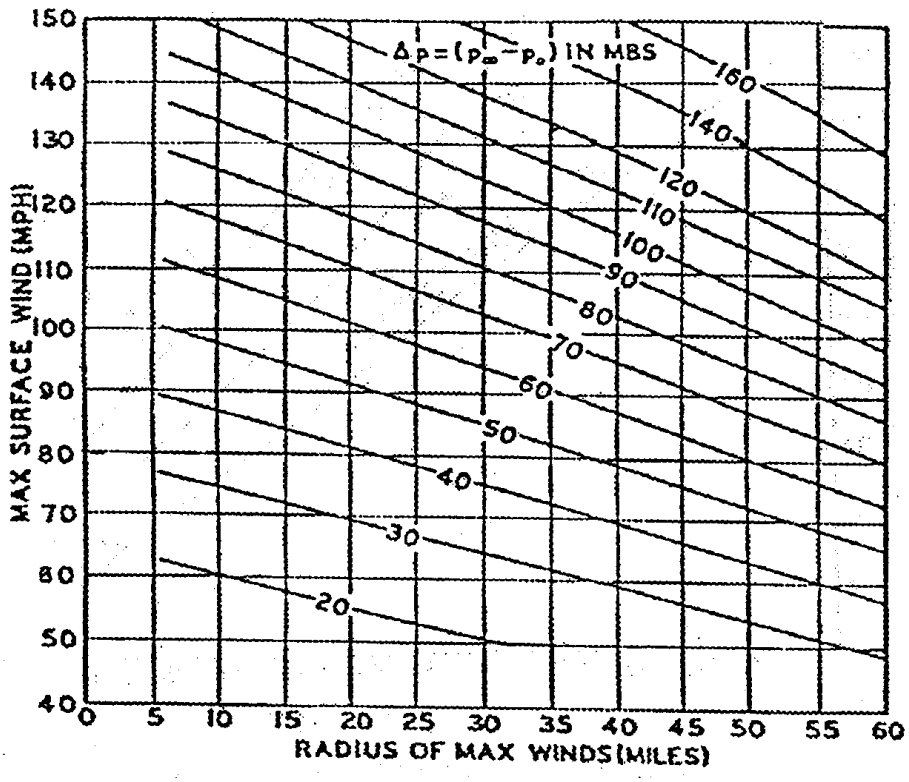

Fig. 2-1: Nomograph from Jelesnianski and Taylor (1973) used to derive radius of maximum winds from given maximum surface winds (long term average, no gusts)

2.4.1 PBL

The PBL (Planetary Boundary layer) is a method for specifying the surface wind field in hurricanes over the ocean by applying a dynamical-numerical model in

hurricanes. The method, requiring as input only a description of the surface pressure field and specification of storm motion and latitude, has been used to model the surface wind field.

The PBL model solves for the surface wind stress and barometric pressure distribution. Wind speeds are computed in the model and then converted to surface wind stress. The PBL model solves the equations of horizontal motion that have been averaged through the depth of the atmospheric boundary layer, following the work of Chow (1971) . Written in general coordinate system fixed to the earth these equations can be expressed as:

$$\frac{dV}{dt} + f\left(\vec{k} \times \vec{V}\right) = -\frac{1}{\rho}\nabla p + \nabla \cdot \left(K_H \nabla \vec{V}\right) - \frac{C_D}{h}\left|\vec{V}\right|\vec{V} \qquad (6)$$

where

$$\frac{d\overline{V}}{dt} = \frac{\partial \overline{V}}{\partial t} + \overline{V} \cdot \nabla \overline{V} \qquad (7)$$

and

$\overline{V}$ = vertically averaged horizontal velocity,

f = Coriolis force parameter,

$\vec{k}$ = unit vector in the vertical direction,

ρ = mean air density,

p = barometric pressure,

K_H = horizontal eddy viscosity coefficient,

C_D = drag coefficient,

h = depth of the boundary layer.

It is assumed that the vertical advection of momentum is small compared to the horizontal advection and can be neglected and that shearing stress vanishes at the top of the PBL. In addition to the storm winds, the PBL model generates a pressure field. The pressure field is axisymmetric and is defined by exponential law which expresses P_c, the pressure at a particular location in the storm, as:

$$P_c = P_{eye} + \Delta p e^{-R_p / r} \tag{8}$$

where,

P_{eye} = the central low pressure at the eye of the storm,

Δp = P- P_{eye}, where P is the normal background pressure (~ 1013 mb),

R_p = scale radius, equivalent to the radius of maximum winds,

r = radial distance from the eye.

These equations are solved using a finite difference formulation, which utilizes a nested rectangular mesh for computations. The computational grid is a rectangular nested grid system consisting of five nests. An example of this type of mesh is shown in Fig. 2-2, where a single quadrant of the complete numerical grid is shown. The grid moves with the storm, therefore the eye of the hurricane is always centered about the point indicated as origin.

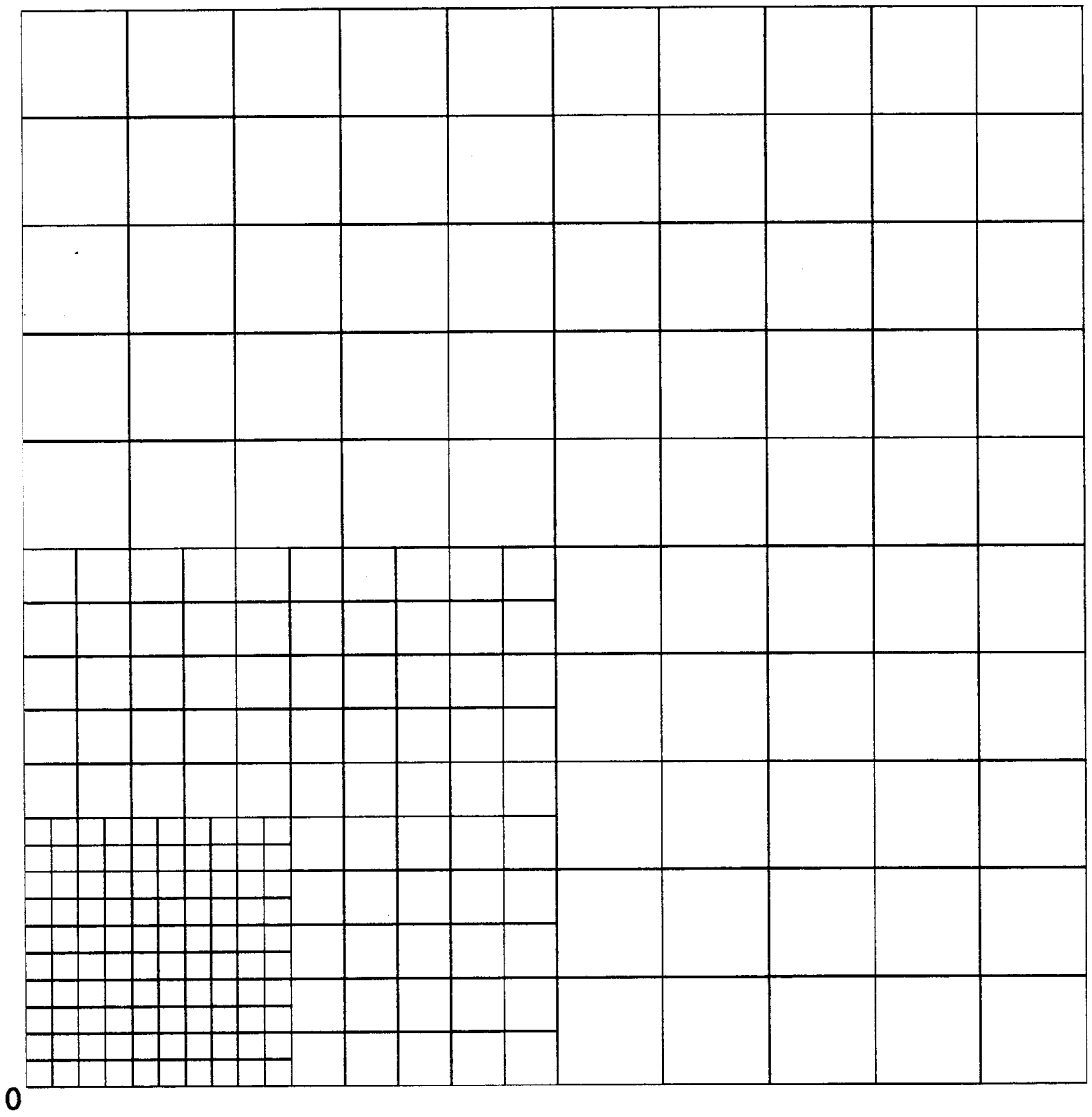

Fig. 2-2: Nested grid system used for hurricane wind computation

The PBL model produces a consistent description of the vertically integrated wind, the surface drag and the wind speed and direction at anemometer height in a moving hurricane with asymmetric horizontal wind distribution over water, with the

strongest winds occurring at the right-hand side of the storm, when facing the direction of travel of storm. The formulation of the model includes momentum, heat, and moisture flux. Equilibrium PBL theory is used to extend the surface wind description to terrain of specified roughness.

The final surface wind stress output of the PBL model is determined from the computed wind speeds using the relationships:

$$\frac{\tau_{s\phi}}{\rho_o} = C_D \frac{\rho_{air}}{\rho_o} \left|\overline{V}\right| \overline{V}_\phi \tag{9}$$

and

$$\frac{\tau_{s\lambda}}{\rho_o} = C_D \frac{\rho_{air}}{\rho_o} \left|\overline{V}\right| \overline{V}_\lambda \tag{10}$$

where,

τ_ϕ, τ_λ = the surface stresses applied in the ϕ and λ directions

ρ_{air}/ρ_o = density ration of air and seawater (~ 0.001293)

$\left|\overline{V}\right|$ = absolute magnitude of the wind velocity

$\overline{V}_\phi, \overline{V}_\lambda$ = components of wind velocity in ϕ and λ directions

C_D = $0.001*(0.75+0.67*\left|\overline{V}\right|)$ frictional drag coefficient

ϕ, λ = directions

A plot of the wind shear stress in a well-developed hurricane is shown in Fig. 2-3, where it is shown that the greatest winds in this case occur north-east of the eye of this north-westerly moving storm.

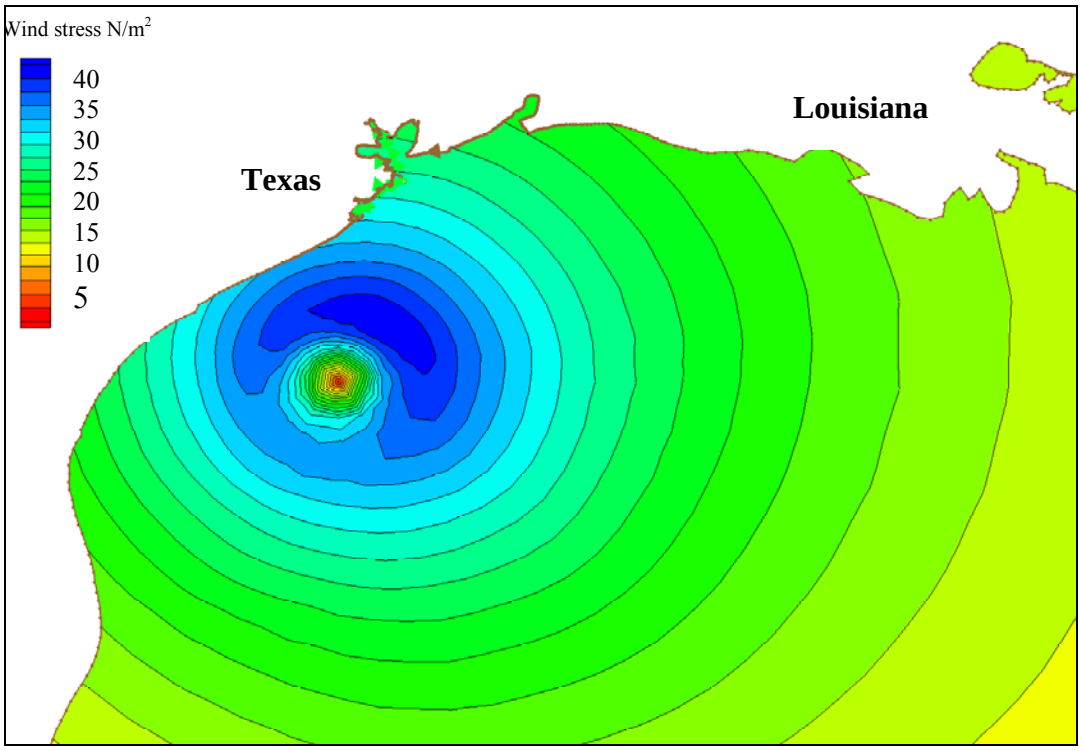

Fig. 2-3: Plot of variation of wind stress for a well-developed hurricane moving towards Texas coast

The wind model is incorporated in a computer program to provide a gridded temporal and spatial history of the surface wind for use in surge calculation. After completing the computations for the wind and pressure fields at each hourly position of the storm, the solution from the nested rectangular grid is superimposed onto a triangular grid for use by ADCIRC. Therefore, when ADCIRC is run with the hurricane wind fields in the PBL format, it is supplied with the components of the surface stress in the ϕ and λ directions and barometric pressure at each node in the FEM grid and at every hour.

3 SLOSH

A numerical-dynamic, tropical storm surge model, was developed for real-time forecasting of hurricane storm surges on continental shelves, across inland water bodies, along coastlines, and for inland routing of water – either from the sea or from inland water bodies. The most valuable application of SLOSH (Sea, Lake, and Overland Surges from Hurricanes) was in the design of evacuation plans for various communities.

SLOSH is a two-dimensional finite difference code, which has been programmed to utilize a variety of curvilinear grid formats, such as polar, elliptical, and hyperbolic (Jelesnianski 1973). The full length of East coast and Gulf coast of the United States is broken down into several regional grids, or model "basins". Each basin in turn is centered about a major bay, inlet or population center. The individual SLOSH basins that are used by NWS are shown in Fig. 3-1. An example of one of these model basins is shown in the grid no. 31 used for Galveston Bay in Fig. 3-2. The results from this grid have been used in this thesis for comparison purposes.

3.1 Development of SLOSH

The National Weather Service (NWS) began its efforts in hurricane storm surge modeling with a relatively simple model referred to as SPLASH (Special Program to List the Amplitude of Storm surges from Hurricanes). This model, like several other simple models for computing storm surge, was restricted to a continental shelf only, with the coastline acting as an artificial vertical wall. No flow through this wall was permitted. Such a model cannot consider inundation across terrain or surges across inland water bodies (Jelesnianski, 1972; Wanstrath and Reid, 1976). An earlier shelf model by Bodine

(1971) was even more restricted. His model required computations carried out on only one seaward line from the coast. Also the storm track was restricted to being nearly perpendicular to the coastline.

The National Weather Service (NWS) embarked on an effort to develop a more comprehensive model to forecast storm surges, which incorporated features not possible with SPLASH. This follow-on model called SLOSH, uses a curvilinear grid system to allow greater resolution in the area of forecast interest, computes surges over bays and estuaries, retains some non-linear terms in the equation of motion, and allows sub-grid scale features such as channels, barriers, and flow of surge up the rivers. More recently the model has been used to delineate coastal areas susceptible to hurricane storm surge flooding.

A curvilinear grid system overcomes many of the problems associated with specifying boundary conditions encountered with earlier models. Instead of limiting an invariant fine mesh to a small region or small basin, the SLOSH model's coordinate system begins as fine mesh in the limited area nearest to the pole point of the grid and stretches continuously to a coarse mesh at distant boundaries of a large basin. The geographical area covered by the entire grid is large and there is detailed description over the fine-mesh region. Moreover, in many cases simple boundary conditions are sufficient (Jelesnianski et al, 1992).

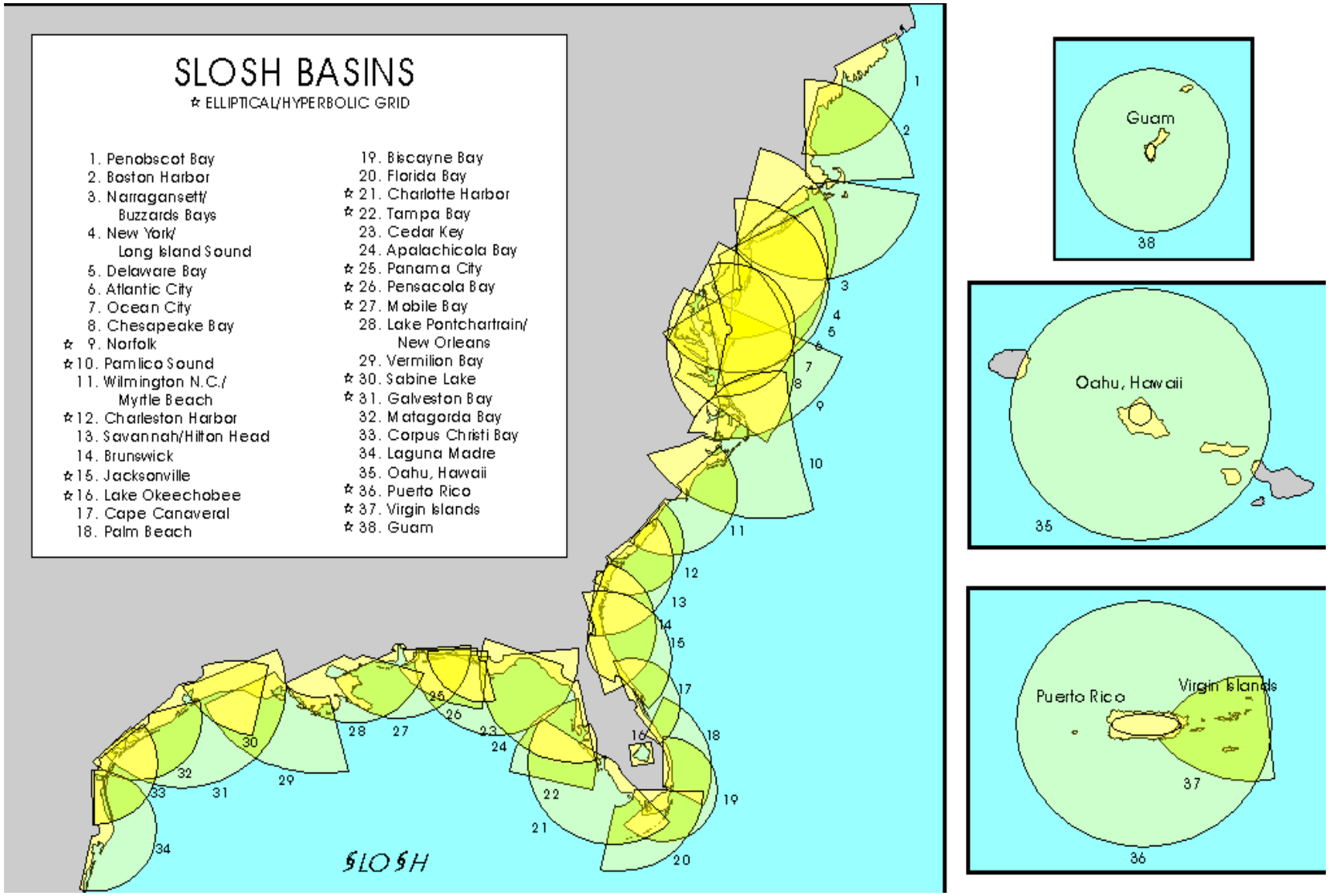

Fig. 3-1: SLOSH model basins for the East and Gulf coastlines of the U.S. (Jelesnianski et al, 1992)

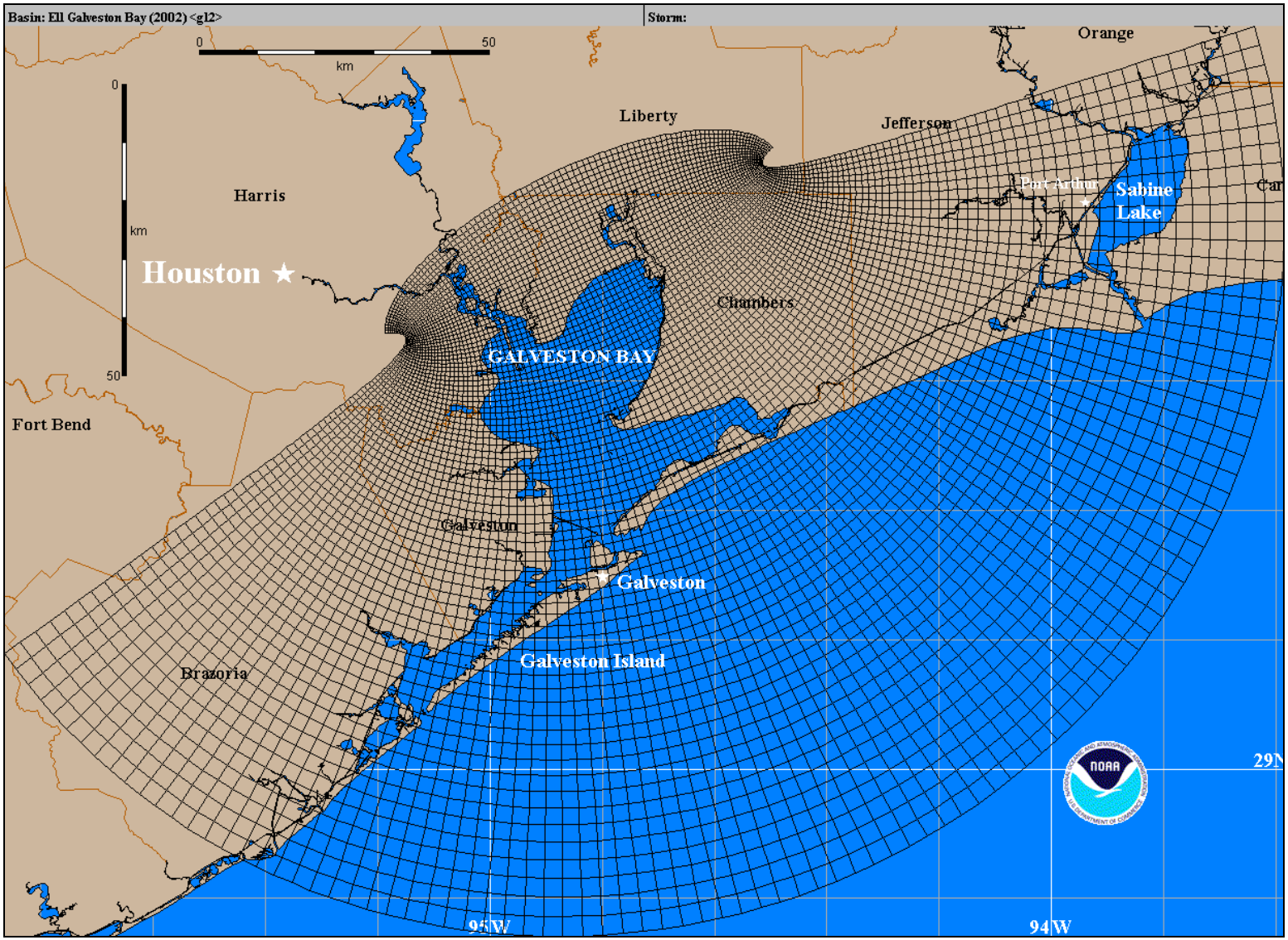

Fig. 3-2: SLOSH model basin for Galveston Bay (Jelesnianski et al, 1992)

3.2 SLOSH Methodology

The transport equations of motion on a Cartesian frame of reference used are:

$$\frac{\partial U}{\partial t} = -g(D+h)\left[Br\frac{\partial(h-h_o)}{\partial x} - B_i\frac{\partial(h-h_o)}{\partial y}\right] + f(A_rV + A_iU) + C_rx_\tau - C_iy_\tau$$

$$\frac{\partial V}{\partial t} = -g(D+h)\left[Br\frac{\partial(h-h_o)}{\partial y} + B_i\frac{\partial(h-h_o)}{\partial x}\right] - f(A_rU - A_iV) + C_ry_\tau + C_ix_\tau \qquad (11)$$

$$\frac{\partial h}{\partial t} = -\frac{\partial U}{\partial x} - \frac{\partial V}{\partial y}$$

where:

U, V = components of transport
g = gravitational constant
D = depth of quiescent water relative to a common datum
h = height of water above datum
h_o = hydrostatic water height
f = Coriolis parameter
x_τ, y_τ = components of surface wind stress
$A_r, .. B_r, . C_i$ = bottom stress terms

The SLOSH model incorporates finite amplitude effects but not advective terms in the equations of motion. It uses time-history bottom stress (Platzman, 1963; Jelesnianski, 1967), corrected for finite amplitude effects. Overtopping of barrier systems, levees and roads, is incorporated. Also, simply turning squares on and off as water inundates or recedes permits inland inundation. Astronomical tide is ignored except for superposition onto the computed surge; it is difficult to phase storm landfall and astronomical tide. A small error in time on track positions will invalidate computations with astronomical tide.

Besides the hydrodynamic model, the most significant part of SLOSH is the wind model that is used to generate hurricane wind fields using simple time-dependent storm data. The storm data required by SLOSH are storm position and central pressure at six-hour intervals. Each model basin is calibrated separately by a single historic event through the use of three empirical coefficients in the model. These tuning coefficients are eddy viscosity, bottom friction factor, and wind drag. They are set to the same value at each node of the model basin, and these values are usually determined by a best-fit approximation. After the initial calibration of the model basin, no additional tuning is made for further model runs.

3.3 SLOSH Output

The final output of the SLOSH model runs gives both local information at selected sites in the grid, and global output for the entire modeled domain. Local, time-dependent data are collected from as many as 60 individual stations. These time histories present the surge elevation, wind speed and wind direction every 10 minutes of simulated time. In addition to the model station output, SLOSH outputs global (values for each node in the grid) surge elevations. The global data is output at three-hour intervals up to the closest approach of the storm, and then every two hours, up until nine hours beyond the closest approach.

There are other factors also that can have a significant influence on the total water level elevation during a storm. In coastal regions, the action of breaking waves can create a quasi-steady-state, long period “set-up” (if not set-down) whereby the original storm surge is altered. This wave action can affect bottom stress in shallow waters. Also, exotic effects occur such as an increase of density from suspended sand particles. Along coastal

regions, during passage of a tropical storm and onset of inundation, the totality of wind-wave effects on surge is now well understood or even well observed. Many theoretical studies of an idealized and piecemeal nature, as well as idealized wave tank experiments, have been made. It is not sufficient to correct a computed surge for one or more long-term interactions. Accordingly, the SLOSH model lumps the long-term interactions into an ad hoc generalized calibration to observed surge data generated by a multitude of historical storms: that is, the short term action from wind waves is absent but crude approximations for the long term effects may be present. The SLOSH model does give an indication of inland flooding but not the pulsating action of wind waves, such as short-term, periodic, sheet flow over barriers (Jelesnianski et al, 1992).

4 THE EMPIRICAL SIMULATION TECHNIQUE

The Empirical Simulation Technique (EST) is a procedure for simulating multiple life-cycle sequences of non-deterministic multi-parameter systems such as storm events and their corresponding environmental impacts. Essentially, it is a "Bootstrap" resampling-with-replacement, interpolation, and subsequent smoothing technique in which random sampling of a finite length database is used to generate a larger database (Borgman et al. 1992). The only assumption is that future events will be statistically similar in magnitude and frequency to past events. As stated above, EST is a generalized procedure applicable to any cyclic or frequency-related phenomena (Scheffner et al, 1999). For example, if one can parameterize storm events as well as obtain or simulate corresponding historical impacts for these events, EST could be used to investigate life-cycle scenarios of storm conditions. The EST begins with an analysis of historical events that have impacted a specific locale. The selected database of events (the training set) is then parameterized to define the characteristics of the event. The interdependence of parameters is computed directly from the respective parameter interdependencies contained in the historic data. In this manner, probabilities are site-specific; do not depend on fixed parametric relationships or assumed joint probability distributions. The impacts of events may be known or may be simulated by other models (e.g., hurricane events can be characterized by parameters such as central pressure, forward speed, etc. and their impact may be simulated with appropriate hydrodynamic and storm wind models). Parameters that describe an event, i.e., a storm in this discussion, are referred to as input parameters or input vectors. Response parameters or response vectors define event-related impacts such as storm surge elevation, inundation, shoreline and dune

erosion, etc. These input parameters and response parameters are then used as a basis for generating life-cycle simulations of hurricane activity with corresponding impacts.

The descriptive characteristics of the storm event with respect to the specific location of interest are determined by the input parameters or input vectors. For tropical storms these input parameters are studied at the point when the eye of the hurricane is closest to the station of interest. These vectors are defined as:

1) tidal phase during the event, with 1.0 corresponding to high water slack, 0.0 MSL at maximum ebb, -1.0 low water slack, these represent relative values that are defined for each station

2) radius of maximum wind for the hurricane when the eye is closest to the hurricane in nautical miles.

3) minimum distance from the eye of the storm to the location of interest in nautical miles.

4) pressure at the hurricane eye in millibars (mb)

5) wind speed in the hurricane at the instant of eye hitting the coast, measured in knots.

6) direction of forward propagation of the eye of the hurricane in knots.

7) tidal range during the event: with spring, neap or mid tide conditions.

The maximum storm surge elevation reached at specified gauge locations is defined as the response vector of the storm at that location. The specified response vector for this study was determined by simulating the specific storm event via the ADCIRC hydrodynamic model using the computational domain shown in Fig. 1-2. The output vector(s) represents the environmental response to the storm. This response is defined at location X and is a direct consequence of the storm via the storm parameter values

defined at the point of nearest proximity of the storm eye to point X. For the case of stage-frequency analyses, maximum surge is assumed to occur when the eye of the storm is nearest to location X.

4.1 Storm Consistency with Past Events

The first major requirement for the use of EST is that future events will be statistically similar to past events. This criterion is maintained by insuring that the input vectors for simulated events are similar to those of past events and the input vectors have similar joint probabilities to those historical events of the training set. For example, a hurricane with a large central pressure deficit and low maximum winds is not a realistic event – the two parameters are not independent although their precise dependency is unknown. The simulation of realistic events is accounted for in the nearest-neighbor interpolation-bootstrap-resampling technique developed by Borgman (Scheffner, et al. 1999 and Borgman, et al. 1992). By using the training set as a basis of for defining future events, unrealistic events are not included in the life cycle of events generated by the EST. Events that are output by EST are similar to those in the training set with some degree of variability from the historic/historically based events. This variability is a function of the nearest neighbor: therefore the deviation from historic conditions is limited to natural variability of the system.

The basic technique can be described as follows. Let X_1, X_2, X_3, . . . X_a be n independent, identically distributed random vectors (historic storm events) each having two components [$X_i=\{\underline{x}i(1),\underline{x}_i(2)\}$; I =1,n]. If there are no hypothetical events, each event X_i has a probability p_i of l/n. If one storm event is used to generate two hypothetical events, then the original storm and each of the two perturbations are

assigned a probability of one-third of l/n. A cumulative probability relationship can be developed in which each storm event of the total training set is assigned a segment of the total probability of 0.0 to 1.0. Therefore each event occupies a fixed portion of the 0.0 to 1.0 cumulative probability spaces according to the total number of events in the training set. A random number from 0 to 1 is then used to identify a storm event from the total storm training set population. The procedure is equivalent to drawing and replacing a random sample from the full storm event population.

The EST is not simply a resampling of historical events technique, but rather an approach intended to simulate the vector distribution contained in the training set data base population. The EST approach is to select a sample storm based on a random number selection from 0 to 1 and then performs a random walk from the event X_i with n number of response vectors to the nearest neighbor vectors. The walk is based on independent uniform random numbers on (-1,1) and has the effect of simulating responses that are not identical to the historical events but are similar to events, which have historically occurred. However it is important to point out that it is possible that the response value of water surface elevation (i.e. tide plus surge) may be greater than the greatest value in the total training set or it could be smaller than the smallest of the training set.

The process can be summarized as follows. Select a specific storm event from the training set and proceed to the location in multidimensional input vector space corresponding to that event. From that location, perform a nearest neighbor random walk to define a new set of input vectors. This new input vector defines a new storm, similar to the original storm but with some variability in parameters.

4.2 Storm Event Frequency

The second criteria to be satisfied is that the number of storm events selected per year must be statistically similar to the number of historical events that have occurred at the area of concern. Given the mean frequency of storm events for a particular region, a Poisson distribution is used to determine the average number of expected events in a given year. For example, a Poisson distribution can be written in the following form:

$$\Pr(s;\lambda) = \frac{\lambda^s \ e^{-\lambda}}{s!} \tag{12}$$

for s=0,1,2,3… The probability Pr(s;λ) defines the probability of having s events per year where λ is the historically based number of events per year. In the present study, historical data were used to define λ as:

λ = 0.2307 (27 historical events/117 years or one event every 4.33 years)

Output from the EST program is N repetitions of T years of simulated storm event responses. For this study, 500 repetitions, N, of a 200 year sequence, T, of storm activity are used. It is from the responses of those 500 life cycle simulations that frequency-of-occurrence relationships are computed. Because EST output is of the form of multiple time–series simulations, post processing of output yields mean value frequency relationships with definable error estimates. The computational procedure followed is based on the generation of a probability distribution function corresponding to each of the T-year of simulated data. In the following section, the approach adopted for using these storms to develop frequency-of-occurrence relationships is given.

4.3 Risk-Based Frequency Analysis

The primary justification for applying the EST to a specific project is to generate risk-based frequency information relating to effectiveness and cost of the project with the level of protection provided. The multiple life-cycle simulations produced by EST can be used for developing design criteria in two approaches. In the first, the actual time series are input to an economics based model that computes couple storm inundation, structure response, and associated economics. The model internally computes variability associated with the risk-based design. The other application is the post processing of multiple time-series to generate single-response frequency relationships and associated variability.

4.4 Frequency-of-Occurrence Relationships

Estimates of frequency-of-occurrence begin with the calculation of a probability distribution function (pdf) for the response vector of interest. Let X_1, X_2, X_3, . . . , X_n be n independent, identically distributed, random response variables with a cumulative pdf given by

$$F_x(x) = \Pr[X < x] \tag{13}$$

where Pr[X<x] represents the probability that the random variable X is less than or equal to some value x, and $F_x(x)$ is the cumulative probability density function ranging from 0.0 to 1.0. The problem is to estimate the value of F_x without introducing some parametric relationship for probability. The following procedure is adopted because it makes use of the probability laws defined by the data and does not incorporate any prior assumptions concerning the probability relationship.

Assuming a set of n observations of data, the n values of x are first ranked in order of increasing size. In the following analysis, the parentheses surrounding the subscript indicate that the data have been rank-ordered. The value x(1) is the smallest in the series and x(n) represents the largest value. Let r denote the rank of the value x(r) such that rank r = 1 is the smallest and rank r = n is the largest.

An empirical estimate of $F_x(x(r))$, denoted by $F_x(x_{(r)})$, is given by Gumbel (1954) (See also Borgman and Scheffner (1991) and Scheffner and Borgman (1992)) as:

$$F_\chi(x_{(r)}) = \frac{r}{(n+1)} \tag{14}$$

for $\{x_{(r)}, r = 1, 2, 3, \ldots, n\}$. This form of estimate allows for future values of x to be less than the smallest observation $x_{(1)}$ with a cumulative pdf of 1/(n+1), and to be larger than the largest values with cumulative pdf of n/(n+1).

The cumulative pdf as defined by Equation (14) is applied to develop stage-frequency relationships as follows. Consider that the cumulative probability for an n-year return period storm can be written as

$$F(n) = 1 - \frac{1}{n} \tag{15}$$

where F(n) is the simulated cumulative pdf for an event with a return period of n years. Frequency-of-occurrence relationships are obtained by linearly interpolating a stage from Equation (14) corresponding to the pdf associated with the return period calculated by Equation (15).

Equations (14) and (15) are applied to each of the N-repetitions of T-years of storm events simulated via the EST. Therefore, there are N frequency-of-occurrence relationships generated. From these results, the standard deviation is determined to

provide an estimate of the variability of the result. The standard deviation is computed for each return period as:

$$\sigma = \sqrt{\left[(1 / N) \sum_{n=1}^{N} (x_n - \bar{x})^2 \right]} \tag{16}$$

where $\bar{x}$ is the mean value of x.

5 PROJECT IMPLEMENTATION

The model as stated before required the generation of finite element grid and application of appropriate boundary conditions in order to simulate tides and coupling with the wind model PBL, to simulate hurricanes and tropical storms. The process required the following tasks:

1. Obtaining Coastline
2. Obtaining Bathymetry
3. Grid generation
4. Boundary conditions
5. Tidal verification
6. Storm verification, simulation and entry into database
7. EST analysis

5.1 Coastline

The coastline is required to define the extents of the model domain. This will become the boundary of the computational mesh. The coastline around our area of interest as well as the ocean defines the domain. The coastline for this purpose is obtained in digital format from GEODAS and NOAA databases. The coastline is in the form of World Vector Shoreline subset at 1:1million resolution (altered) format. Since the obtained coastline was ragged in nature, it was smoothened before being used for grid generation.

5.2 Bathymetry

The bathymetry in the Gulf of Mexico varies dramatically, as is illustrated in the Fig. 1-3. Bathymetric data in most of the Gulf was obtained from the grid developed by Scheffner et al. (2003), GeoDas (a database developed by National Oceanic and Atmospheric Administration, NOAA), USACE surveys, surveys conducted by Texas A&M University in the area of interest, and USGS terrain data. The terrain data was in the form of 30-meter grid digital elevation models (DEM). These data are based on the USGS 7.5 minute x 7.5-minute quads maps and are interpolated from 5-foot elevation contours.

5.3 Grid Generation

The grid was generated as a combination of finite element grid developed by Scheffner et al. (2003) and modified in the area of interest with details added. The grid in the area of interest was developed using SMS (Surface Modeling System). To get a mesh/grid with density radiating from the center of the Freeport channel, size functions in SMS were used along with celerity and wavelength functions so that smaller elements are obtained closer to the shore to correctly model the area of interest.

5.4 Boundary Conditions and Model Setup

Boundary conditions are imposed on the solutions of ordinary differential equations and partial differential equations, to fit the solutions to the actual problem.There are many kinds of possible boundary conditions, depending on the formulation of the problem, number of variables involved, and (crucially) the mathematical nature of the equation.

The boundary conditions used within ADCIRC for this study were:

- External boundary with no normal flow as an essential boundary condition and no constraint on tangential flow. This is applied by zeroing the normal boundary flux integral in the continuity equation and by zeroing the normal velocity in the momentum equations. This boundary condition should satisfy no normal flow in a global sense and no normal flow at each boundary node. This type of boundary represents a mainland boundary with a strong no normal flow condition and free tangential slip.
- Internal boundary with no normal flow treated as an essential boundary condition and no constraint on the tangential flow. This is applied by zeroing the normal boundary flux integral in the continuity equation and by zeroing the normal velocity in the momentum equations. This boundary condition should satisfy no normal flow in a global sense and no normal flow at each boundary node. This type of boundary represents an island boundary with a strong normal flow condition and free tangential slip.
- External boundary with non-zero normal flow as an essential boundary condition and no constraint on the tangential flow. This is applied by specifying the non-zero contribution to the normal boundary flux integral in the continuity equation and by specifying the non-zero normal velocity in the momentum equations. This boundary condition should correctly satisfy the flux balance in a global sense and the normal flux at each boundary node. This type of boundary represents a river inflow or open ocean boundary with a strong specified normal flow condition and free tangential slip.

There are several other boundary conditions that can be applied in ADCIRC but they were not needed for the present model. The model was "spun up" (started with progressively increasing forcing such as tides or winds) from homogeneous initial conditions using a time ramp to avoid problems with short period gravity modes and vortex modes in the sub internal frequency range. A very smooth hyperbolic tangent ramp function, which acts over approximately one day, was applied to both boundary conditions and direct forcing functions. A 6-day spin-up was determined to be more than adequate for all conditions of interest.

A time step of 6 sec was used for tidal propagation and a time step of 2 seconds was used for storm simulation in order to accommodate the strong gradients associated with strong winds for storm conditions. Using higher time steps resulted in oscillations and long-term instabilities. The optimal time step was calculated based on Courant number criteria. The Courant Number criteria is usually expressed in the one-dimensional form as follows:

$$\text{Courant number} = \frac{v\Delta t}{\Delta x}$$

where:

Δx = nodal spacing

v = average linear velocity

Δt = incremental time step

The Courant Number constraints provide the necessary conditions for the finite element mesh design and the selection of time steps in transport modeling. The Courant Number constraint requires that the distance traveled by advection during one time step is not larger than one spatial increment. Based on wave celerity, it ranged from 0.0025 to

0.82. Time weighing factors of 0.35, 0.30 and 0.35 were used in the GWCE (Generalized Wave Continuity Equations). The parameter τ_0 was set equal to –0.005 as this signals ADCIRC to use 0.005 in deep water and 0.02 in shallow water, so that a balance is set between the primitive continuity and wave equation portions of the GWCE equation.

Table 5-1: List of stations used for tidal verification

S. No	Location	Longitude °	Latitude °
1	Corpus Christi	-97.38928	27.08113
2	Freeport Harbor	-95.34277	28.95019
3	Sabine Pass	-93.83873	29.68882
4	Galveston Bay entrance south jetty	-94.69849	29.32304
5	Round Point Galveston Bay	-94.78059	29.31827
6	Galveston Bay entrance	-94.70587	29.34739
7	Bolivar Roads	-94.78388	29.34029
8	Galveston (channel) (2)	-94.78774	29.31305
9	Galveston Pleasure Pier	-94.78747	29.28495
10	Galveston Channel	-94.80136	29.31203
11	Jamaica Beach	-95.00899	29.19919
12	Morgan Point	-94.9766	29.6756
13	Clear Lake	-95.06118	29.55583
14	Lynchburg Landing	-95.09607	29.77917
15	San Luis Pass	-95.12016	29.07968

5.5 Tidal Verification

Tidal water surface elevation data computed with the ADCIRC model were recorded at 15 locations for verification purposes. These locations are listed in Table 5-1. Storm surge water surface elevations were archived for 35 locations within the area of interest for subsequent computation of frequency-of-occurrence relationships.

The verification of the model had to be done to ensure that grid resolution, bathymetry, and boundary conditions were acceptable to properly simulate conditions in the defined domain. For comparison of tidal simulations with observed tides, verification was accomplished using 8-constituents (M_2, S_2, N_2, N_1, K_1, O_1, Q_1, and P_1), as these constituents comprise most of the tidal energy, with tidal elevations calculated using software XTIDE which in turn uses published harmonic series, and NOS published tidal records. The use of fewer tidal constituents resulted in less accurate simulation of tides in the study area.

Tidal circulation was simulated within ADCIRC by specifying a surface elevation time series at the Florida Strait and just south of the Yucatan Strait as shown in the computational grid of Fig. 1-2. This boundary condition specification is accomplished by reconstructing an 8-constituent tidal elevation time series at each open water boundary node of the grid based on amplitudes and Greenwich epoch values obtained from a database incorporated in the SMS software also known as LeProvost database. Additionally, tidal potential terms are specified at each node of the computational grid. The ADCIRC model has an internal harmonic analysis option in which individual constituent amplitudes and epochs are computed at user specified locations during the tidal simulation.

Verification of tidal circulation was made by comparing both ADCIRC computed harmonic constituents and ADCIRC computed time series with existing constituent data and reconstructed time series at each of the 15 verification locations listed in Table 5-1. Comparisons of ADCIRC versus published Harmonic Analysis (HA) computed constituent amplitudes and Greenwich epochs (G) are shown in Table 5-2 for two locations. Because the Gulf of Mexico is a semi-enclosed body of water, approximately 10 to 15 days of spin up time were required for the tide to come to a dynamic equilibrium, i.e. when the tides are acceptably reproduced. The harmonic analysis used for the comparisons in Table 5-2 were based on a 43-day simulation of tides and during this time the harmonic analysis was computed for the 29-day (one lunar month) period of days 15 through 43. A period with little wind activity was chosen to effectively compare the real-time data and ADCIRC simulated time-series. In order to demonstrate a degree of acceptability for the constituent comparisons shown in Table 5-2, a tidal elevation time series for days 15 through 43 is shown in Fig. 5-1 and Fig. 5-2 at different recording stations. As shown, the comparisons are quite acceptable and fully adequate for the statistical generation of stage-frequency relationships. The period of little wind activity is useful in comparisons with NOS published time series whereas in the case of comparison with XTIDE wind or lack of it, does not affect the comparison. This is because XTIDE tidal time series do not have the effect of wind.

Table 5-2:Tidal verification of ADCIRC along open coast

Constituents	Galveston Pleasure Pier		Freeport Harbor	
	Amp – m Mod / HA	G – deg Mod / HA	Amp – m Mod / HA	G – deg Mod / HA
K_1	.162/. 197	33.2/42.6	.175/. 188	18.7/26.6
O_1	.162/. 187	20.8/32.1	.167/. 178	13.2/15.9
P_1	.051/. 056	14.2/18.5	.059/. 065	17.1/21.6
Q_1	.034/. 043	11.6/16.2	.037/. 046	2.2/4.8
N_2	.025/. 037	290.2/285.1	.024/. 035	261.1/258.4
M_2	.102/. 138	317.6/295.7	.092/. 101	273.5/265.2
S_2	.024/. 040	278.9/282.6	.033/. 035	284.3/178.9
K_2	.009/. 011	271.3/282.1	.014/. 015	266.1/272.6

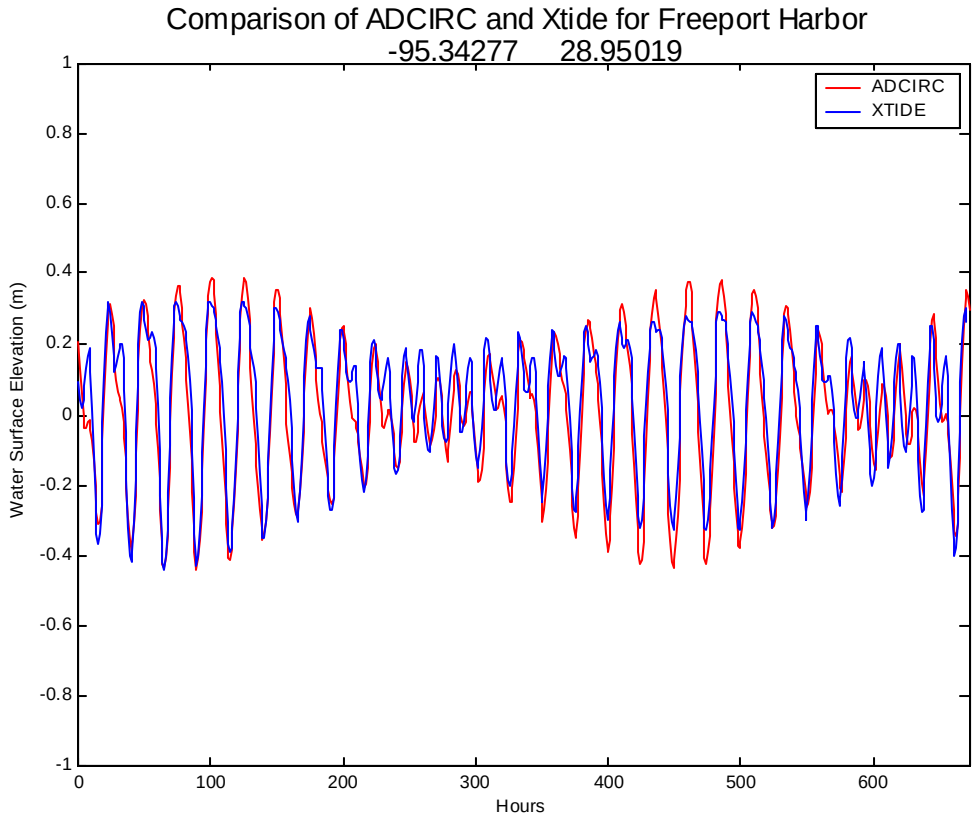

Fig. 5-1:Comparison of tides at Freeport Harbor

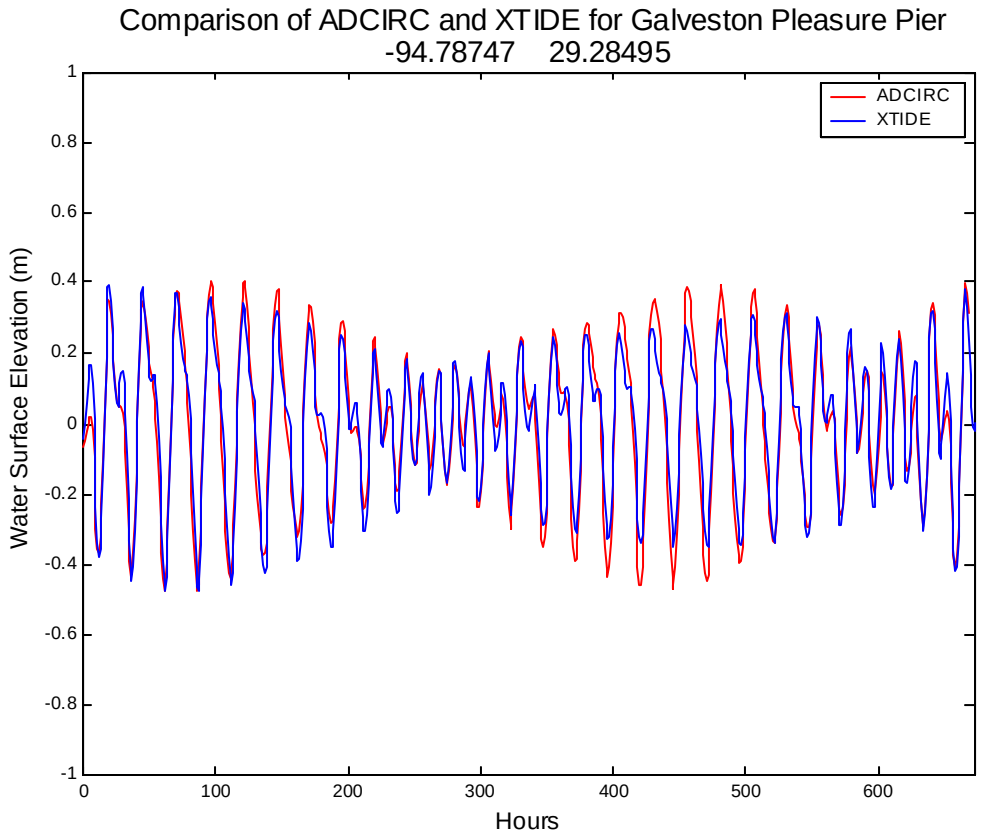

Fig. 5-2: Comparison of tides at Pleasure Pier

Comparison of tides was also made with NOS published time series. The comparison is not as good as the tide gages record instantaneous water surface variations, which includes wind waves. Fig. 5-3 shows this comparison and Fig. 5-4 shows the wind speeds at the same location. It can be seen that differences are observed between simulated and observed data whenever there is higher wind action in the region resulting in wind waves. This is because the model ADCIRC in this particular case does not account for wind.

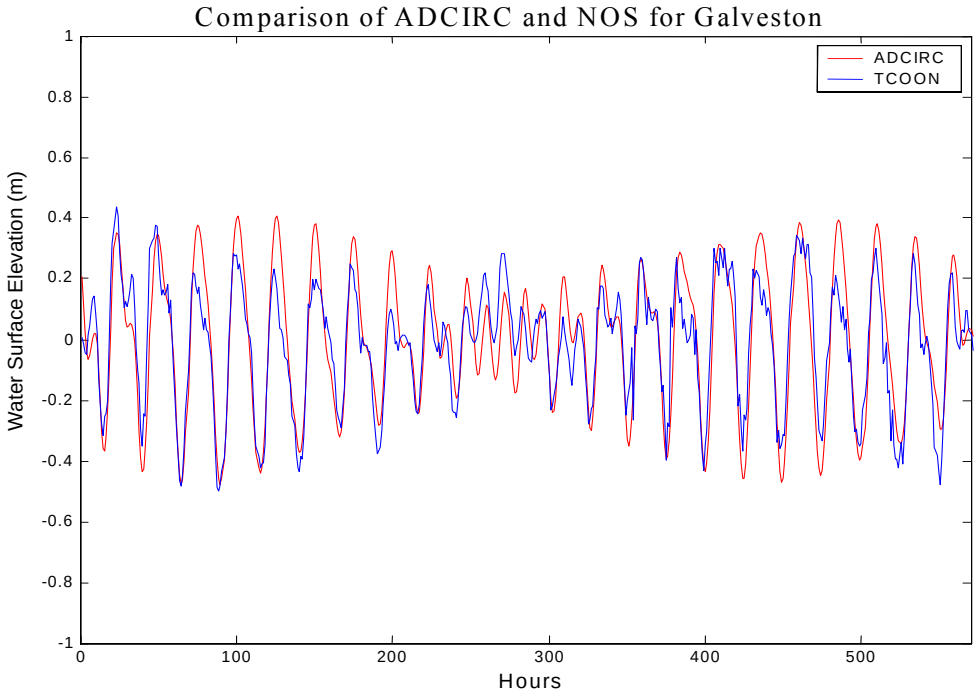

Fig. 5-3: Comparison of tides at Pleasure Pier with NOS gage

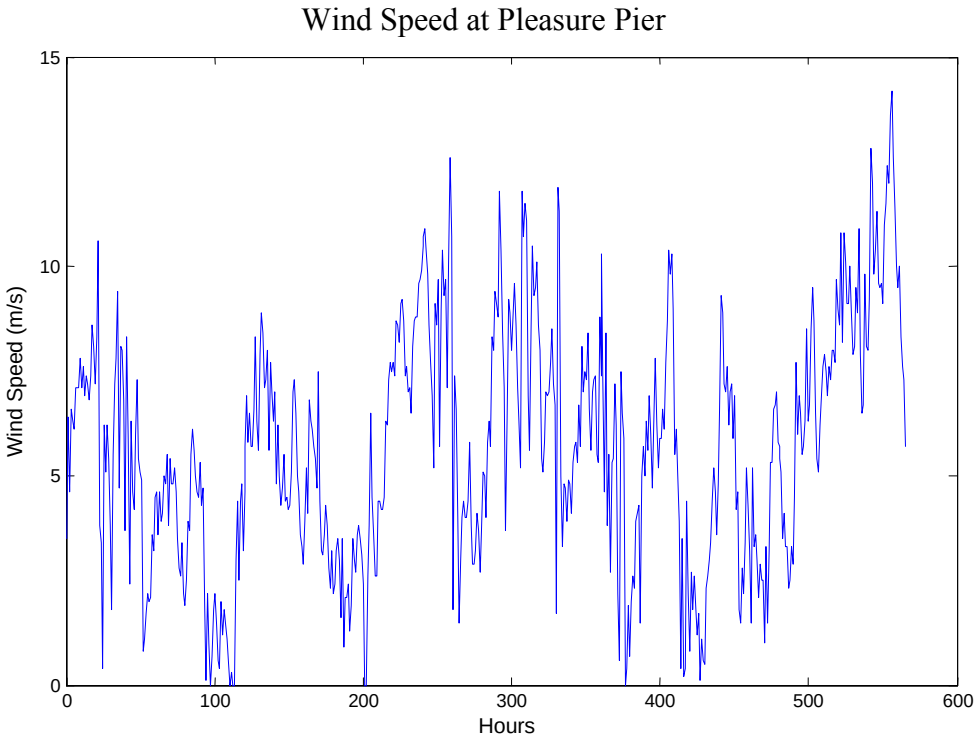

Fig. 5-4: Wind speeds at Pleasure Pier

It was only necessary to show that the model acceptably reproduced water levels for all gauges to demonstrate approximate verification in a more global sense with verification efforts concentrated on the study area. However, in order to demonstrate that the overall verification was acceptable, all model to reconstructed prototype tidal time series are presented in Appendix A. As shown, the comparisons are acceptable and demonstrate that the ADCIRC model is properly reproducing tides throughout the general area of interest as well as in the specific study area.

5.6 Tropical Storm Surge

The PBL model was used during this study and was coupled with ADCIRC in the form of a wind file, which can be input to the ADCIRC model to simulate wind effects of the storms of interest for the study area. Peripheral atmospheric pressures were assumed equal to the standard atmospheric pressure of 1013 millibars (mb) and the geostrophic wind speeds were specified as 6 knots in the same direction as the moving eye of the storm. All additional data were computed from data contained in the National Oceanic and Atmospheric Administration's (NOAA) Hurricane DATabase (HURDAT) of tropical storm events (Jarvinen, Neumann, and Davis 1988). This database is updated yearly and now contains descriptions of all hurricane, tropical storm, and severe tropical depressions that have impacted the east coast of the United States, Gulf of Mexico, and Caribbean Sea from 1886 through 2002. The database contains latitude and longitude locations of the eye of the hurricane with the corresponding central pressure and maximum wind speeds at 6-hour intervals. The recent Hurricane Claudette (July 2003) was simulated by using track data from weather databases, which contain track information: latitude, longitude, time along with minimum pressure and maximum wind.

The goal of this component of the study was to compute frequency-of-occurrence relationships for storm surge plus tide in the Freeport area. In order to develop these relationships, it was necessary to identify tropical storms that have historically impacted the study area. This was accomplished by making use of the tropical storm database (Scheffner, et al, 1994) that was generated through simulation of 134 historically based storm events along the east coast, Gulf of Mexico, and Caribbean Sea. The database uses the HURDAT database described above as input. For 486 discrete locations along the U.S. coast, peak storm surge values corresponding to storm events, which produced a surge of at least 0.305 m, were archived and indexed according to event, location, and surge magnitude. The database was used to select 26 storm events for the present study beginning with the hurricane of 1886 and extending through Hurricane Claudette (2003). These events, shown in Table 5-3, represent the selected historical set of storms. An example plot of the storm track and location every 6 hours of Hurricane Claudette is shown in Fig. 5-5. The track for each storm event of the historical training set is shown in Appendix B.

Table 5-3: Tropical storms set

HURDAT No./Name	Date of Storm	HURDAT No./Name	Date of Storm
1. #5	8/12/1886	14. #602 – Carla	9/3/1961
2. #117	8/27/1900	15. #690 – Celia	7/31/1970
3. #183	7/13/1909	16. #703 – Edith	9/5/1971
4. #211	8/5/1915	17. #704 – Fern	9/3/1971
5. #232	8/1/1918	18. #722 – Delia	9/1/1973
6. #295	6/27/1929	19. #809 – Chris	9/9/1982
7. #310	8/12/1932	20. #812 – Alicia	8/15/1983
8. #324	7/25/1933	21. #841 – Bonnie	6/23/1986
9. #397	8/2/1940	22. #867 – Chantal	7/30/1989
10. #405	9/16/1941	23. #874 – Jerry	10/12/1989
11. #445	8/24/1945	24. #923 – Dean	7/28/1995
12. #565 – Audrey	6/25/1957	25. #965 – Frances	9/8/1998
13. #586 – Debra	7/23/1959	26. #1001 – Allison	6/5/2001
		27. #1016 - Claudette	7/5/2003

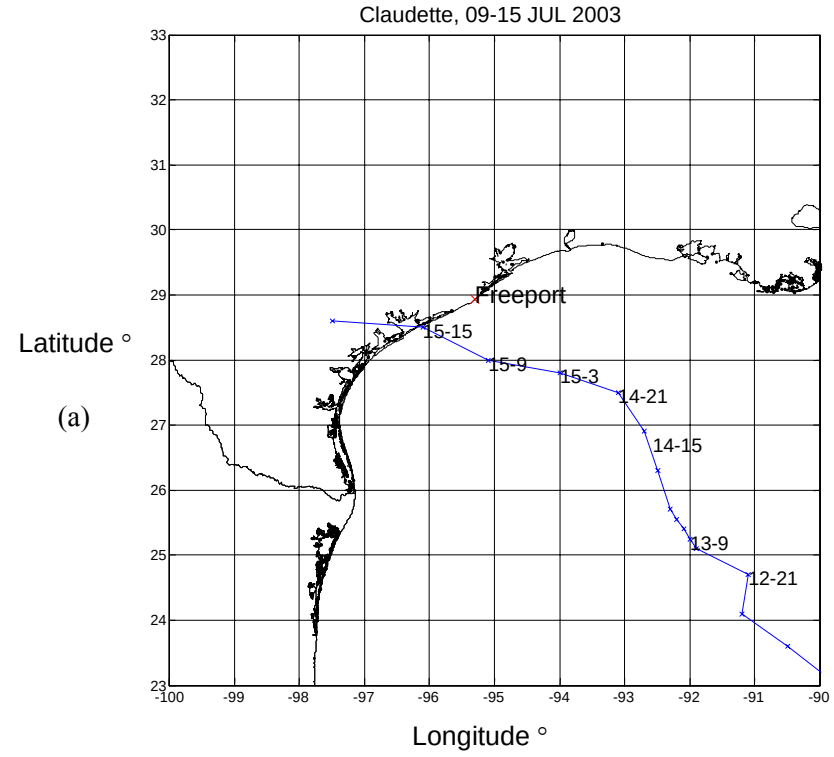

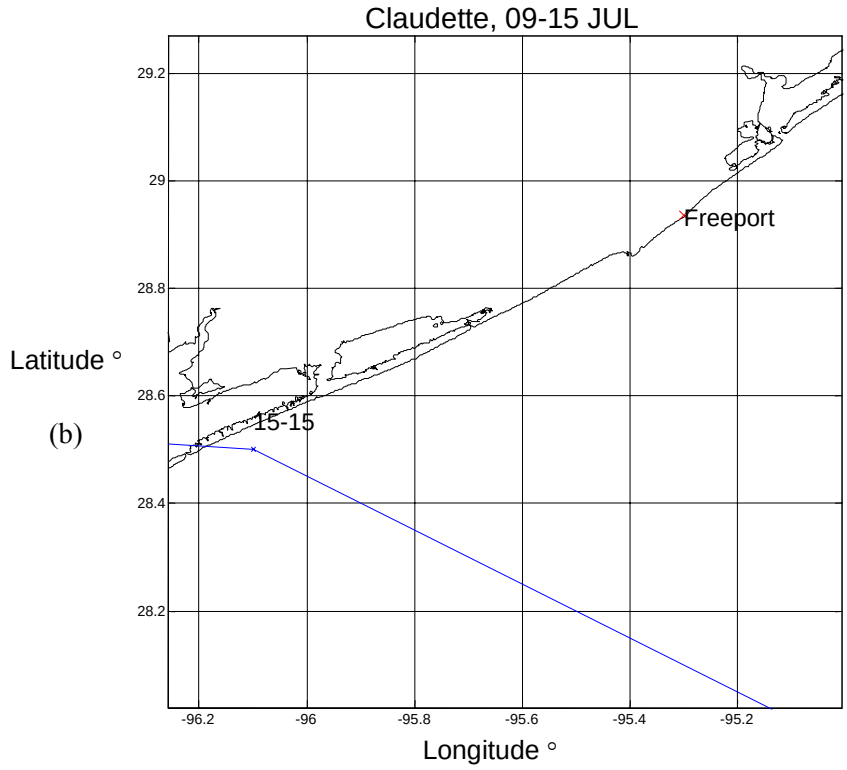

Fig. 5-5: (a) Large and (b) small scale plots of Hurricane Claudette's track

This set of tropical storms is verified by comparing National Ocean Survey (NOS) measured tide gage records taken at Pleasure Pier and Freeport Harbor. These data are ideal for storm event verification effort as it allows calibration of the radius of maximum wind that is an important input to the PBL model to optimize the model for comparison of the set of storms for the area of interest. Due to spin-up time of 10-15 days required for tidal simulations, the decision was taken to compare storm surge elevations without tidal forcing. Therefore, surge only time-series were constructed by removing the astronomical tide from the raw NOS tide gage records, and the ADCIRC surge was computed without tidal forcing. For example, Fig. 5-6 shows a time series of NOS data for Freeport for Hurricane Claudette (2003). As is evident from Fig. 5-6, the storm surge is accurately captured; however, the tides are not accurately simulated due to spin-up time required for tidal simulation in the Gulf. In Fig. 5-7, surge-only data is shown, which is computed by subtracting tides and pre-storm datum from the raw signal.

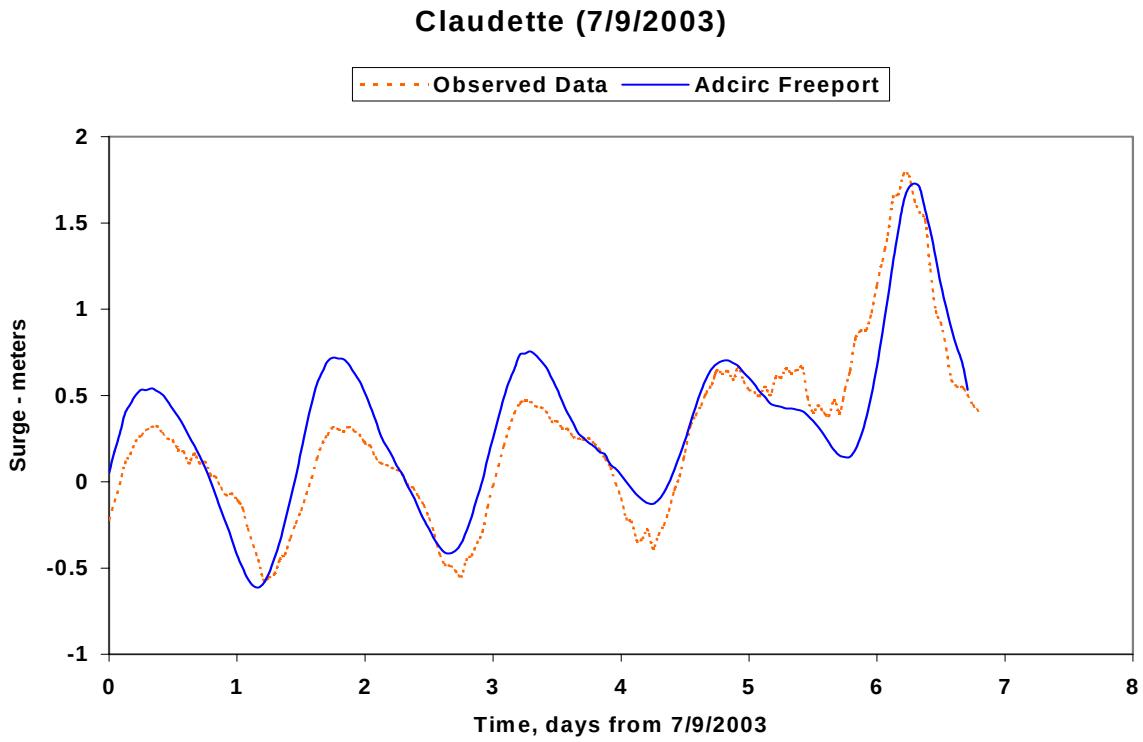

Fig. 5-6: **Raw surface elevation data for Hurricane Claudette at Freeport Harbor**

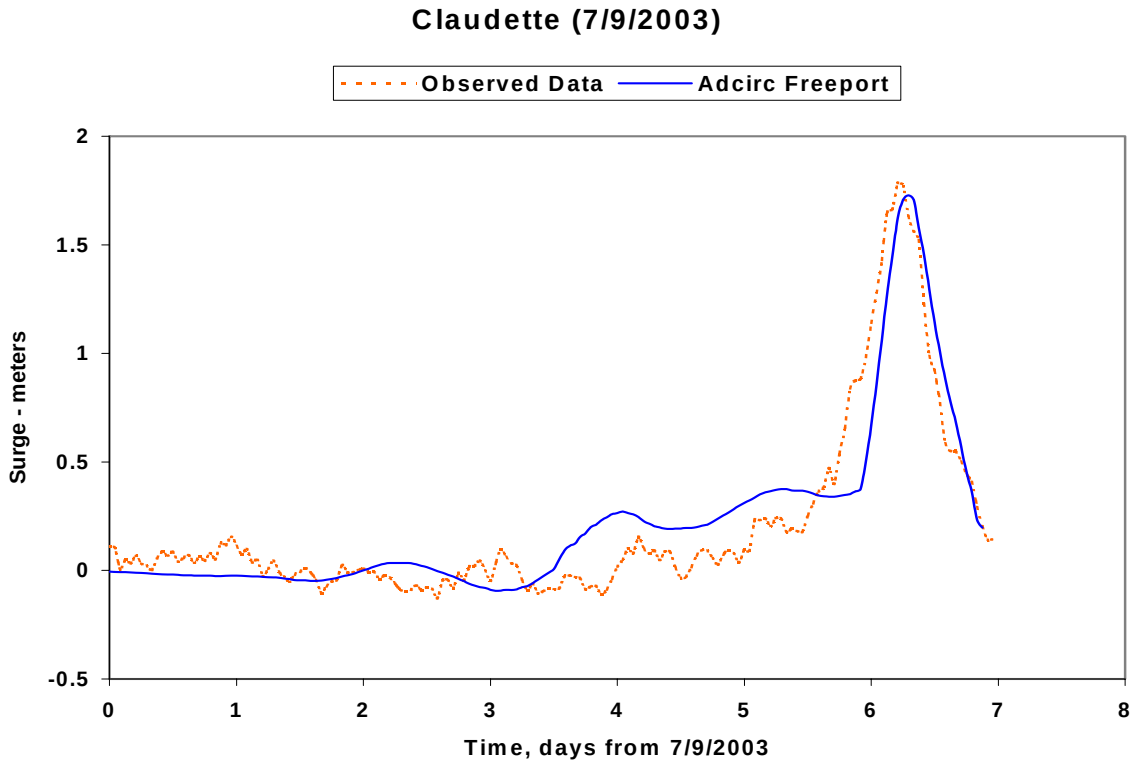

Fig. 5-7: Surge only surface elevation data for Hurricane Claudette

NOS Data are available for Pleasure Pier for the period starting August 1957 through August 2003. Data for Freeport Harbor is available only for the period starting March 1995 through August 2003. The data for Clear Lake is available starting August 1991. This period represents almost a 50-year period and encompasses majority of the storms in the Galveston bay and Freeport.

All storms shown in Table 5-3 were simulated using ADCIRC model without tide. Storm surge peak values for events before August 1957 were compared to anecdotal data from National Hurricane Center's historical archives by removing tides. Storm event simulated hydrographs for events after August 1957 were compared to the NOS hydrographs at Pleasure pier, Freeport Harbor and Clear Lake gage stations. Results and

comparisons of peak surge values in meters relative to mean sea level for each event for which data are available are shown in Table 5-4.

Table 5-4: Comparison of storm surge computations with observed data measured from MSL

Storm No.	Pleasure Pier (m, msl)		Freeport Harbor (m, msl)		Clear Lake shores (m, msl)	
	ADCIRC	NOS	ADCIRC	NOS	ADCIRC	NOS
1. #5	0.796		0.880		1.068	
2. #117	2.141		0.788		1.216	
3. #183	1.493		0.931		1.475	
4. #211	3.059		1.372		3.369	
5. #232	0.780		0.576		0	
6. #295	1.875		0.917		1.123	
7. #310	3.040		0.612		3.9232	
8. #324	0.689		0.687		0.688	
9. #397	0.264		0.270		0.37	
10. #405	2.155		2.159		3.234	
11. #445	1.002		1.351		2.391	
12. #565 – Audrey	0.516		0.449		0.514	
13. #586 – Debra	1.105	0.954	0.562		2.64	
14. #602 – Carla	2.314	2.46	3.295		3.811	
15. #690 – Celia	0.952	0.91	1.525		1.466	
16. #703 – Edith	1.158	1.25	0.927		1.172	
17. #704 – Fern	1.477	1.32	1.446		2.067	
18. #722 – Delia	1.227	1.14	1.227		1.965	
19. #809 – Chris	0.434	0.401	0.409		0.553	

Table 5-4: Continued

Storm No.	Pleasure Pier (m, msl)		Freeport Harbor (m, msl)		Clear Lake shores (m, msl)	
	ADCIRC	NOS	ADCIRC	NOS	ADCIRC	NOS
21. #841 – Bonnie	0.431	0.69	0.327		0.511	
22 #867 - Chantal	0.593	0.682	0.325		0.459	
23. #874 – Jerry	1.39	0.997	0.967		1.869	
24. #923 – Dean	0.859	0.84	0.498		1.177	0.921
25. #965 – Frances	0.791	0.84	0.877	0.865	1.15	1.31
26. #1001 – Allison	0.605	0.792	0.345	0.585	0.81	0.985
27.#1016- Claudette	1.481	1.523	1.707	1.772	1.595	1.563

Fig. 5-8 shows a comparison of simulated-adjusted raw data for Hurricane Carla (1961) for the Freeport Harbor. A comparison of simulated-observed data for Hurricane Alicia (1983) is also provided in Fig. 5-9 for pleasure Pier. Hurricane Alicia represents the most intense storm for which the observed data are available. As shown, the model generated surge matches the observed data very closely with respect to maximum surge as well as shape. The maximum observed surge at Pleasure Pier for Hurricane Alicia was 2.710 m and the maximum surge computed from ADCIRC was 2.334 m, giving an error of approximately 0.14 m. Model generated storm surge hydrographs and comparisons wherever available are included in Appendix B along with hurricane track plots.

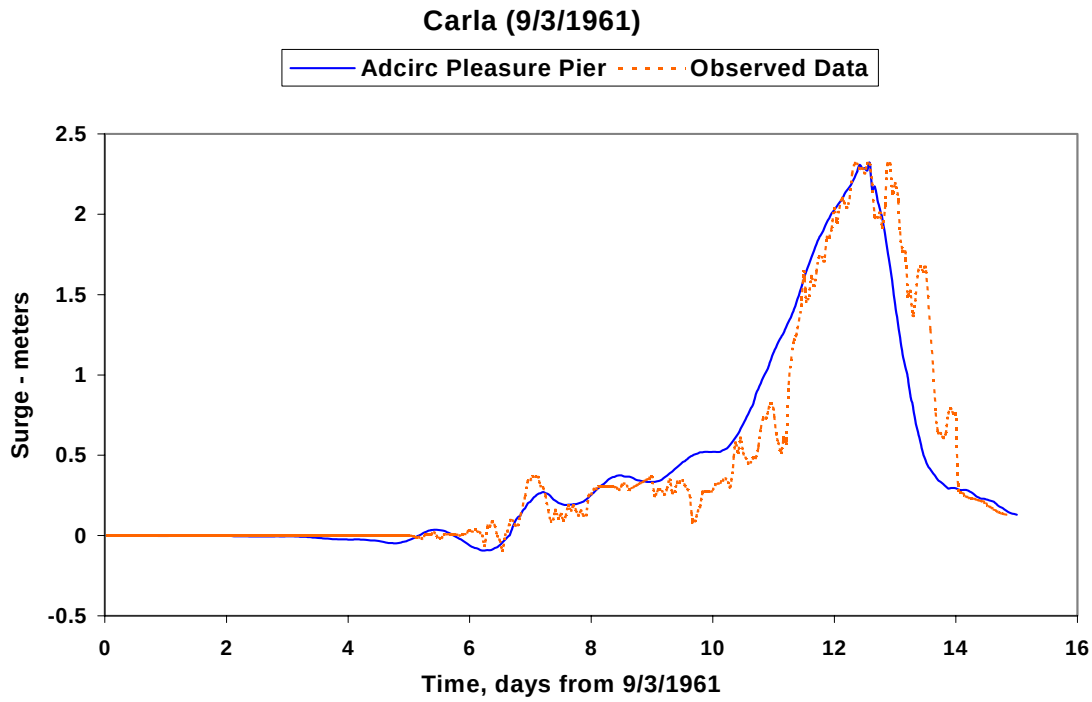

Fig. 5-8: Simulated-observed data for Hurricane Carla (1961) for Pleasure Pier

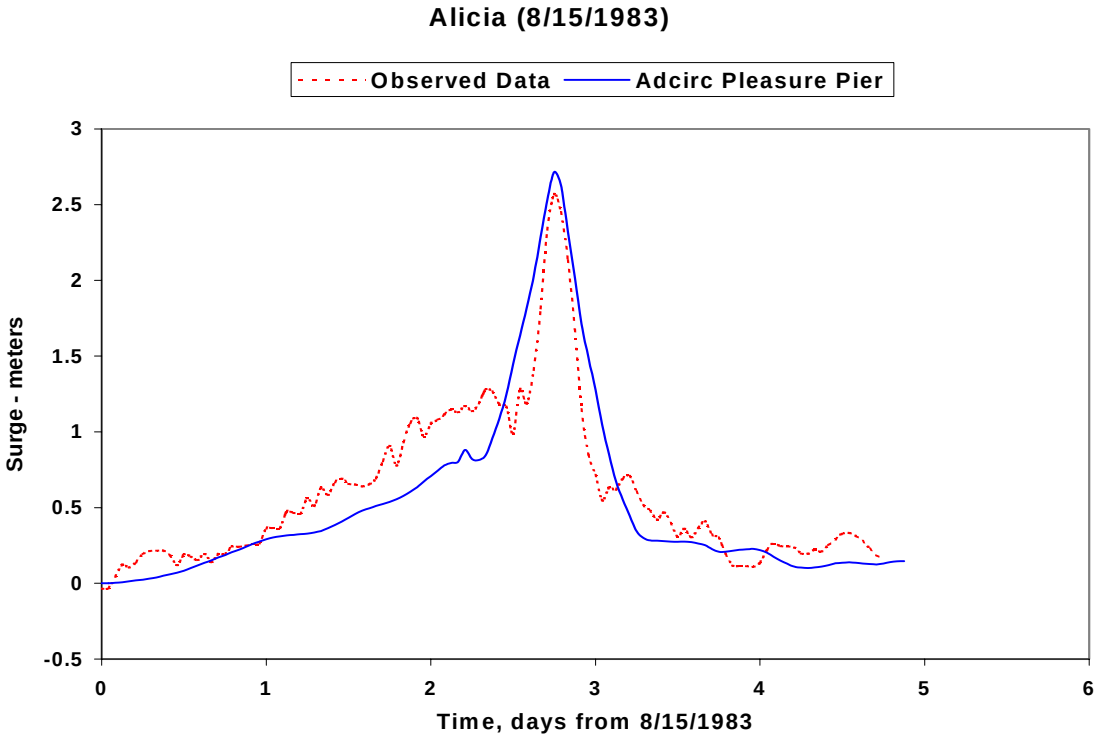

Fig. 5-9: Simulated-observed data for Hurricane Alicia (1983) for Pleasure Pier

A spatial distribution snapshot plot of the maximum surge at the approximate time of peak surge for Hurricane Claudette (2003) along the open coast area of Freeport is shown in Fig. 5-10. Model results agree very well with observed data reported from NOS database where storm surge of 1.3 - 2 meters above normal tides was observed and both the barrier islands were inundated.

Model simulations for tidal elevations are considered to be acceptable for use in the frequency analysis. Additionally, model results compare well to available storm surge data for a variety of storm events and qualitatively compare well to post-storm visual surveys. The conclusion of the tidal and storm surge verification effort is that the model reasonably reproduces known historical events such as tide and tropical storms.

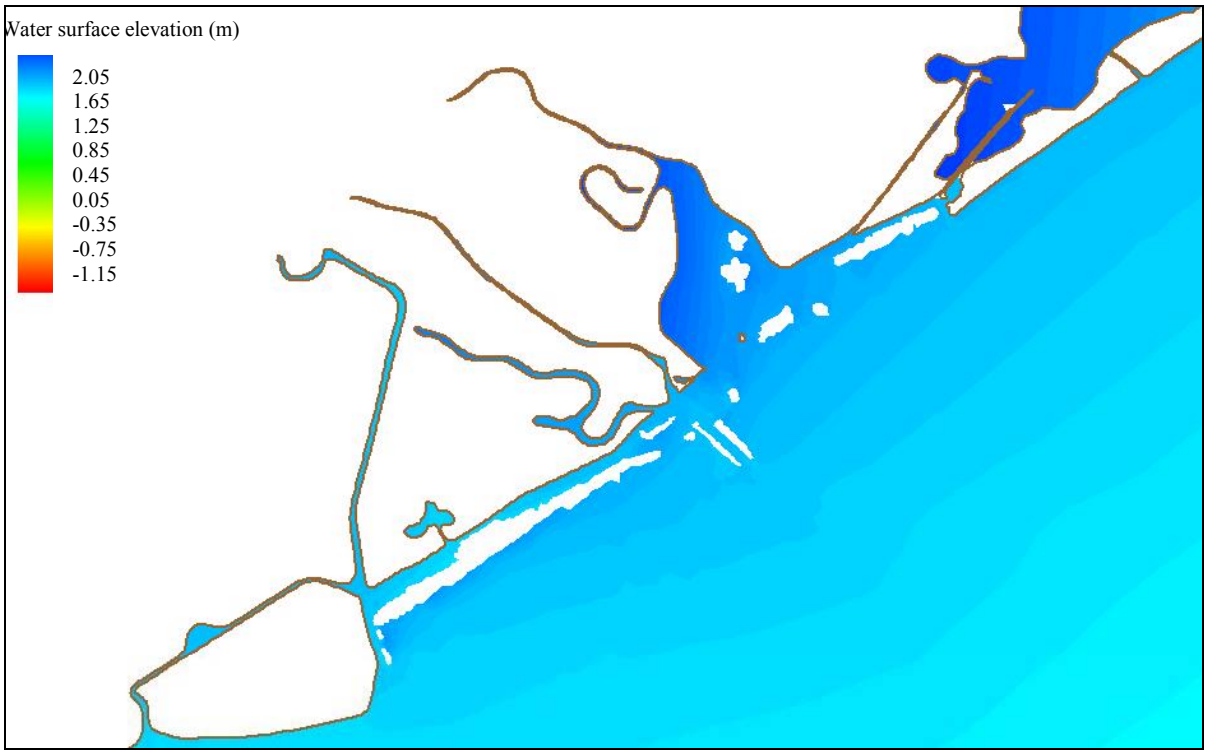

Fig. 5-10: Maximum surge at the approximate time of peak surge for Hurricane Claudette along the area of Freeport coast

Although this study is based on a historical storm set, it is important to consider not only historical storm events but also potential storm events that could reasonably be expected to occur. For example it is reasonable to assume that the storm could easily have tracked within ± one degree of the actual track. Therefore, in order to insure that the most severe events have been included for the area of interest, simulations include hypothetical events that could occur. For example, the tracks of the most intense events in the historical storm events are shifted along the coast such that all maximum storm surge events that could occur are taken into consideration. Two events were defined as perturbations for each of HURDAT storms 117 (August 1900), 211 (August 1915), 310 (August 1932), Carla (September 1961) and Alicia (August 1983) to augment the historical storm set. Each perturbation is represented by a shift of the storm track reported in HURDAT database as indicated in Table 5-5. These events have been shown to be among the most severe storms to have impacted the study area between 1886 and 2003. Use of these 10 hypothetical events increases the total to 37 storms that are used as a "training set" for the study. Thus the training set is comprised of 27 historical storm events plus the 10 perturbations.

Table 5-5: Hypothetical storm events

Storm Event	Perturbation shift in degrees longitude
#117 August 1900 - 2 events	+/- 1.0 degree longitude
#211 August 1915 - 2 events	+/- 1.0 degree longitude
#310 August 1932 - 2 events	+/- 1.0 degree longitude
Carla September 1961 - 2 events	+/- 1.0 degree longitude
Alicia August 1983 - 2 events	+/- 1.0 degree longitude

5.7 Application of EST

In order to establish the training set of storms 27 historical events and 10 storm perturbations were used to produce a total of 37 events. Each of the 37 storms was simulated without tide to produce a set of surge-only responses at the stations. The storms are then assumed to have taken place at different phases of the astronomical tides: 1) high tide, 2) mean (MSL = 0.0) tide, and 3) low tide. It is further assumed that the storm could occur during the lunar cycles of: 1) spring tide, 2) between spring and neap, and 3) neap tide. Input vectors representing these phases of the tide are described above. This combination of tide and lunar cycle produces 9 surface elevations for each of the 27 storm events of Table 5-3 and 10 hypothetical storm events at the station locations shown in

Fig. 5-11. This procedure produces a total input/response vector training set of 333 (37*9), tide plus surge events for each station location. It is also considered that the mid-tide level would have twice the probability of occurrence on the MHHW or the MLLW. Similarly the mean tidal range would have twice the probability of occurrence as spring or neap tide.

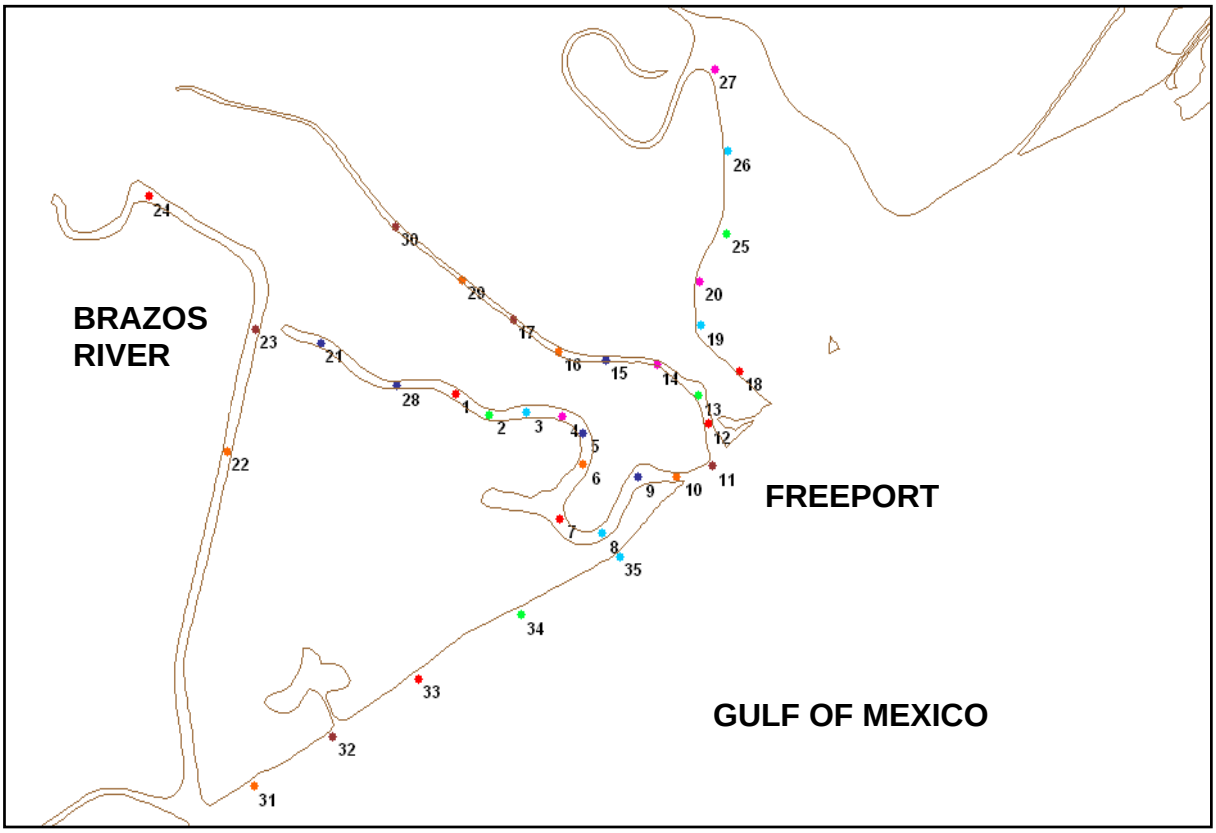

Fig. 5-11: Location of points used for input to EST model

The water surface elevation that is one of the response vectors for the EST analysis was calculated as follows. Analysis of tidal values for the tides at Freeport harbor show that the approximate peak tidal elevation at spring, mid, and neap cycle is 0.35, 0.268, and 0.20 m. The four primary model-generated diurnal and semi-diurnal tidal constituents for the Freeport Harbor study area are the K_1, O_1, M_2, and S_2 with the amplitudes of 0.137, 0.125, 0.07, and 0.02 m respectively. The values of spring and neap tides are calculated using these constituents as follows assuming that most of the tidal energy is contained in these constituents, using the relationship:

spring high tide = $K_1 + O_1 + M_2 + S_2$

mid spring/neap high tide = $K_1 + O_1$

neap high tide = $K_1 - O_1 + M_2 + S_2$

This relationship generates an acceptable approximation of 0.352, 0.261, and 0.191 m versus 0.35, 0.268, and 0.2 m for the 9 combinations, as explained earlier, of astronomical and lunar tidal effects. Therefore this relationship was used for all locations. Similar steps are used for Galveston Pleasure Pier and Clear Lake locations.

The model simulations are used to generate a database of historical and historically based storm events for use in generating maximum surface elevation frequency-of-occurrence relationships at the sites as shown in Fig. 5-11. The statistical approach used to generate multiple life-cycle simulations of storm-activity for the study area and the subsequent post-processing of results to generate surge versus frequency-of-occurrence relationships is described here.

An example set of 500 frequency relationships and the mean value for the Freeport Harbor are shown in Fig. 5-12. Fig. 5-13 shows the mean value with the +/- one standard deviation error bounds. The extreme event storm surge for locations around the Freeport levee for 200, 100 and 50-year storms are shown in Fig. 5-14 through 5-16. The storm surge frequency-of-occurrence tables for all the 35 locations are provided in Appendix C.

Surge elevations are affected by many variables such as offshore bathymetry, storm/shoreline orientation, location with respect to the Gulf of Mexico, and the local topography. Therefore, the frequency-indexed surge distribution varies from one end of the study area to the other.

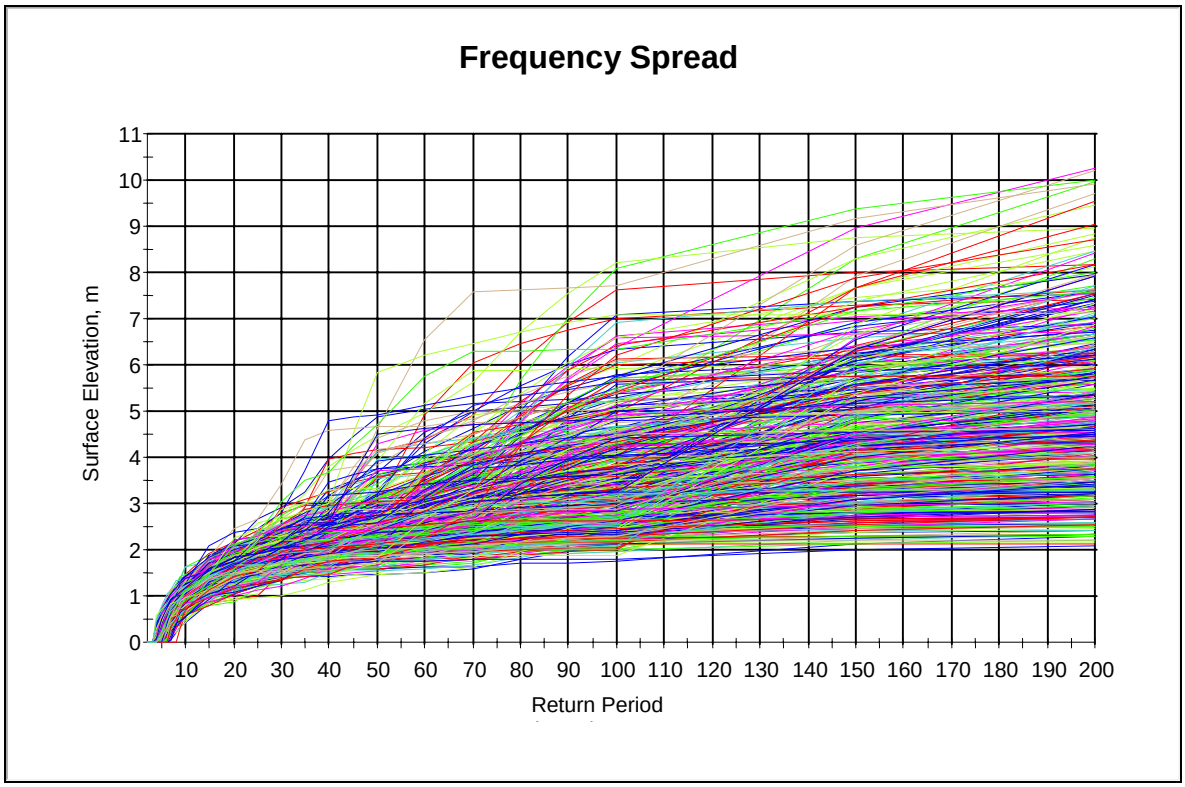

Fig. 5-12: Frequency relationship for the Freeport Harbor for 500 simulations of 200 years

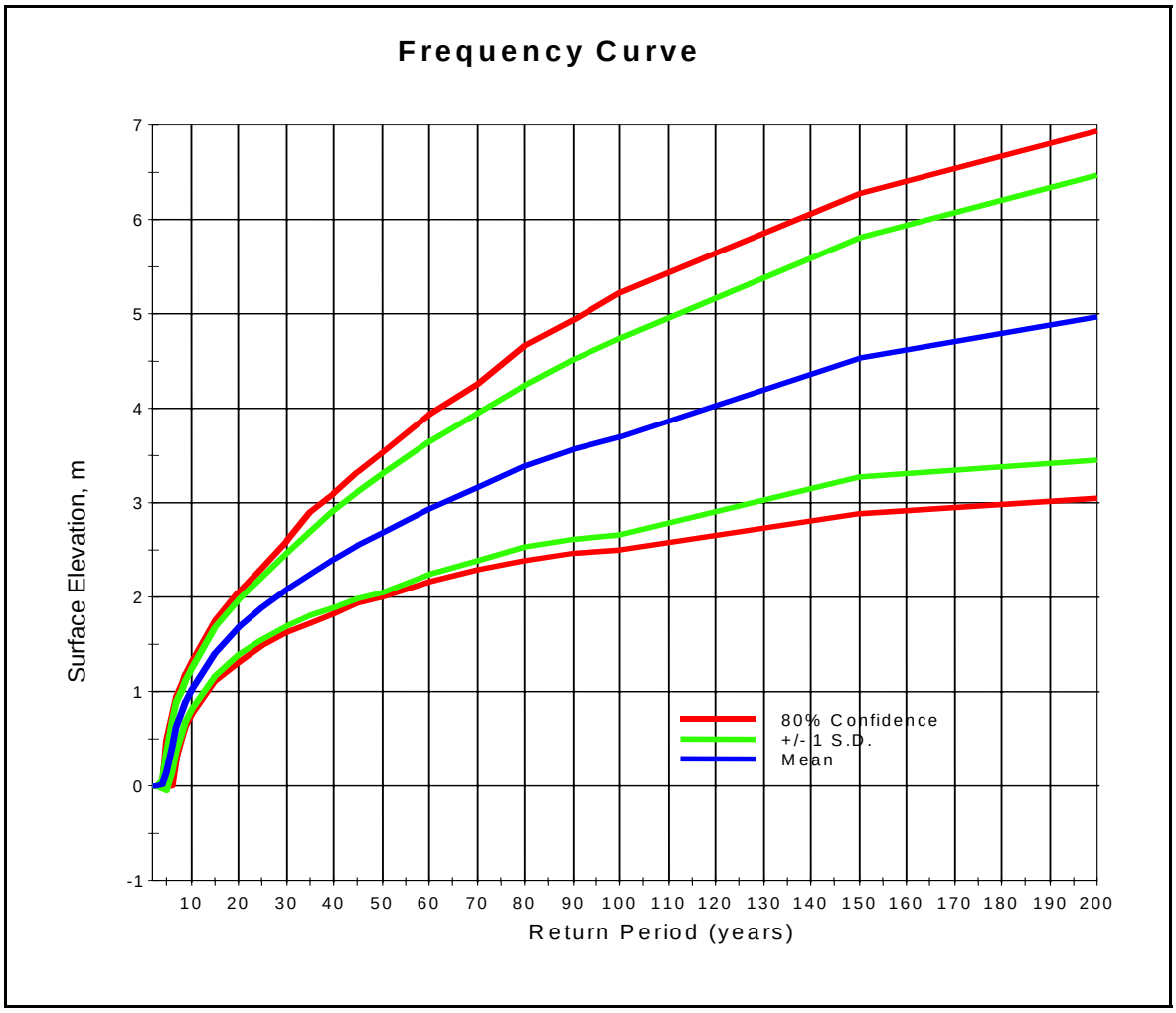

Fig. 5-13: Mean Value of surface elevation with standard deviation bounds for Freeport Harbor

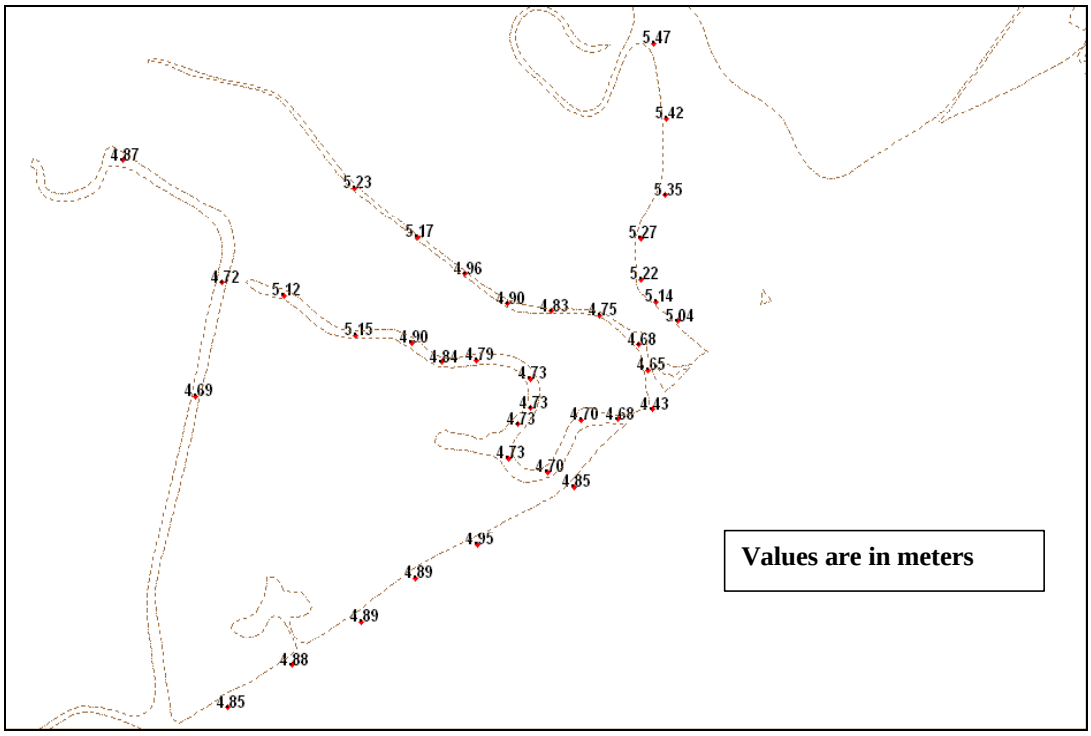

Fig. 5-14: 200 year storm surge values around the Freeport Levee System

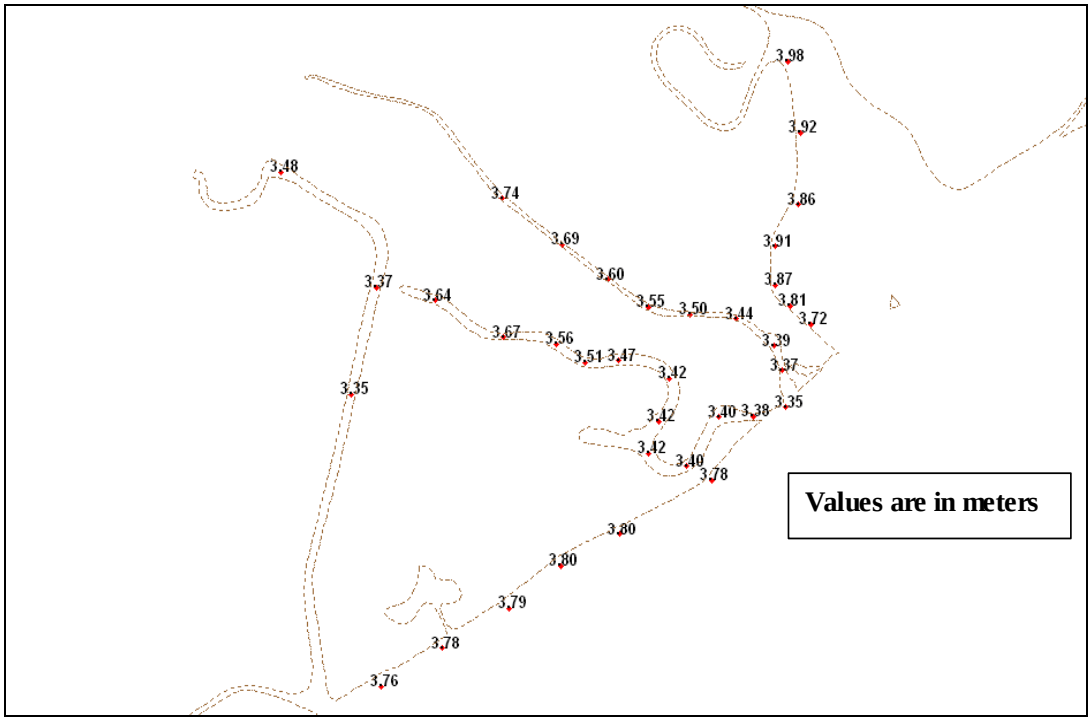

Fig. 5-15: 100 year storm surge values around the Freeport Levee System

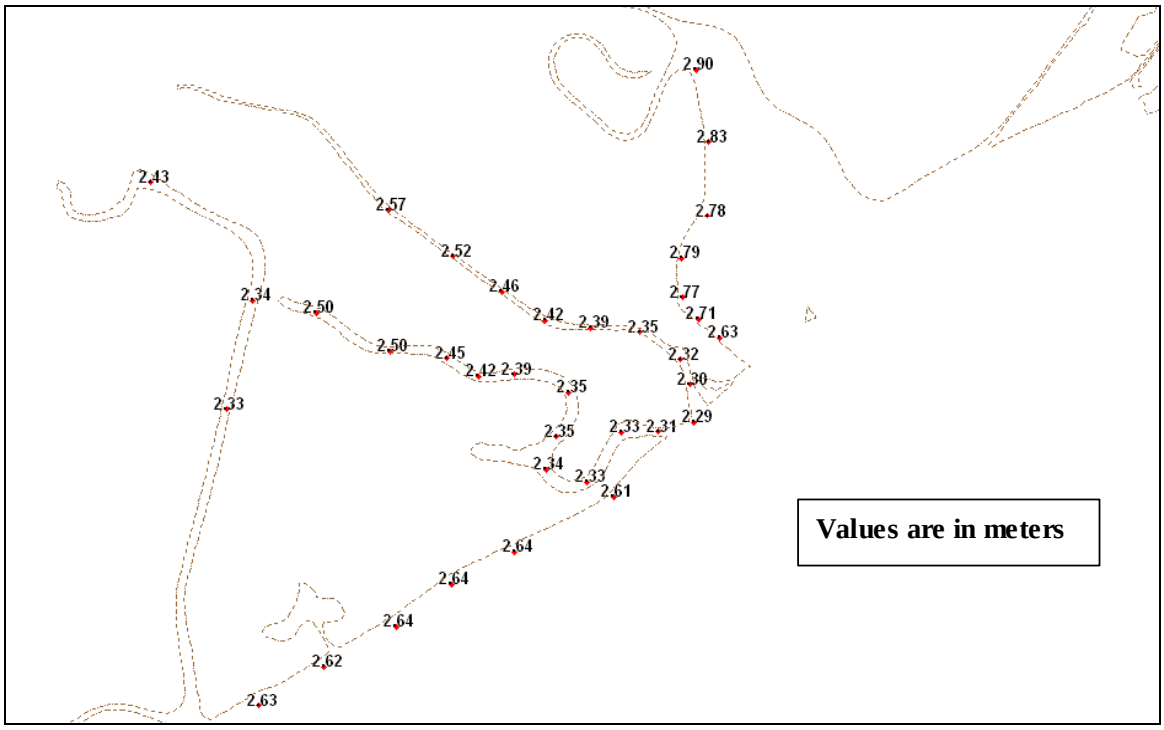

Fig. 5-16: 50-year storm surge values around the Freeport Levee System

The ADCIRC-EST approach can thus be used to estimate and predict life cycle storm surge values at any given site as shown above. These values can hence be used for design purposes or for evacuation and planning purposes. The model SLOSH is currently used by federal authorities in the United States for hurricane evacuation and planning. The next section presents a comparison between this approach and the SLOSH approach.

6 COMPARISON WITH SLOSH

The SLOSH numerical model is used to prepare an atlas of pre-computed surges. On-site computations with several tracks, tropical cyclone intensities and sizes may require many computer runs. During a real time situation this can overload computer facilities and personnel, and require unacceptably time consuming analysis of the output.

To generate a database of pre-computed atlases of storm surges for a particular basin with inland water bodies and complicated terrain features, recourse is made to a tropical cyclone climatology, which gives a broad view of the tropical cyclone types likely to affect a given region. Historical tropical cyclones affecting a region are stratified into preferred track directions, intensities, and sizes. Such families of equally spaced, parallel tracks for surge computations gently curve to reflect climatological data, but should all correspond in the vicinity of the landfall points.

6.1 Methodology of Storm Atlas

The family of tracks account for alternate landfall points for a given direction along a coastal area of interest (or else alternate distances from the coast for alongshore moving tropical cyclones). It is recognized that the generated surge normally is strongly dependent on the angle the track makes with the coast, several hours before and after landfall. Thus, the remaining track segments affect the surge only mildly. Thus, although the location of a tropical cyclone far out to sea and its landfall point may be significantly in error, the family, or families, representing the broad approach to land can be used to estimate the likely surge consequences.

For simplification, it is assumed that the cyclone translation speed, central pressure and size remain constant along the track. Alternate values of these parameters

can be used for each track family to provide a more comprehensive database. The embedded, identical tropical cyclone model in each family of tracks also can be designed to alter the tropical-cyclone central pressure and size with time after landfall to represent any explosive filling and core changes of the tropical cyclone.

After a study of potential surges with idealized tracks from the atlas, runs are then made to fine tune a surge forecast that includes relevant details from the actual cyclone.

6.2 Maximum Envelope of Waters (MEOW)

An atlas of pre-computed surges can be a bulky document and collating the several possible tropical cyclone conditions from the many into a composite potential of surges is a demanding chore. Since each computer run gives an envelope of highest waters in a basin for the life history of a tropical cyclone, it is a simple computer chore to determine the highest possible surge at all vulnerable coastal locations from a particular family of tracks. The resulting map is called a Maximum Envelope of Waters, or MEOW.

Model runs are made using hypothetical tropical cyclones stratified by the Saffir/Simpson scale of intensity categories and sizes. To generate the MEOW, the maximum surge value from the entire family of cyclones at each grid square of a basin is saved; regardless of which cyclone was responsible. The resulting composite of peak surges makes up a MEOW such as that shown in Fig. 6-1. Other MEOWs can be developed for a range of cyclone profiles and conditions. This provides an easily accessible summary of the "worst case" surge scenario given the uncertainty in the current forecast situation.

6.3 Storm Atlas for Harris/ Brazoria County

The model SLOSH was run for imaginary storms with varying intensities (category 1–5) and the effect of storm making landfall at a relative distance from Galveston channel was studied. These results were produced in the form of Maximum Storm Surge Penetration Maps in the Storm Atlas (College of Architecture 1994).

There are five MEOWs, which indicate the worst case MEOWs (or MOMS, Maximum of MEOWs) for each category of hurricane making landfall from 87 nautical miles right to 70 nautical miles left of Galveston channel. For each of these landfall areas, a high and a low MEOW were produced.

The high (maximum) is produced by taking all of the various MEOW movement directions and forward movement speeds and using the high surge elevations. The low (minimum) is produced by using the lowest surge elevations. As will be noticed, the differences between high (maximum) and low (minimum) surge estimates for the same category of hurricane are quite extreme. This illustrates the extreme range of possibilities in modeling with SLOSH as only hypothetical events are used.

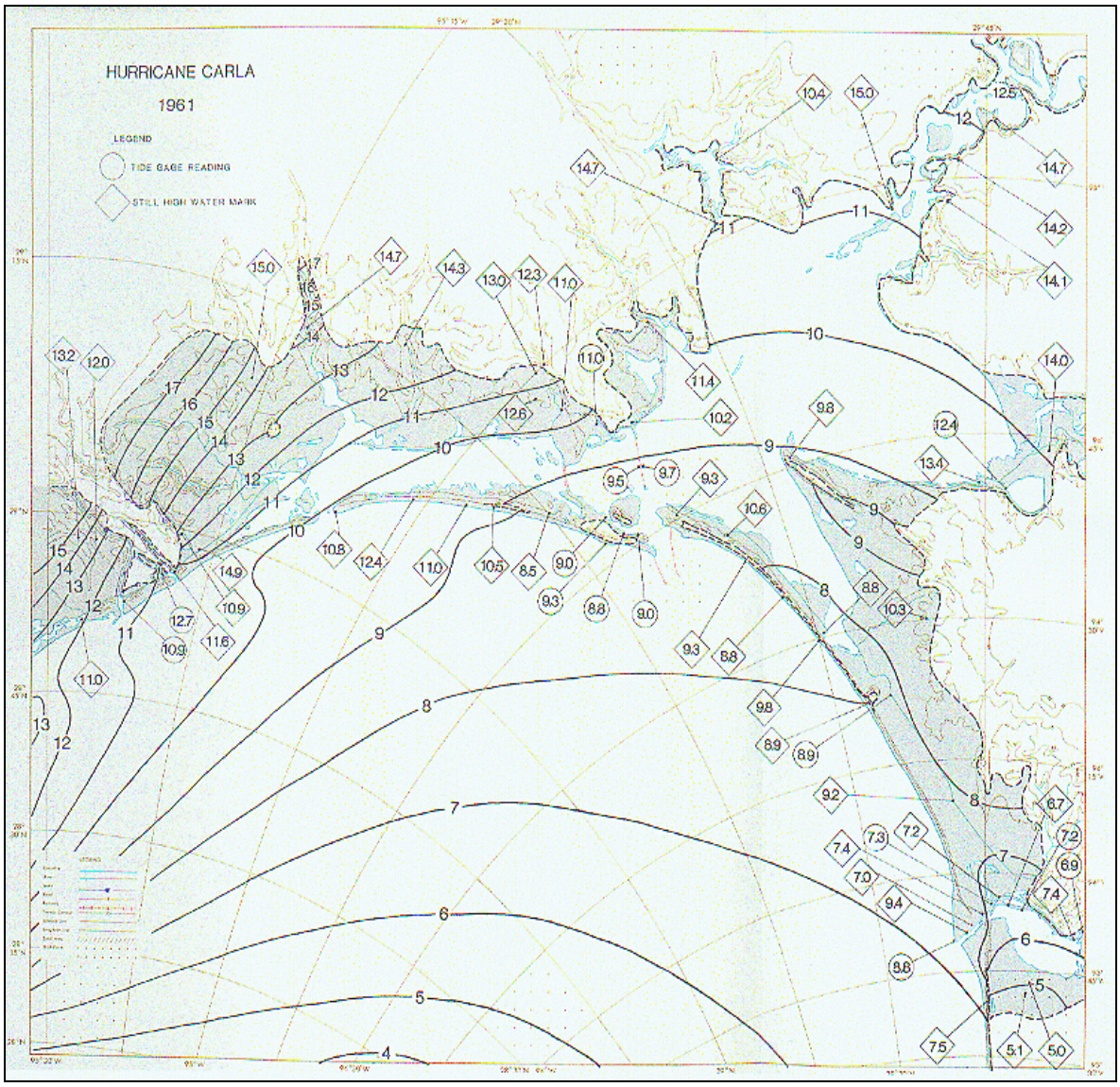

Fig. 6-1: MEOW for Hurricane Carla (1961) for Galveston Bay (units of elevation are in feet (Jelesnianski et al, 1992))

6.4 Comparison with ADCIRC

For comparison of ADCIRC simulated storm surge with SLOSH predicted surges, the hurricanes used in the study were arranged according to the approach used in the storm atlas that is on the basis of the Saffir-Simpson scale category and the distance from Galveston ship channel as shown in Table 6-1.

Table 6-1: Characteristics of hurricane database used in the study

Storm No.	Pressure (mb)	Distance from Galveston channel (n-miles)	Max Wind (knots)	Category	Radius Max Wind (nm)
5	984	131.698	85	2	21.28
117	964	17.921	115	4	41.37
117(+1.0)	964	56.765	115	4	41.37
117(-1.0)	964	42.596	115	4	50.83
183	986	43.156	120	4	31.91
211	953	35.912	125	4	50.83
211(+1.0)	953	86.889	125	4	17.73
211(-1.0)	953	14.758	125	4	50.83
232	980	115.608	90	2	50.83
295	988	56.221	75	1	40.19
310	955	19.599	125	4	31.91
310(+1.0)	942	80.955	125	4	41.37
310(-1.0)	942	40.514	125	4	41.37
324	981	352.513	80	1	44.92
397	973	106.709	70	1	34.28
405	977	86.896	80	1	50.83

Table 6-1: Continued

Storm No.	Pressure (mb)	Distance from Galveston channel (n-miles)	Max Wind (knots)	Category	Radius Max Wind (nm)
445	987	126.904	120	4	50.83
565 – Audrey	972	88.699	125	4	50.83
586 – Debra	989	34.993	75	1	50.83
602 – Carla	931	171.81	145	5	49.82
602 – Carla(+1.0)	931	246.148	145	5	49.82
602 – Carla(-1.0)	931	97.423	145	5	49.82
690 – Celia	950	232.38	110	3	29.55
703 – Edith	978	249.656	140	5	28.37
704 – Fern	979	139.846	80	1	43.73
722 – Delia	987	56.211	60	1	50.83
809 – Chris	994	77.112	55	1	37.82
812 – Alicia	963	38.474	100	3	22.46
812 – Alicia(+1.0)	963	107.395	100	3	22.46
812 – Alicia(-1.0)	963	7.211	100	3	37.82
841 – Bonnie	992	53.89	75	1	18.91
867 – Chantal	984	34.603	70	1	26
874 – Jerry	983	26.869	65	1	20.09
923 – Dean	999	42.472	40	1	50.83
965 – Frances	990	195.874	55	1	50.83
1001 – Allison	1003	40.109	45	1	50.83
1016 - Claudette	983	127.365	75	1	41.37

MEOW charts from the storm atlas are read and the corresponding maximum and minimum values for a storm are read based on its distance from the Galveston ship channel and its category. These values are then plotted along with ADCIRC simulated

value in the return period frequency charts. The ADCIRC simulated surge values for different hurricanes are plotted on the frequency curve and the SLOSH maximum/minimum surge values corresponding to that category of hurricane and its distance from Galveston ship channel are plotted along with it. The ADCIRC value corresponds to '+' marker, whereas the values from SLOSH are represented by 'x' marker. The comparison was made for three different locations, Pleasure Pier in Galveston Island, Freeport harbor and Clear Lake and is shown in Fig. 6-2, 6-3 and 6-4.

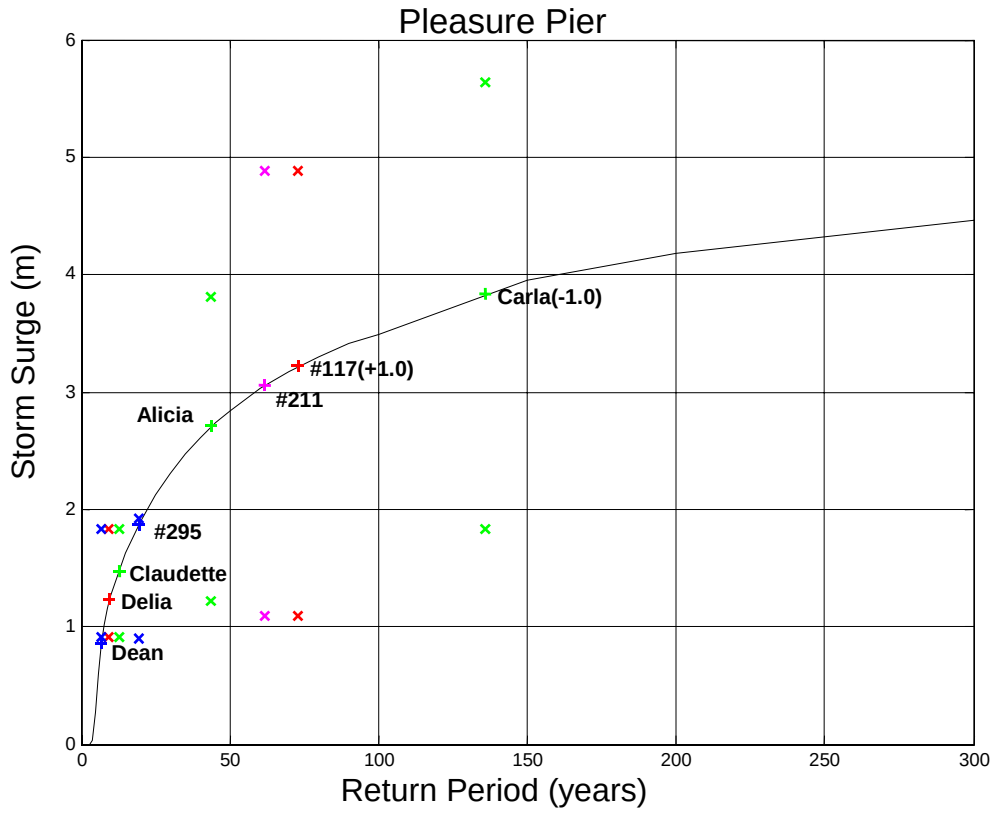

Fig. 6-2: Comparison of ADCIRC/EST and SLOSH generated surge values for Pleasure Pier

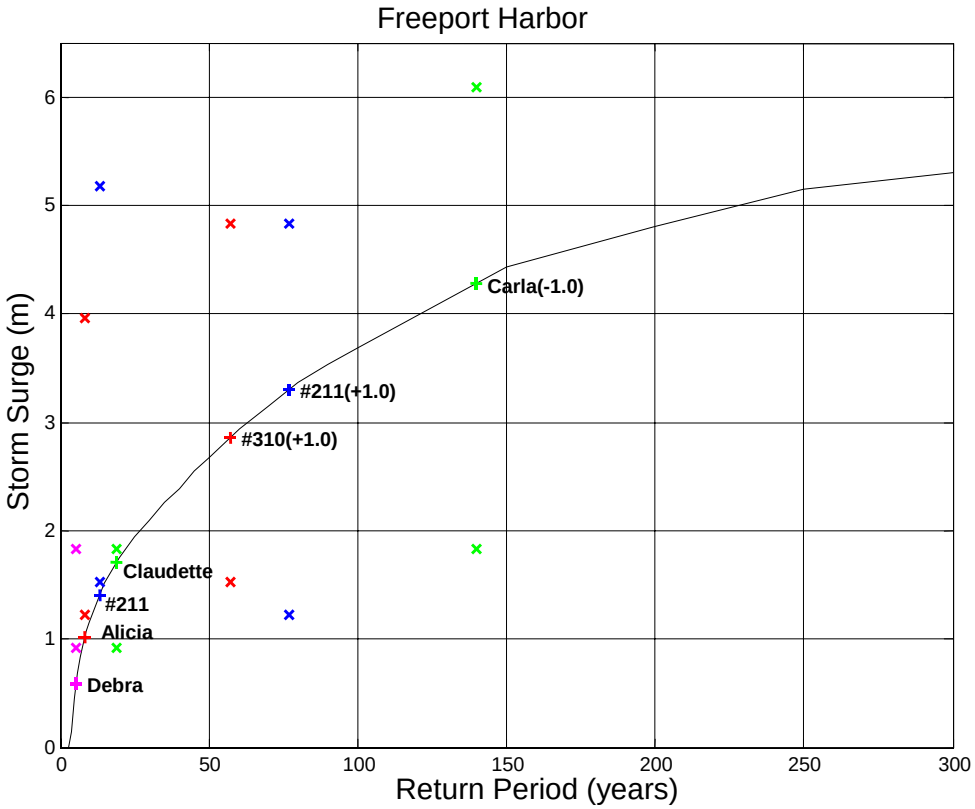

Fig. 6-3: Comparison of ADCIRC/EST and SLOSH generated surge values for Freeport Harbor

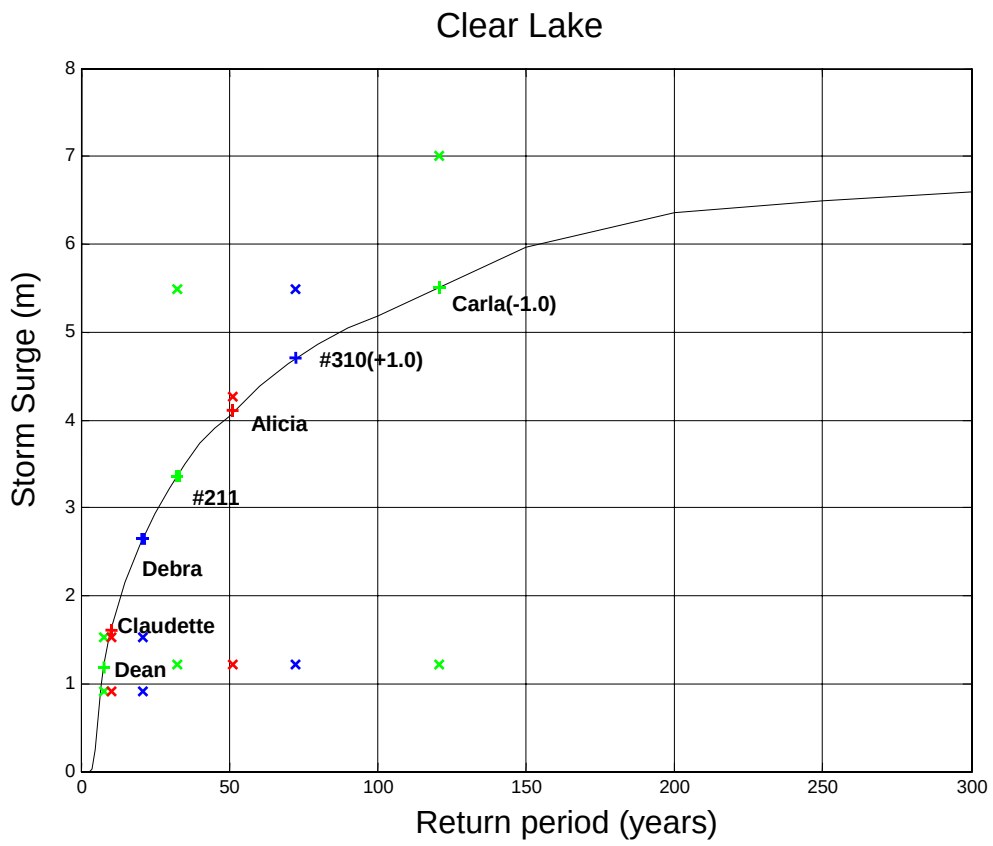

Fig. 6-4: Comparison of ADCIRC/EST and SLOSH generated surge values for Clear Lake

As evident from the Figs, there is a large amount of scatter in the case of SLOSH values, especially in the case for Freeport harbor. This may be because the SLOSH runs with simulated hurricanes whose distances were measured from Galveston ship channel. The distance between Freeport Harbor and the ship channel being 80 miles, the SLOSH analysis is not accurate for Freeport area. In the case of storm surge at Freeport due to Hurricane Alicia (1983), SLOSH estimates that a hurricane of its intensity and at a distance of 38.45 n-miles from Galveston ship channel should produce a maximum surge of 3.96 m and a minimum surge of 1.2192 m. However, the ADCIRC generated surge due to Alicia was 1.023 m. The anecdotal surge due to Alicia (Garcia and Flor, 1984) was reported to be around 1 m. Thus SLOSH over-estimates the surge in this case. This is due

to the fact that Alicia made landfall around 50 miles to the right of Freeport looking landward. In the northern hemisphere due to rotation of earth, the effect of storm surge is more pronounced on the right side of hurricane center rather than left side. This effect is not taken into account in the approach used for producing the storm atlas using SLOSH. Hence the storm surge values from the storm atlas are accurate only for centrally located regions in the SLOSH grid. Also this approach assumes that all the storms of same category making landfall within the distance of 46 n-miles right to 23 n-miles left of a location will produce the same surge. This may be true for some ideal cases but imagine an intense hurricane of category 5 having Rmax (Radius of maximum winds) of 29 n-miles making landfall 10 miles right of the central location. In this case areas 35-52 n-miles from the central location will experience high values of surge of the order of 3-4 meters but the areas on the left hand side of landfall location will experience much less storm surge, assuming the bathymetry around the area is similar.

Some of the problems associated with SLOSH are thus identified as follows:

1. Although storm-induced flooding along the coast of the United States can be predicted fairly accurately using SLOSH, storm surges in bays and estuaries are often poorly predicted using this method because of irregular coastline and local topography.

2. The simplification used for preparing of these atlases is that the cyclone translation speed, central pressure and size remain constant along the track. This assumption is generally not true. For example the hurricane of 1915 (7/13/1915) had its maximum winds (120 knots) at a distance of approximately 120 miles from its landfall and had winds of much lower value (85 knots) at landfall. Thus the assumption of constant size of storm and constant winds results in over-estimation of surges.

3. For the same landfall location and category storms, the storm atlas gives the same results. It is accepted that the peak surge on the open coast is not always monotonically related to the parameter, maximum wind speed of the storm. In fact, the peak surge may increase or decrease according to the manner in which the other storm parameters are affected by the change in maximum wind speed. The pressure drop, size scale and shape of the wind profile also have an effect on the peak surge. For example Hurricane Camille (1969) that was an ordinarily sized storm though it was a category five storm and resulted in storm surge of 6 meters in Gulfport, Mississippi. However, SLOSH gives prominence to maximum wind speeds during analysis.

4. The SLOSH model's polar grid as shown in Fig. 3-2 is generally very coarse compared to the ADCIRC grid. For the study area Freeport, a high-resolution grid was needed to effectively calculate storm surges all along the existing levee system. The SLOSH grid covers the whole Freeport area in just 24 squares.

5. Since we do not completely understand the processes of hurricane formation and hence cannot model these accurately, using empirical relations to simulate them is a wrong approach. Thus the approach of using historical storms to generate database of storm surge and then using a return period concept to calculate maximum storm surges may be more reliable instead of just simulating different storms, where not all the storms have similar features. Using the same coefficients for all these different storms also is not advisable.

6. Risk assessment by definition necessitates a probabilistic approach whereas SLOSH uses an event-driven approach.

The SLOSH model results are taken manually from the contour plots provided in the Storm Atlas. Due to difficulties reading the SLOSH values from the contour plots, the

values in the table should only be considered approximate (+/- 0.5 feet) and only used for a broad and general comparison.

6.5 Alternate Approach

The database consisting of 37 storms, which is extended to 333 storms with addition of neap, spring tides, high and low tides, is used for this EST analysis. Two different type of analysis were done. In one case the pressure difference between the eye of the hurricane and ambient is used as a response vector with all other input vectors remaining the same as in storm surge analysis with addition of storm surge associated with that hurricane as an input vector. The other case is repeated with maximum wind speed being used as a response vector. The lower bands of pressure difference values and maximum wind speeds for different categories of hurricanes, based on Saffir Simpson scale are read from Table 6-2. These two plots are shown in Fig. 6-5 and Fig. 6-6.

Table 6-2: Saffir Simpson scale

Category	Pressure Difference (mb)	Maximum Wind Speed (knots)
1	33	64
2	33	83
3	48	96
4	68	114
5	93	135

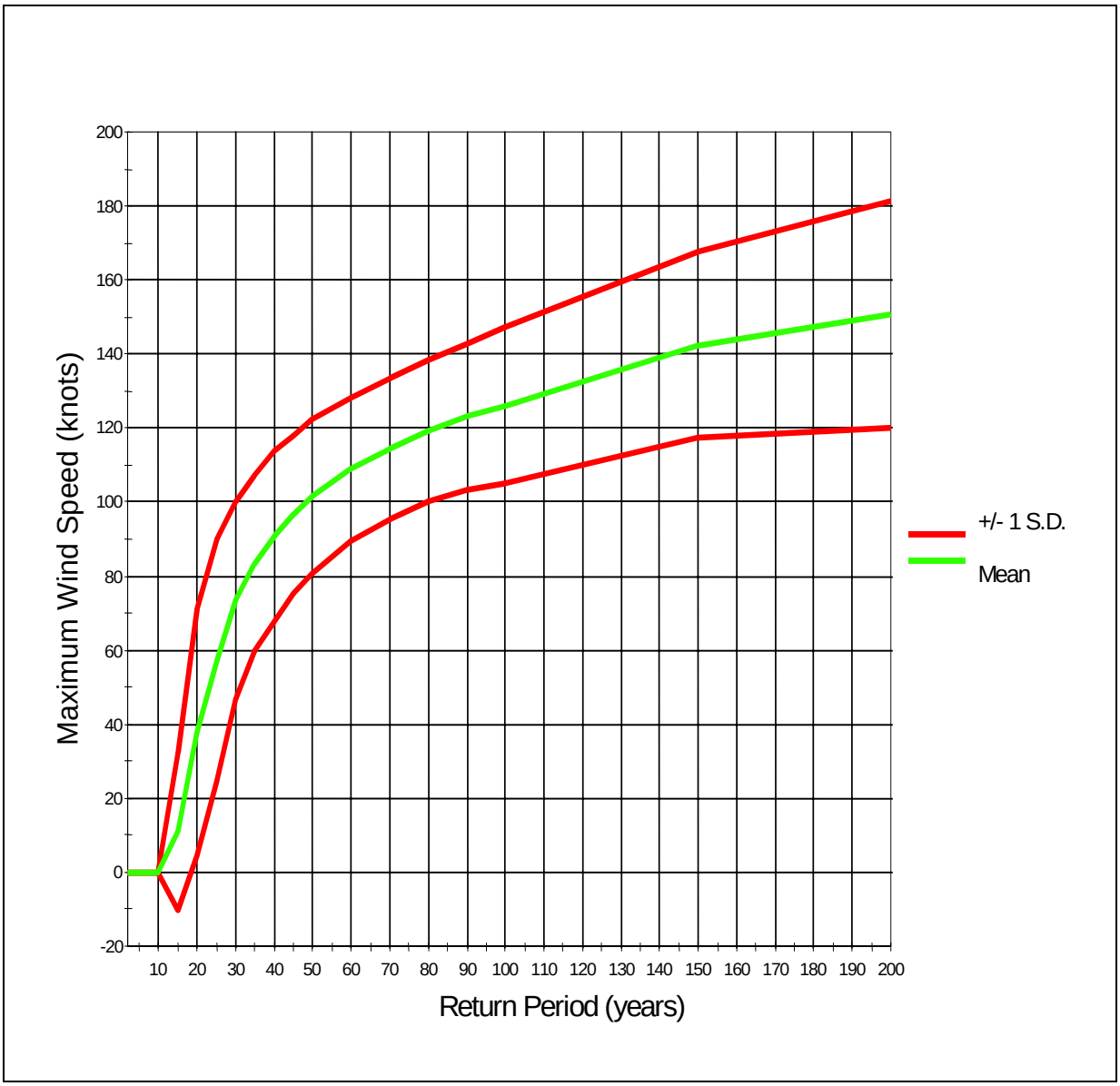

Fig. 6-5: **Frequency plot for maximum wind speeds**

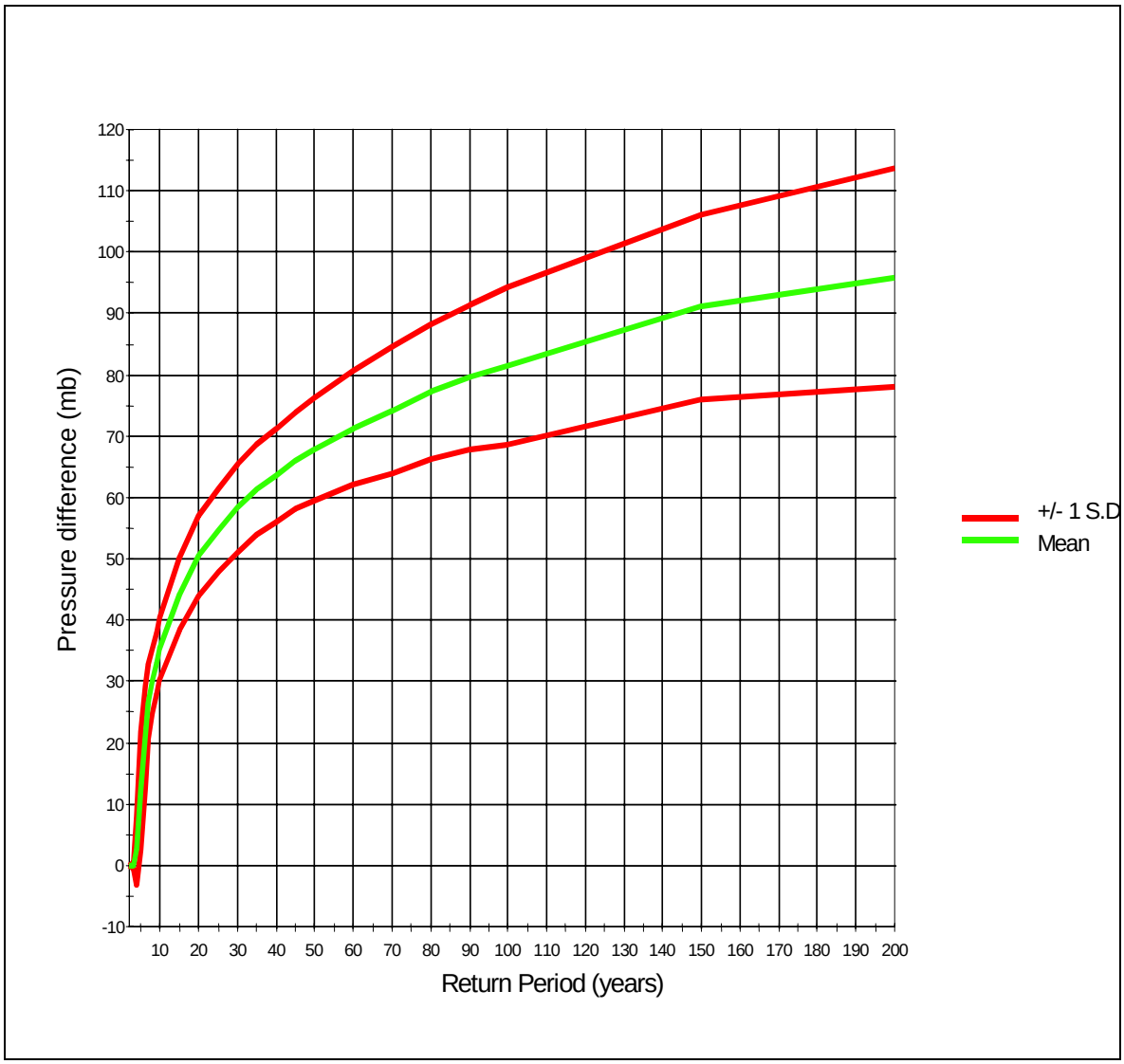

Fig. 6-6: **Frequency plot for pressure difference**

From the EST curve return periods corresponding to the pressure difference and maximum wind speed values as in Table 6-2 are recorded and are shown in Table 6-3. These return periods are then used along with storm surge frequency plots in order to obtain bands for different category of hurricanes. These bands are marked on the plots as shown in Fig. 6-7, 6-8 and 6-9. The expected surge corresponding to different category of hurricanes can be read from these plots. In order to validate this approach some

hurricanes were simulated and checked for their acceptability with the return periods predicted.

Table 6-3: Return periods for different categories of hurricanes

Category	Return Periods based on Pressure Difference, years	Return Periods based on Wind speed, years
1	-	-
2	12	32
3	26	45
4	52	62
5	168	116

6.6 Validation

In order to validate this approach some more hypothetical hurricanes were simulated in addition to the existing ones. Since SLOSH model assumes that the size and intensity of a hurricane remain constant throughout its track, Hurricane Carla (1961) was manipulated to obtain medium range category 2,3,4 and 5 hurricanes. Further, the track of Carla was perturbed by shifting it by -1.0 and –1.5 degree longitude from its normal track to obtain the maximum effect around the Freeport and Galveston Bay areas respectively. The storm surges from these hurricanes were plotted on the categorized storm surge return period graphs and are shown in Figures 6-7, 6-8 and 6-9.

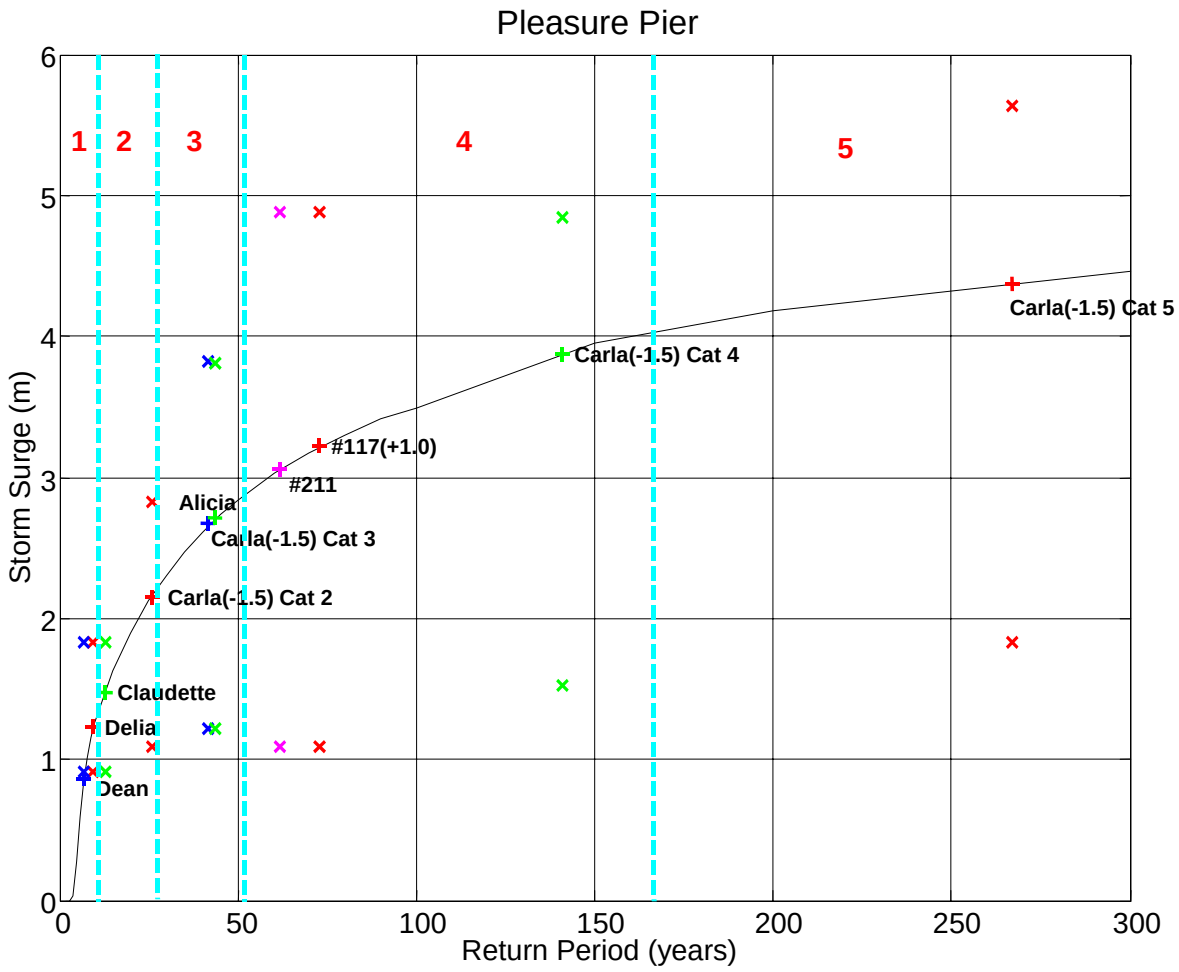

Fig. 6-7: Category bands for Galveston Pleasure Pier

Fig. 6-8: Category bands for Freeport Harbor

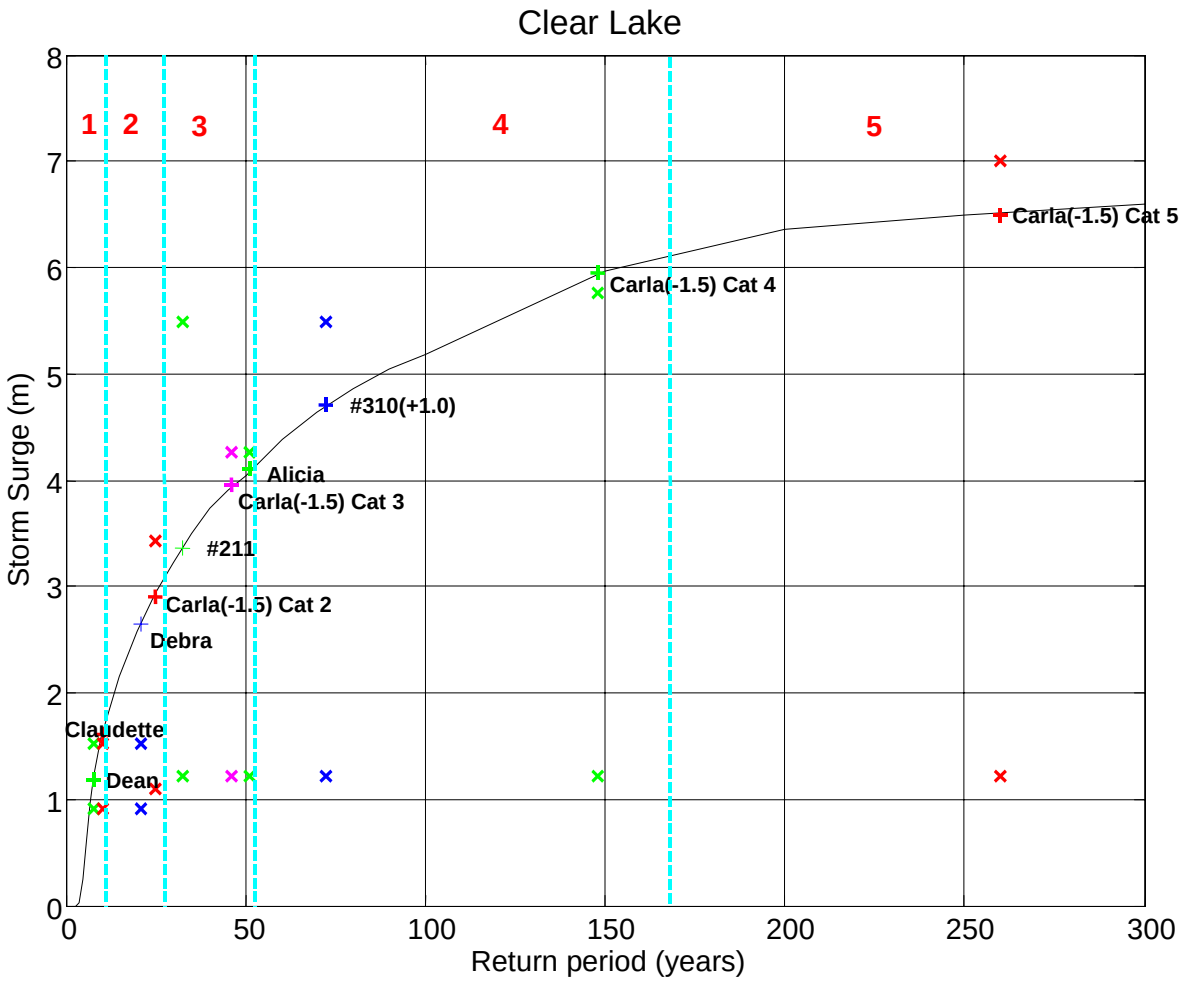

Fig. 6-9: Category bands for Clear Lake

The return periods for pressure difference are used in this study, as they seem to be more accurate and also conform to the HURISK return periods (Neumann C.J. 1994). The reason for this may be because maximum wind speeds are a function of central pressure difference and radius of maximum winds (Jelesnianski 1972), and since we still can not simulate Radius of maximum winds accurately, there seems to be some flaw in using maximum winds for calculating return periods for categories of hurricanes. Also, the fact that hurricane database consists of wind speeds greater than 64 knots, introduces some error in EST analyses for lower values of wind speeds response vector.

The hypothetical hurricanes like Carla (-1.0) and (-1.5) longitude whose maximum effect occurs at the respective locations Freeport and Galveston Bay fall well within the bands for their category as predicted. This is because these hurricanes make landfall within the distance of 30-50 miles left of the respective sites. Hence these hurricanes produce their maximum surge at these locations. As we move away from the landfall location, surge will reduce. However on the right hand side of the landfall location due to opposing wind directions surge is also reduced.

Let us consider the case of Hurricane #211. It was a medium range category 4 hurricane according to the Saffir Simpson scale. It made landfall at a distance of 31.2 miles from Galveston ship channel. It produced a surge consistent with the expected value read from Fig. 6-7 for Pleasure Pier. However it has a different impact at Freeport. It made landfall at a distance of 18 miles to the right and resulted in a surge of 1.34 meters. This is much less than its expected value that is within range of 2.6-4.5 meters. This is due to its making landfall right of Freeport. Thus it had an effect of a category 2 hurricane in the vicinity of Freeport.

Similarly Hurricane Alicia made landfall 33.5 miles left of ship channel and resulted in a storm surge of 2.7 meters and lies within its expected category in the frequency curves. However with respect to Freeport, it made landfall right of Freeport at a distance of 15 miles. Here again the frequency plots do not capture the storm surge associated due to it. This is again due to its making landfall right of Freeport.

The return period bands cover a wide range of storm surge, thus in order to predict a value that a hurricane can result, care must be taken. Storm surge being a complicated process, dependent on a large number of parameters, the predicted value will always have some inherent errors in it. Since the EST approach tries to take into effect all the factors that influence storm surge, the approach is more reliable compared to other approaches. A hurricane belonging to a category can, still be classified further into weaker, modest and stronger based on the ranges. Hence a weaker hurricane would correspond to a lower value of storm surge in that band and so on. The effect of distance of the site from landfall also plays an important role in the storm surge expected at that site. Based on the radius of maximum winds for the hurricane, the value must be selected from the plots considering the fact that surge is greater at a distance of around 30-40 miles from the landfall location. As we move away from the landfall location the storm surge is greatly reduced. Thus relative distance plays a very important role in storm surge expected due to a hurricane.

The present prediction and forecasting techniques do not accurately capture the effect of relative distance. Thus a method needs to be established in order to quantify storm surge due to a hurricane of given intensity and size on the basis of its relative distance from the landfall location. The prevalent forecasting techniques do a good job in

estimating maximum surge that can be expected based on Saffir-Simpson scale category of storms.

7 CONCLUSIONS

The results of this thesis illustrate the use of the hydrodynamic model ADCIRC in conjunction with statistical model EST for storm surge simulation and generation of frequency return curves for a location. Comparisons have been presented that show model output from ADCIRC and observed water level data for various hurricanes that have significantly impacted Texas coast during last 117 years.

The simulated data for most of the hurricanes compares well with the measured data wherever available. The model was able to accurately simulate the time and duration of the highest storm surge level. However the model is not able to fully capture storm surges due to tropical storms like Allison (2001). This inadequacy most likely results from the simplified vortex flow representation of the wind field by the wind model PBL, which may not accurately model the actual hurricane wind field particularly for a tropical storm as a storm approaches and passes over a coastal boundary. The other cause may be the method used to estimate the radius of maximum winds, which is the nomograph of Fig. 2-1. Though this nomograph in general is able to predict the radius of maximum winds, it is not able to do so for all storms equally as well. In this study the observed values of radius were used wherever available as in Hurricane Claudette (2003) resulting in fairly accurate storm surge simulation as shown in Fig. 5-7. Another factor may be that the modeled distribution of wind magnitudes along the axis of storm may not be representative of the actual storm, where wind speeds may not decay at the rate assumed by the PBL model. The approach used in this study of using the whole Gulf of Mexico as the computation domain takes care of the limitations of PBL model near to the shore.

The study extends the storm surge simulation using the EST model to arrive at life-cycle return period curves for storm surge at a particular location. These values can

be used to give a realistic idea of typical ”design” storm surge values that may help engineers to design new structures and maintain existing structures. EST encompasses all the parameters that affect the storm surge at a location for an individual hurricane like relative distance from landfall. Thus the results give a more realistic picture of the damage potential to the engineers.

This approach is also compared with the SLOSH approach used by federal authorities to delineate coastal areas susceptible to hurricane storm surge flooding and evacuation studies. The shortcomings in the model SLOSH and the storm atlas approach are pointed out in the study. An alternate way for estimating storm surge at a location based on Saffir-Simpson categorization scale of hurricanes is presented in the study. This method utilizes the database of historical and hypothetical storms to arrive at return periods for different categories of hurricane and then uses these periods for estimating storm surges due to different category of hurricanes.

This approach needs to be applied for localized areas, as there are many local factors that may influence the storm surge. The local bathymetry may play an important role in the final storm surge value; hence the computational grid used for populating the database should have required resolution in order to capture the local bathymetry. The shape of the coastline also has a strong effect on the size of a storm surge. A concave coastline is favored for greater storm surge, as water can be funneled toward the center of the coastline. For example, the coast of North Carolina has many concave areas that can influence the size of a storm surge. For example, in 1996, Hurricane Fran made landfall at Cape Fear, NC and produced a storm surge of 3.2 m at Carolina Beach, NC. Hurricane Hazel (1954) made landfall at the border of North and South Carolina, as a rapidly moving hurricane. This area of North Carolina's coastline to the right of Hazel was

concave. Hazel was also a stronger, faster moving storm than Fran and it produced a peak storm surge of 5.5 m on the south facing beaches south west of Carolina Beach, while Carolina Beach had a peak storm surge of less than 3.0 m. Hence these coastline effects again call for a good resolution of the computational grid.

There are certain improvements that can be made to the model. One is to include shoaling effect. This refers to water forced from deep water into shallow water, where it converges to the shoreline. The more shoaling that occurs, the higher the potential storm surge. The waves also play an important role in potential storm surge. Strong hurricane winds may result in high wave setups. Hence coupling of the hydrodynamic ADCIRC model with a wave model would be helpful in estimating these factors. Also, high rainfall amounts can lead to fresh water flooding, which can exacerbate the storm surge problem. If a hurricane makes landfall in a location where several rivers empty into the ocean, the runoff from the rivers can increase flooding. An example of this is Bangladesh, which is located in a low-lying flood plain where several rivers empty into the Indian Ocean. Future models may also include the effect of rainfall and river-runoffs to completely calculate and estimate storm surges.

After evaluating the limitations of the present storm surge calculation and estimation approach, it still provides useful information about surge levels for sites, particularly for sites that are located to the east of a storm. The good feature of this approach is its relative simplicity, as it can model a storm using only the most basic information. Also as it is based on actual historical storm rather than possible hypothetical ones, it is more credible.

REFERENCES

Bodine, B.R., (1971) “Storm surge on the open coast: fundamentals and simplified prediction.” *Corps of Engineers Technical Memorandum No. 35*, USACE, WES, Vicksburg, MS.

Borgman, L.E., Miller, M.C., Butler, H.L., and Reinhard, R.D., (1992) Empirical simulation of future hurricane storm histories as a tool in engineering and Economic Analysis. *Proc. Civil Engineering in the Oceans,* ASCE, New York, 2-5.

Borgman, L.E. and Scheffner, N.W., (1991) “The simulation of time sequences of wave height, period, and direction.” *TR-DRP-91-2*. US Army Corps of Engineers, Waterways Experiment Station, Vicksburg, MS.

Cardone, V.J., Greenwood, C.V., and Greenwood, J.A., (1992) “Unified program for the specification of hurricane boundary layer winds over surfaces of specified roughness,” *contract report CERC-92-1*, US Army Corps of Engineers, Waterways Experiment Station, Vicksburg, MS.

Chow, S (1971) “A diagnostic model of the hurricane PBL.” *Journal of Atmospheric Sciences* 29(2), 419–426.

College of Architecture, (1994) ”Storm atlas for Brazoria, Galveston and Harris Counties.” Texas A&M University, College Station, TX.

Flather, R.A., (1988) “A numerical model investigation of tides and diurnal-period continental shelf waves along Vancouver Island.” *Journal of Physical Oceanography* 18, 115-139.

Garcia, A. W. and Flor, T. H., (1984) “Hurricane Alicia storm surge and wave data,” *Technical report CERC-84-6*, US Army Corps of Engineers, Waterways Experiment Station, Vicksburg, MS.

Ho, F.P., (1987) “Hurricane climatology for the Atlantic and Gulf coasts of the United States.” *NOAA Technical Report NWS 38*, NOAA, Washington, DC.

Jarvinen, B.R., Neumann, C.J., and Davis, M.A.S., (1988) “A tropical cyclone data tape for the North Atlantic Basin, 1886-1983: Contents, limitation and uses,” *NOAA Technical Memorandum NWS NHC 22*, NOAA, Washington, DC.

Jelesnianski, C.P., (1972) “SPLASH (Special program to list amplitudes of surges from hurricanes)” *NOAA Technical Memorandum* NWS TDL-46, NOAA, Washington, DC.

Jelesnianski, C.P., (1967) “Numerical computation of storm surges with bottom stress.” *Monthly Weather Review*, 95,740-756.

Jelesnianski, C.P., Chen J. and Shaffer W.A., (1992) “SLOSH: Sea, lake, and overland surges from hurricanes.” *NOAA Technical Report NWS 48*, NOAA, Washington, DC.

Jelesnianski, C.P. and Taylor, A.D., (1973) “A preliminary view of storm surges before and after storm modifications.” *NOAA Technical Memorandum ERL WMPO-3*, Weather Modification Program Office, Boulder CO.

Kolar, R.L., Gray, W.G., Westerink, J.J., and Luettich, R.A. (1994) “Shallow water modeling in spherical coordinates: Equation formulation, numerical implementation, and application,” *Journal of Hydraulic Research* 32(1), 3-24.

Le Provost, C., Genco M. L., Lyard F., Vincent P., and Canceil P. (1994) “Spectroscopy of the world ocean tides from a finite element hydrodynamic model,” *Journal of Geophysics Research* 94, 777-797.

Luettich, R.A., Westerink, J.J., and Scheffner, N.W., (1992) “ADCIRC: An advanced three-dimensional circulation model for shelves, coasts, and estuaries Report 1:Theory and methodology of ADCIRC-2DDI and ADCIRC-3DL,” *Technical report DRP-92-6*, US Army Engineer Waterways Experiment Station, Vicksburg, MS.

Neumann C.J., (1994) “ The National Hurricane Center Risk Analysis Program (HURISK),” Science Applications International Corporation, Miami, FL.

Platzman, G.W., (1963) “The dynamical prediction of wind tides on Lake Erie.” *Meteorological Monographs*, 4, 44-48.

Scheffner, N.W., Carson, F.C., Rhee, J.P., Mark, D.J., (2003) “Coastal erosion study for the open coast from Sabine Pass to San Luis Pass, Texas: Tropical storm surge frequency analysis,” US Army Corps of Engineers, Waterways Experiment Station, Vicksburg, MS.

Scheffner, N. W., Clausner, J. E., Militello, A., Borgman, L. E., Edge, B. L., and Grace, P. E, (1999) “Use and application of the empirical simulation technique: Users guide,”

Technical Report CHL-99-21, US Army Corps of Engineers, Waterways Experiment Station, Vicksburg, MS.

Scheffner, N.W., Mark D.J., Blain, C.A., Westerink, J.J., and Luettich, R.A., (1994) "ADCIRC: An advanced three-dimensional circulation model for shelves, coasts, and estuaries report 5:A tropical storm data base for the East and Gulf of Mexico coasts of the United States," *Technical Report DRP-94-4*, U.S. Army Corps of Engineers, Waterways Experiment Station, Vicksburg, MS.

Wanstrath, J.J. Reid, R.O., (1976) "Storm surge simulation in transformed coordinates", *Technical Report No. 76-3*, US Army Corps of Engineers, Waterways Experiment Station, Vicksburg, MS.

Westerink, J.J., Luettich, R.A., and Scheffner, N.W., (1993) "ADCIRC: An advanced three-dimensional circulation model for shelves, coasts, and estuaries report 3: Development of a tidal constituent database for the western North Atlantic and Gulf of Mexico," *Technical Report DRP-93-2*, US Army Corps of Engineers, Waterways Experiment Station, Vicksburg, MS.

APPENDIX A

COMPARISON OF MODEL GENERATED TIDES AND XTIDE

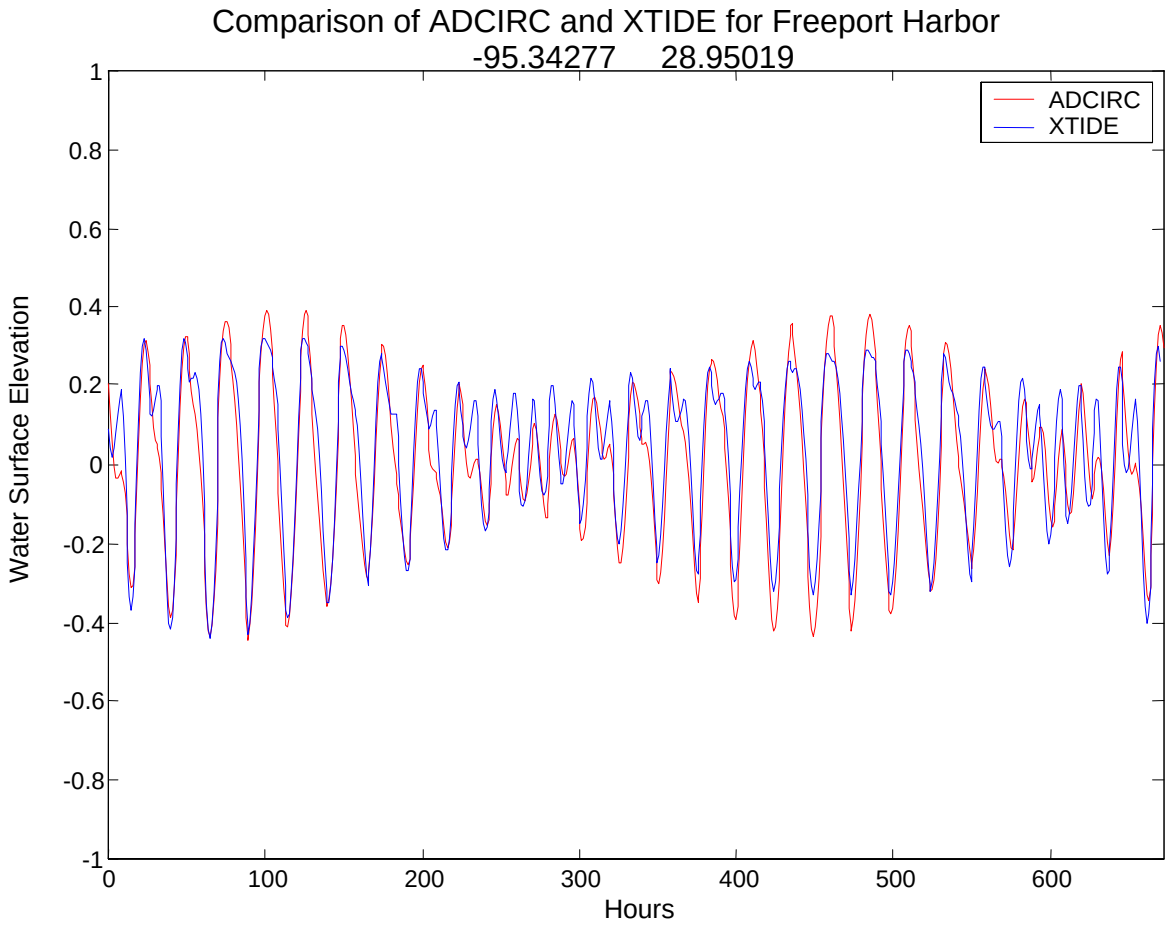
Comparison of ADCIRC and XTIDE for Freeport Harbor
-95.34277 28.95019
ADCIRC
XTIDE
Water Surface Elevation
Hours
1
0.8
0.6
0.4
0.2
0
-0.2
-0.4
-0.6
-0.8
-1
0
100
200
300
400
500
600

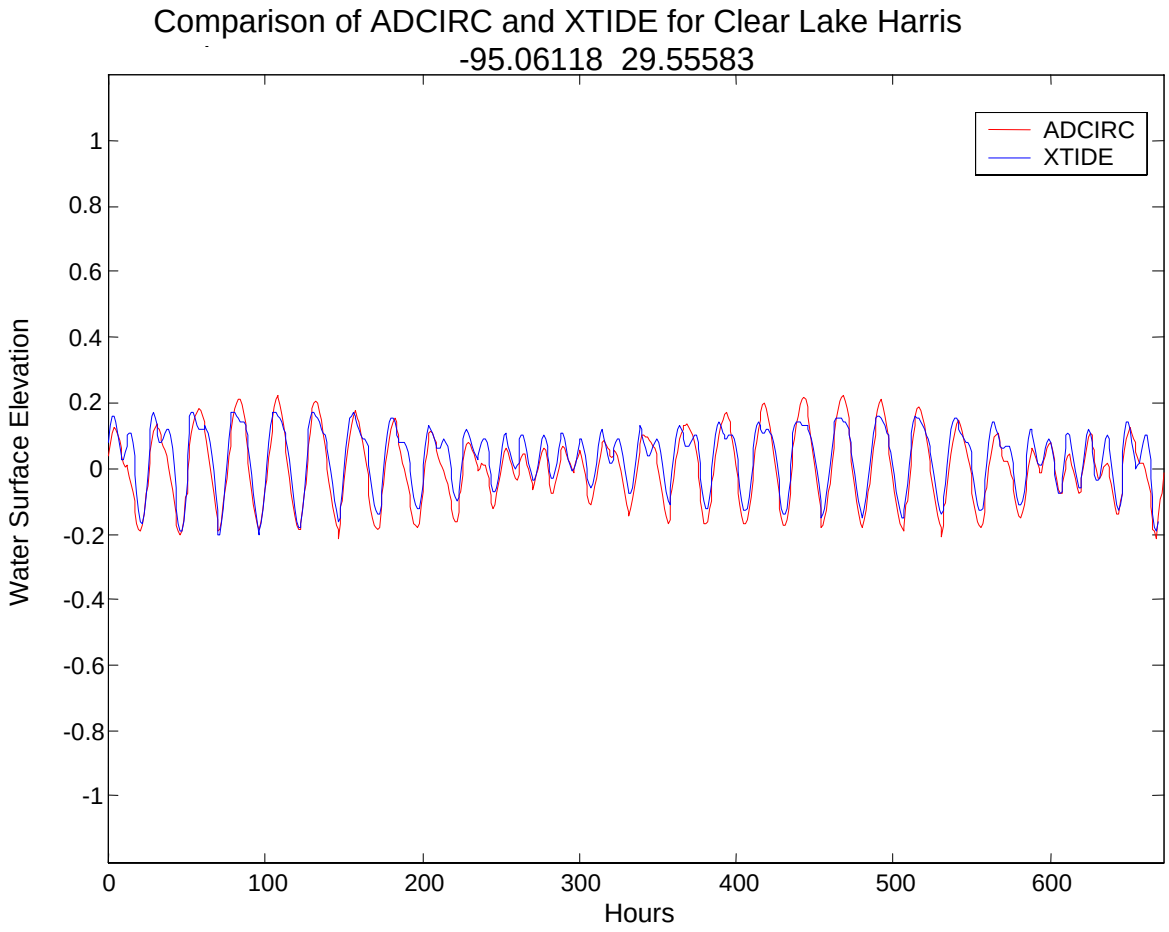
Comparison of ADCIRC and XTIDE for Clear Lake Harris
-95.06118 29.55583
ADCIRC
XTIDE
Water Surface Elevation
Hours
1
0.8
0.6
0.4
0.2
0
-0.2
-0.4
-0.6
-0.8
-1
0
100
200
300
400
500
600

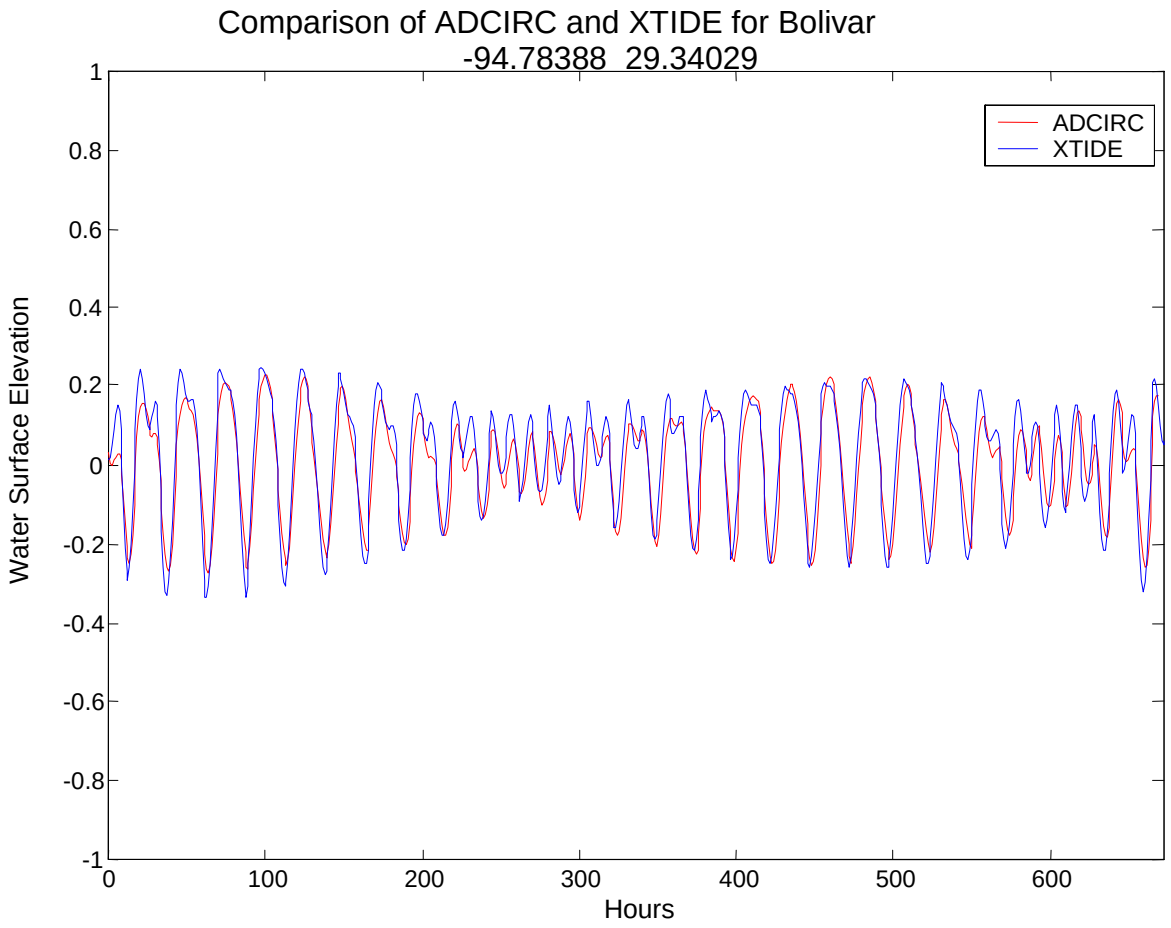
Comparison of ADCIRC and XTIDE for Bolivar
-94.78388 29.34029
ADCIRC
XTIDE
Water Surface Elevation
Hours
1
0.8
0.6
0.4
0.2
0
-0.2
-0.4
-0.6
-0.8
-1
0
100
200
300
400
500
600

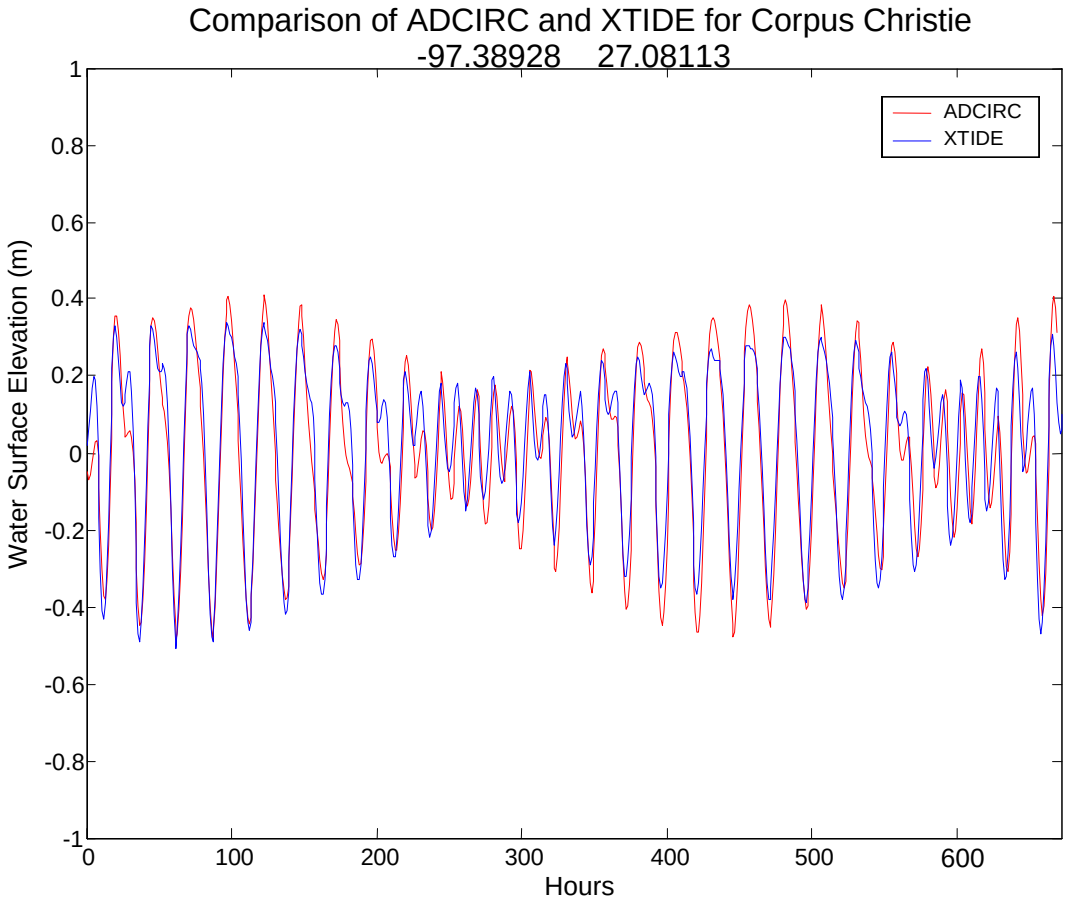
Comparison of ADCIRC and XTIDE for Corpus Christie
-97.38928 27.08113
ADCIRC
XTIDE
Water Surface Elevation (m)
Hours
1
0.8
0.6
0.4
0.2
0
-0.2
-0.4
-0.6
-0.8
-1
0
100
200
300
400
500
600

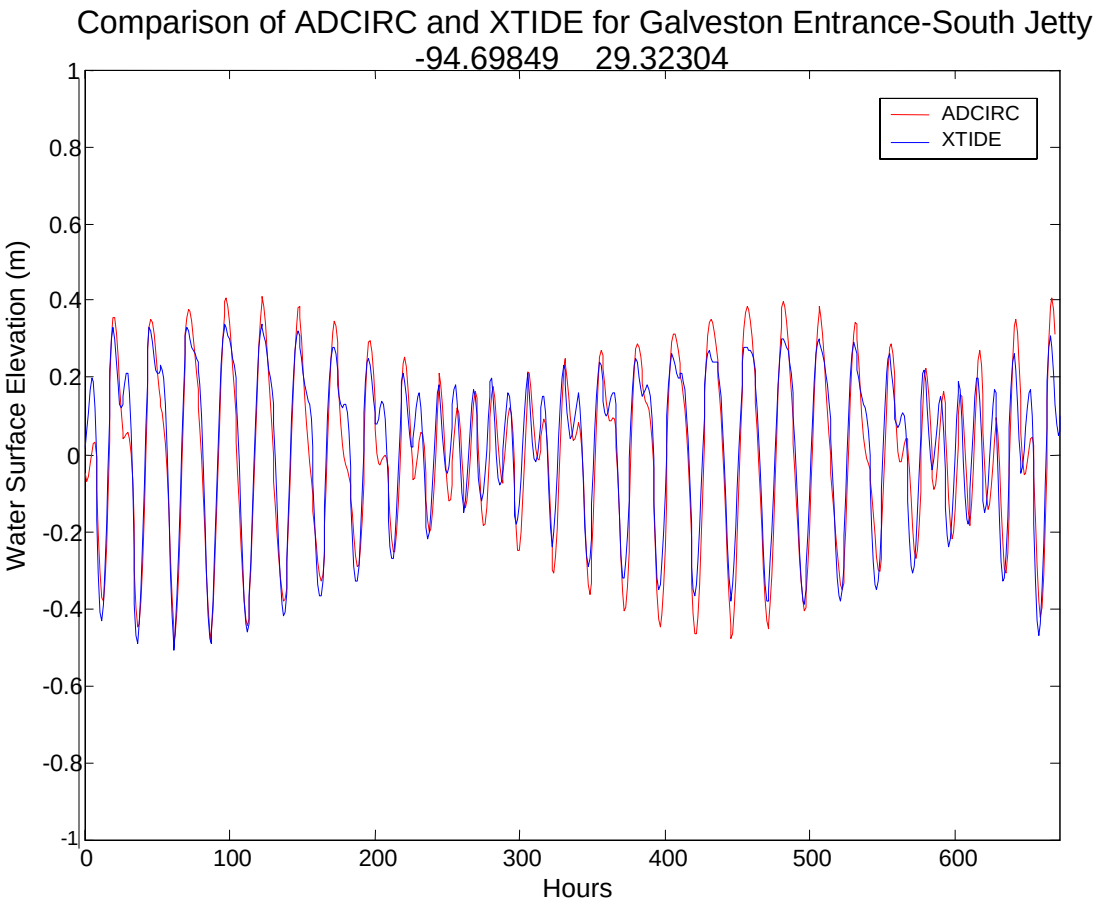
Comparison of ADCIRC and XTIDE for Galveston Entrance-South Jetty
-94.69849 29.32304
ADCIRC
XTIDE
Water Surface Elevation (m)
Hours
1
0.8
0.6
0.4
0.2
0
-0.2
-0.4
-0.6
-0.8
-1
0
100
200
300
400
500
600

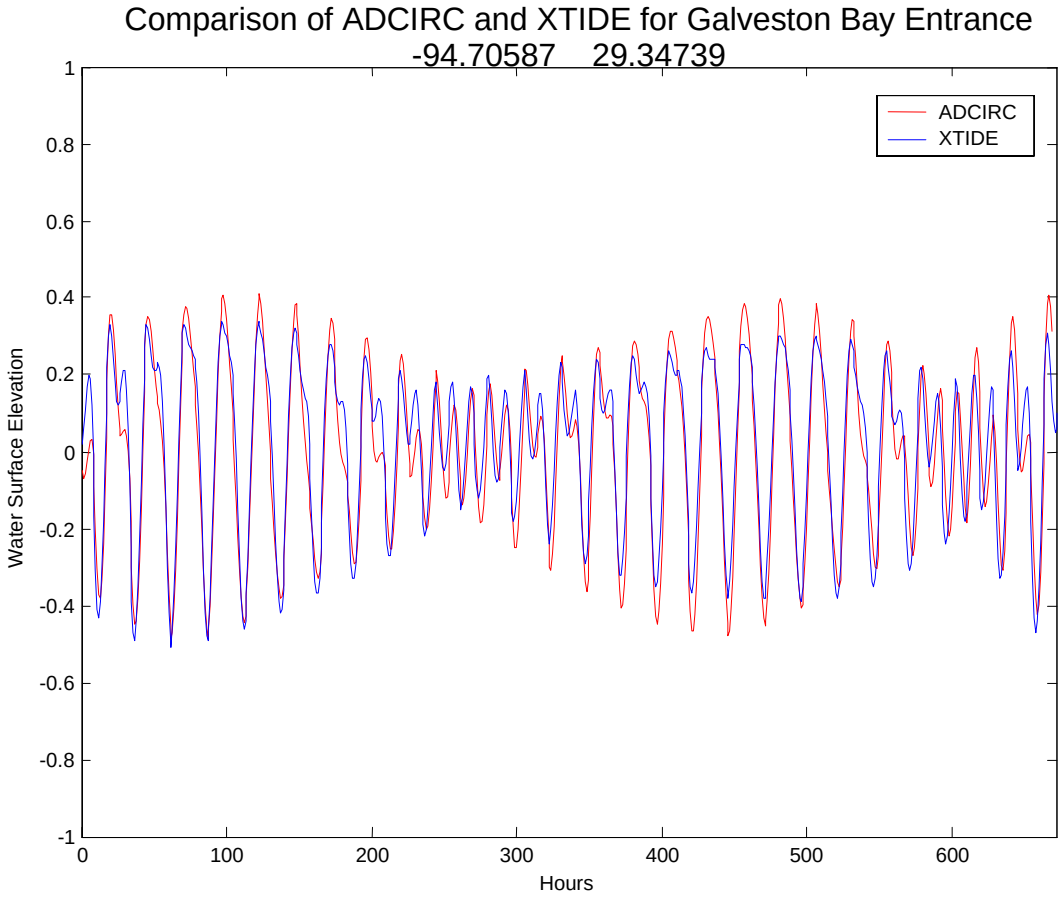
Comparison of ADCIRC and XTIDE for Galveston Bay Entrance
-94.70587 29.34739
ADCIRC
XTIDE
Water Surface Elevation
Hours
1
0.8
0.6
0.4
0.2
0
-0.2
-0.4
-0.6
-0.8
-1
0
100
200
300
400
500
600

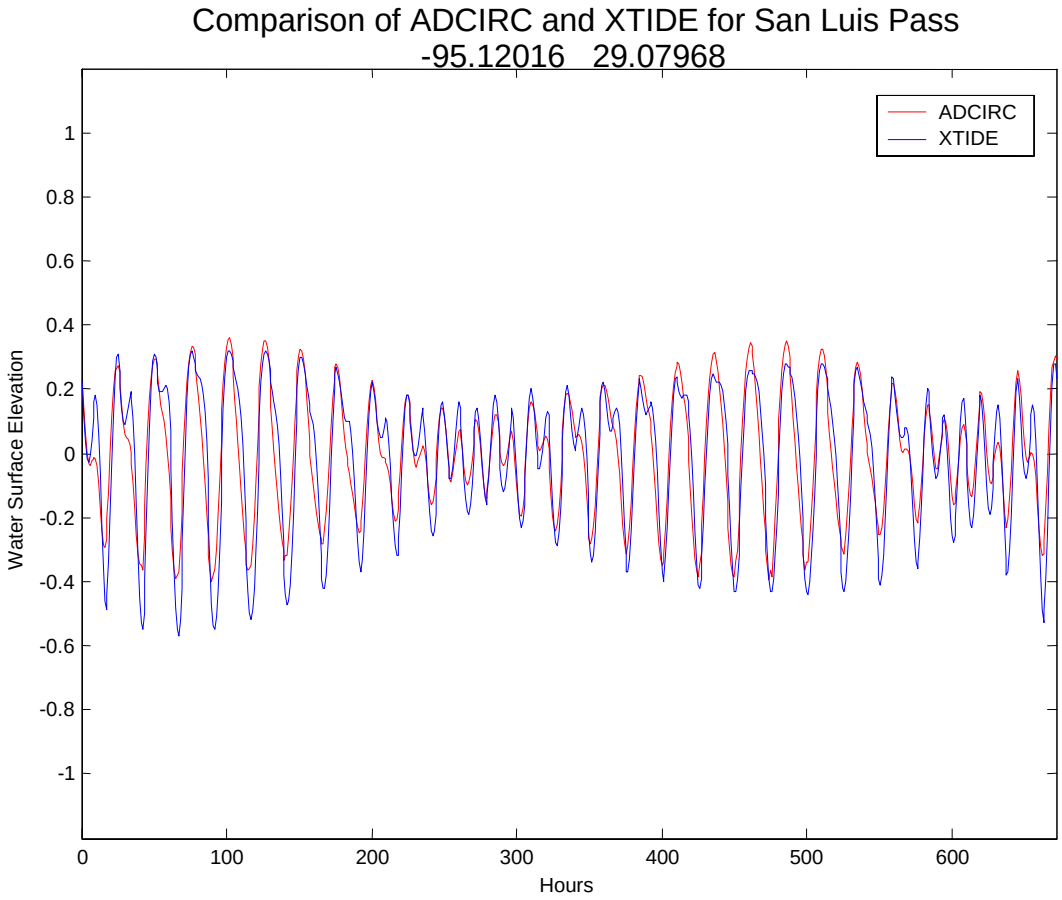
Comparison of ADCIRC and XTIDE for San Luis Pass
-95.12016 29.07968
ADCIRC
XTIDE
Water Surface Elevation
Hours
1
0.8
0.6
0.4
0.2
0
-0.2
-0.4
-0.6
-0.8
-1
0
100
200
300
400
500
600

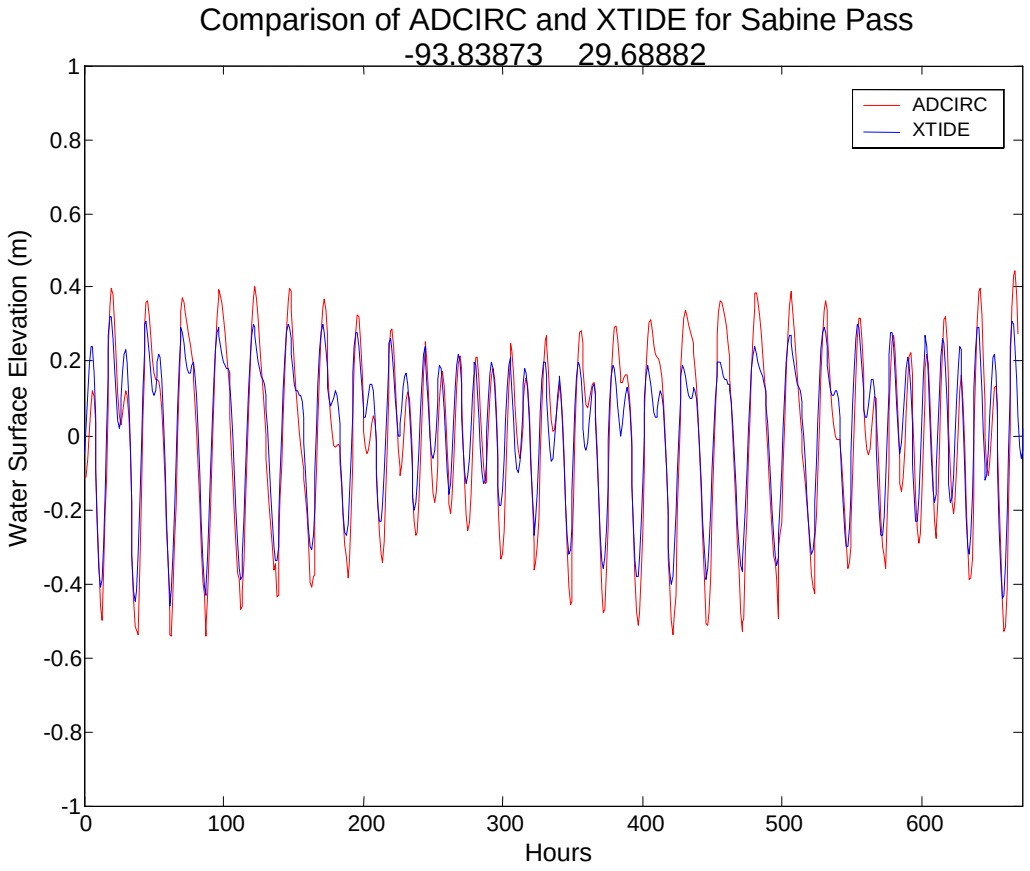
Comparison of ADCIRC and XTIDE for Sabine Pass
-93.83873 29.68882
ADCIRC
XTIDE
Water Surface Elevation (m)
Hours
1
0.8
0.6
0.4
0.2
0
-0.2
-0.4
-0.6
-0.8
-1
0
100
200
300
400
500
600

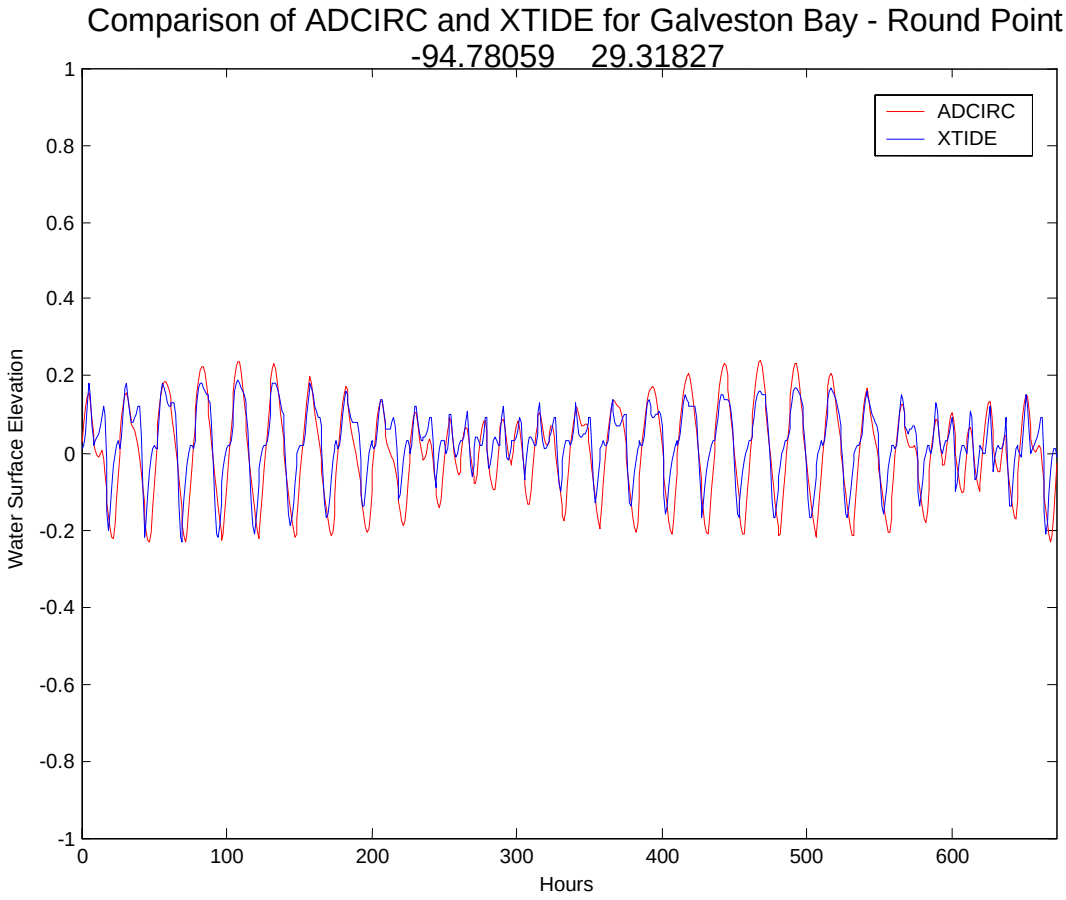
Comparison of ADCIRC and XTIDE for Galveston Bay - Round Point
-94.78059 29.31827
ADCIRC
XTIDE
Water Surface Elevation
Hours
1
0.8
0.6
0.4
0.2
0
-0.2
-0.4
-0.6
-0.8
-1
0
100
200
300
400
500
600

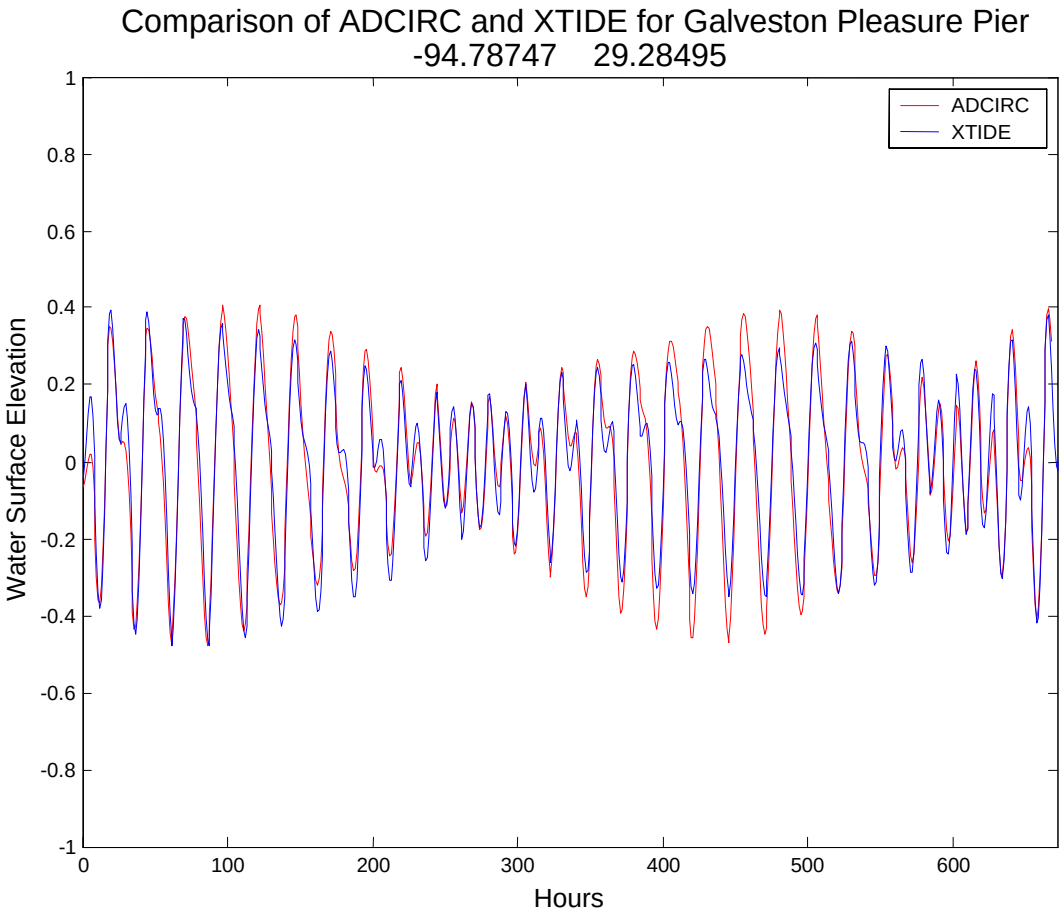
Comparison of ADCIRC and XTIDE for Galveston Pleasure Pier
-94.78747 29.28495
ADCIRC
XTIDE
Water Surface Elevation
Hours
1
0.8
0.6
0.4
0.2
0
-0.2
-0.4
-0.6
-0.8
-1
0
100
200
300
400
500
600

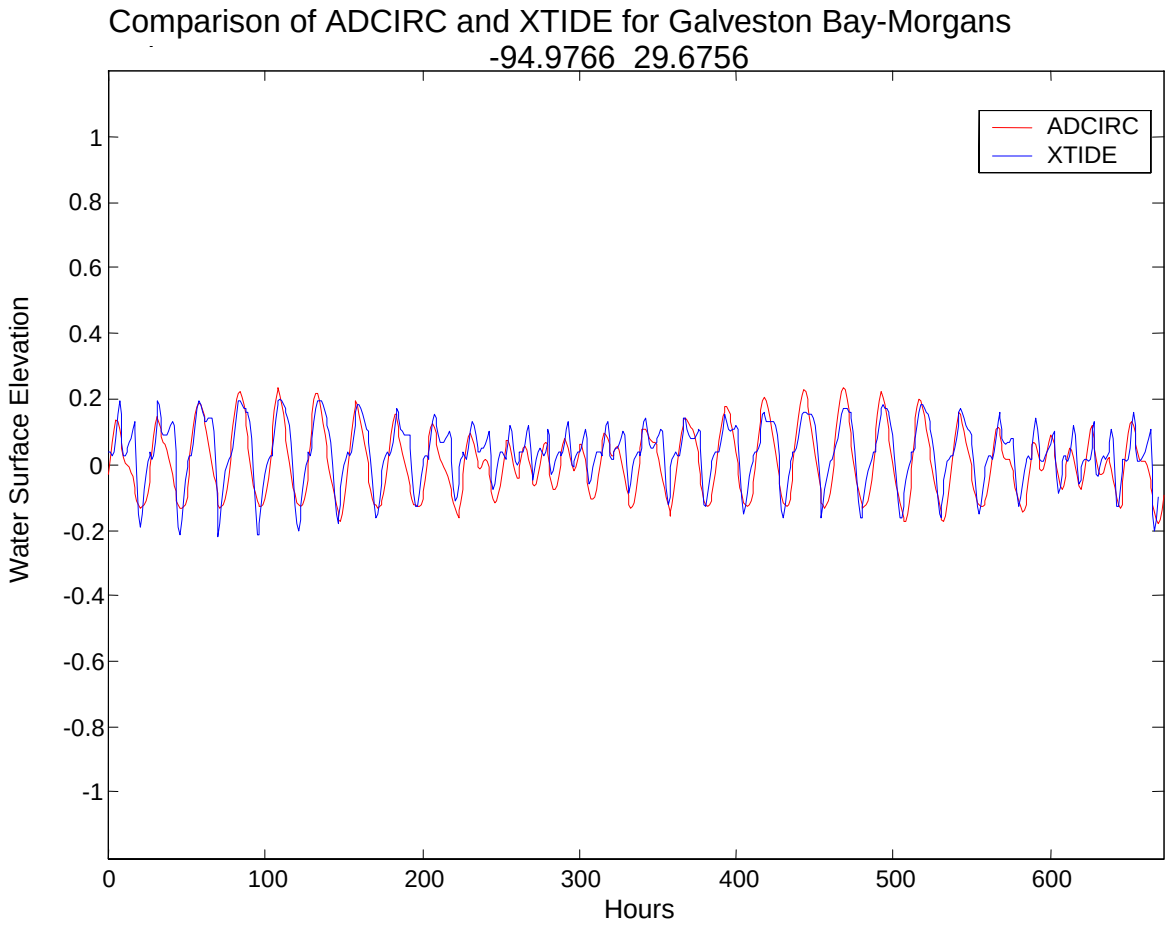
Comparison of ADCIRC and XTIDE for Galveston Bay-Morgans
-94.9766 29.6756
ADCIRC
XTIDE
Water Surface Elevation
Hours
1
0.8
0.6
0.4
0.2
0
-0.2
-0.4
-0.6
-0.8
-1
0
100
200
300
400
500
600

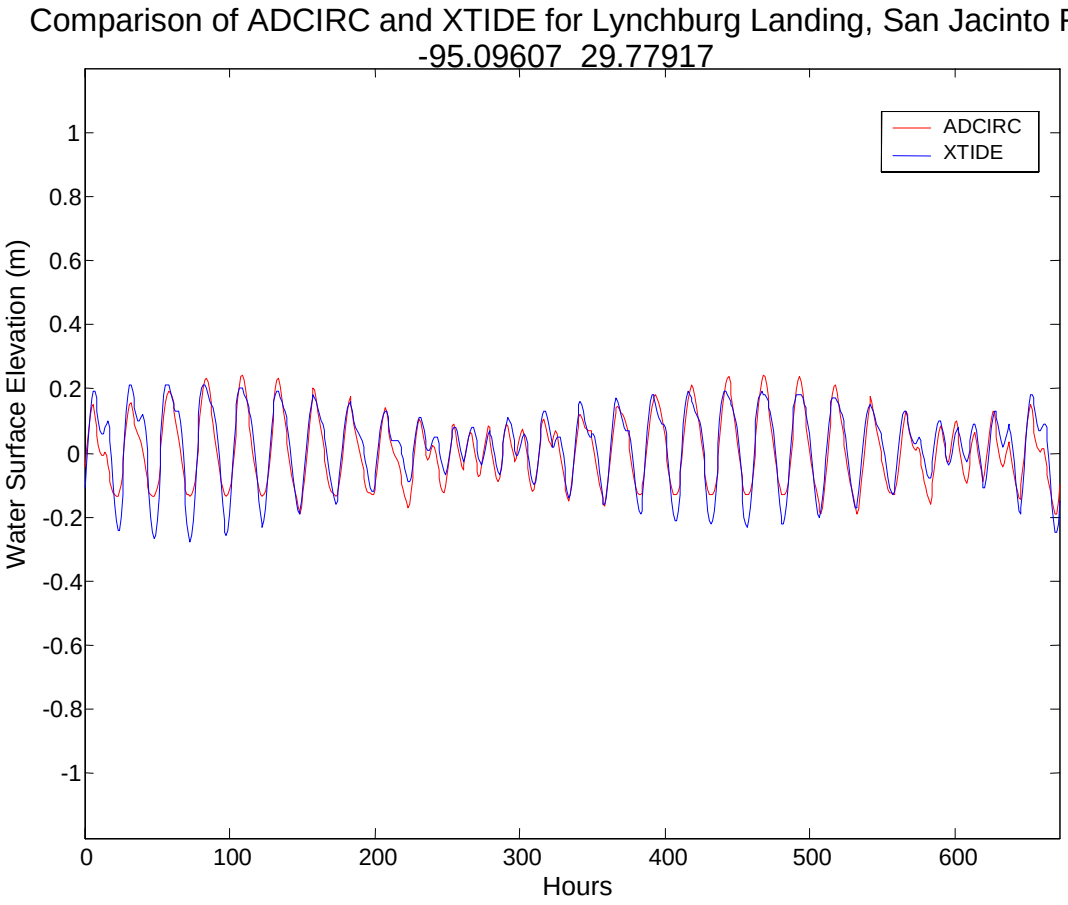
Comparison of ADCIRC and XTIDE for Lynchburg Landing, San Jacinto River
-95.09607 29.77917
ADCIRC
XTIDE
Water Surface Elevation (m)
1
0.8
0.6
0.4
0.2
0
-0.2
-0.4
-0.6
-0.8
-1
0
100
200
300
400
500
600
Hours

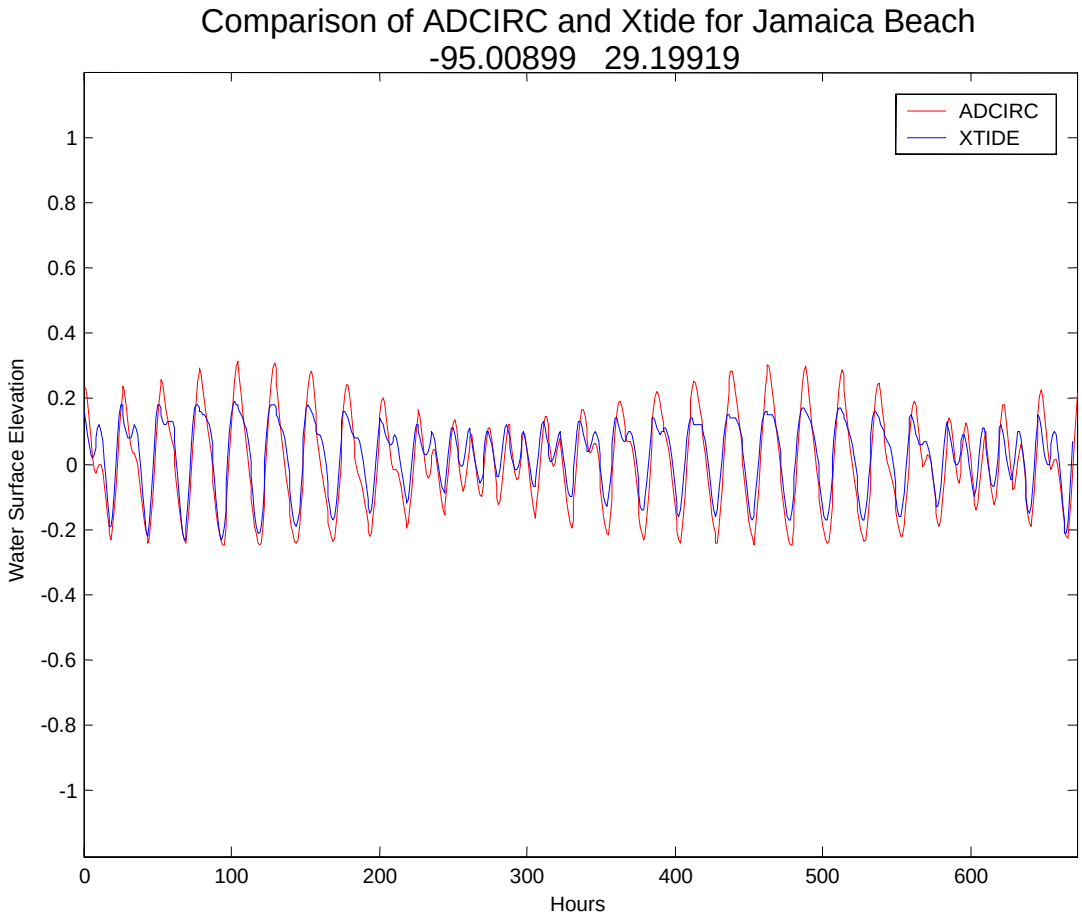
Comparison of ADCIRC and Xtide for Jamaica Beach
-95.00899 29.19919
ADCIRC
XTIDE
Water Surface Elevation
Hours
1
0.8
0.6
0.4
0.2
0
-0.2
-0.4
-0.6
-0.8
-1
0
100
200
300
400
500
600

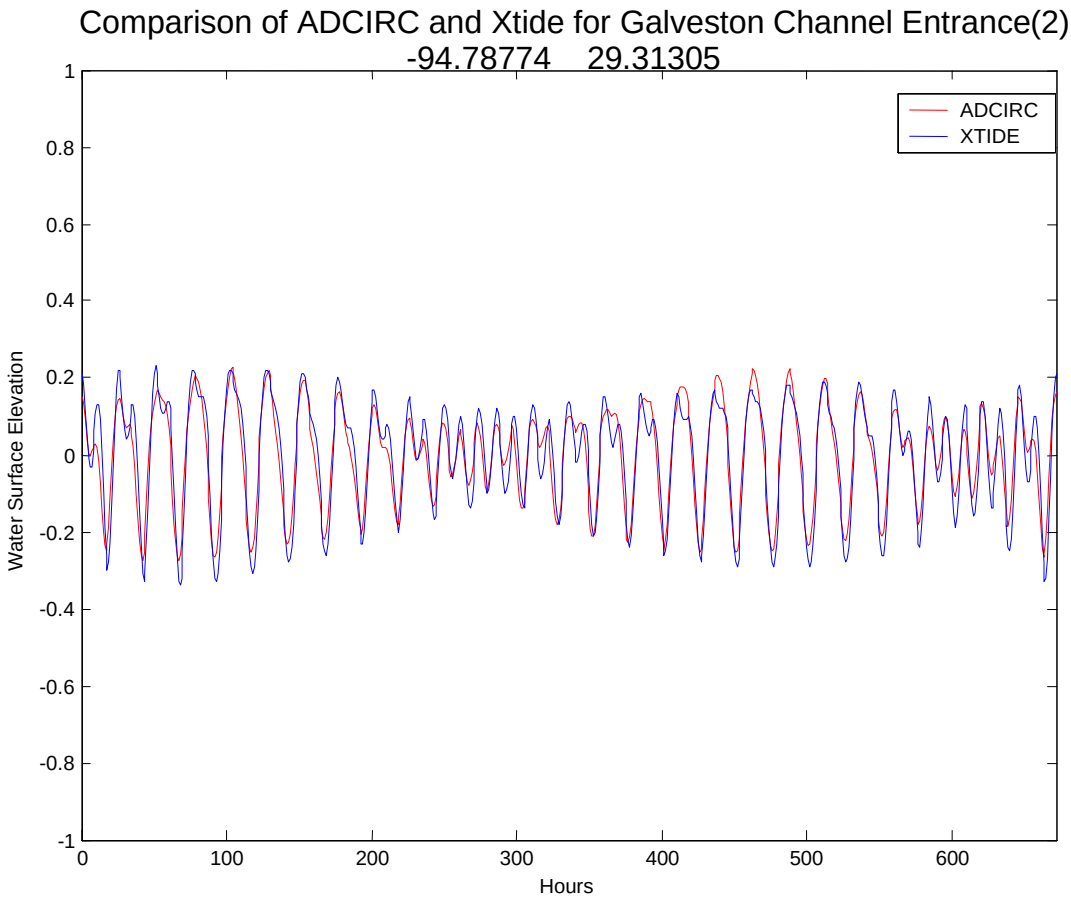
Comparison of ADCIRC and Xtide for Galveston Channel Entrance(2)
-94.78774 29.31305
ADCIRC
XTIDE
Water Surface Elevation
Hours
1
0.8
0.6
0.4
0.2
0
-0.2
-0.4
-0.6
-0.8
-1
0
100
200
300
400
500
600

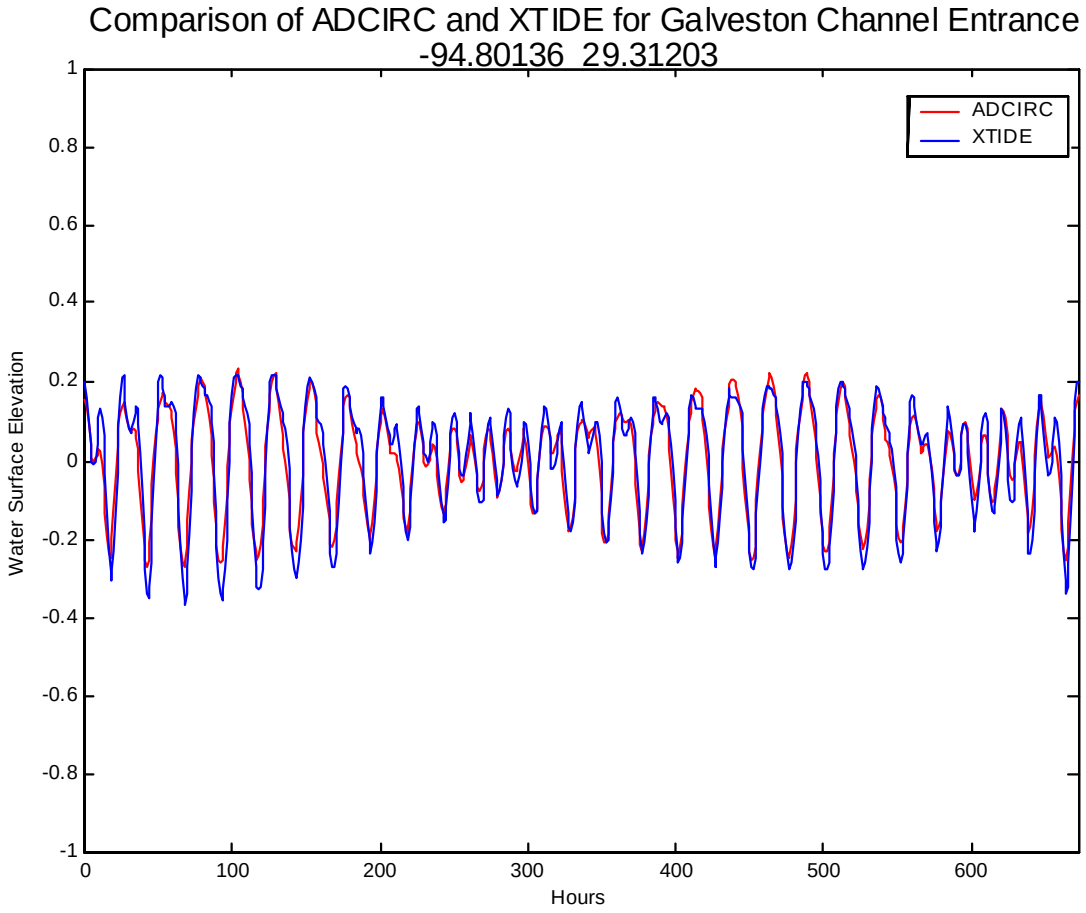
Comparison of ADCIRC and XTIDE for Galveston Channel Entrance
-94.80136 29.31203
ADCIRC
XTIDE
Water Surface Elevation
Hours
1
0.8
0.6
0.4
0.2
0
-0.2
-0.4
-0.6
-0.8
-1
0
100
200
300
400
500
600

APPENDIX B

STORM TRACKS AND SURGE PLOTS

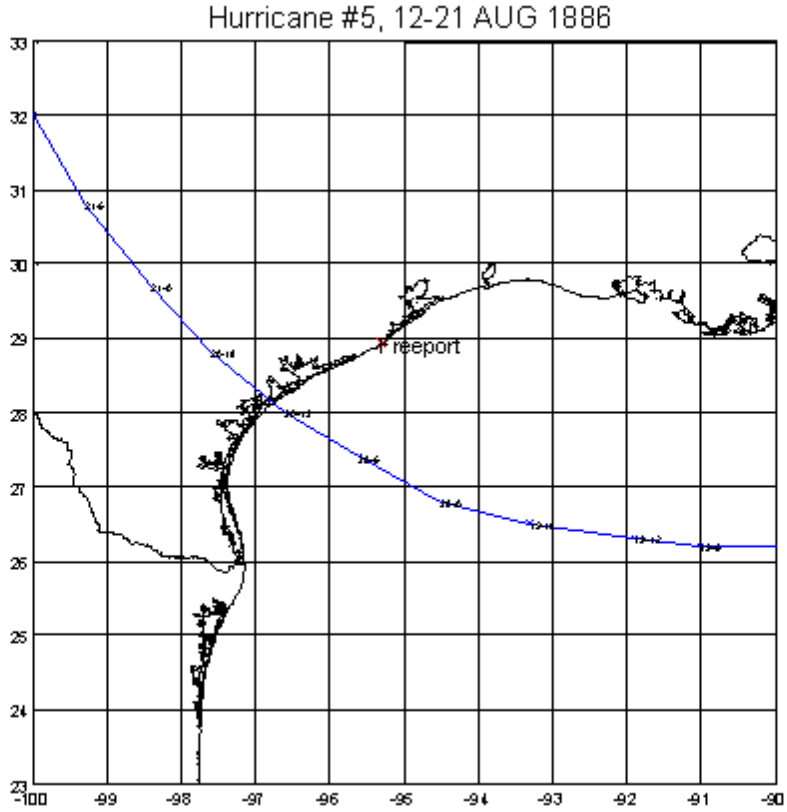
Hurricane #5, 12-21 AUG 1886
Freeport
33
32
31
30
29
28
27
26
25
24
23
-100
-99
-98
-97
-96
-95
-94
-93
-92
-91
-90

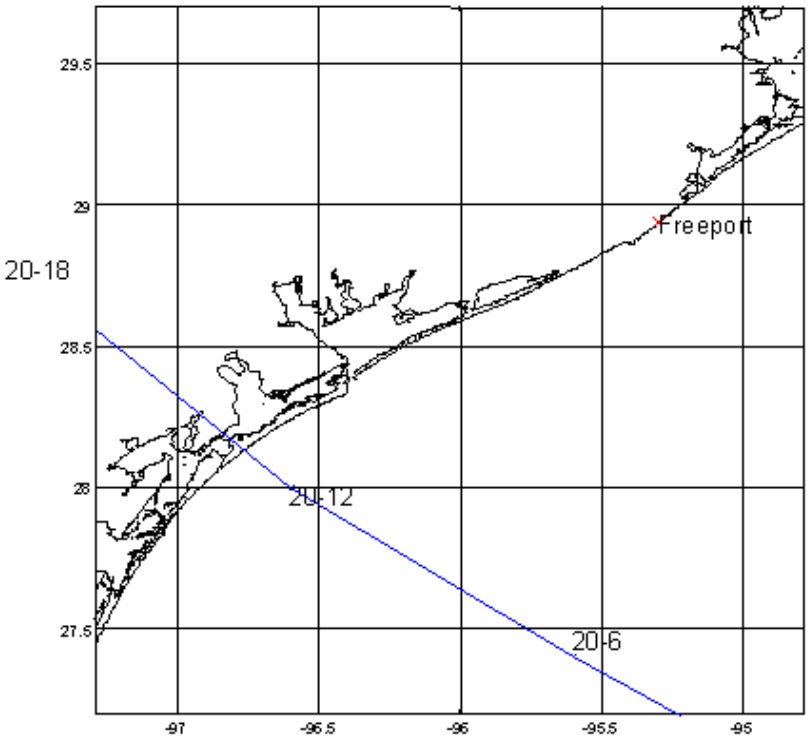
Freeport
20-18
20-12
20-6
29.5
29
28.5
28
27.5
-97
-96.5
-96
-95.5
-95

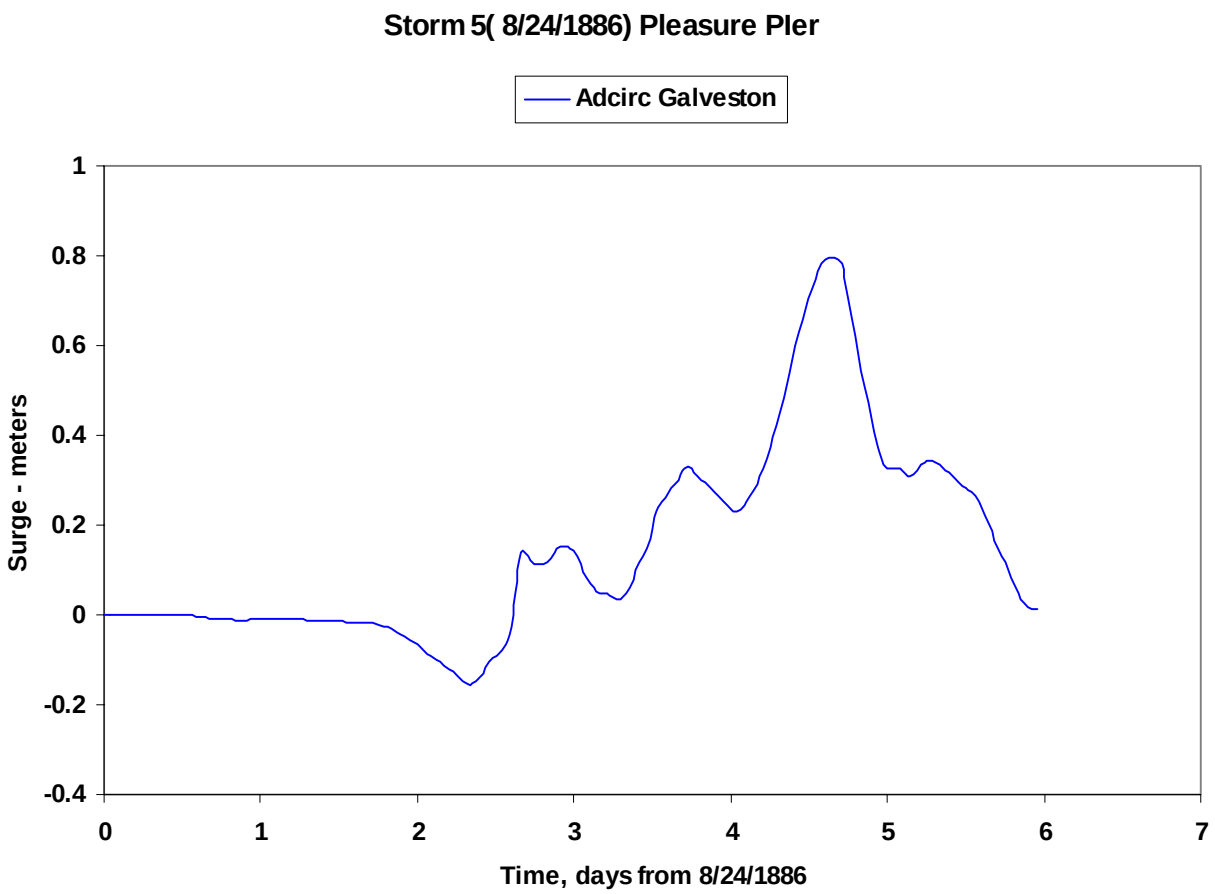
Storm 5(8/24/1886) Pleasure Pier
Adcirc Galveston
Surge - meters
1
0.8
0.6
0.4
0.2
0
-0.2
-0.4
0
1
2
3
4
5
6
7
Time, days from 8/24/1886

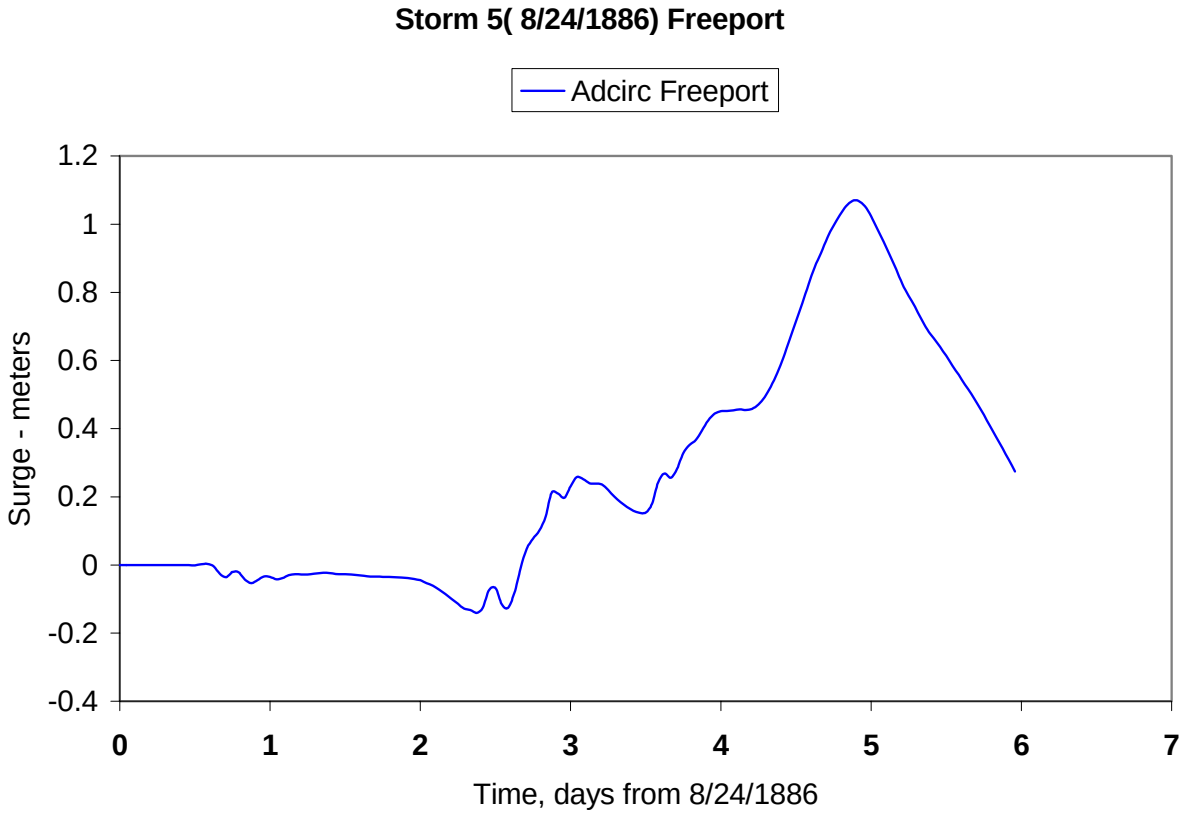
Storm 5(8/24/1886) Freeport
Adcirc Freeport
Surge - meters
1.2
1
0.8
0.6
0.4
0.2
0
-0.2
-0.4
0
1
2
3
4
5
6
7
Time, days from 8/24/1886

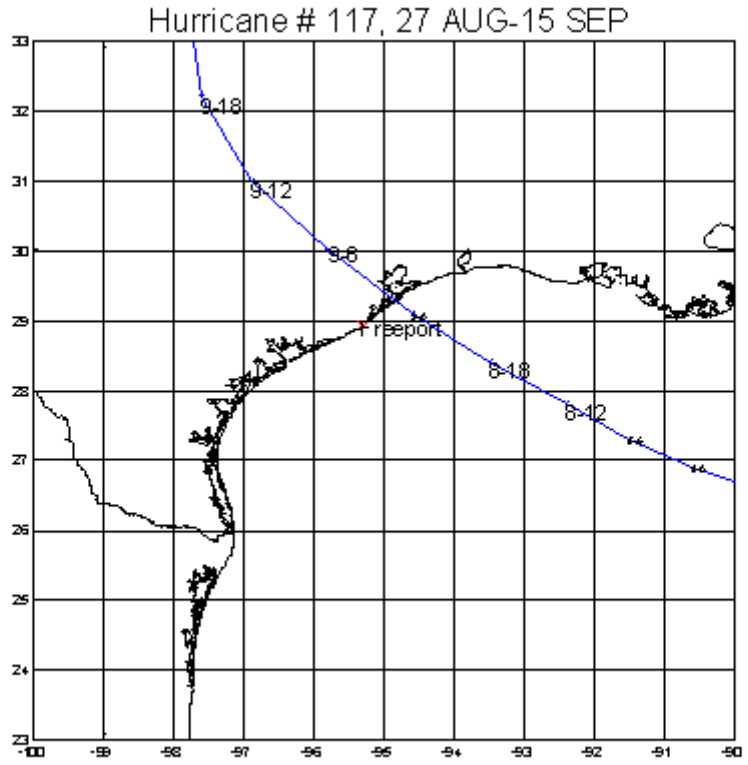
Hurricane # 117, 27 AUG-15 SEP
9-18
9-12
9-6
Freeport
8-18
8-12

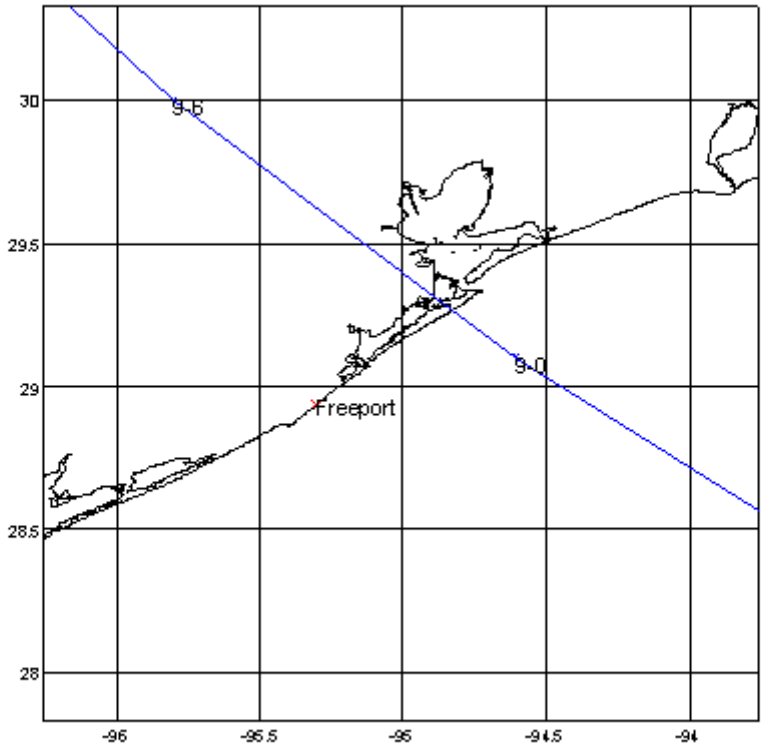
9-6
9-0
Freeport
30
29.5
29
28.5
28
-96
-95.5
-95
-94.5
-94

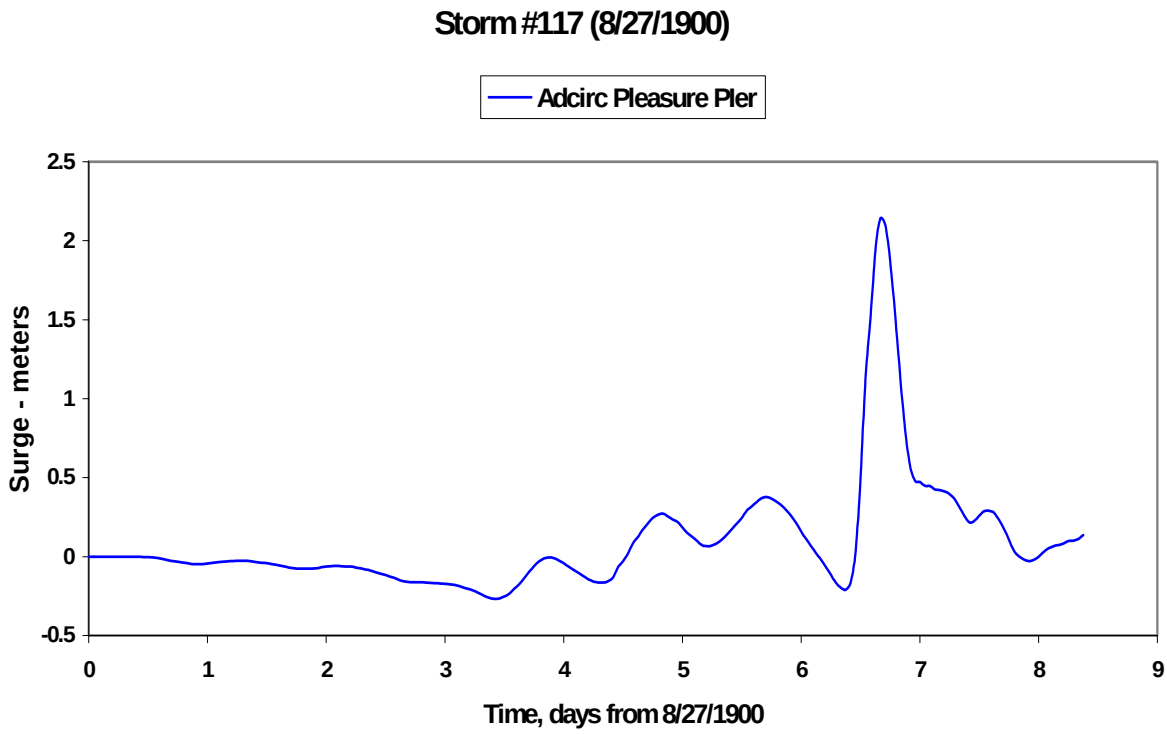
Storm #117 (8/27/1900)
Adcirc Pleasure Pier
Surge - meters
2.5
2
1.5
1
0.5
0
-0.5
0
1
2
3
4
5
6
7
8
9
Time, days from 8/27/1900

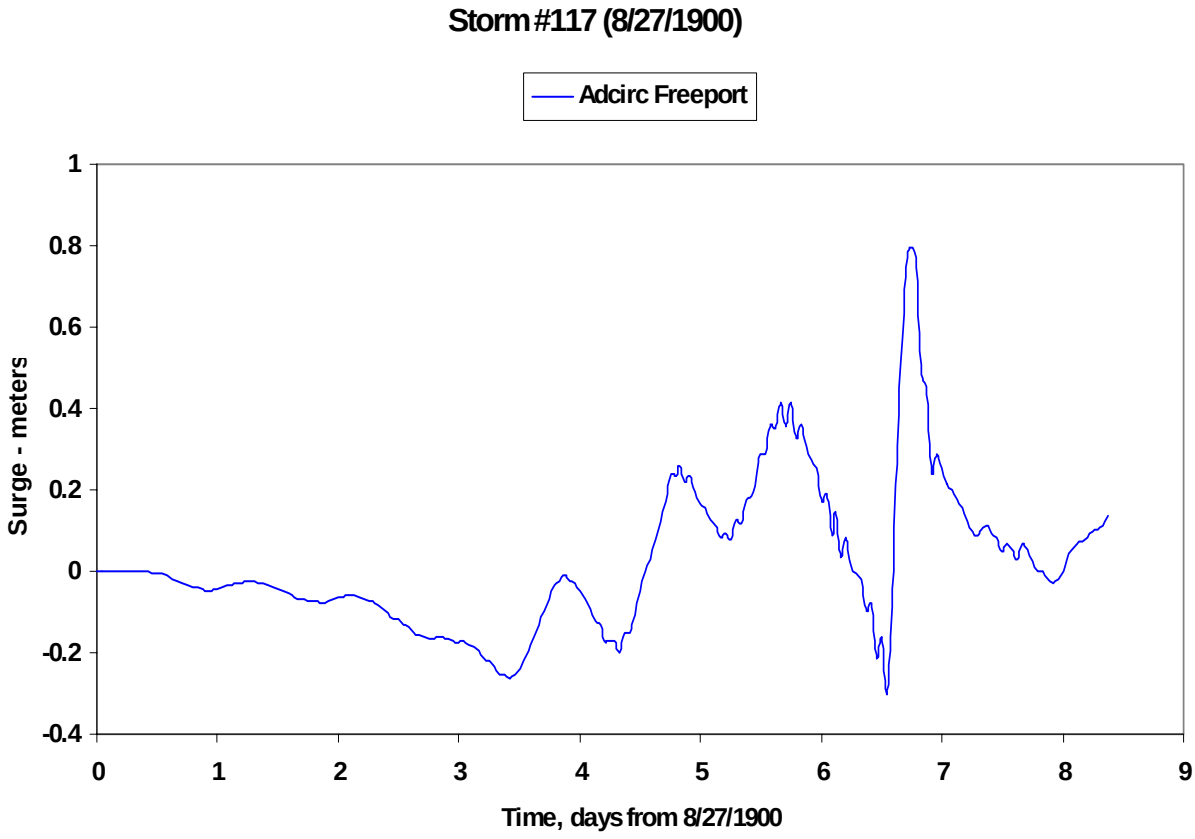
Storm #117 (8/27/1900)
Adcirc Freeport
Surge - meters
1
0.8
0.6
0.4
0.2
0
-0.2
-0.4
0
1
2
3
4
5
6
7
8
9
Time, days from 8/27/1900

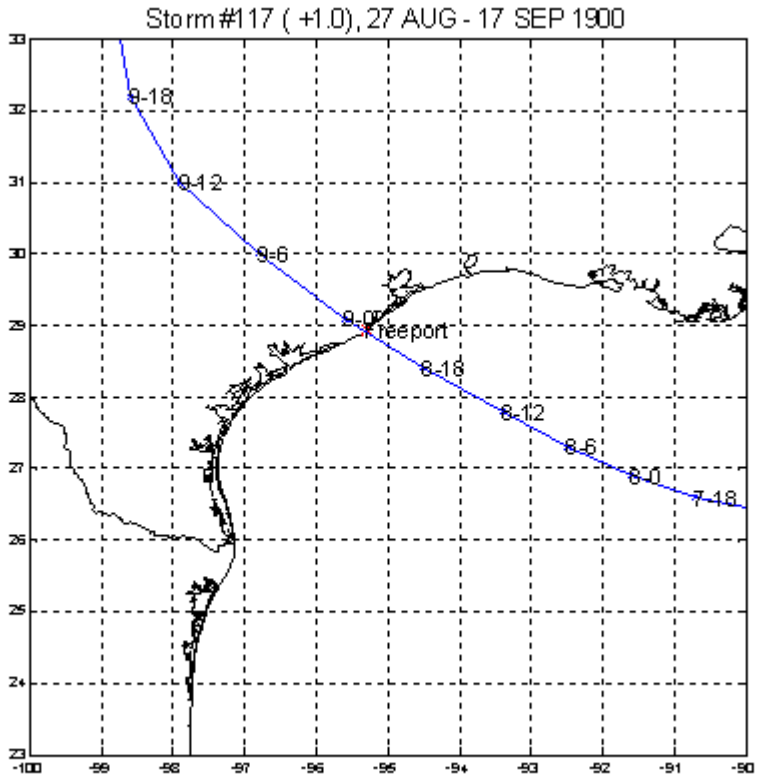
Storm #117 (+1.0), 27 AUG - 17 SEP 1900
9-18
9-12
9-6
9-0
Freeport
8-18
8-12
8-6
8-0
7-18

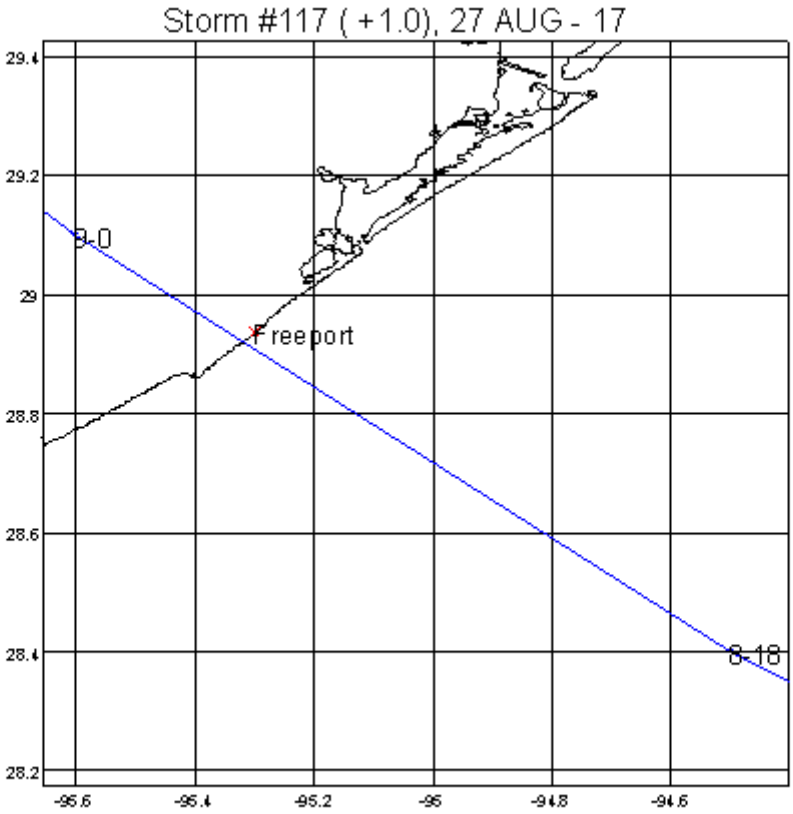
Storm #117 (+1.0), 27 AUG - 17
9-0
Freeport
8-18

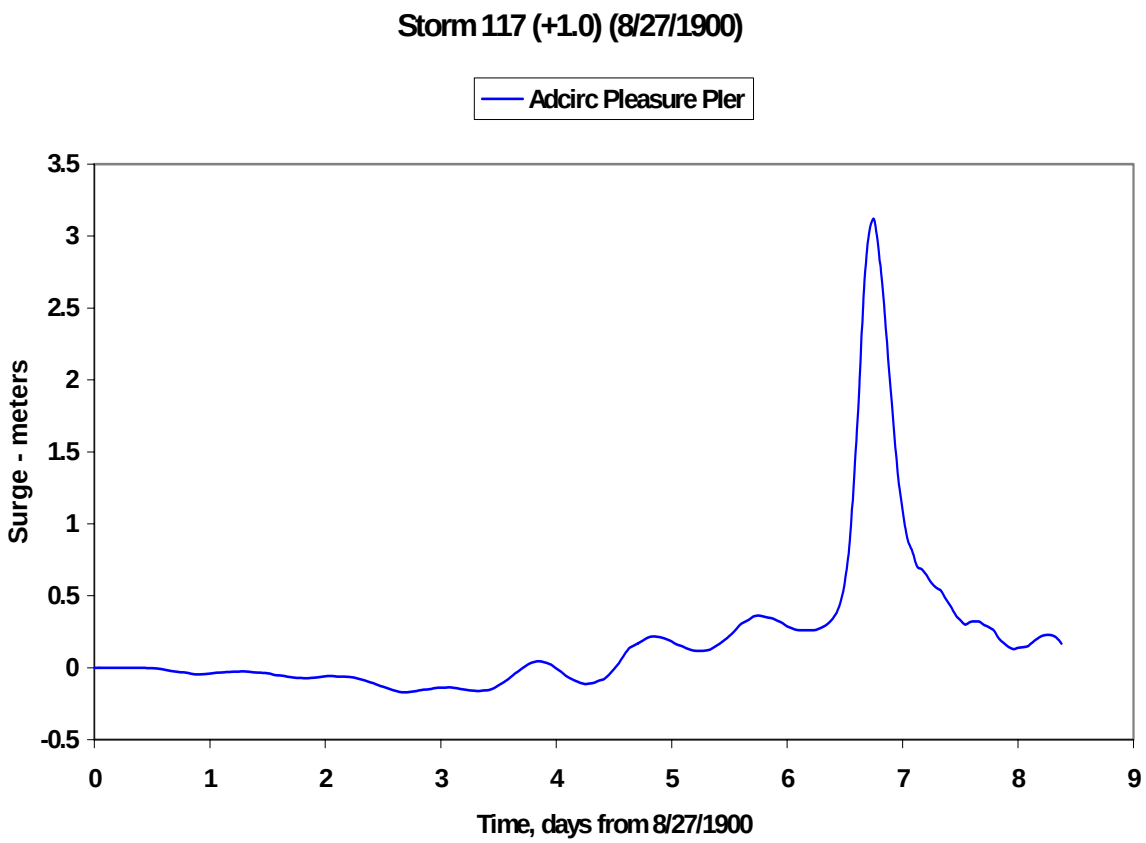
Storm 117 (+1.0) (8/27/1900)
Adcirc Pleasure Pier
Surge - meters
Time, days from 8/27/1900
3.5
3
2.5
2
1.5
1
0.5
0
-0.5
0
1
2
3
4
5
6
7
8
9

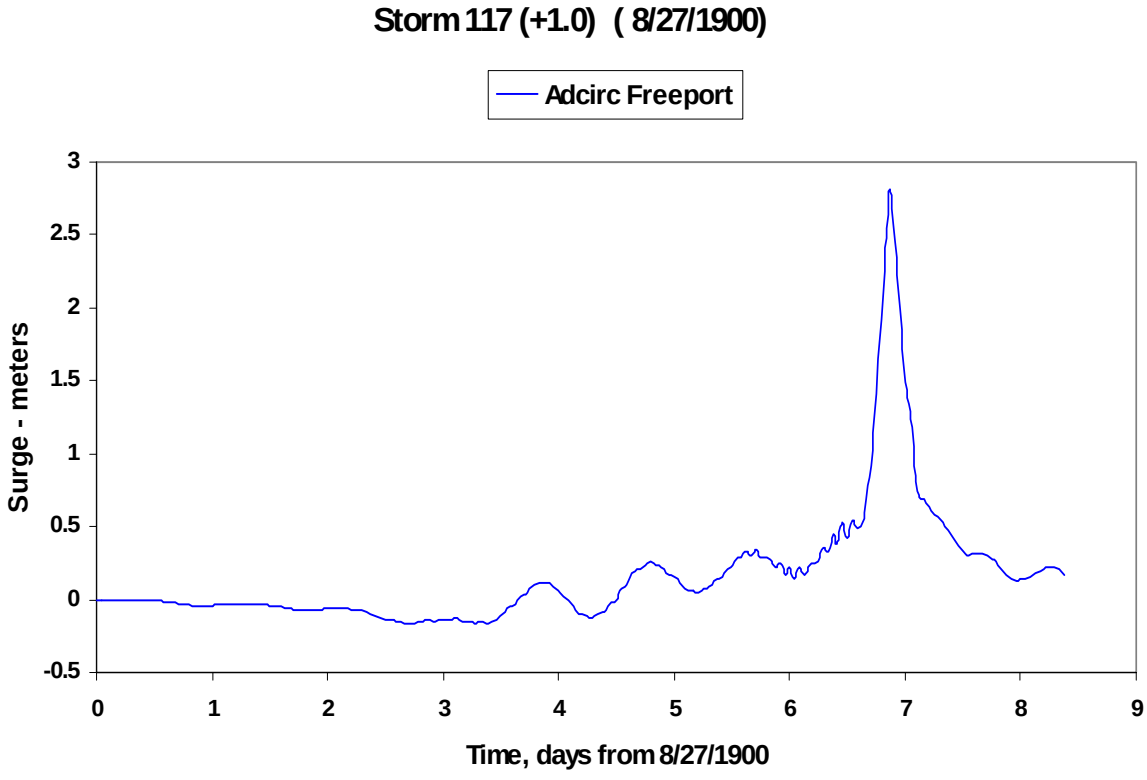
Storm 117 (+1.0) (8/27/1900)
Adcirc Freeport
Surge - meters
Time, days from 8/27/1900
3
2.5
2
1.5
1
0.5
0
-0.5
0
1
2
3
4
5
6
7
8
9

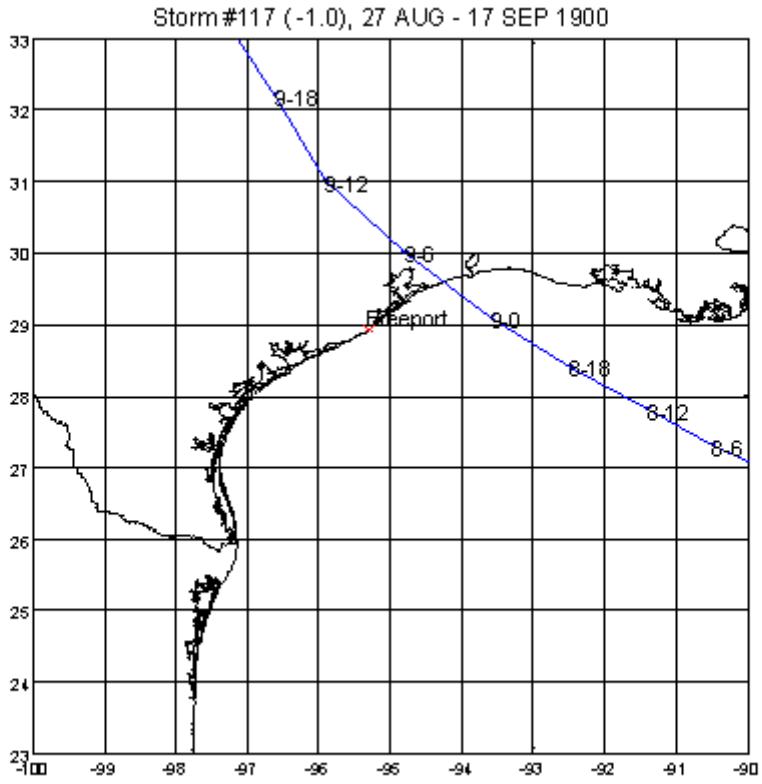
Storm #117 (-1.0), 27 AUG - 17 SEP 1900
9-18
9-12
9-6
Freeport
9-0
8-18
8-12
8-6
33
32
31
30
29
28
27
26
25
24
23
-100
-99
-98
-97
-96
-95
-94
-93
-92
-91
-90

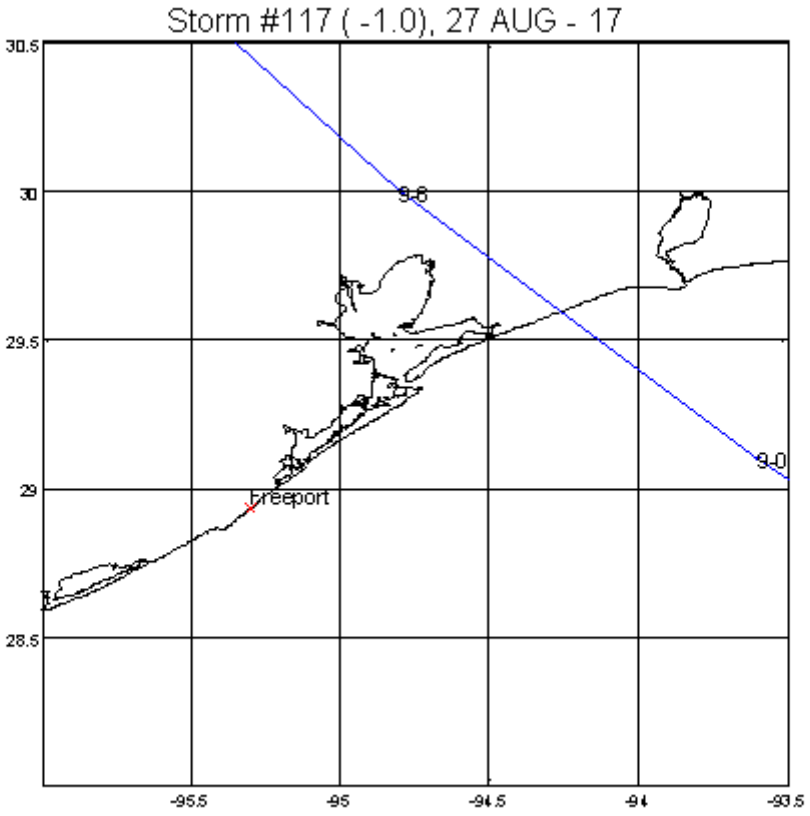
Storm #117 (-1.0), 27 AUG - 17
9-6
9-0
Freeport
30.5
30
29.5
29
28.5
-95.5
-95
-94.5
-94
-93.5

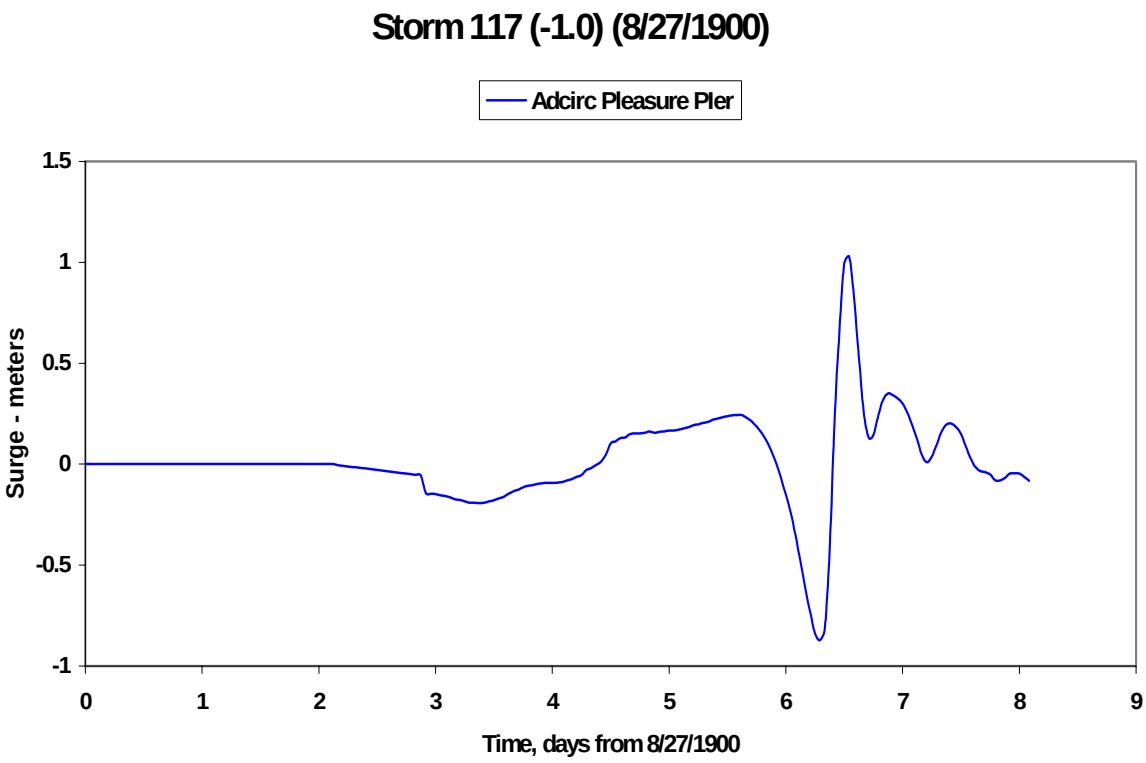
Storm 117 (-1.0) (8/27/1900)
Adcirc Pleasure Pier
Surge - meters
1.5
1
0.5
0
-0.5
-1
0
1
2
3
4
5
6
7
8
9
Time, days from 8/27/1900

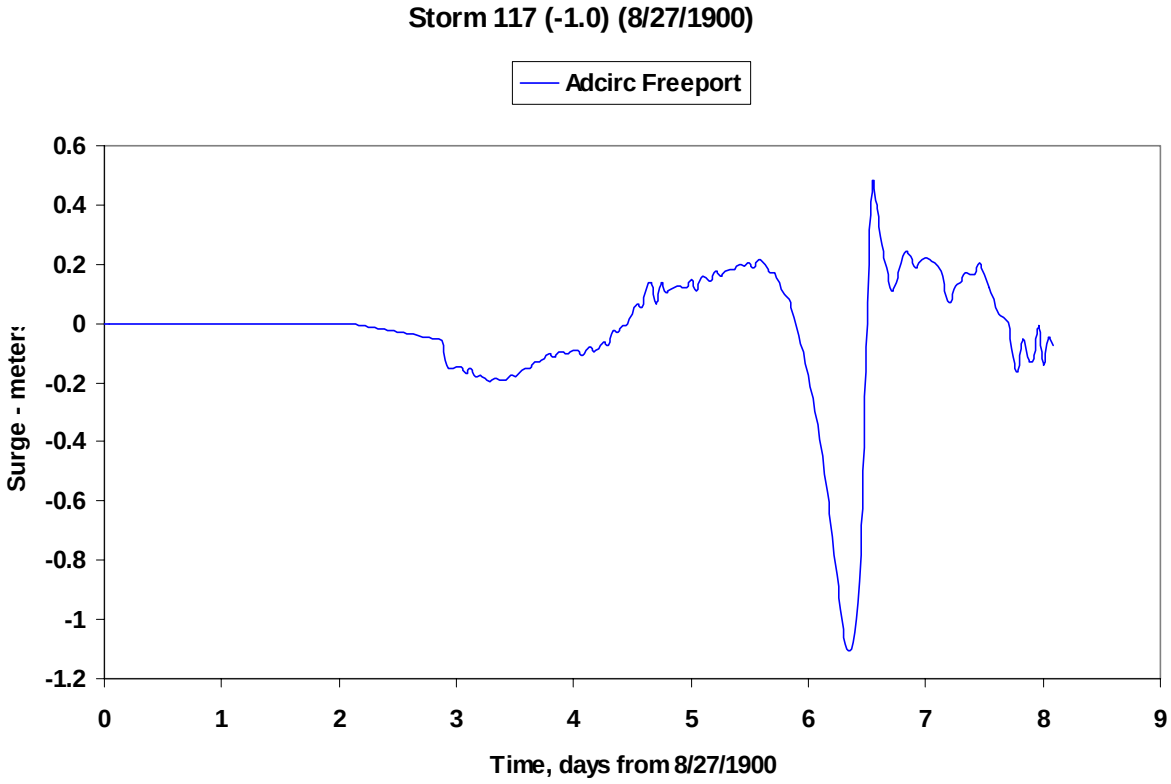
Storm 117 (-1.0) (8/27/1900)
Adcirc Freeport
Surge - meters
0.6
0.4
0.2
0
-0.2
-0.4
-0.6
-0.8
-1
-1.2
0
1
2
3
4
5
6
7
8
9
Time, days from 8/27/1900

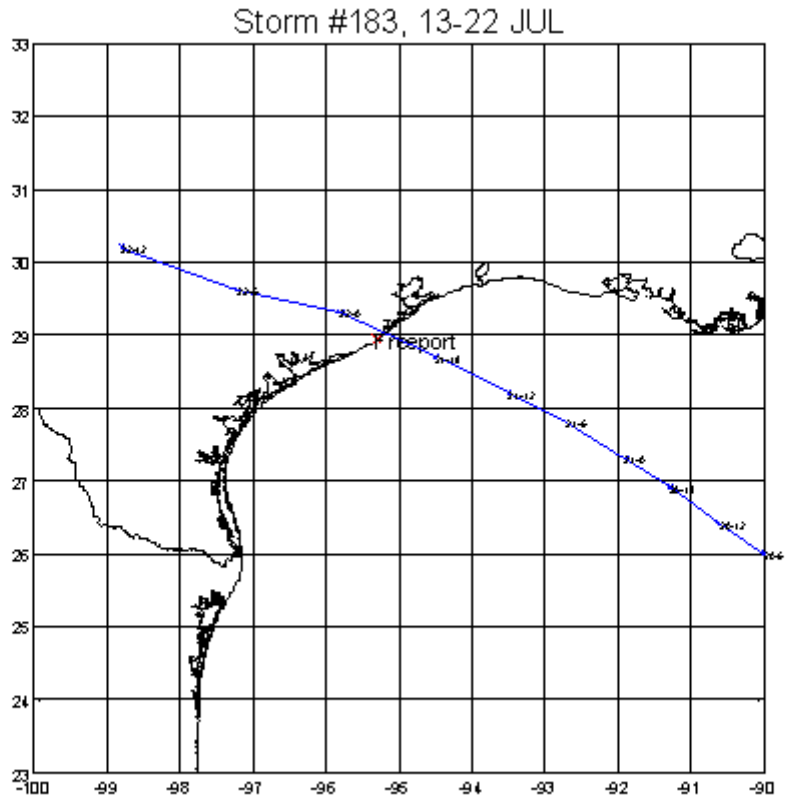
Storm #183, 13-22 JUL
Freeport

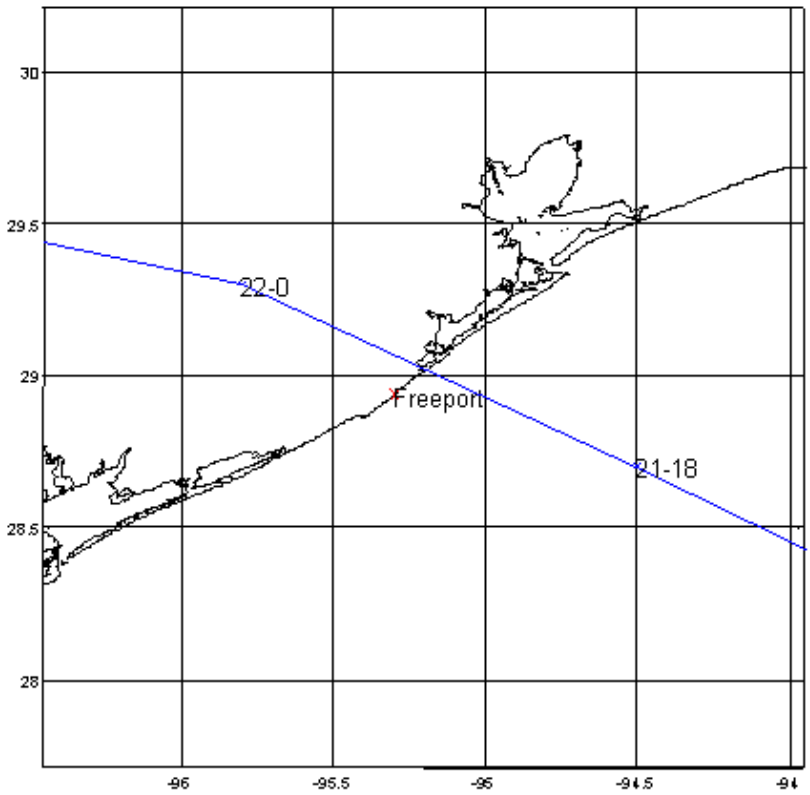
22-0
Freeport
21-18

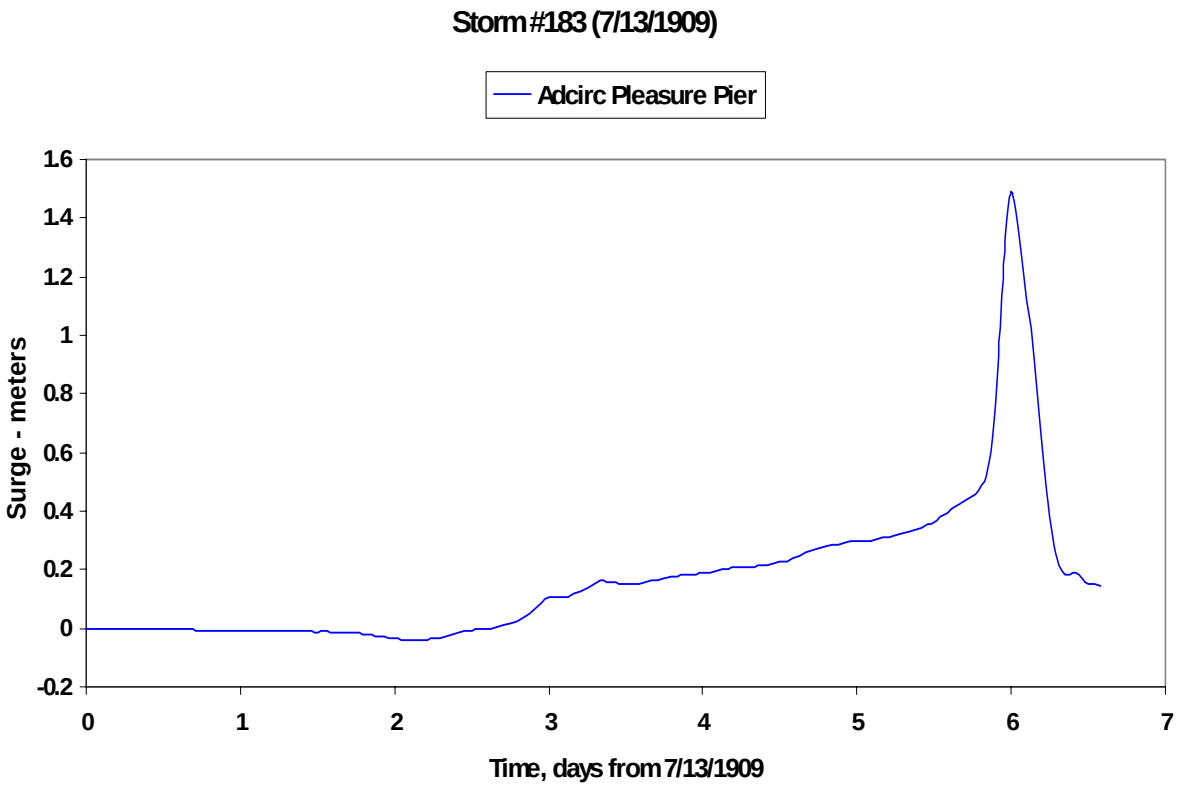
Storm #183 (7/13/1909)
Adcirc Pleasure Pier
Surge - meters
1.6
1.4
1.2
1
0.8
0.6
0.4
0.2
0
-0.2
0
1
2
3
4
5
6
7
Time, days from 7/13/1909

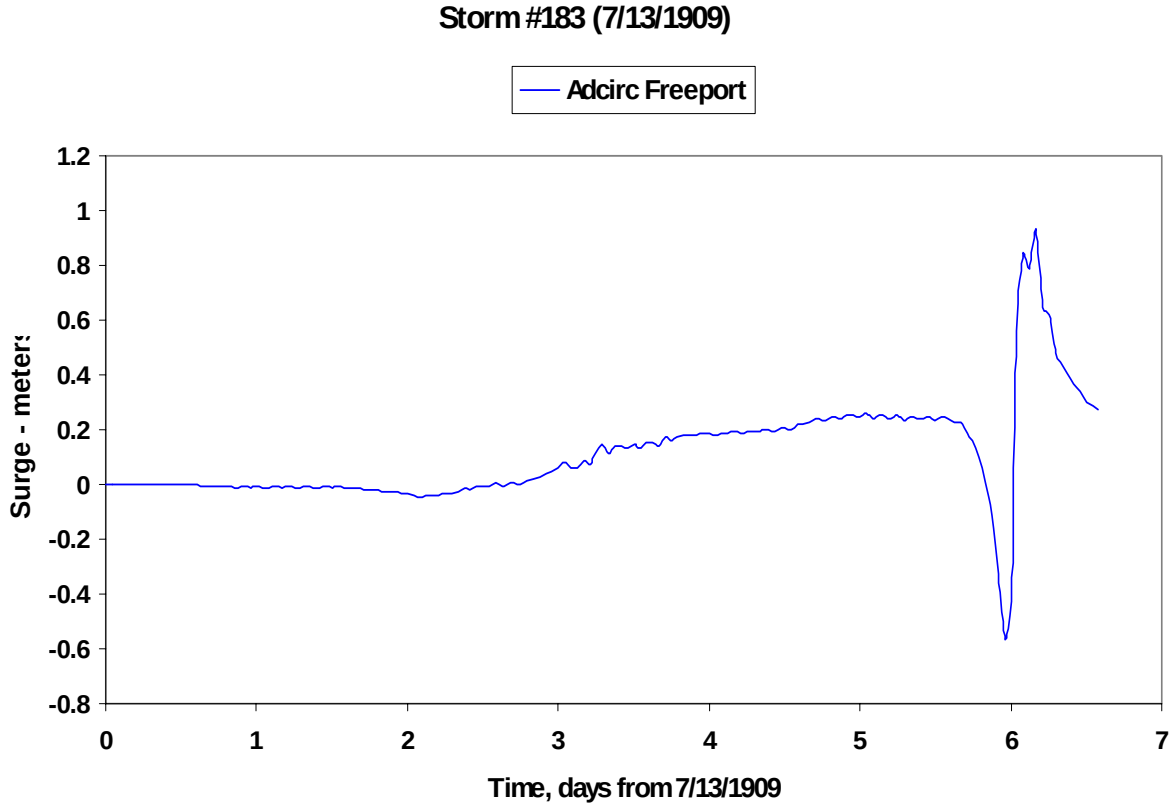
Storm #183 (7/13/1909)
Adcirc Freeport
Surge - meters
1.2
1
0.8
0.6
0.4
0.2
0
-0.2
-0.4
-0.6
-0.8
0
1
2
3
4
5
6
7
Time, days from 7/13/1909

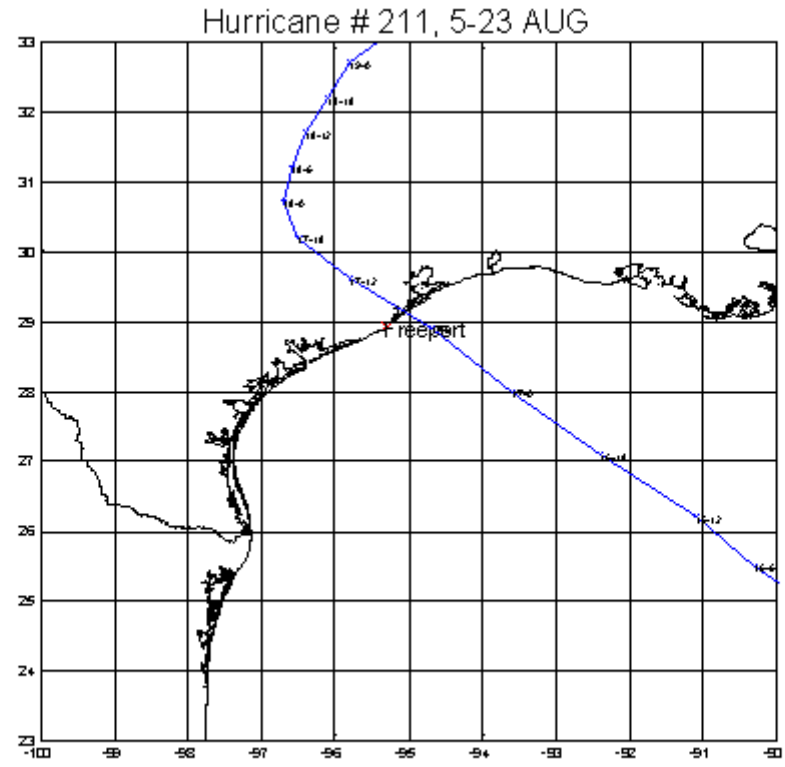

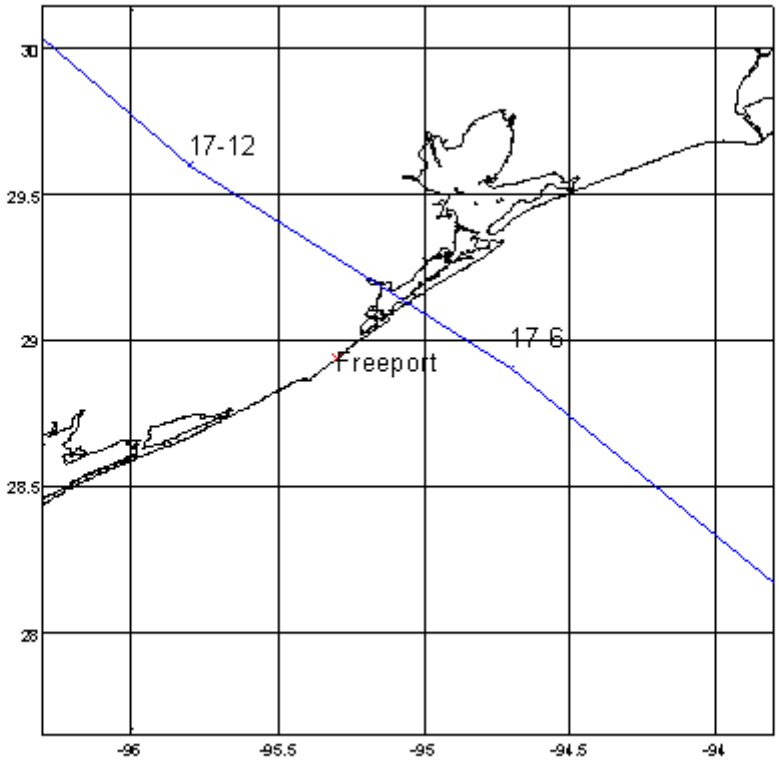

17-0

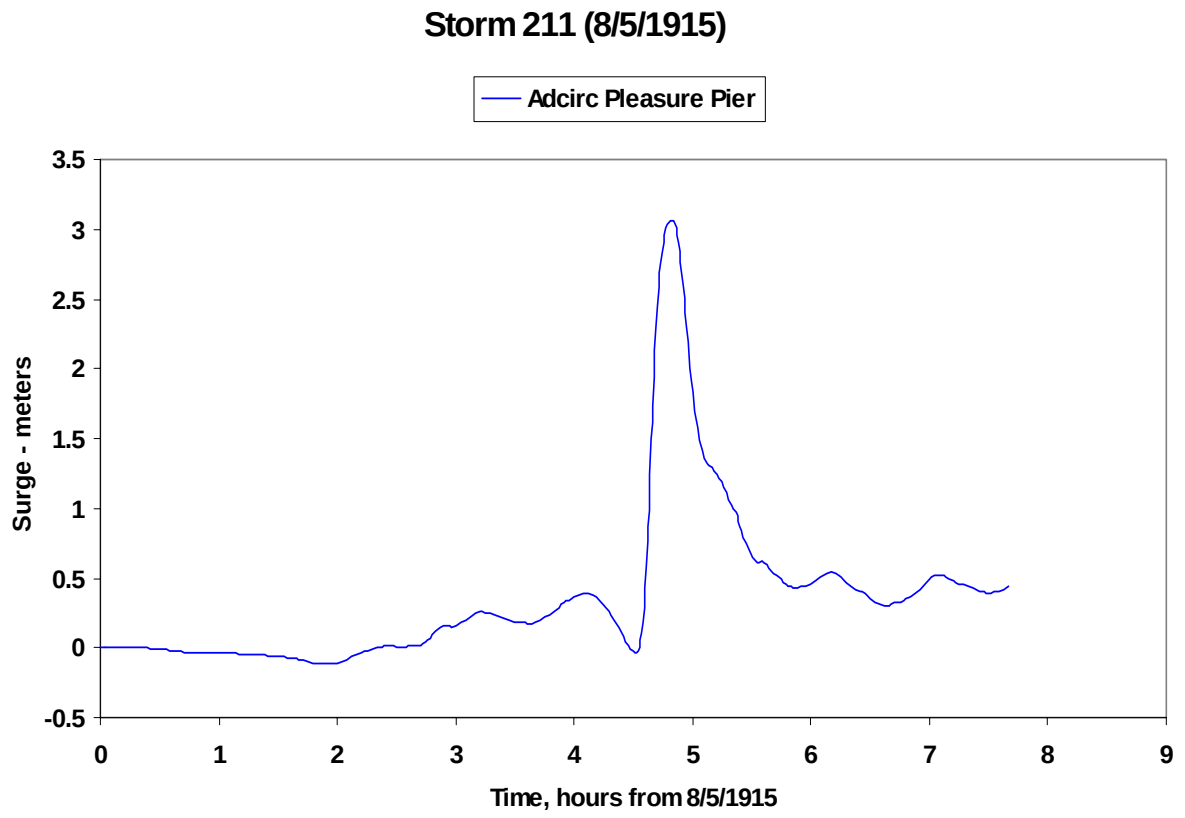
Storm 211 (8/5/1915)
Adcirc Pleasure Pier
Surge - meters
3.5
3
2.5
2
1.5
1
0.5
0
-0.5
0
1
2
3
4
5
6
7
8
9
Time, hours from 8/5/1915

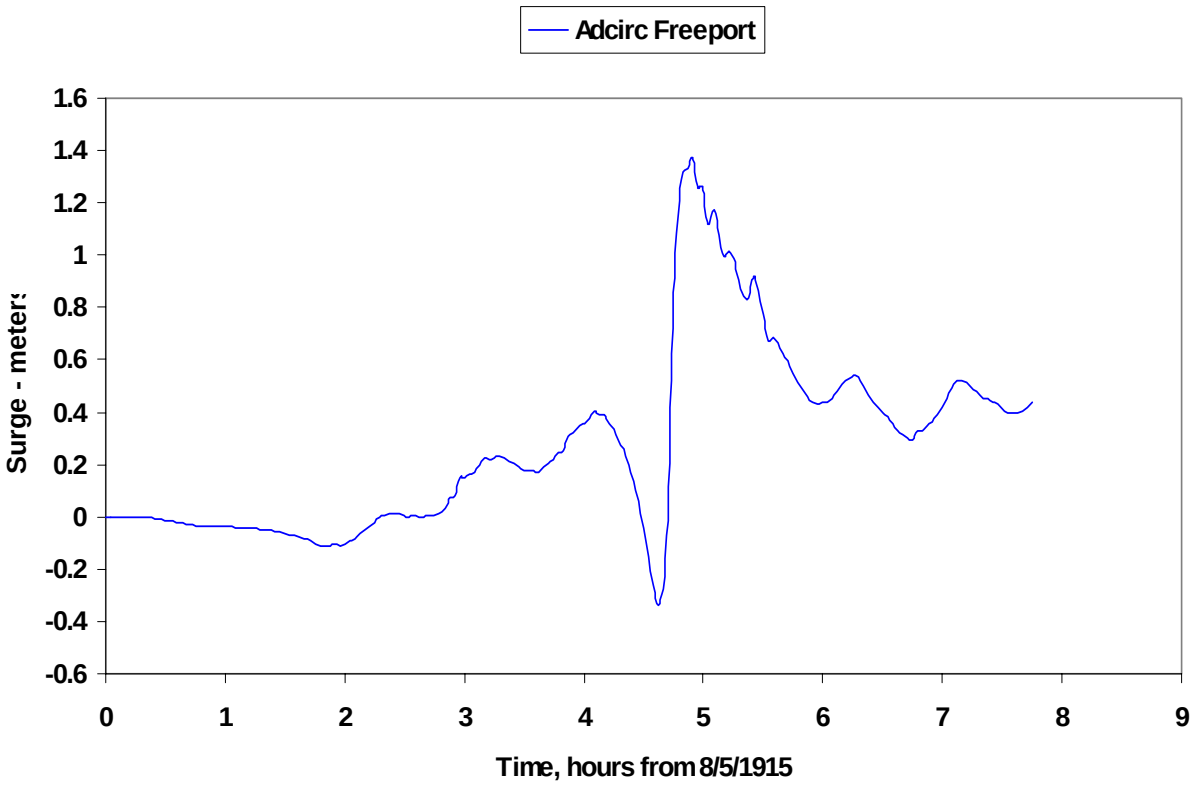
Storm 211 (8/5/1915)
Adcirc Freeport
Surge - meters
1.6
1.4
1.2
1
0.8
0.6
0.4
0.2
0
-0.2
-0.4
-0.6
0
1
2
3
4
5
6
7
8
9
Time, hours from 8/5/1915

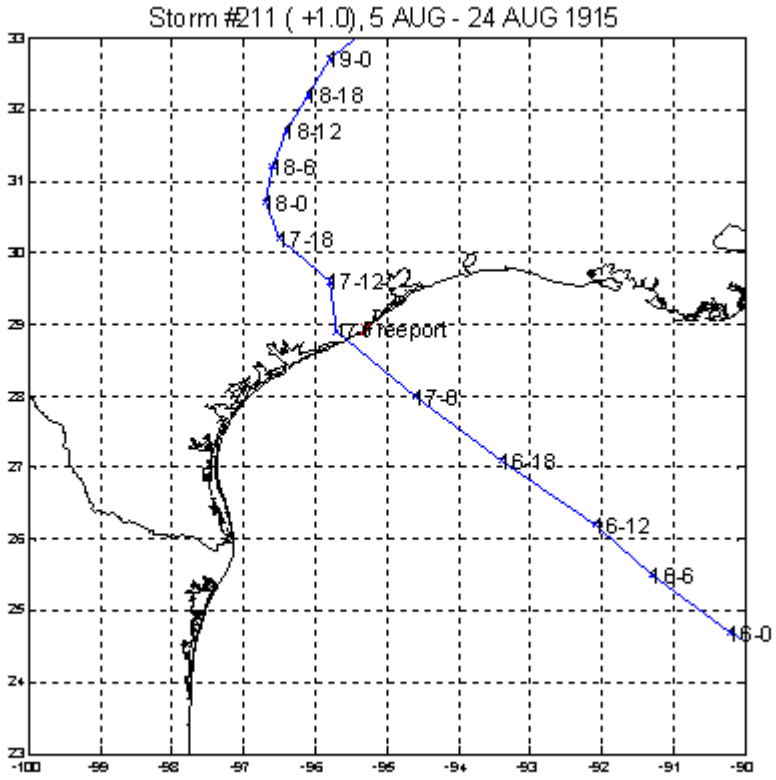
Storm #211 (+1.0), 5 AUG - 24 AUG 1915
19-0
18-18
18-12
18-6
18-0
17-18
17-12
Freeport
17-6
16-18
16-12
16-6
16-0

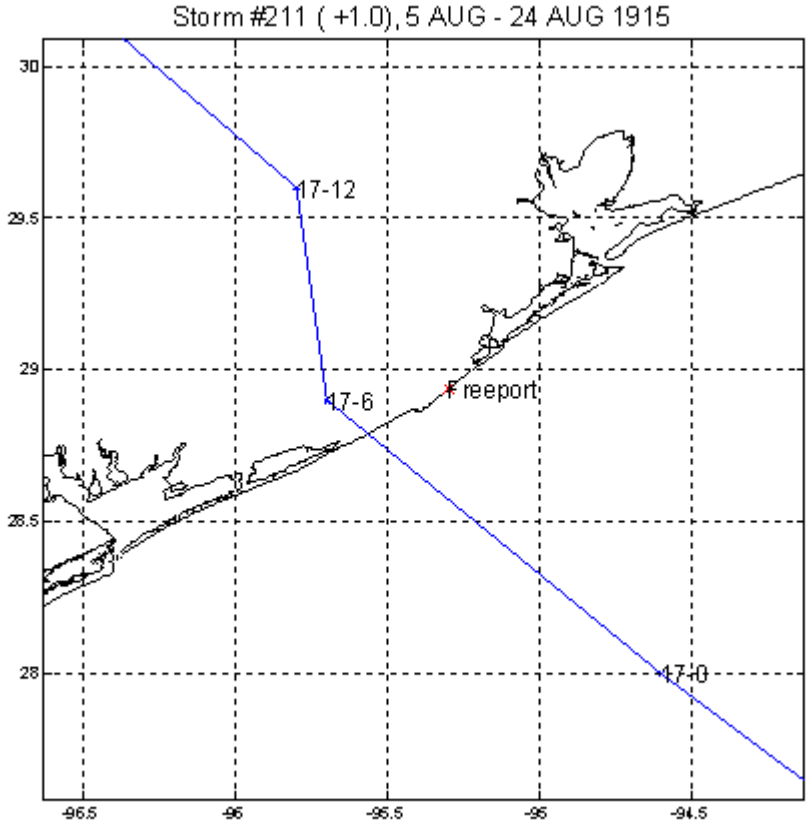
Storm #211 (+1.0), 5 AUG - 24 AUG 1915
17-12
17-6
Freeport
17-0

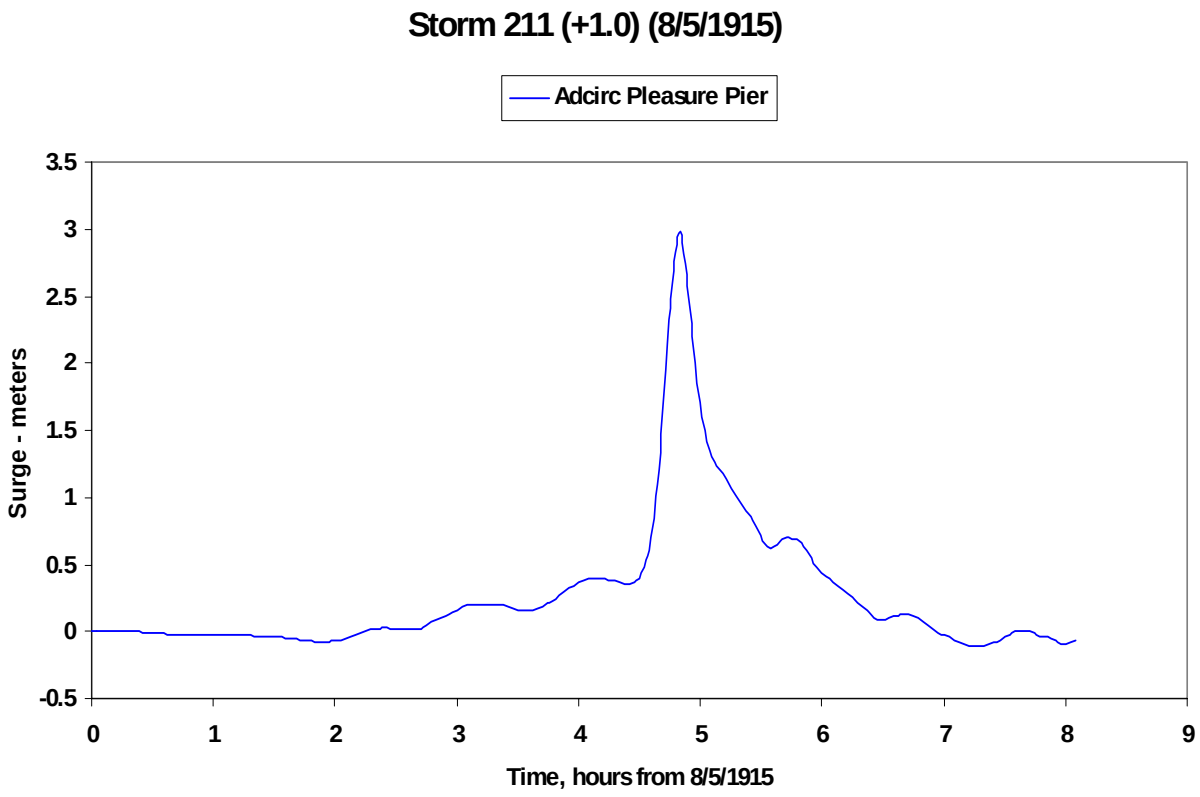
Storm 211 (+1.0) (8/5/1915)
Adcirc Pleasure Pier
Surge - meters
3.5
3
2.5
2
1.5
1
0.5
0
-0.5
0
1
2
3
4
5
6
7
8
9
Time, hours from 8/5/1915

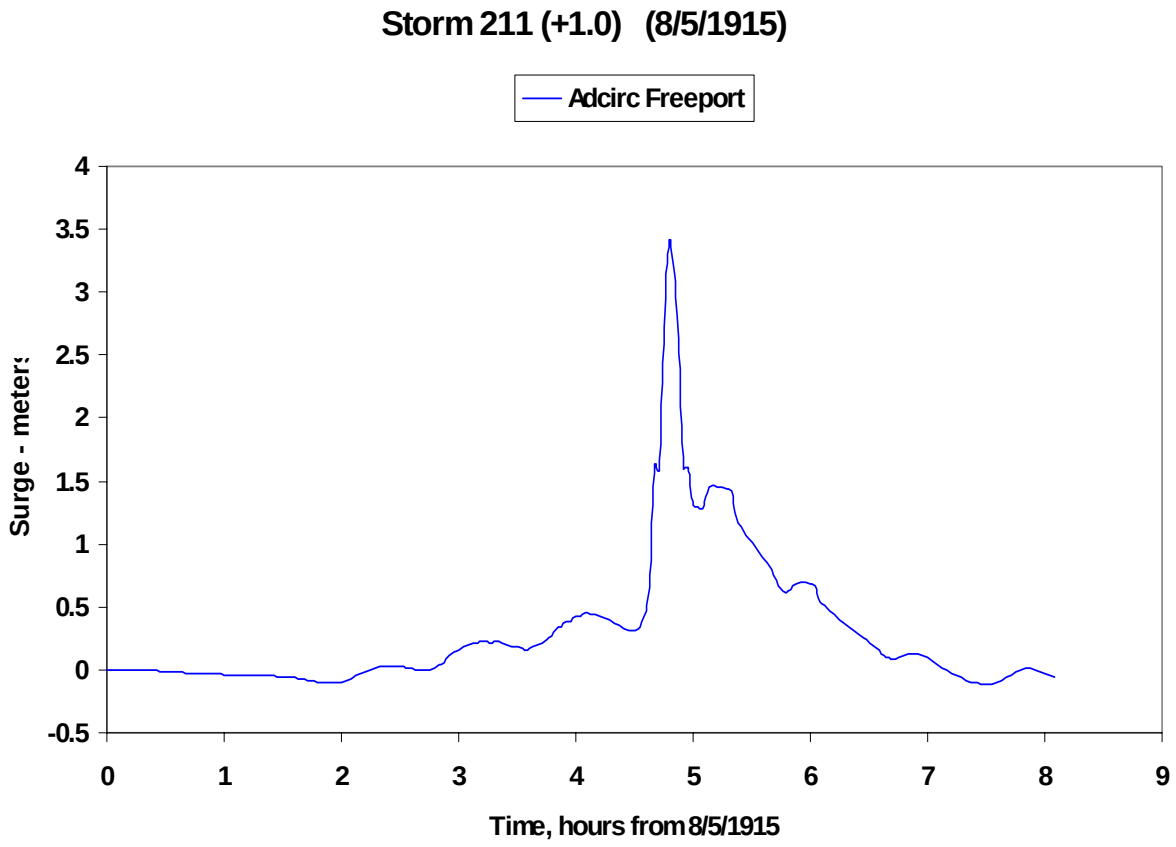
Storm 211 (+1.0) (8/5/1915)
Adcirc Freeport
Surge - meters
4
3.5
3
2.5
2
1.5
1
0.5
0
-0.5
0
1
2
3
4
5
6
7
8
9
Time, hours from 8/5/1915

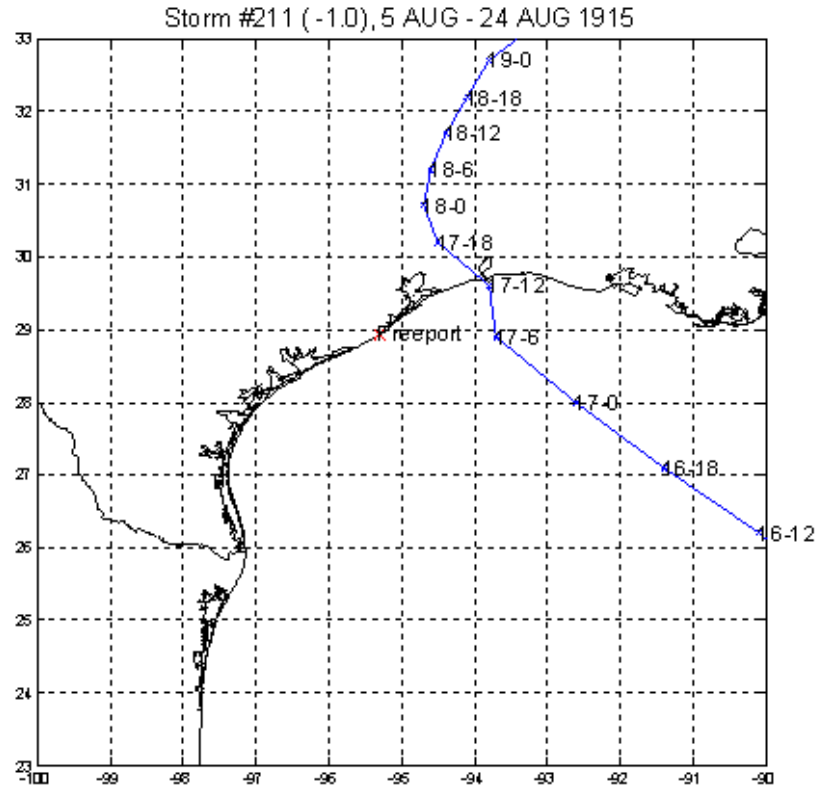
Storm #211 (-1.0), 5 AUG - 24 AUG 1915
19-0
18-18
18-12
18-6
18-0
17-18
17-12
Freeport
17-6
17-0
16-18
16-12
33
32
31
30
29
28
27
26
25
24
23
-100
-99
-98
-97
-96
-95
-94
-93
-92
-91
-90

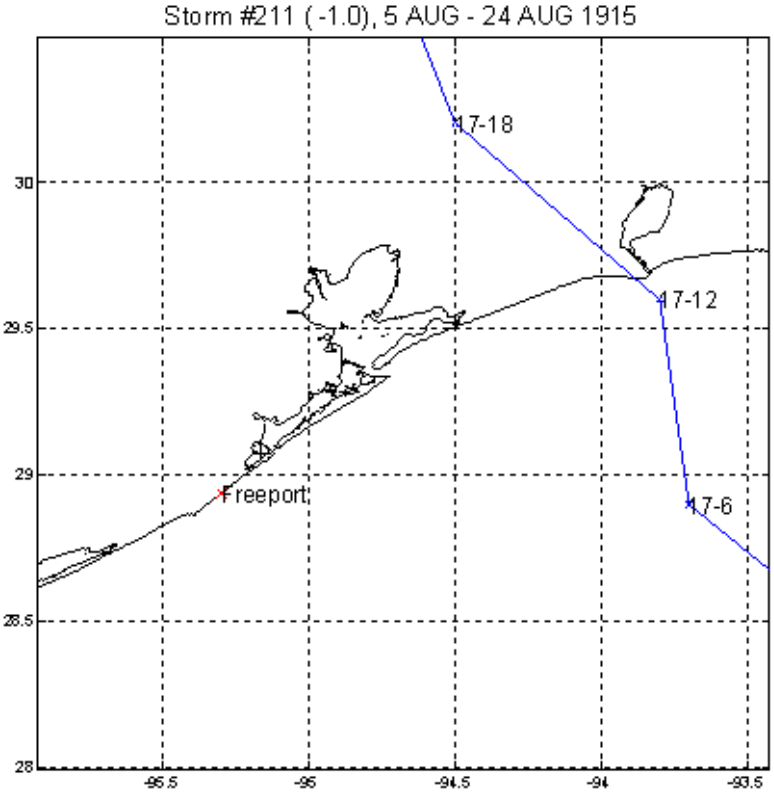
Storm #211 (-1.0), 5 AUG - 24 AUG 1915
17-18
17-12
Freeport
17-6
30
29.5
29
28.5
28
-95.5
-95
-94.5
-94
-93.5

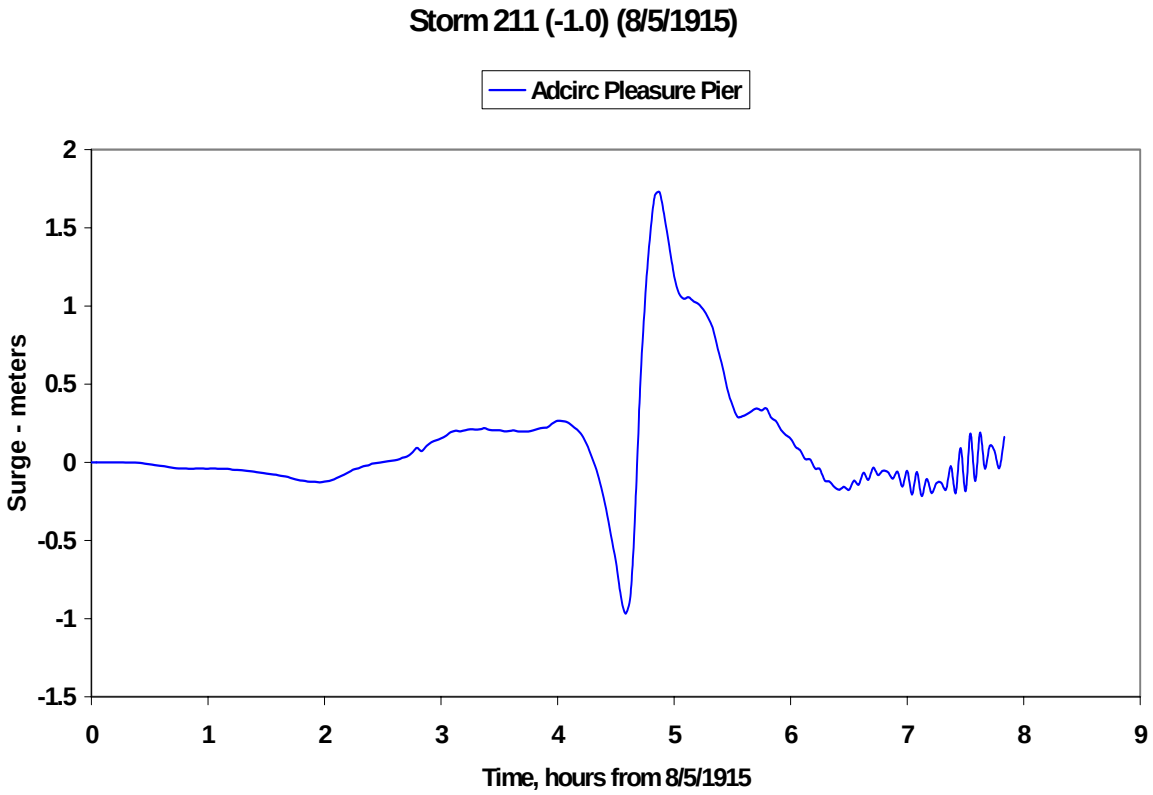
Storm 211 (-1.0) (8/5/1915)
Adcirc Pleasure Pier
Surge - meters
2
1.5
1
0.5
0
-0.5
-1
-1.5
0
1
2
3
4
5
6
7
8
9
Time, hours from 8/5/1915

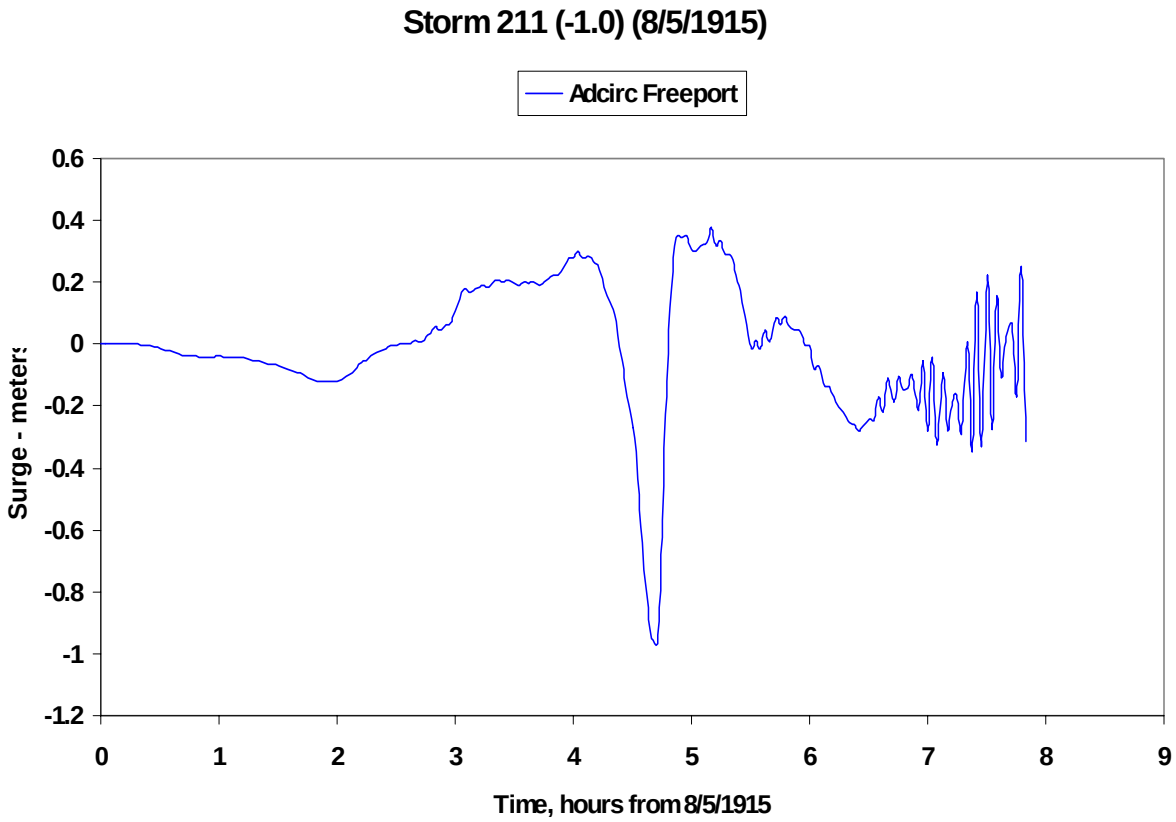
Storm 211 (-1.0) (8/5/1915)
Adcirc Freeport
Surge - meters
0.6
0.4
0.2
0
-0.2
-0.4
-0.6
-0.8
-1
-1.2
0
1
2
3
4
5
6
7
8
9
Time, hours from 8/5/1915

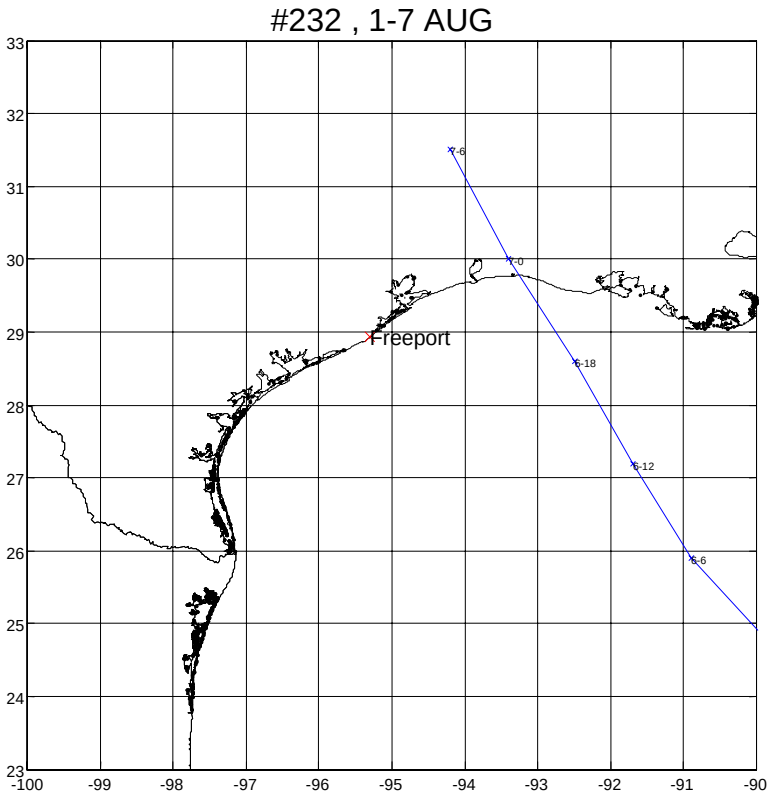
#232 , 1-7 AUG
Freeport
7-6
7-0
6-18
6-12
6-6

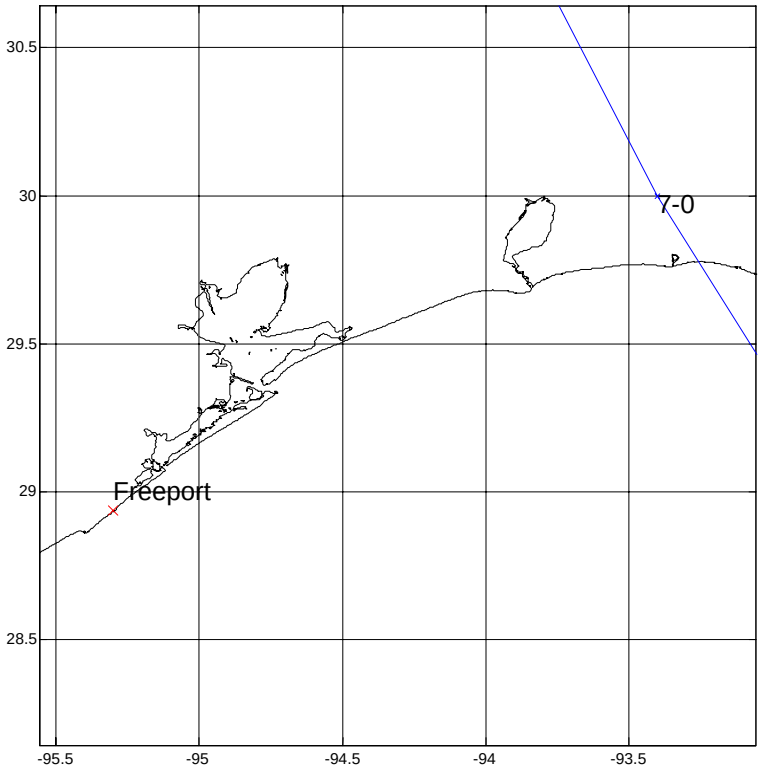
Freeport
7-0
P

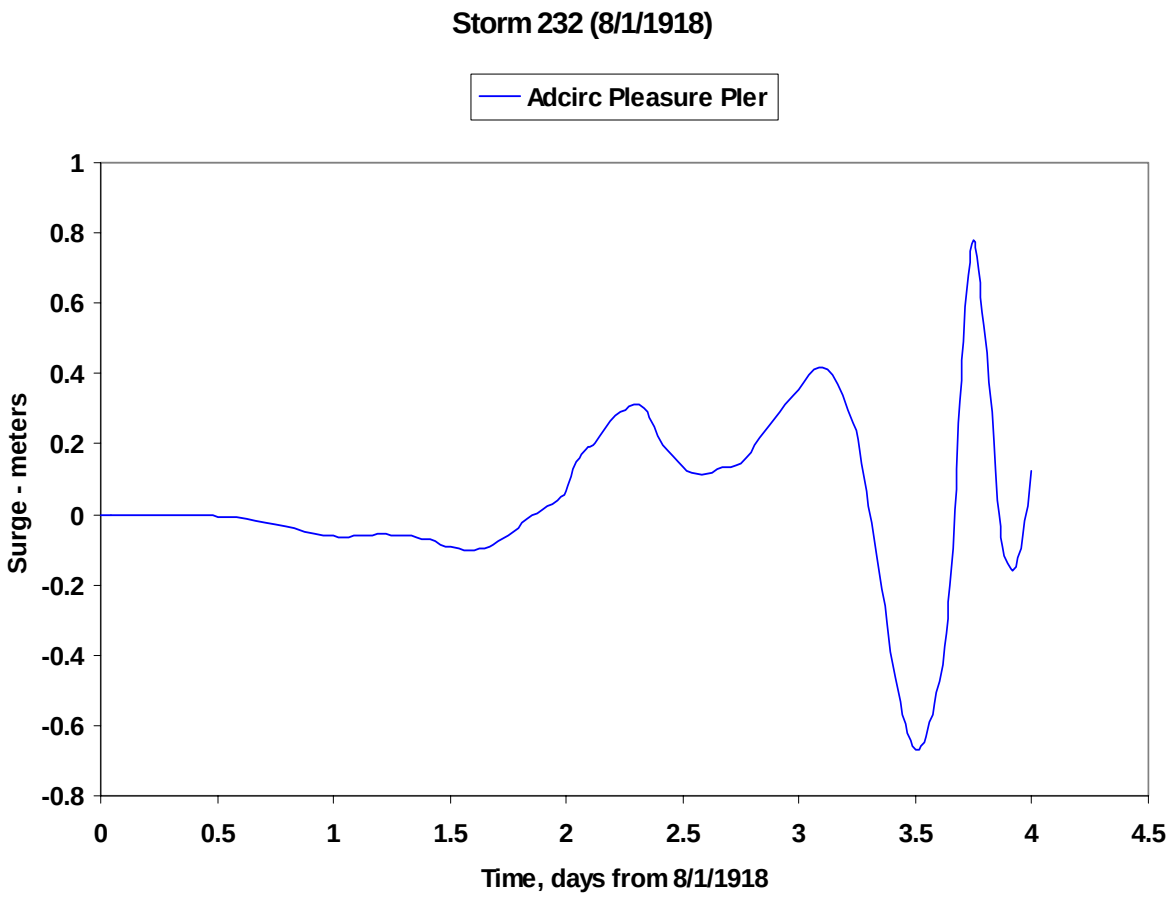
Storm 232 (8/1/1918)
Adcirc Pleasure Pier
Surge - meters
1
0.8
0.6
0.4
0.2
0
-0.2
-0.4
-0.6
-0.8
0
0.5
1
1.5
2
2.5
3
3.5
4
4.5
Time, days from 8/1/1918

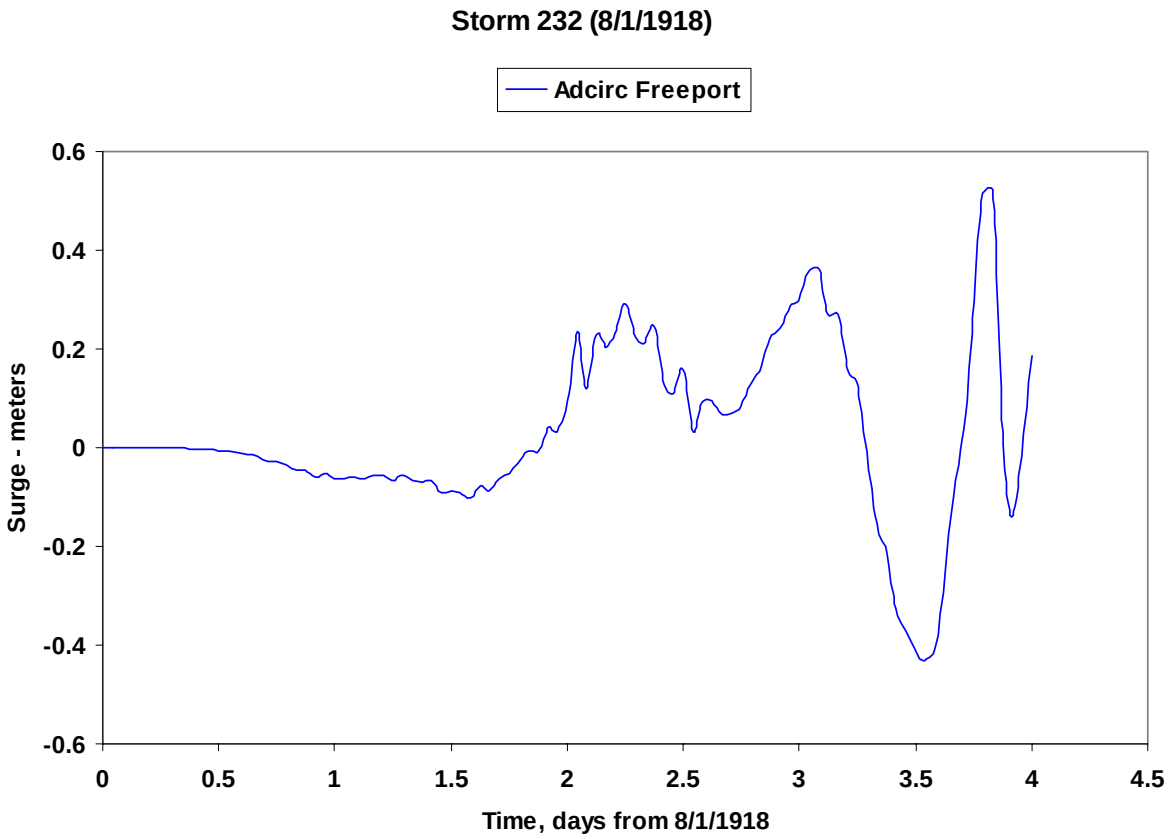
Storm 232 (8/1/1918)
Adcirc Freeport
Surge - meters
0.6
0.4
0.2
0
-0.2
-0.4
-0.6
0
0.5
1
1.5
2
2.5
3
3.5
4
4.5
Time, days from 8/1/1918

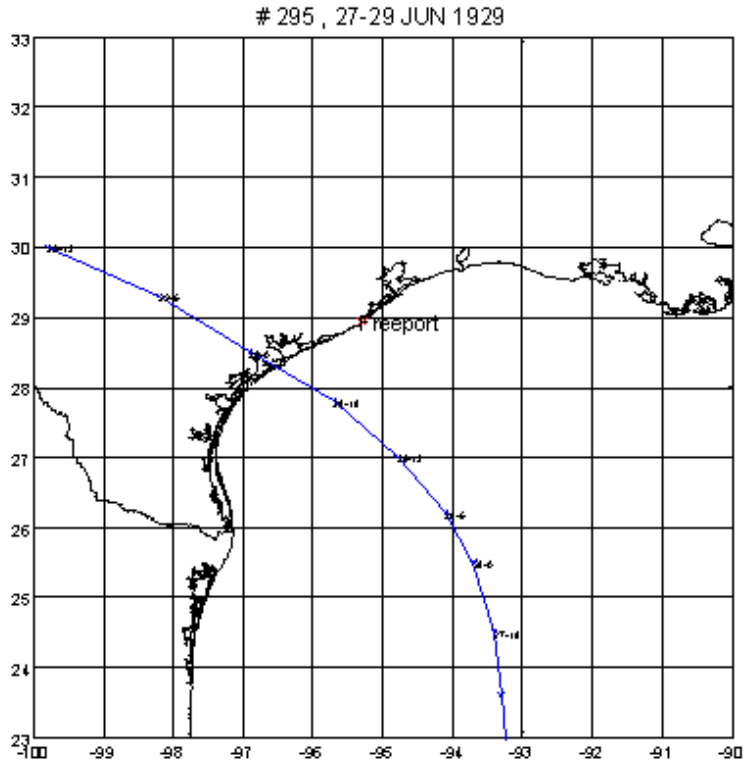
295 , 27-29 JUN 1929
Freeport

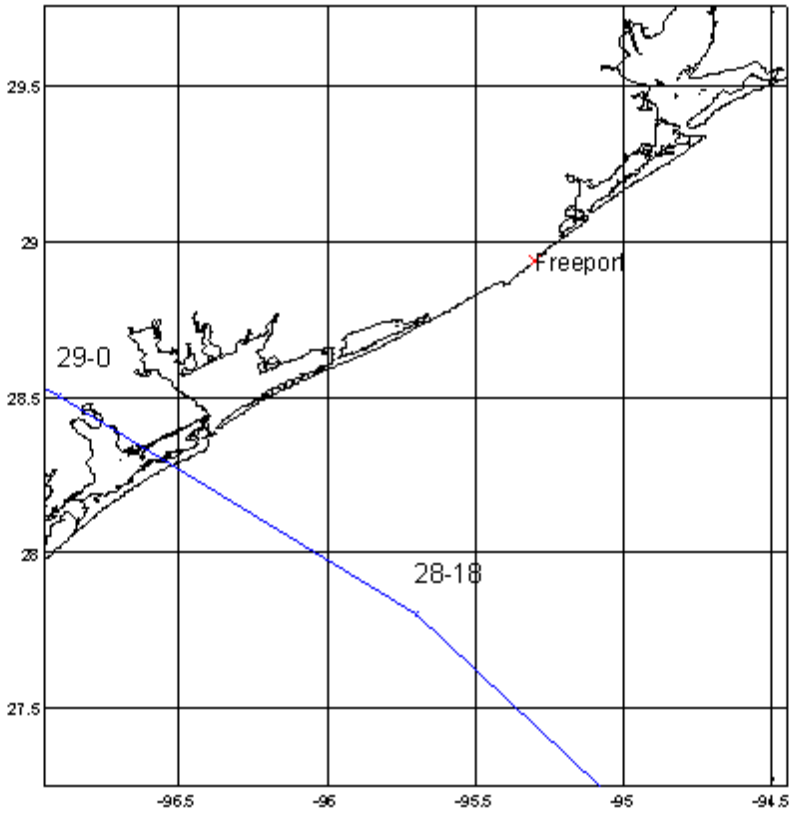
Freeport
29-0
28-18

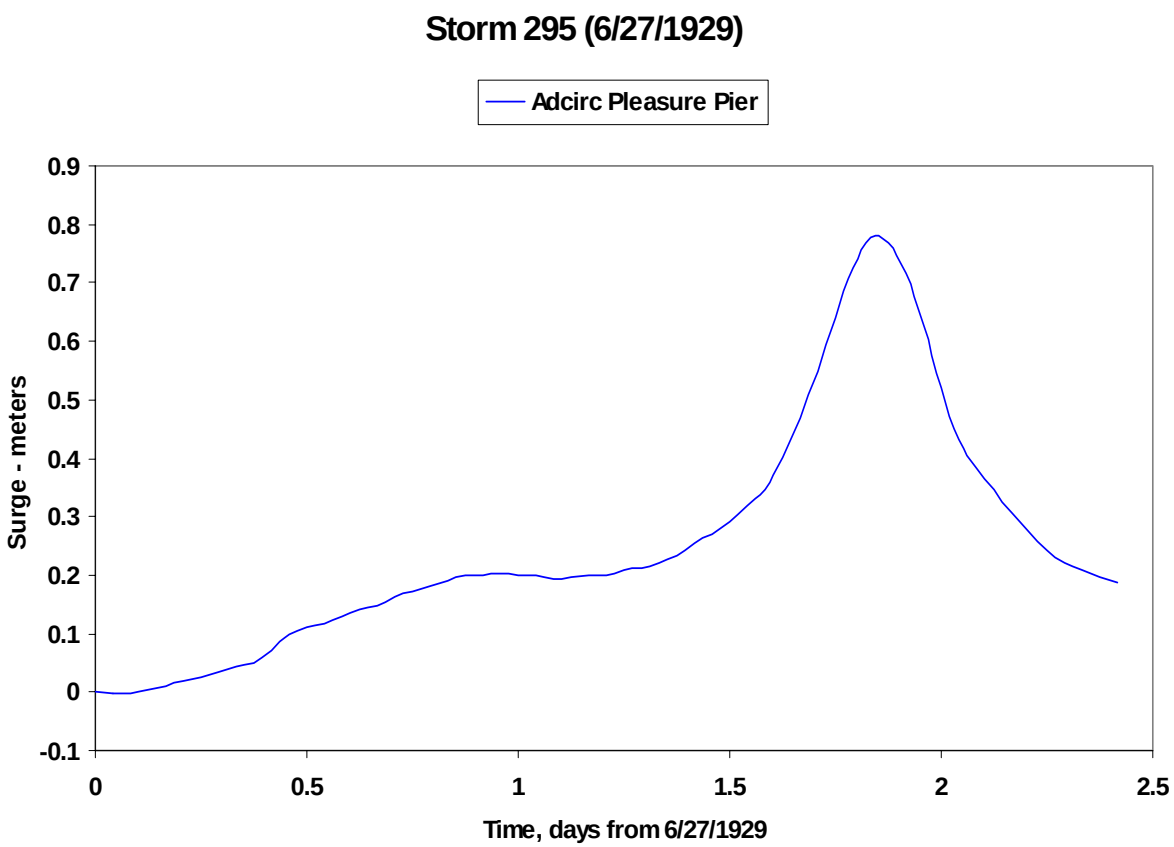
Storm 295 (6/27/1929)
Adcirc Pleasure Pier
Surge - meters
0.9
0.8
0.7
0.6
0.5
0.4
0.3
0.2
0.1
0
-0.1
0
0.5
1
1.5
2
2.5
Time, days from 6/27/1929

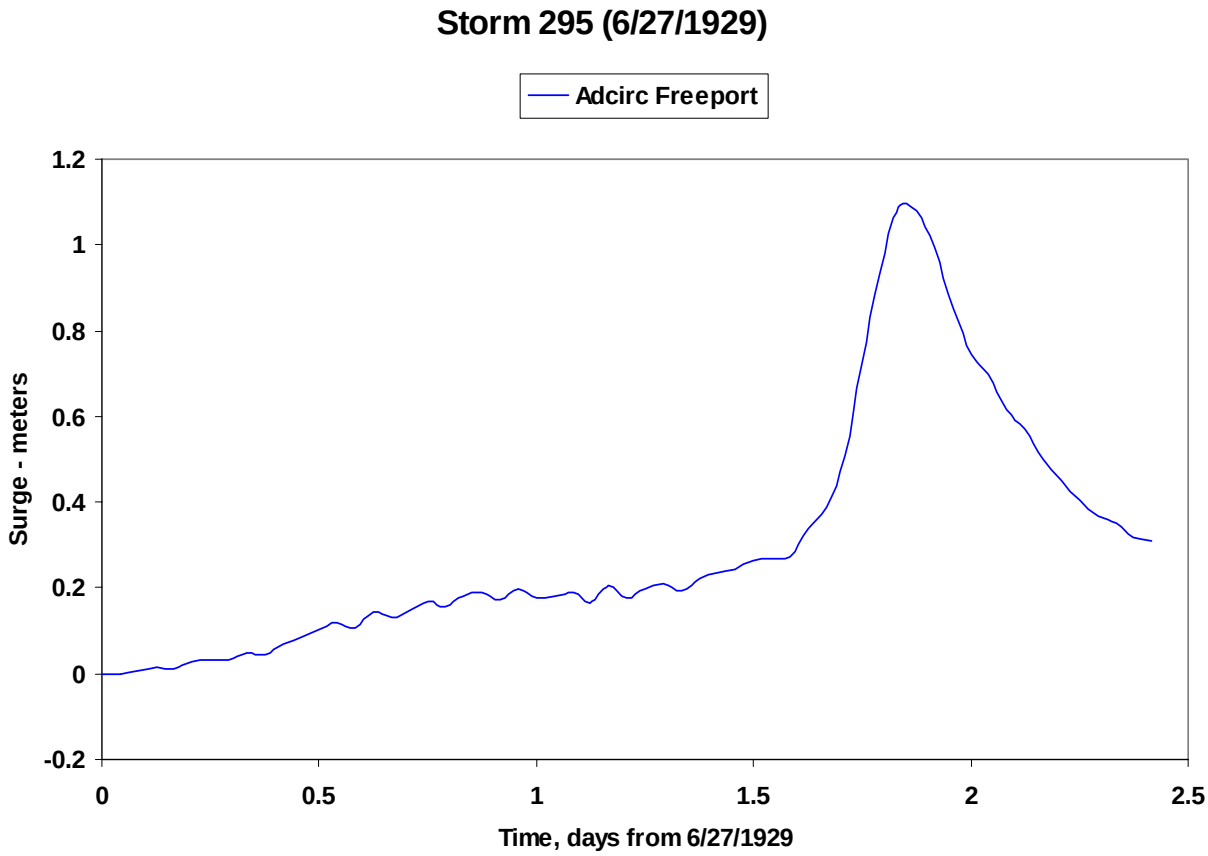
Storm 295 (6/27/1929)
Adcirc Freeport
Surge - meters
1.2
1
0.8
0.6
0.4
0.2
0
-0.2
0
0.5
1
1.5
2
2.5
Time, days from 6/27/1929

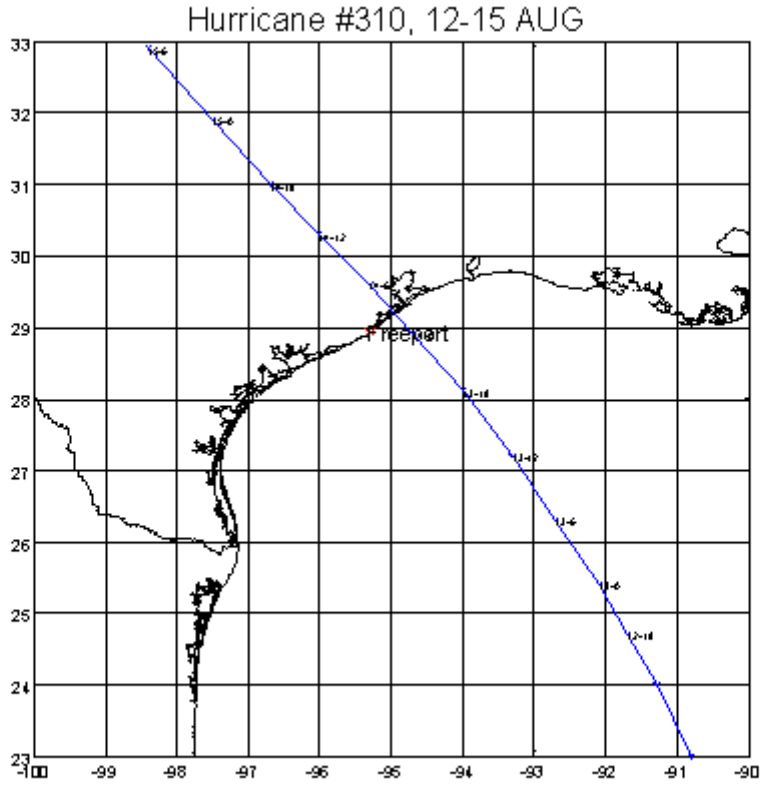
Hurricane #310, 12-15 AUG
Freeport
33
32
31
30
29
28
27
26
25
24
23
-100
-99
-98
-97
-96
-95
-94
-93
-92
-91
-90

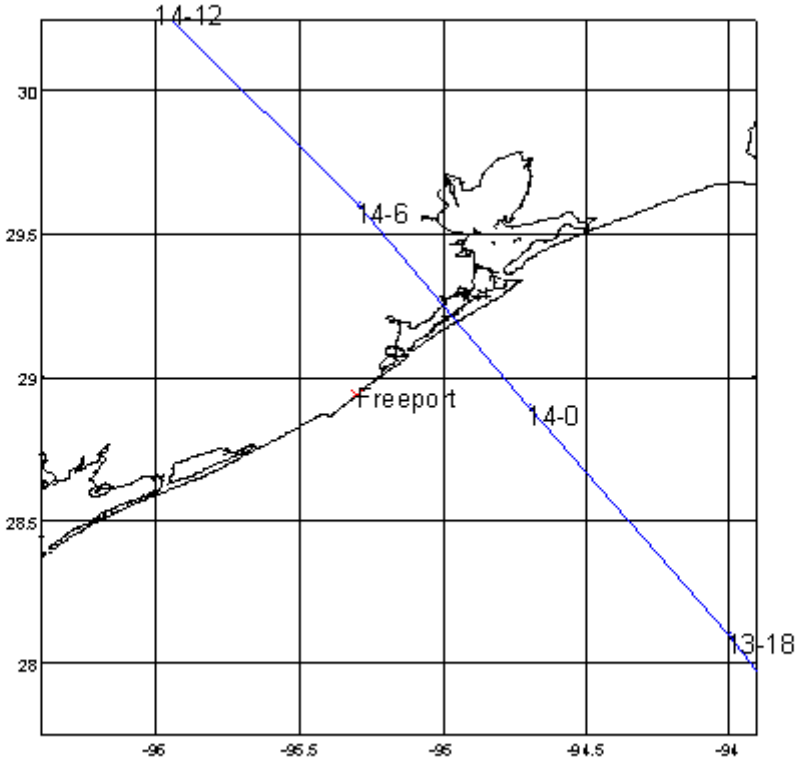
14-12
14-6
14-0
13-18
Freeport
30
29.5
29
28.5
28
-96
-95.5
-95
-94.5
-94

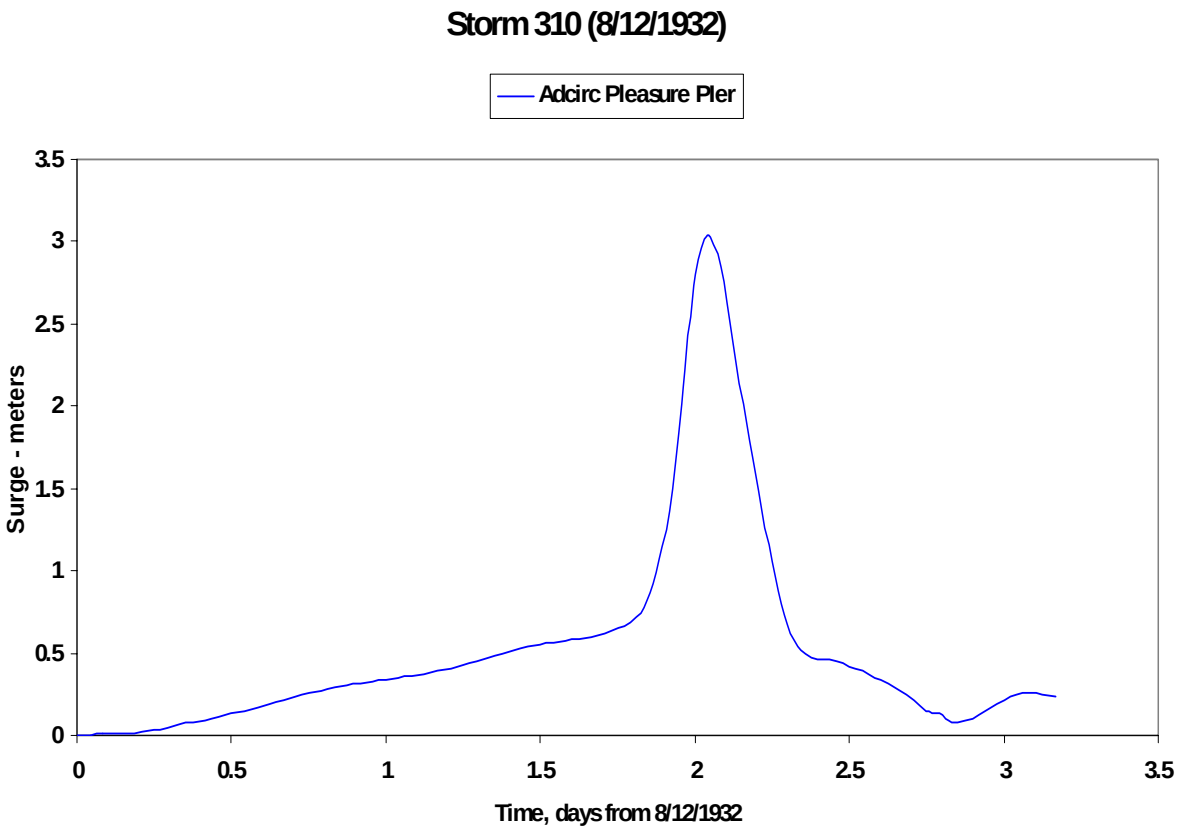
Storm 310 (8/12/1932)
Adcirc Pleasure Pier
Surge - meters
Time, days from 8/12/1932
0
0.5
1
1.5
2
2.5
3
3.5

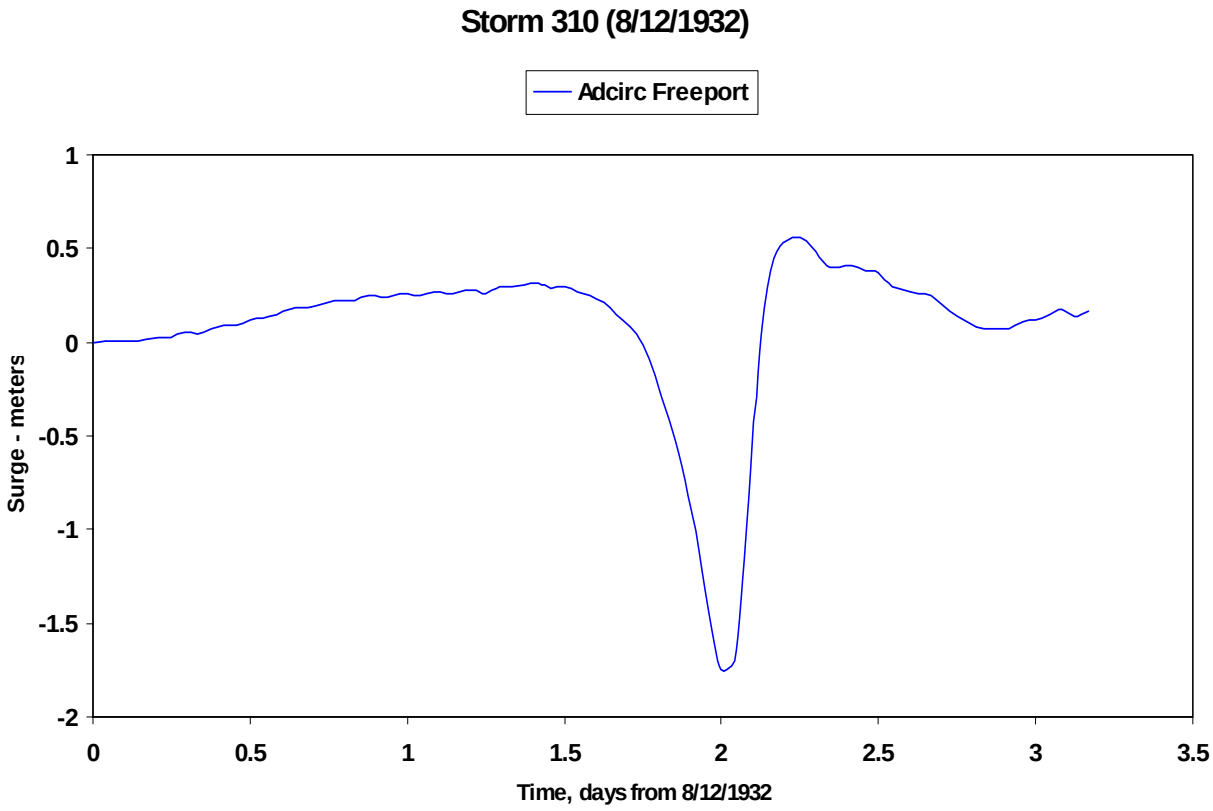
Storm 310 (8/12/1932)
Adcirc Freeport
Surge - meters
Time, days from 8/12/1932
1
0.5
0
-0.5
-1
-1.5
-2
0
0.5
1
1.5
2
2.5
3
3.5

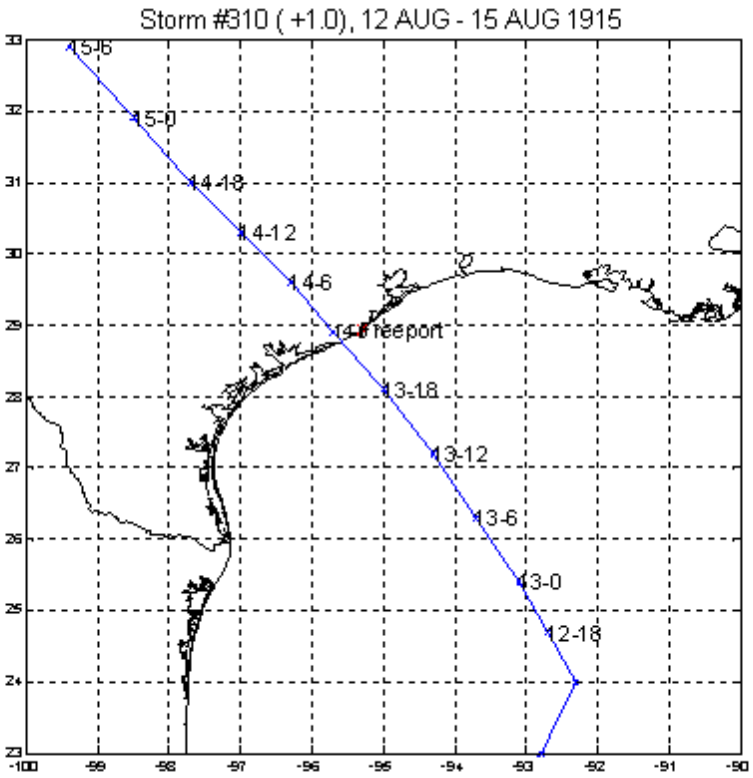
Storm #310 (+1.0), 12 AUG - 15 AUG 1915
15-6
15-0
14-18
14-12
14-6
14-0
Freeport
13-18
13-12
13-6
13-0
12-18

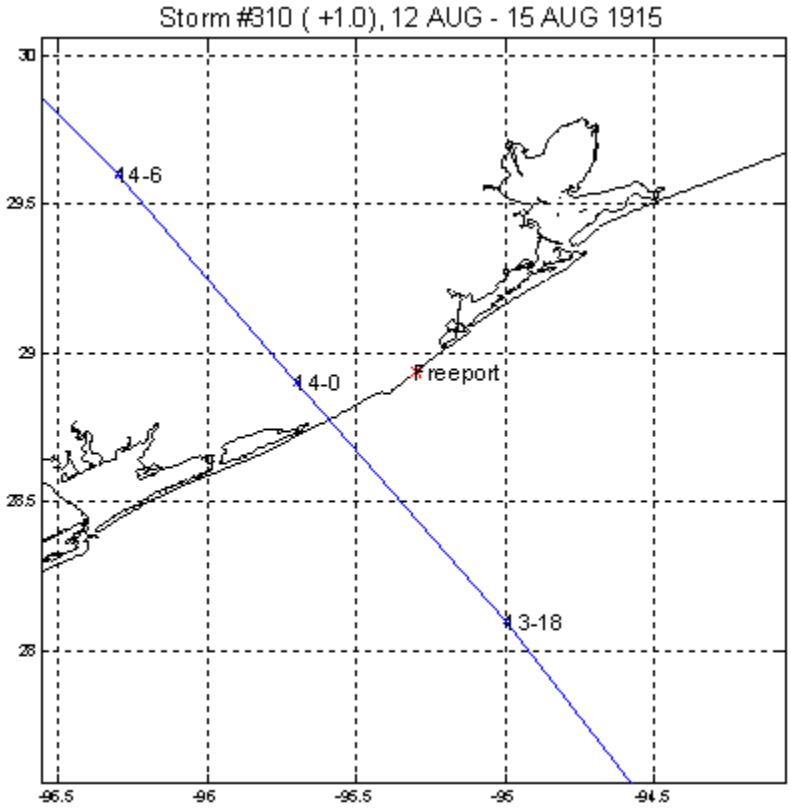
Storm #310 (+1.0), 12 AUG - 15 AUG 1915
14-6
14-0
Freeport
13-18

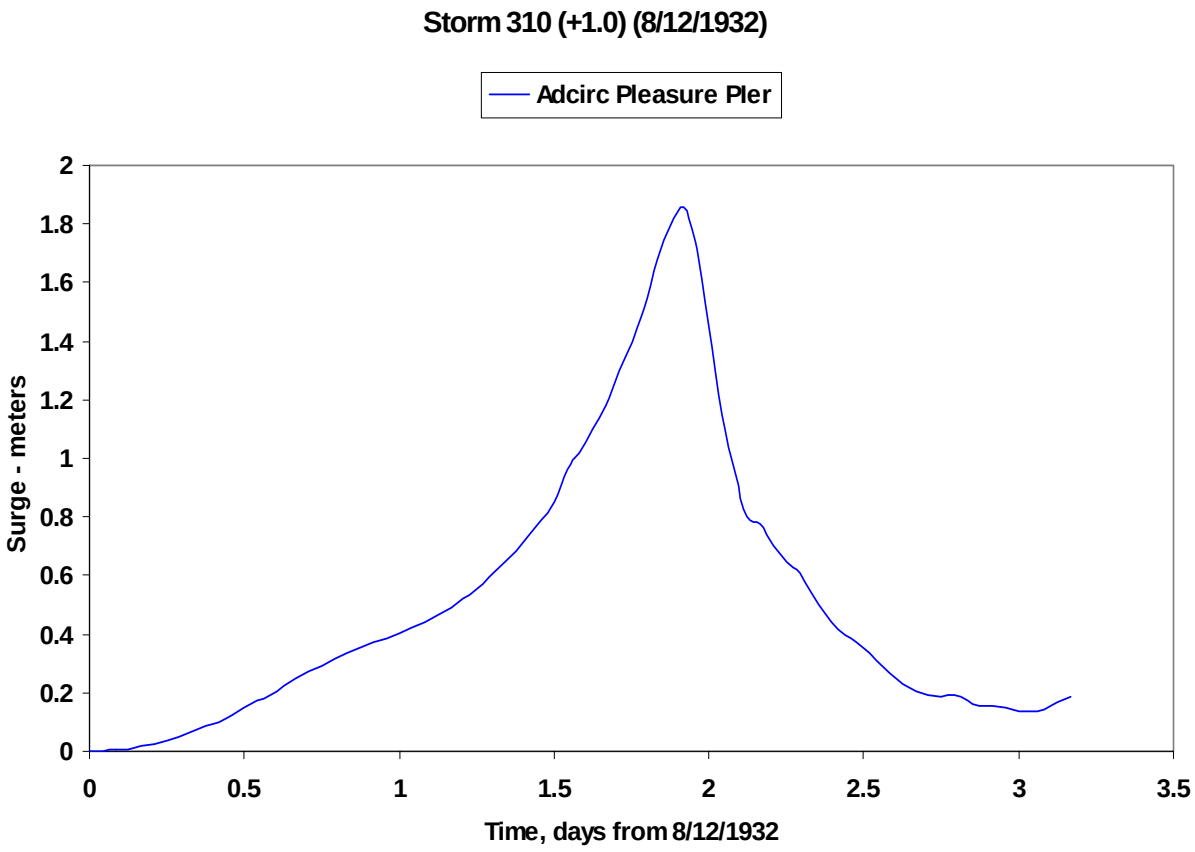
Storm 310 (+1.0) (8/12/1932)
Adcirc Pleasure Pier
Surge - meters
0
0.2
0.4
0.6
0.8
1
1.2
1.4
1.6
1.8
2
0
0.5
1
1.5
2
2.5
3
3.5
Time, days from 8/12/1932

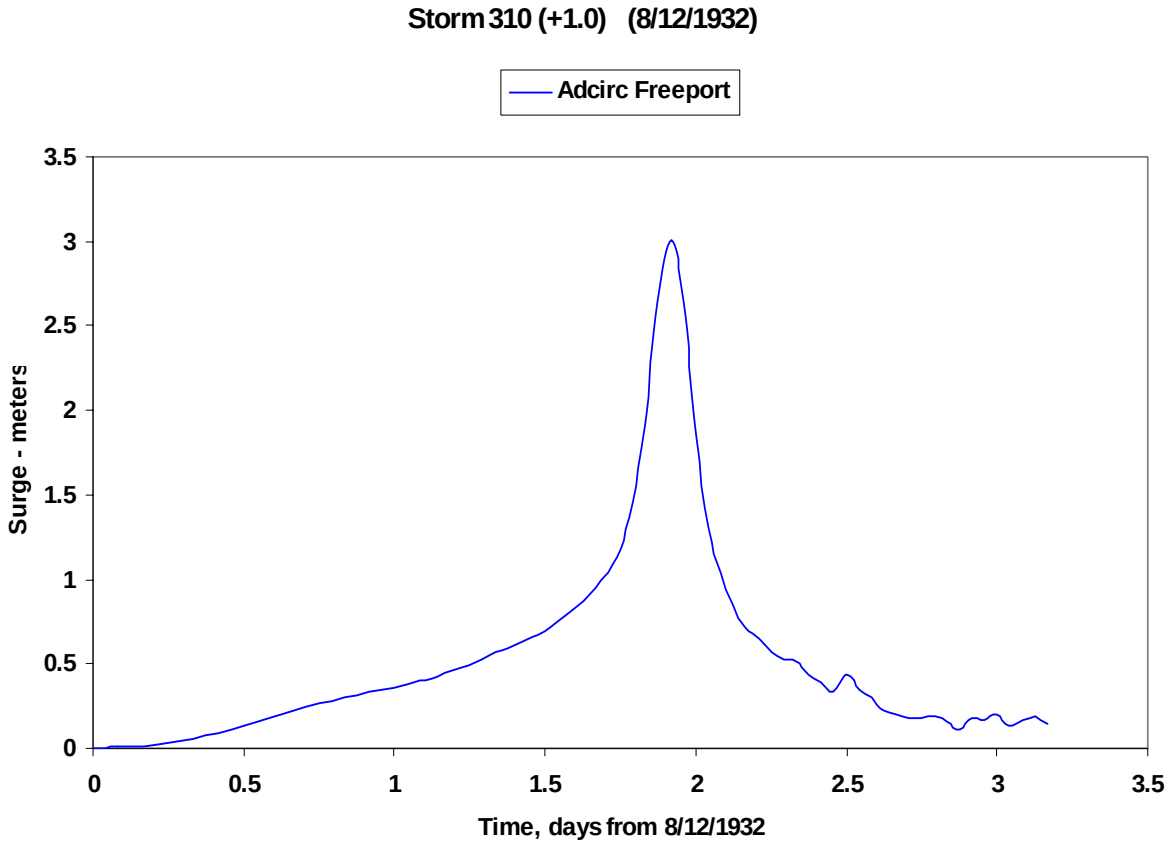
Storm 310 (+1.0) (8/12/1932)
Adcirc Freeport
Surge - meters
0
0.5
1
1.5
2
2.5
3
3.5
0
0.5
1
1.5
2
2.5
3
3.5
Time, days from 8/12/1932

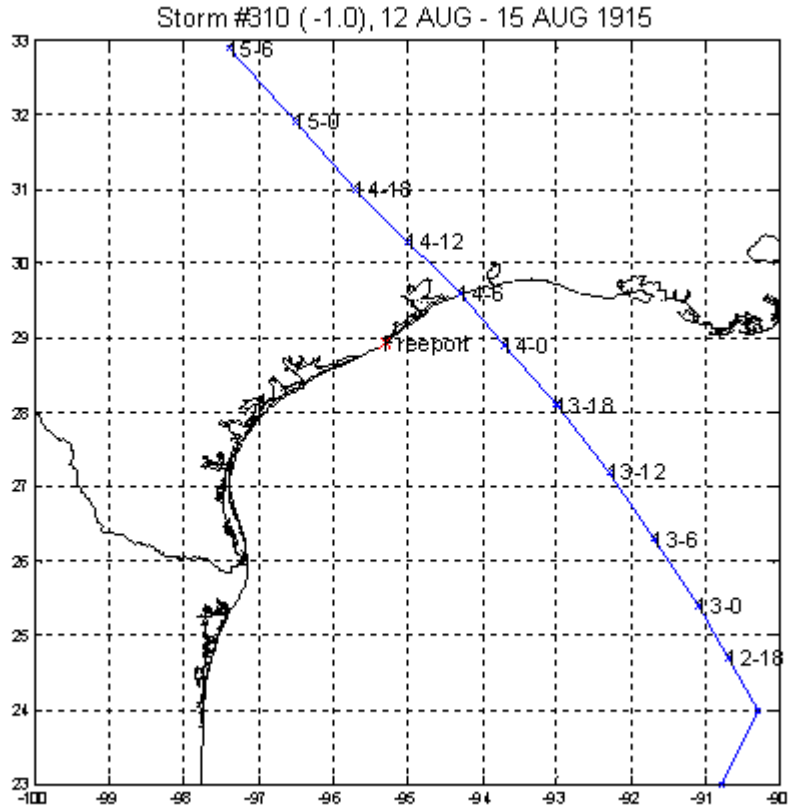
Storm #310 (-1.0), 12 AUG - 15 AUG 1915
15-6
15-0
14-18
14-12
14-6
Freeport
14-0
13-18
13-12
13-6
13-0
12-18

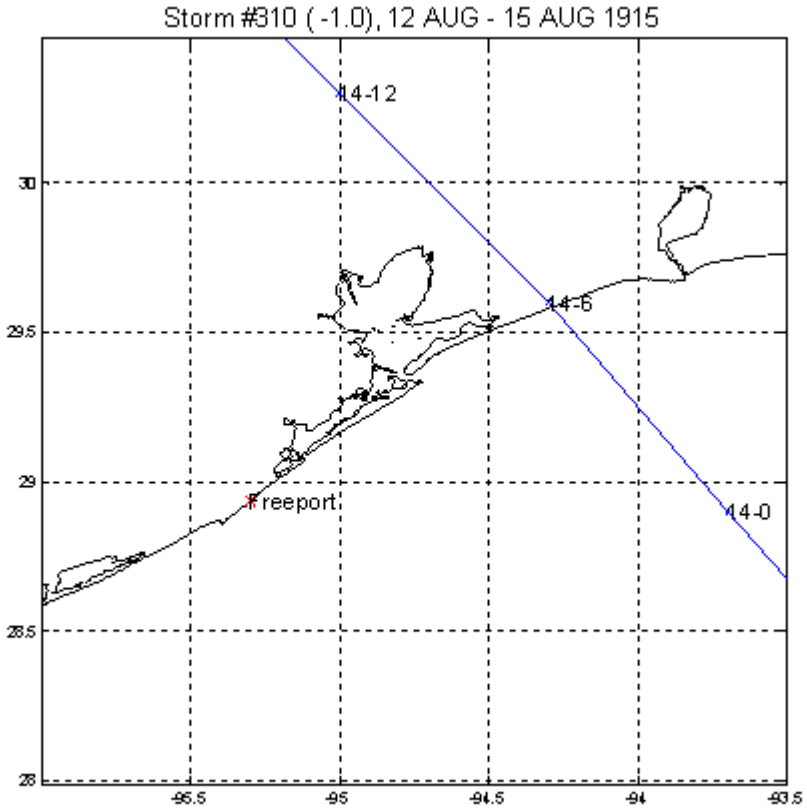
Storm #310 (-1.0), 12 AUG - 15 AUG 1915
14-12
14-6
Freeport
14-0

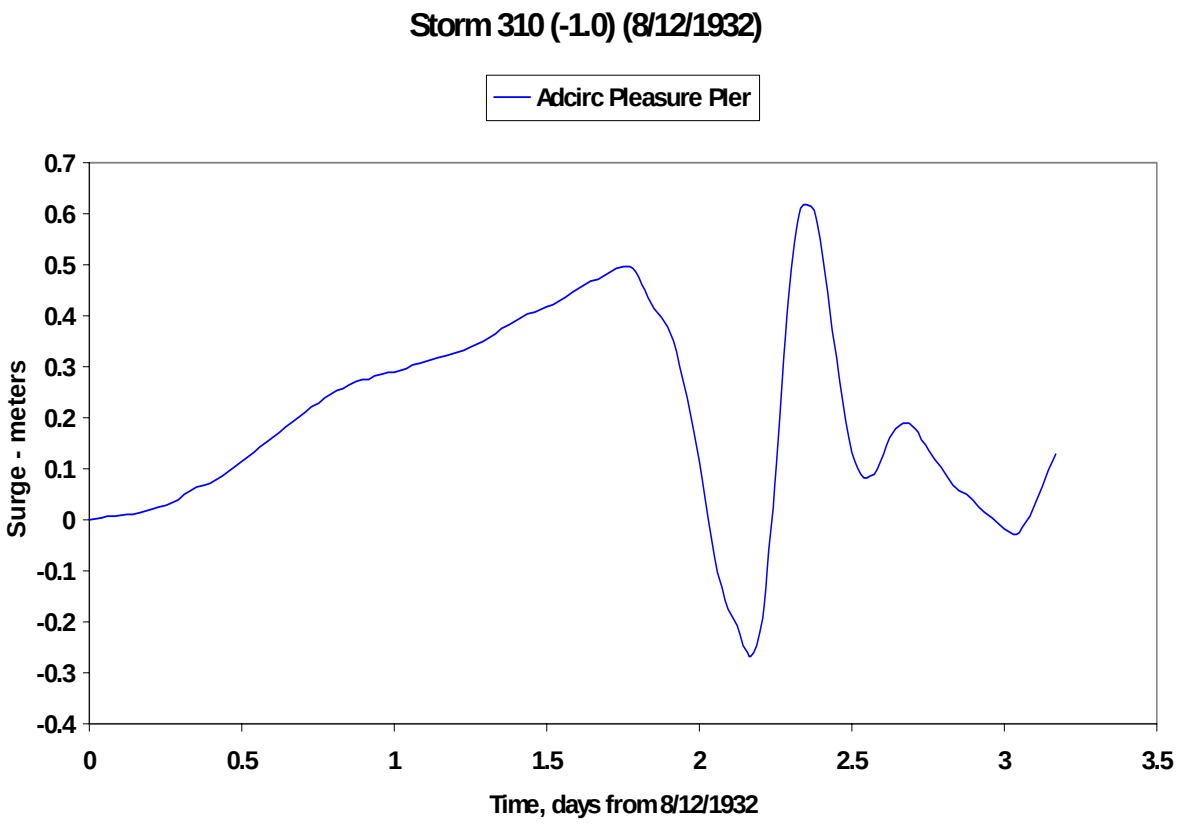
Storm 310 (-1.0) (8/12/1932)
Adcirc Pleasure Pier
Surge - meters
0.7
0.6
0.5
0.4
0.3
0.2
0.1
0
-0.1
-0.2
-0.3
-0.4
0
0.5
1
1.5
2
2.5
3
3.5
Time, days from 8/12/1932

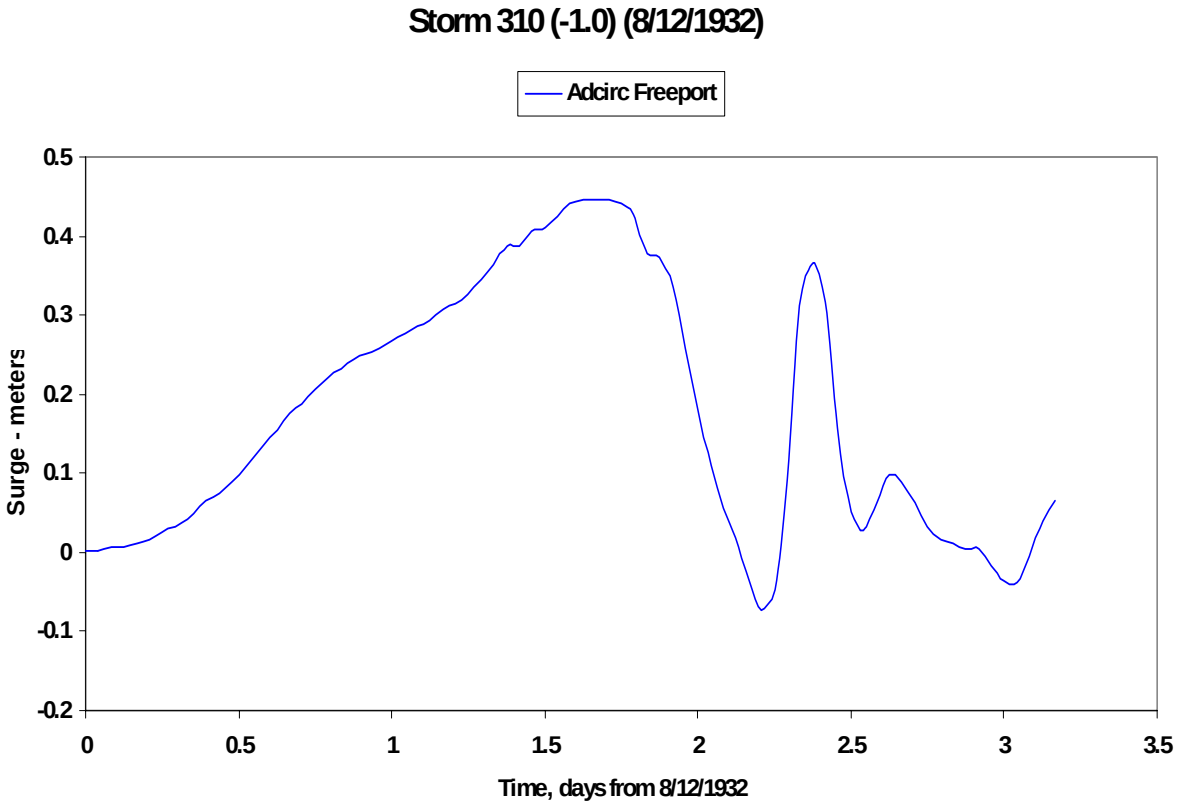
Storm 310 (-1.0) (8/12/1932)
Adcirc Freeport
Surge - meters
0.5
0.4
0.3
0.2
0.1
0
-0.1
-0.2
0
0.5
1
1.5
2
2.5
3
3.5
Time, days from 8/12/1932

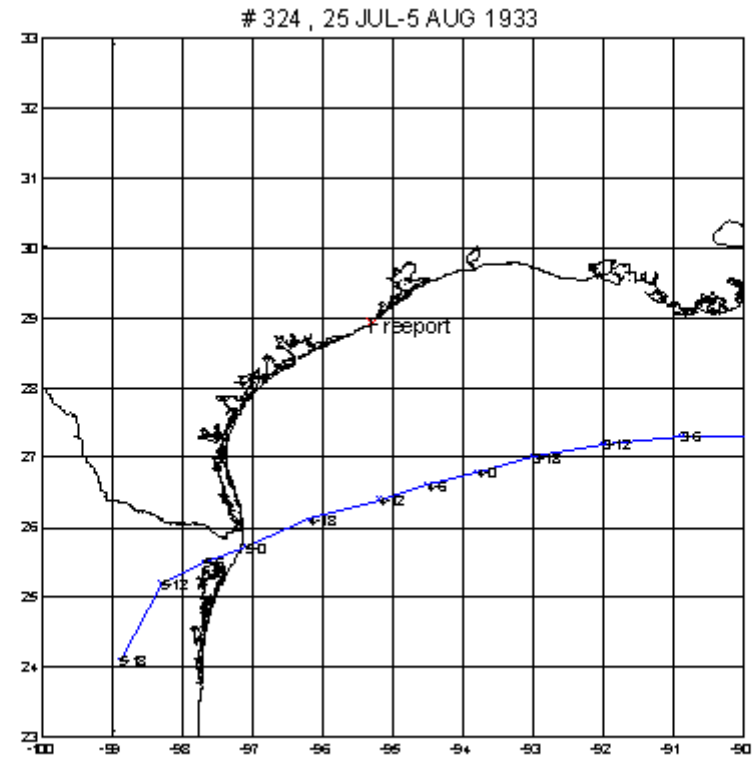
324 , 25 JUL-5 AUG 1933
Freeport
5-0
5-12
5-18
6-0
6-6
6-12
6-18
7-0
7-6
7-12
7-18
8-0
8-6
8-12
8-18
9-0
9-6

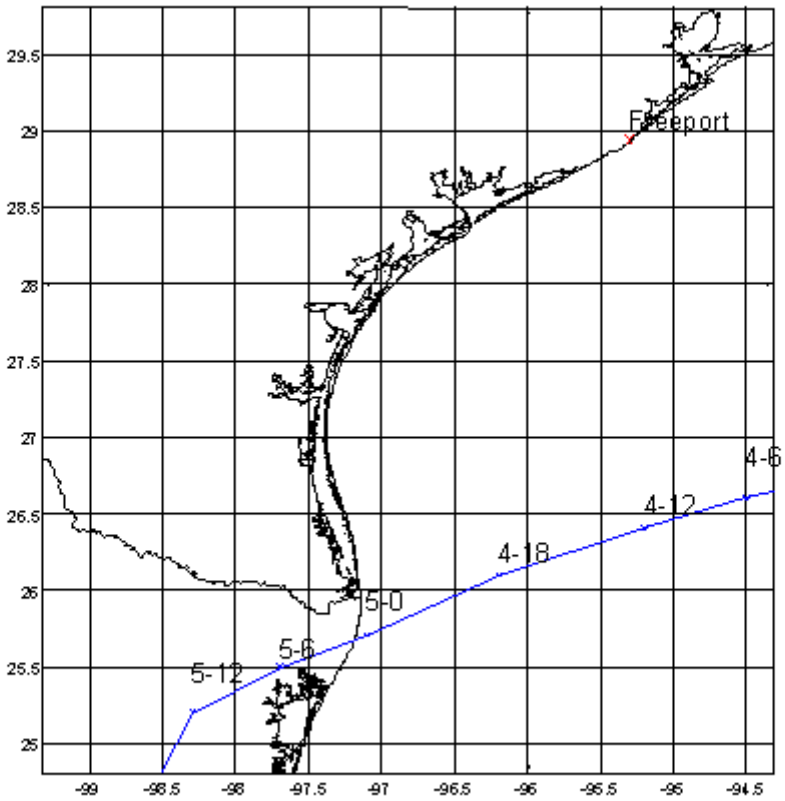
Freeport
4-6
4-12
4-18
5-0
5-6
5-12

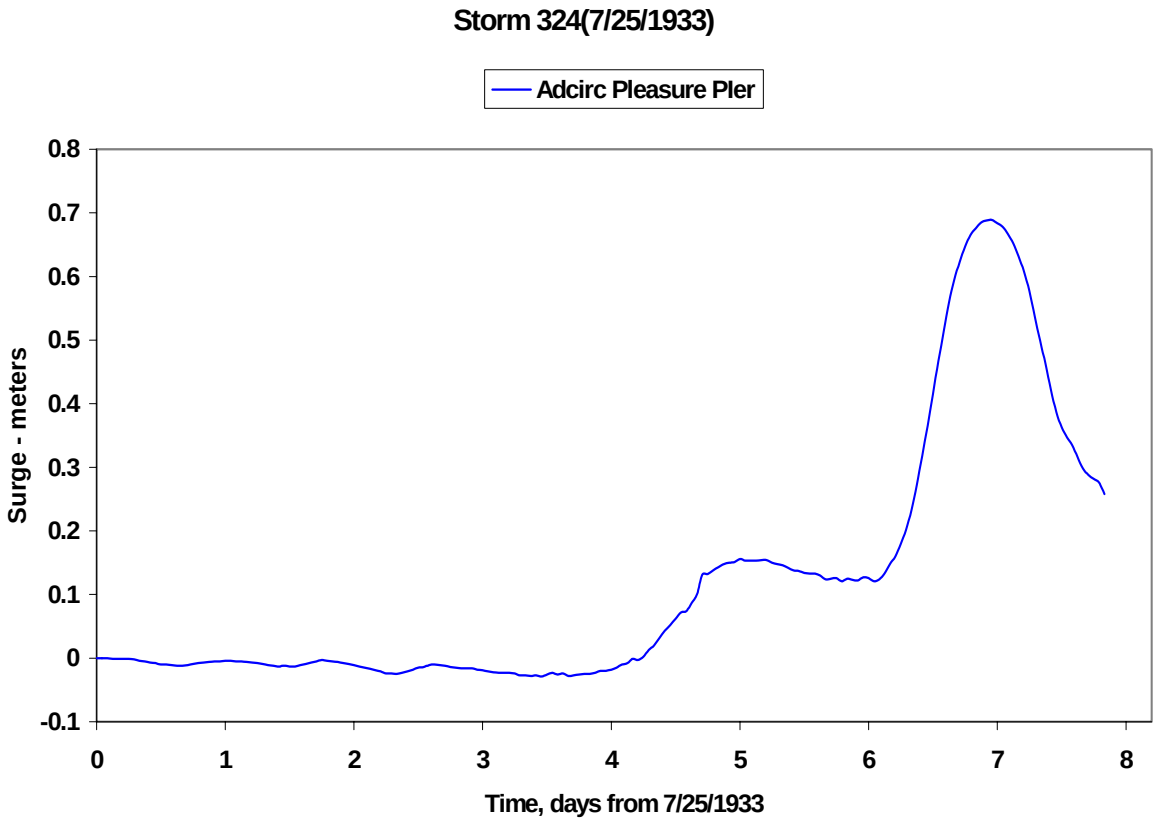
Storm 324(7/25/1933)
Adcirc Pleasure Pier
Surge - meters
0.8
0.7
0.6
0.5
0.4
0.3
0.2
0.1
0
-0.1
0
1
2
3
4
5
6
7
8
Time, days from 7/25/1933

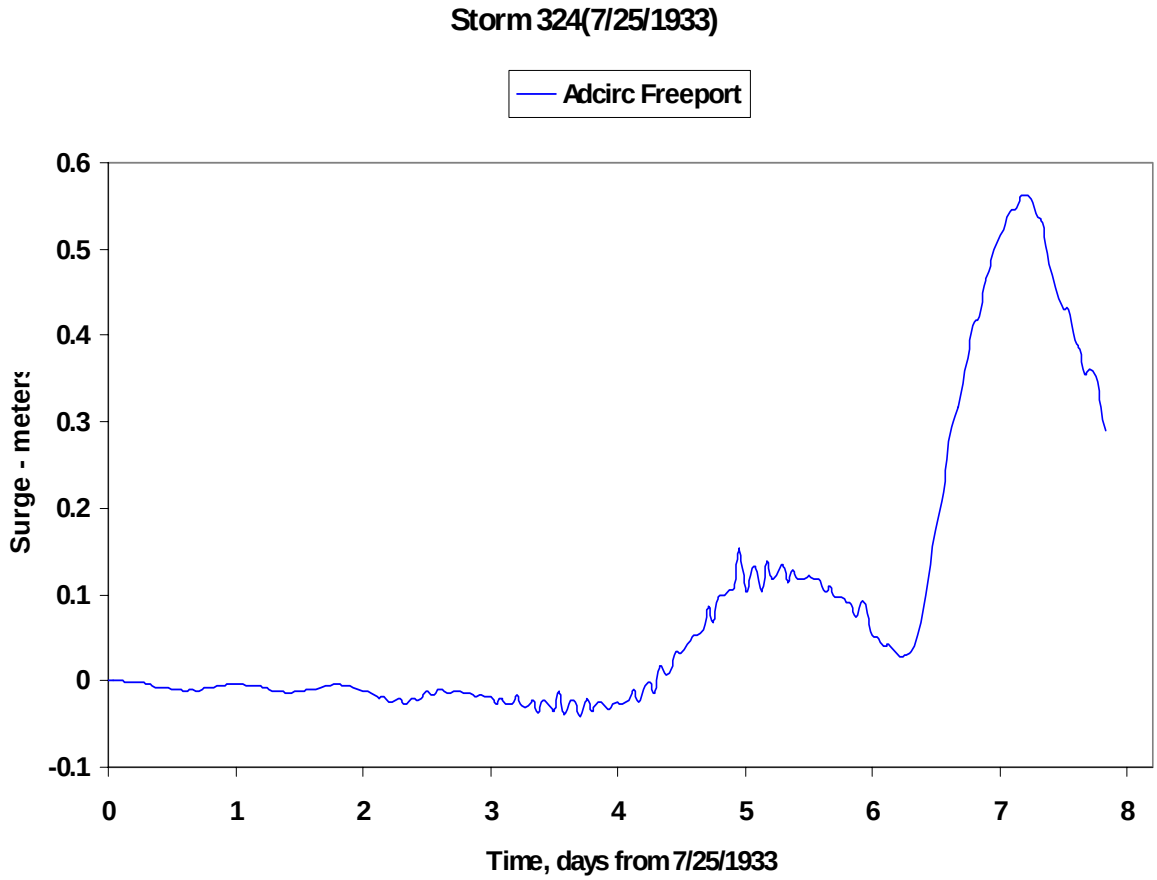
Storm 324(7/25/1933)
Adcirc Freeport
Surge - meters
0.6
0.5
0.4
0.3
0.2
0.1
0
-0.1
0
1
2
3
4
5
6
7
8
Time, days from 7/25/1933

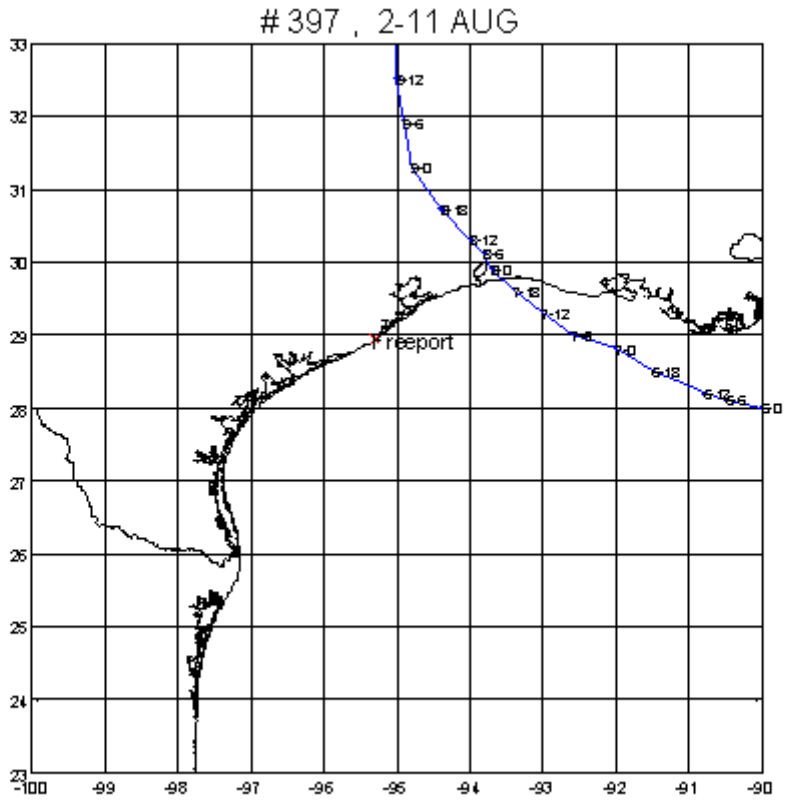
397 , 2-11 AUG
Freeport

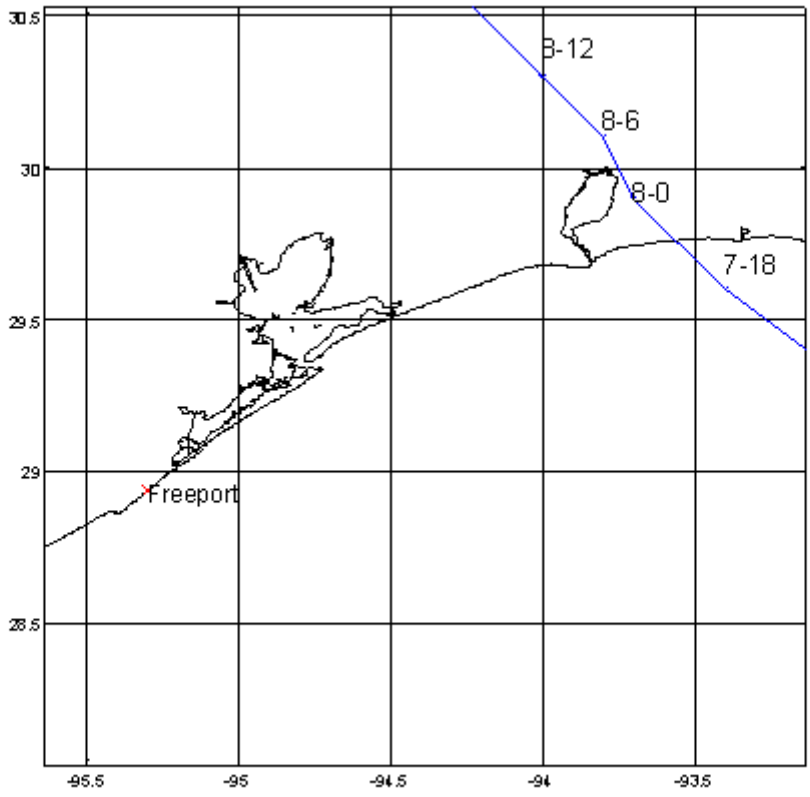
8-12
8-6
8-0
7-18
Freeport

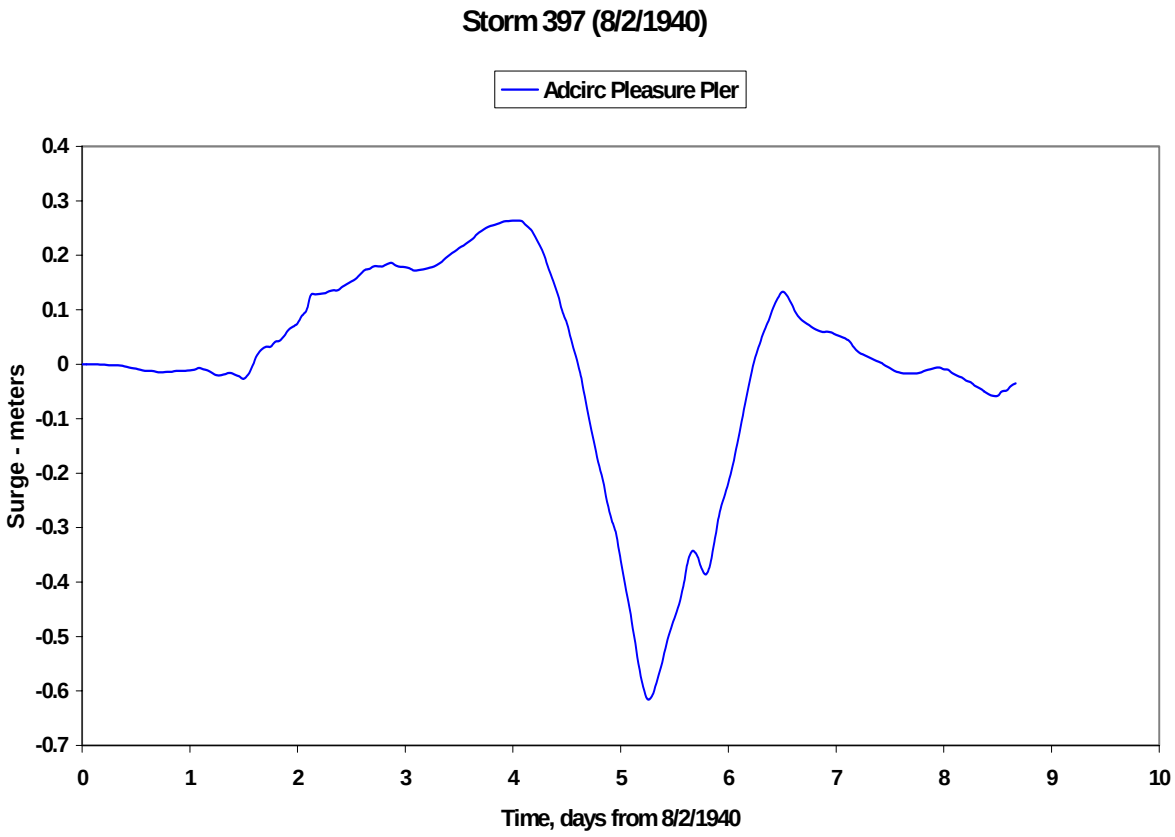
Storm 397 (8/2/1940)
Adcirc Pleasure Pier
Surge - meters
0.4
0.3
0.2
0.1
0
-0.1
-0.2
-0.3
-0.4
-0.5
-0.6
-0.7
0
1
2
3
4
5
6
7
8
9
10
Time, days from 8/2/1940

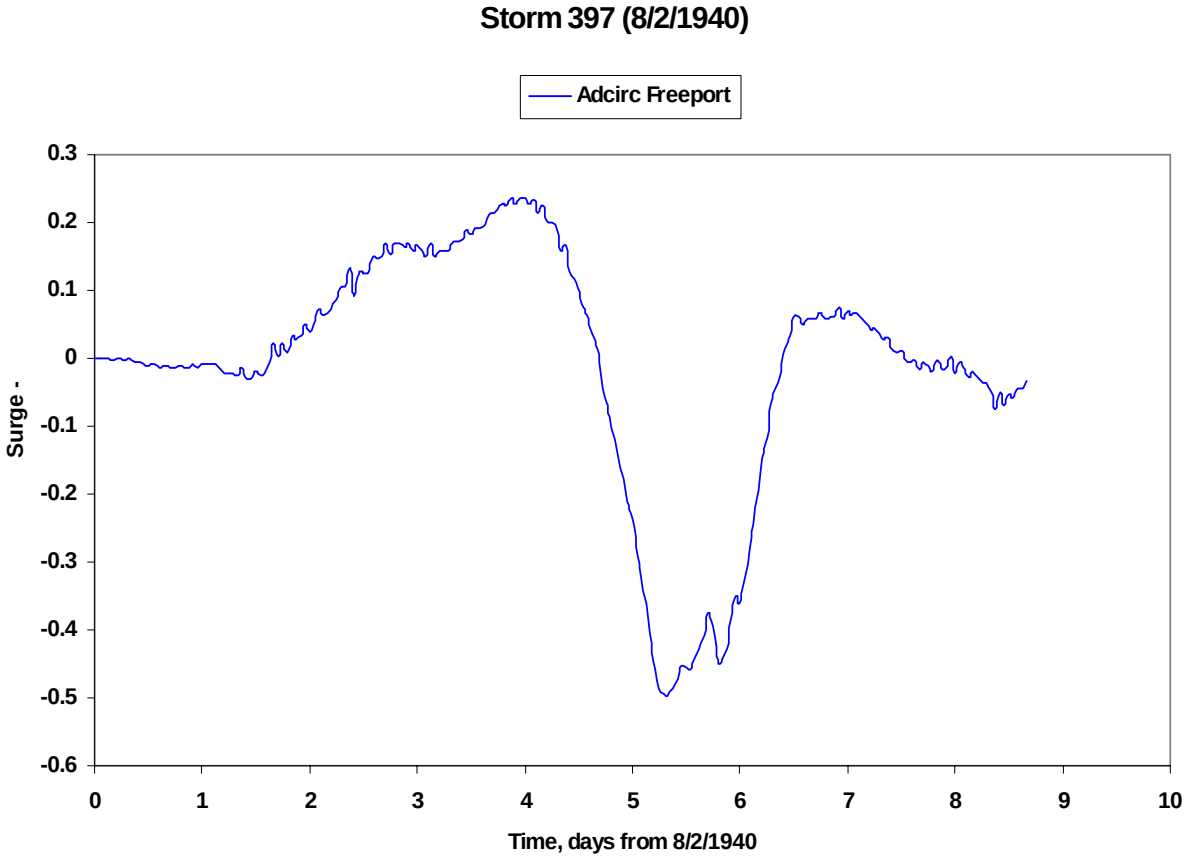
Storm 397 (8/2/1940)
Adcirc Freeport
Surge -
0.3
0.2
0.1
0
-0.1
-0.2
-0.3
-0.4
-0.5
-0.6
0
1
2
3
4
5
6
7
8
9
10
Time, days from 8/2/1940

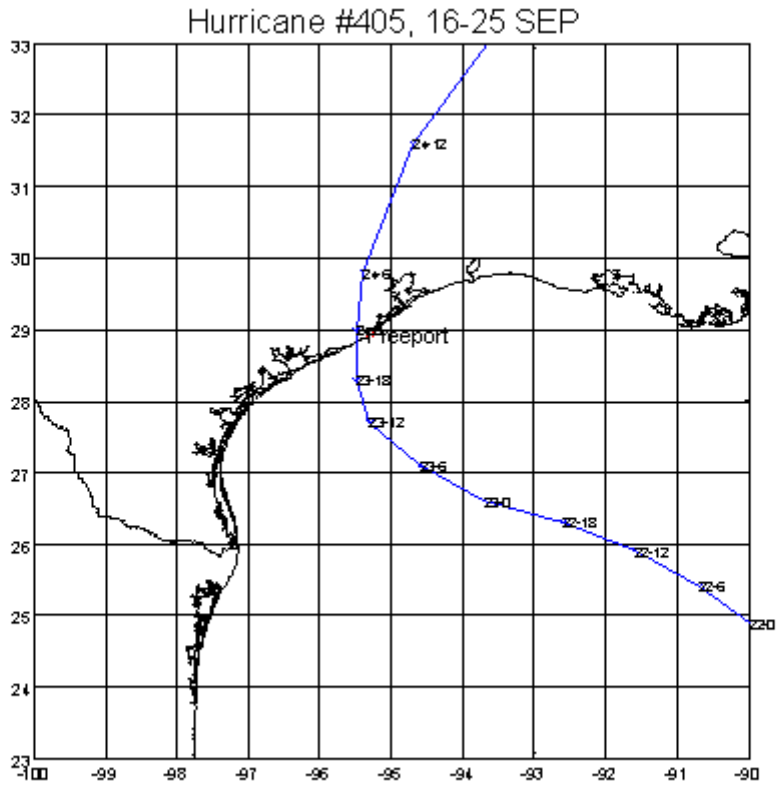
Hurricane #405, 16-25 SEP
Freeport
2-12
2-6
23-18
23-12
23-6
23-0
22-18
22-12
22-6
22-0

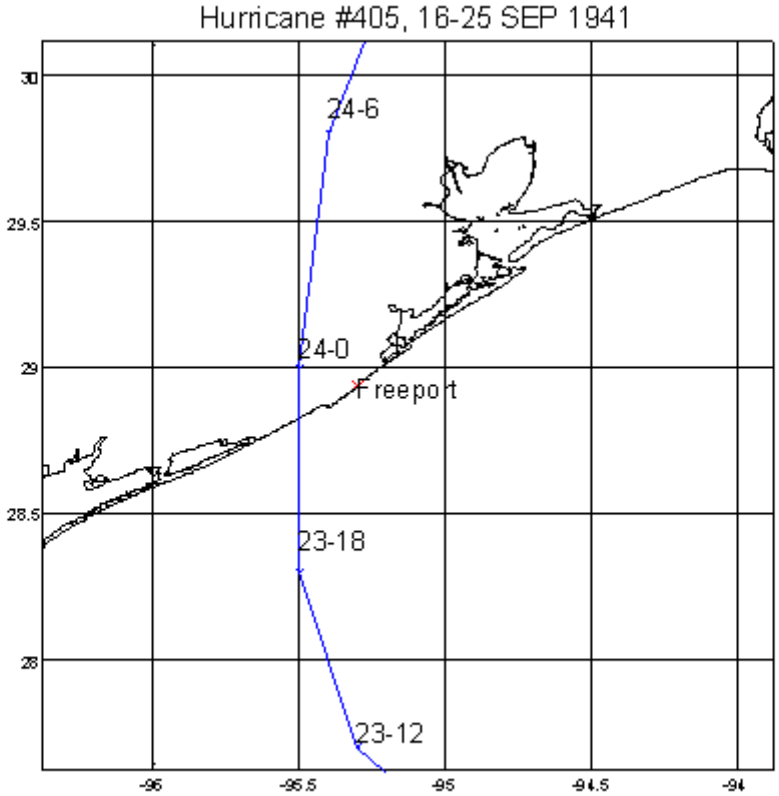
Hurricane #405, 16-25 SEP 1941
24-6
24-0
Freeport
23-18
23-12

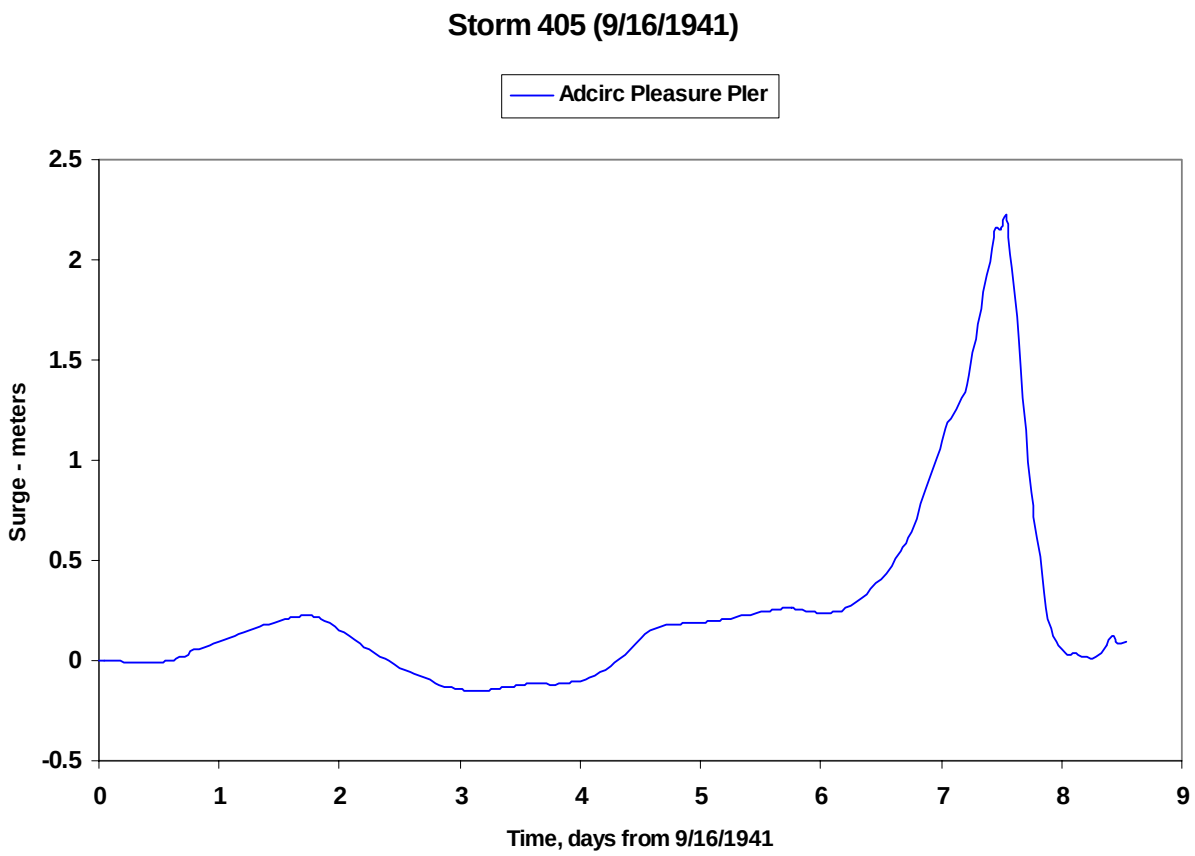
Storm 405 (9/16/1941)
Adcirc Pleasure Pier
Surge - meters
2.5
2
1.5
1
0.5
0
-0.5
0
1
2
3
4
5
6
7
8
9
Time, days from 9/16/1941

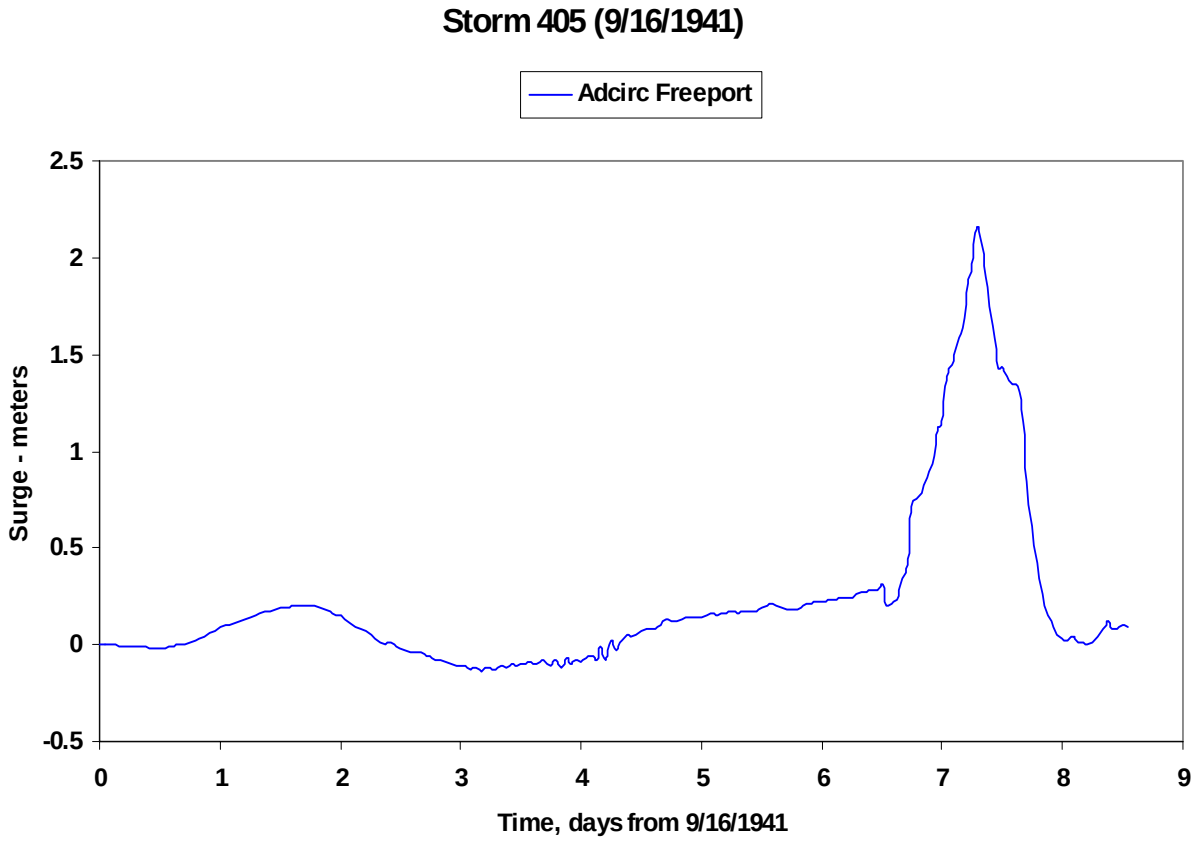
Storm 405 (9/16/1941)
Adcirc Freeport
Surge - meters
2.5
2
1.5
1
0.5
0
-0.5
0
1
2
3
4
5
6
7
8
9
Time, days from 9/16/1941

Hurricane #445, 24-29 AUG 1945

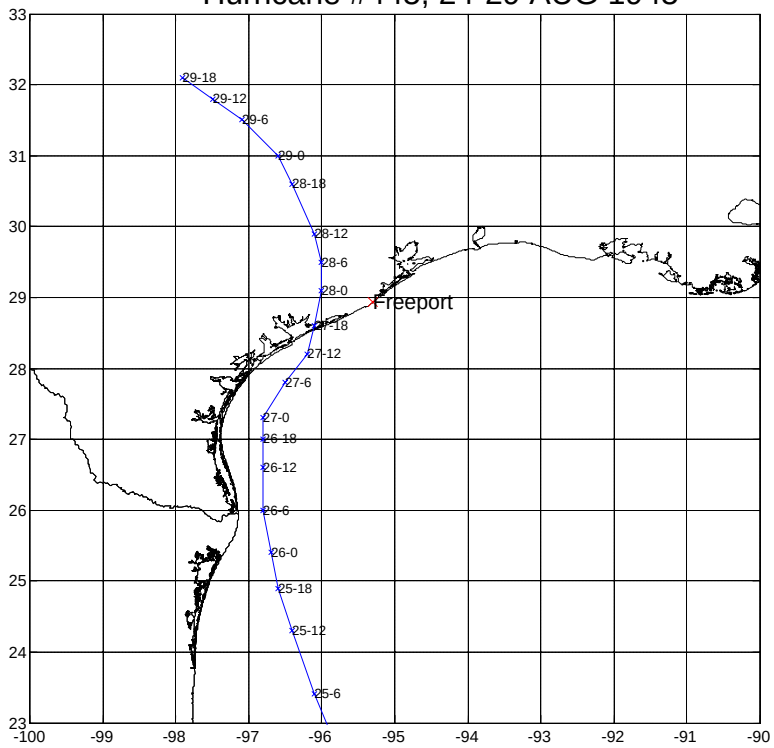

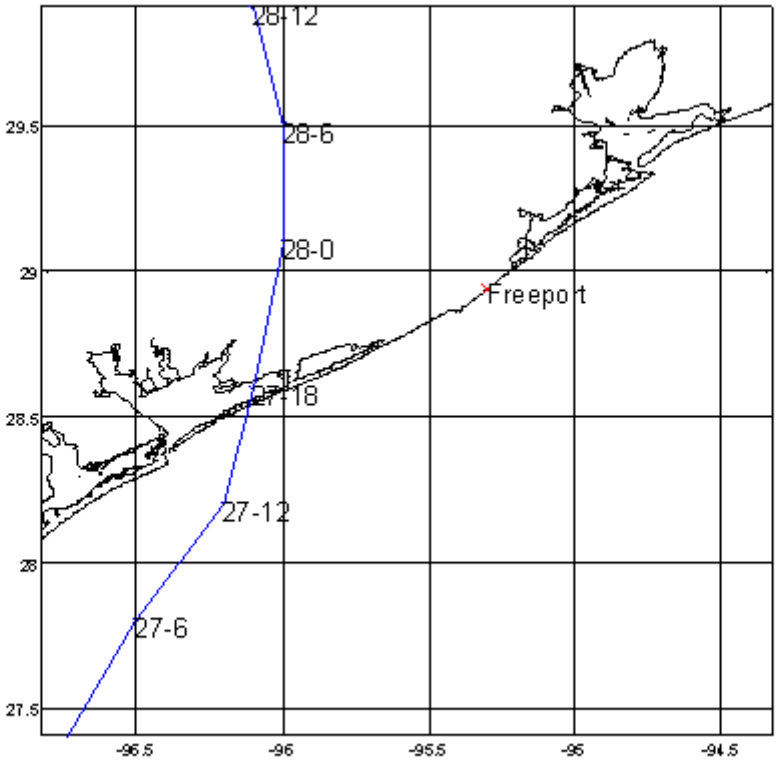

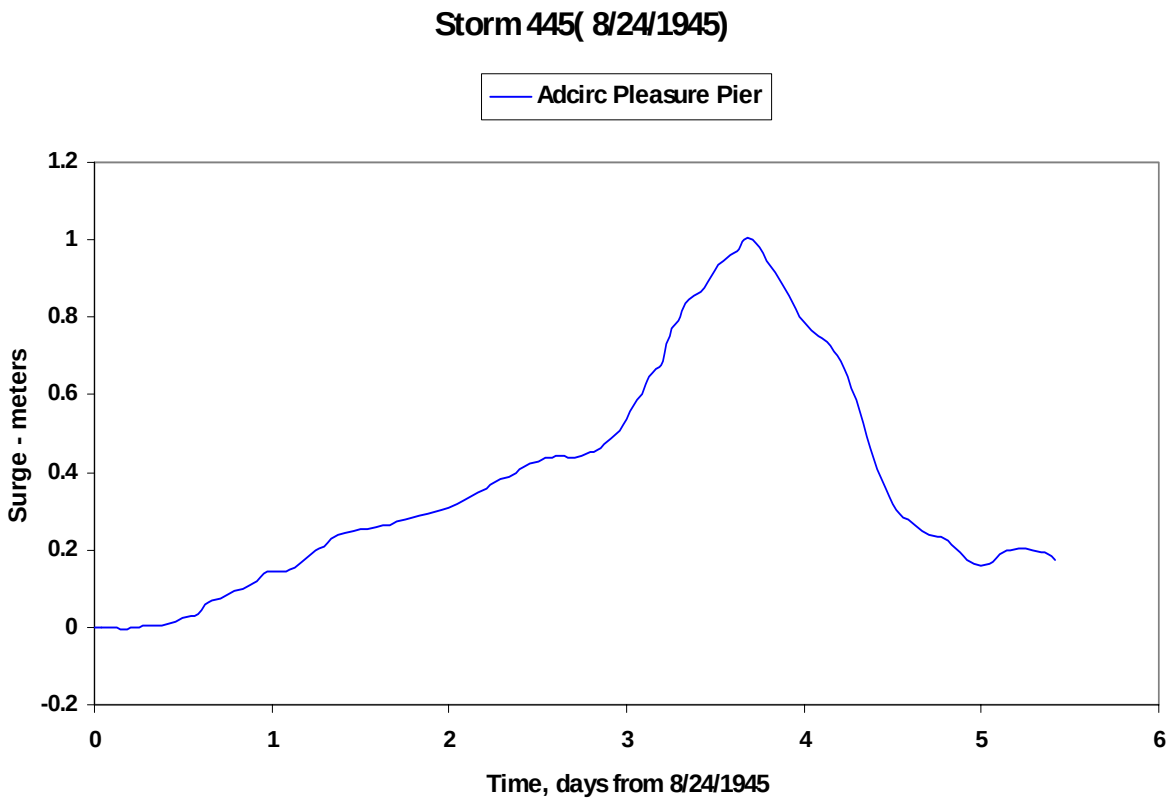
Storm 445(8/24/1945)
Adcirc Pleasure Pier
Surge - meters
1.2
1
0.8
0.6
0.4
0.2
0
-0.2
0
1
2
3
4
5
6
Time, days from 8/24/1945

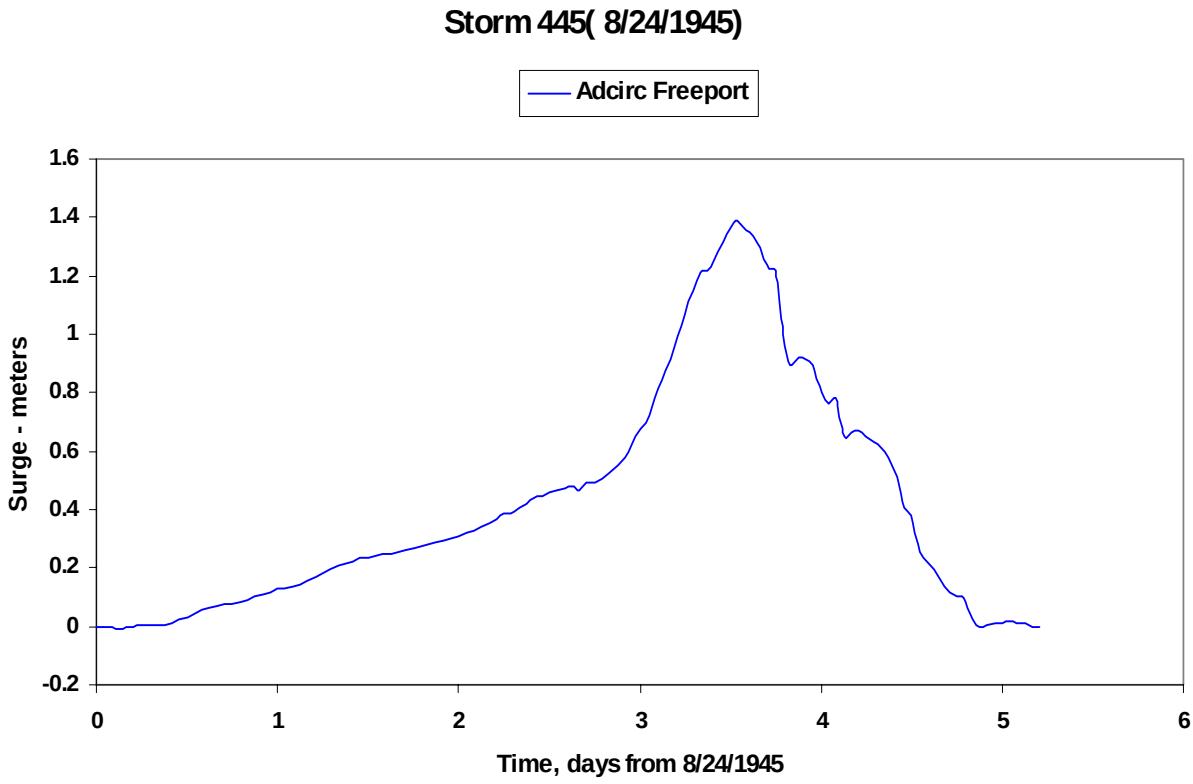
Storm 445(8/24/1945)
Adcirc Freeport
Surge - meters
1.6
1.4
1.2
1
0.8
0.6
0.4
0.2
0
-0.2
0
1
2
3
4
5
6
Time, days from 8/24/1945

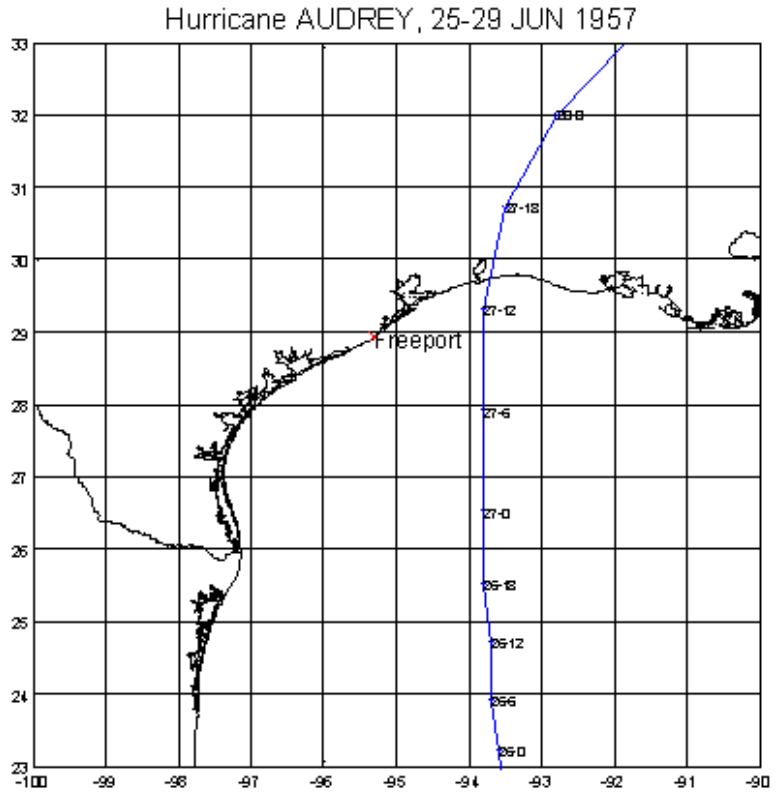
Hurricane AUDREY, 25-29 JUN 1957
Freeport
27-18
27-12
27-6
27-0
26-18
26-12
26-6
26-0
33
32
31
30
29
28
27
26
25
24
23
-100
-99
-98
-97
-96
-95
-94
-93
-92
-91
-90

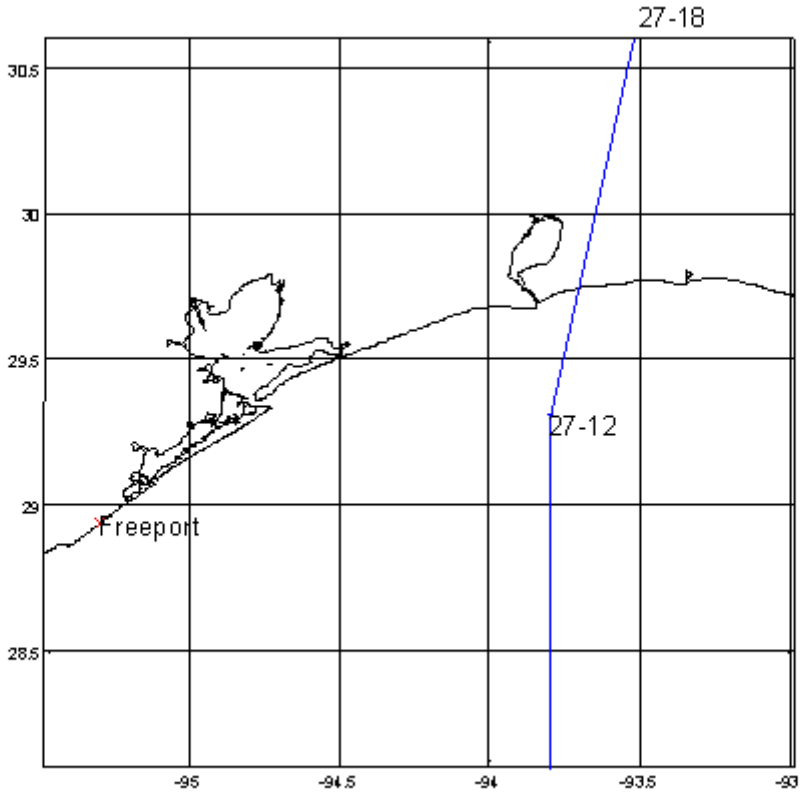
27-18
27-12
Freeport
30.5
30
29.5
29
28.5
-95
-94.5
-94
-93.5
-93

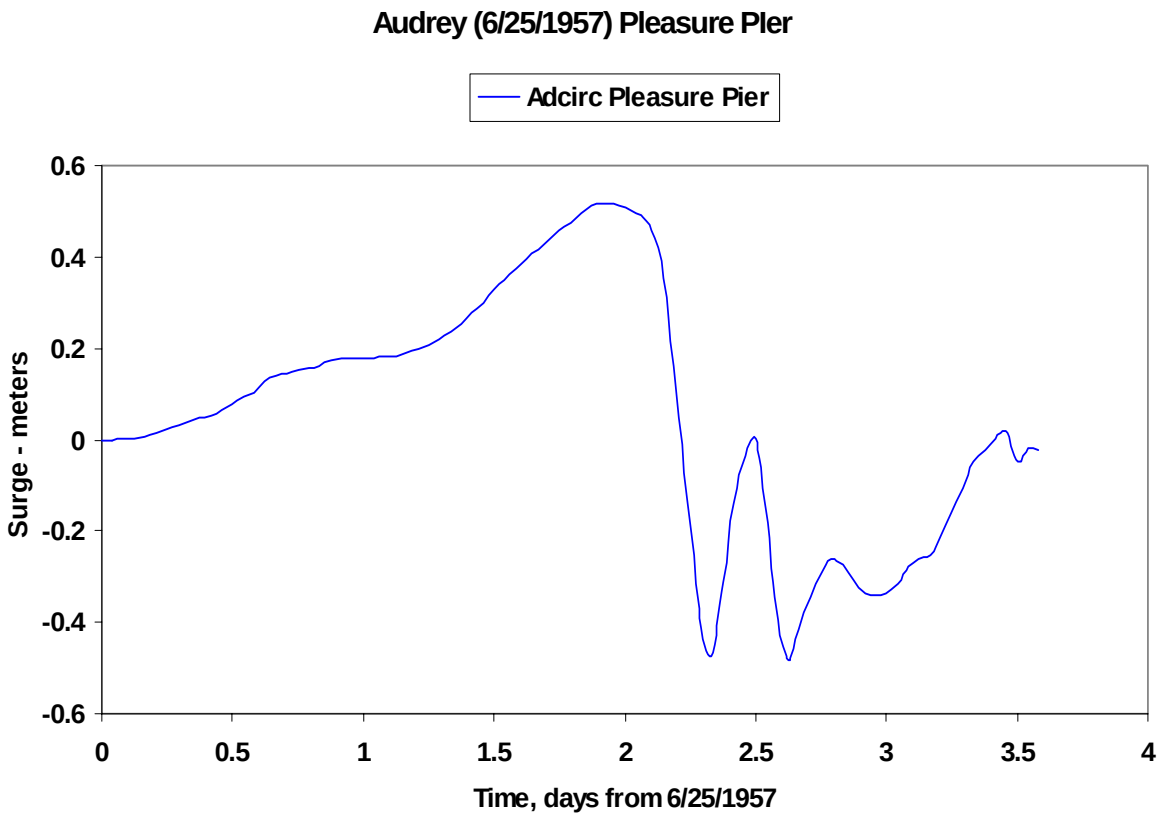
Audrey (6/25/1957) Pleasure Pier
Adcirc Pleasure Pier
Surge - meters
0.6
0.4
0.2
0
-0.2
-0.4
-0.6
0
0.5
1
1.5
2
2.5
3
3.5
4
Time, days from 6/25/1957

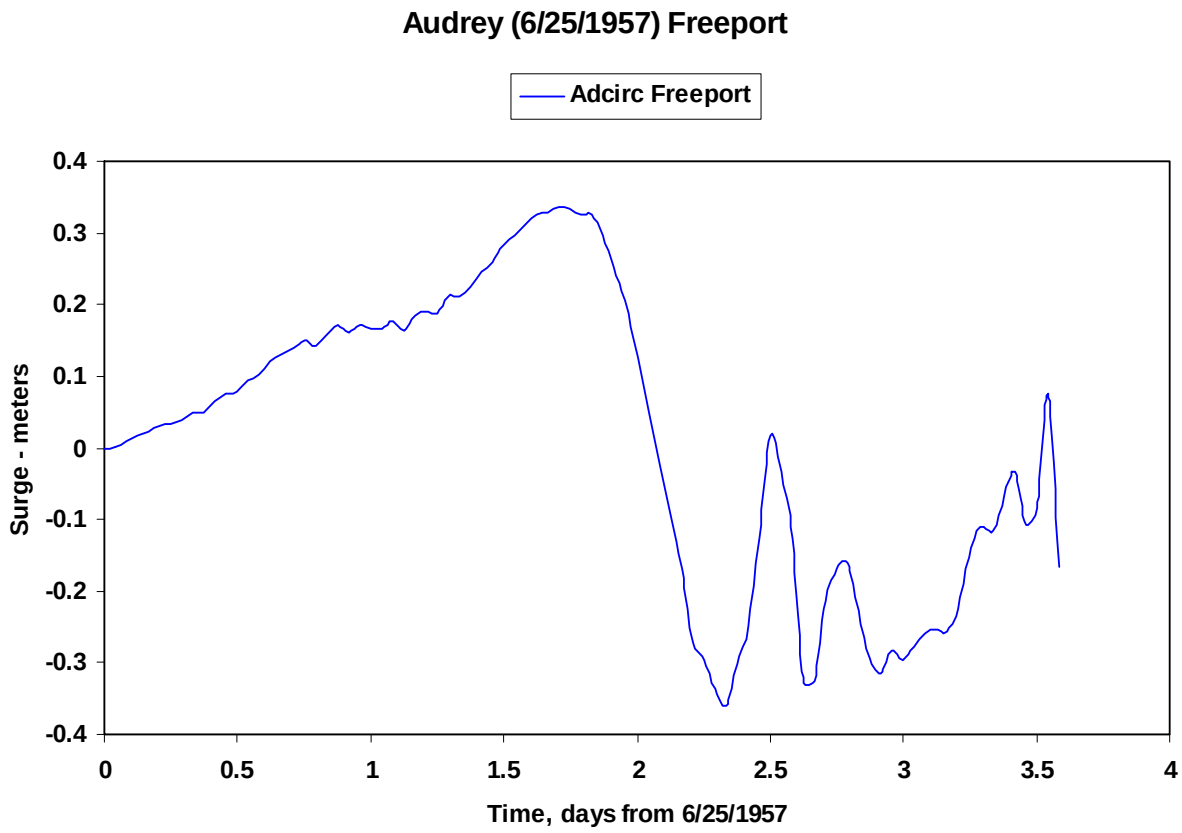
Audrey (6/25/1957) Freeport
Adcirc Freeport
Surge - meters
0.4
0.3
0.2
0.1
0
-0.1
-0.2
-0.3
-0.4
0
0.5
1
1.5
2
2.5
3
3.5
4
Time, days from 6/25/1957

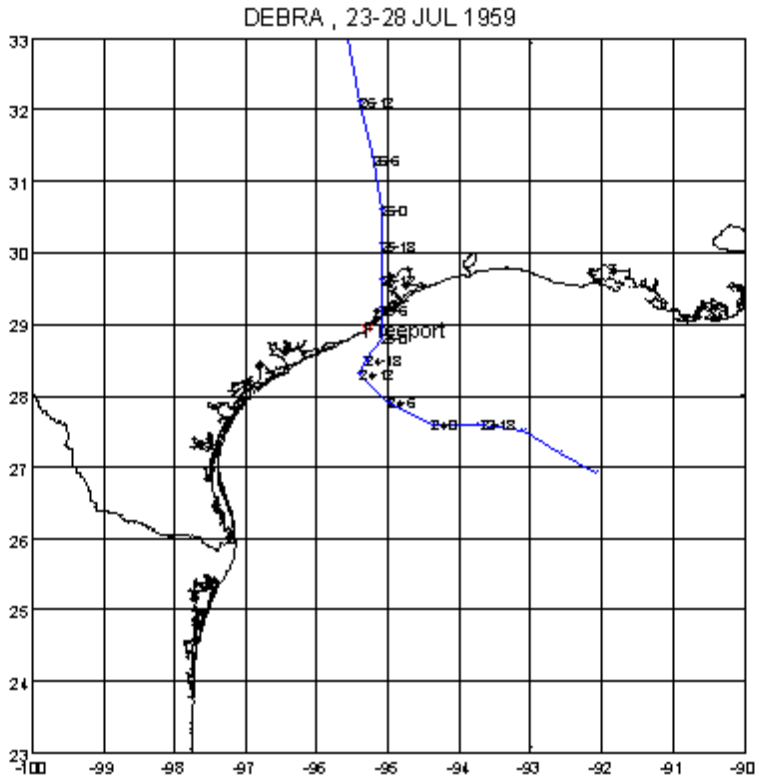
DEBRA , 23-28 JUL 1959
Freeport

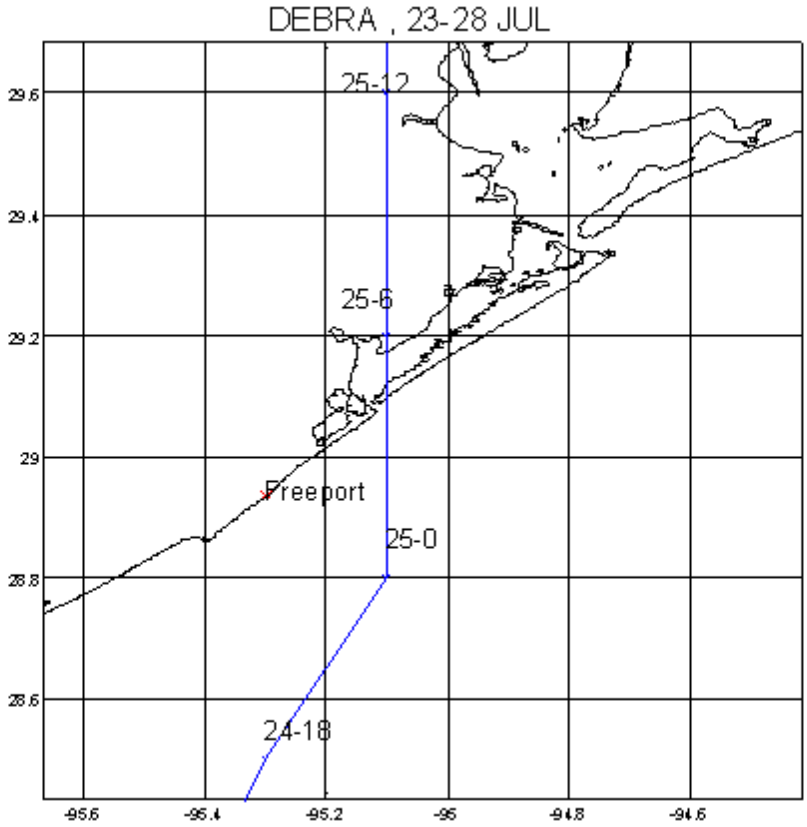
DEBRA , 23-28 JUL
25-12
25-6
Freeport
25-0
24-18

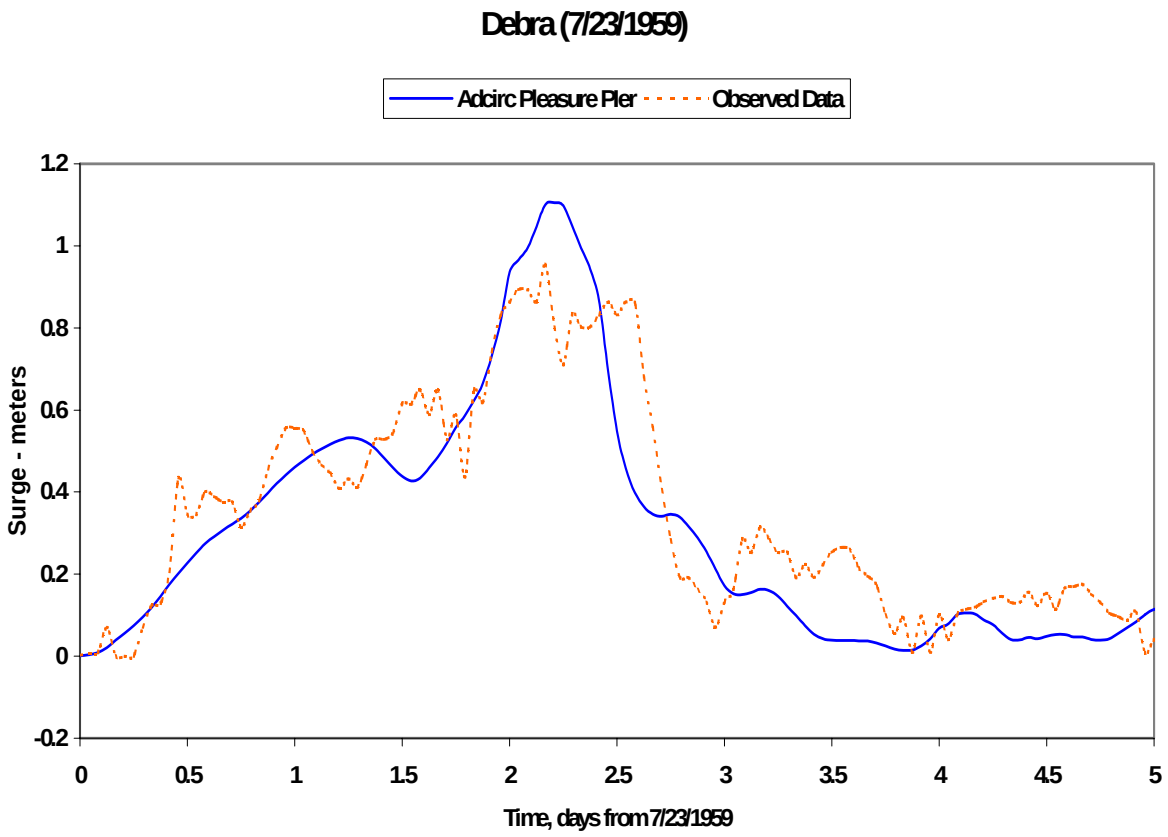
Debra (7/23/1959)
Adcirc Pleasure Pier
Observed Data
Surge - meters
1.2
1
0.8
0.6
0.4
0.2
0
-0.2
0
0.5
1
1.5
2
2.5
3
3.5
4
4.5
5
Time, days from 7/23/1959

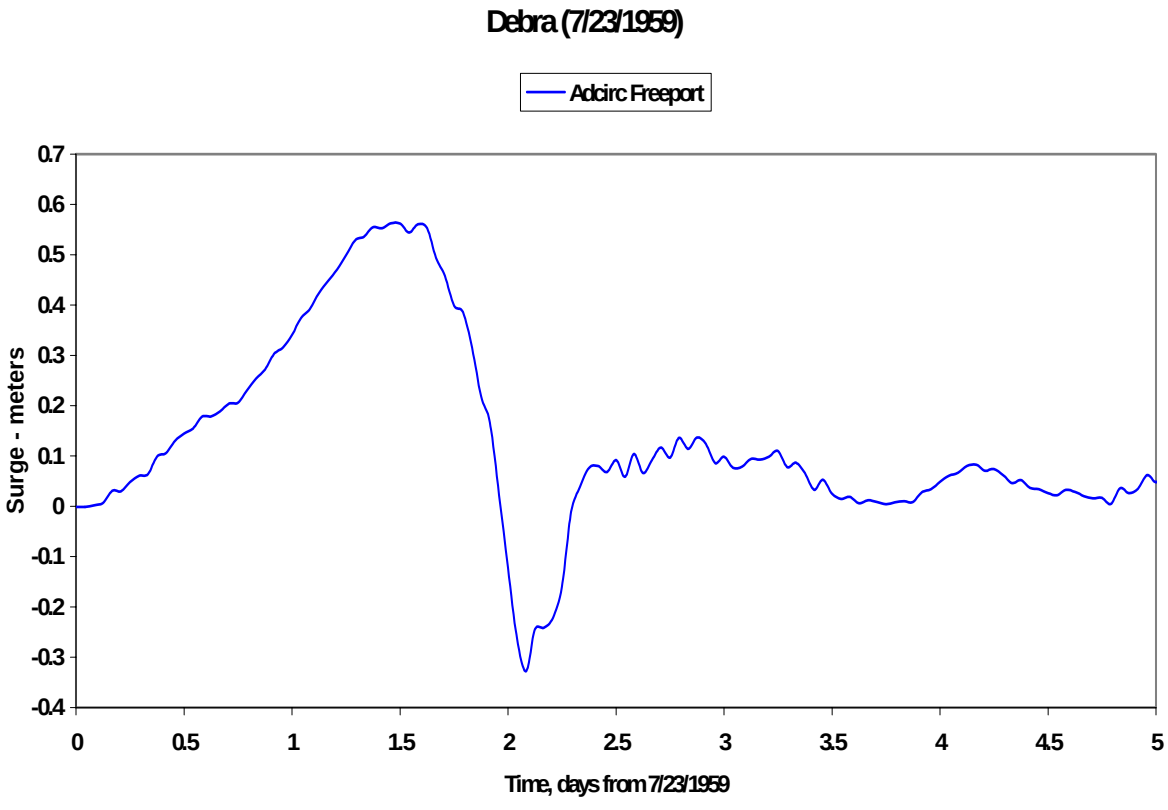
Debra (7/23/1959)
Adcirc Freeport
Surge - meters
0.7
0.6
0.5
0.4
0.3
0.2
0.1
0
-0.1
-0.2
-0.3
-0.4
0
0.5
1
1.5
2
2.5
3
3.5
4
4.5
5
Time, days from 7/23/1959

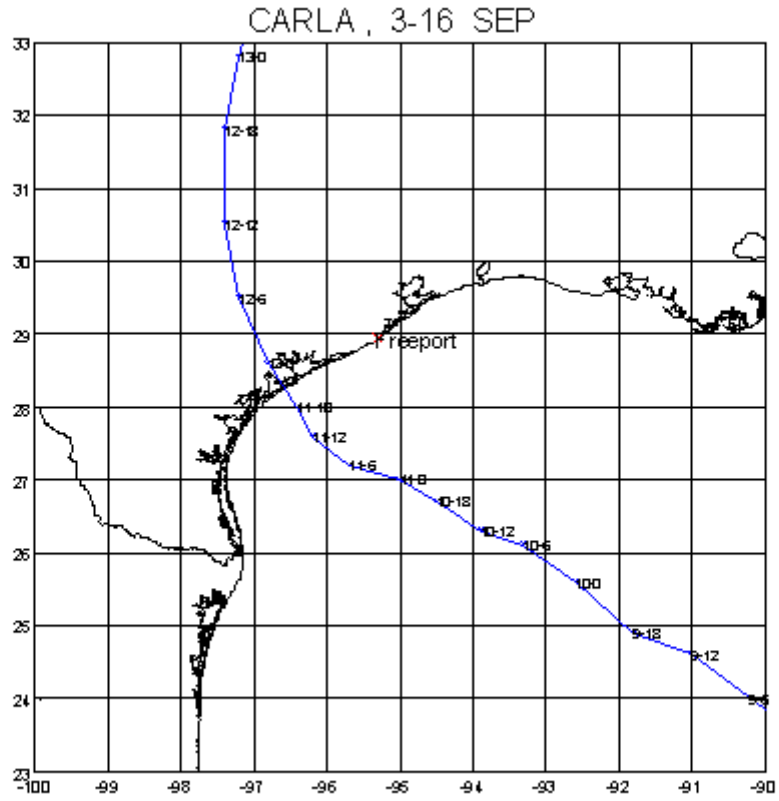
CARLA , 3-16 SEP
Freeport
12-18
12-12
12-6
11-18
11-12
11-6
11-0
10-18
10-12
10-6
10-0
9-18
9-12
33
32
31
30
29
28
27
26
25
24
23
-100
-99
-98
-97
-96
-95
-94
-93
-92
-91
-90

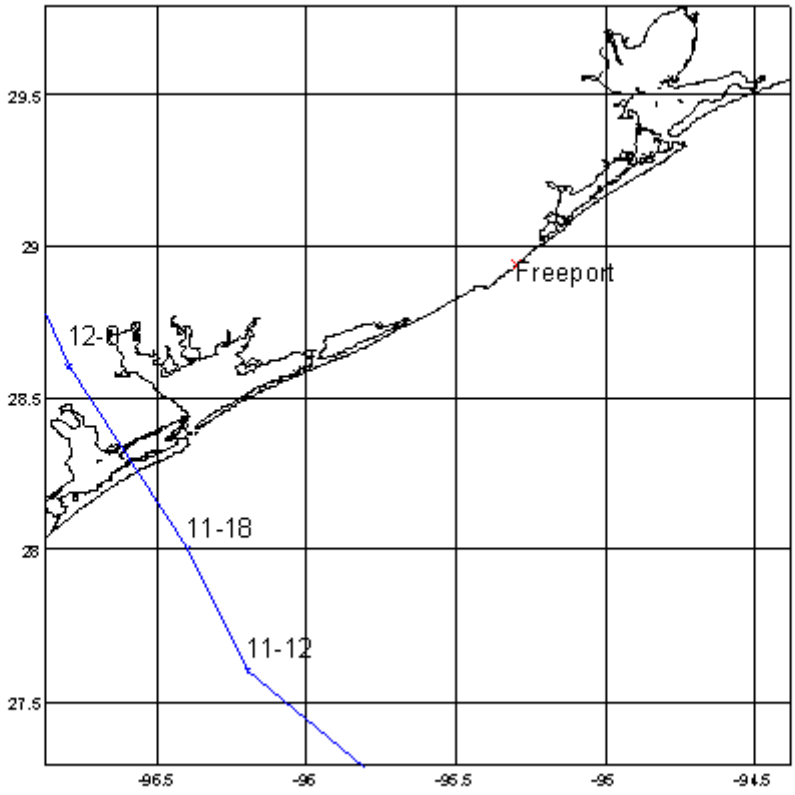
Freeport
12-0
11-18
11-12
29.5
29
28.5
28
27.5
-96.5
-96
-95.5
-95
-94.5

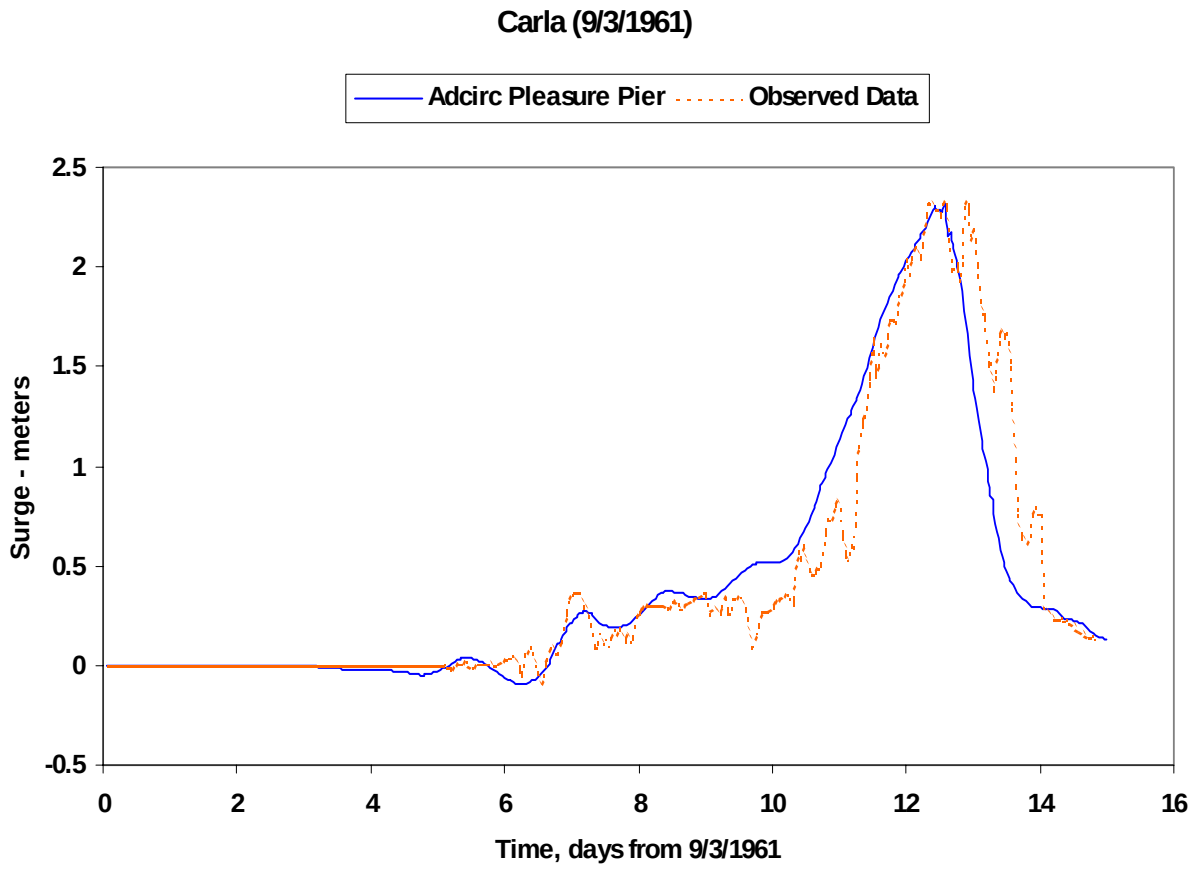
Carla (9/3/1961)
Adcirc Pleasure Pier
Observed Data
Surge - meters
2.5
2
1.5
1
0.5
0
-0.5
0
2
4
6
8
10
12
14
16
Time, days from 9/3/1961

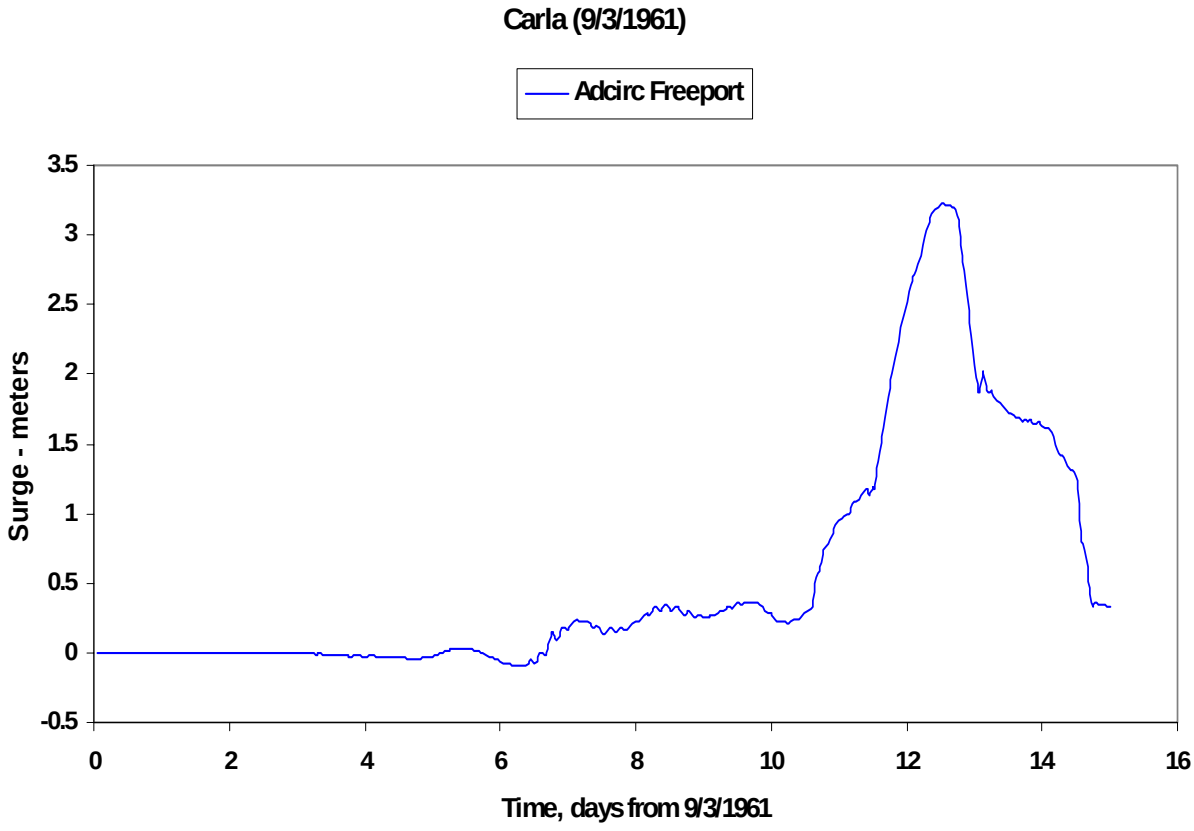
Carla (9/3/1961)
Adcirc Freeport
Surge - meters
3.5
3
2.5
2
1.5
1
0.5
0
-0.5
0
2
4
6
8
10
12
14
16
Time, days from 9/3/1961

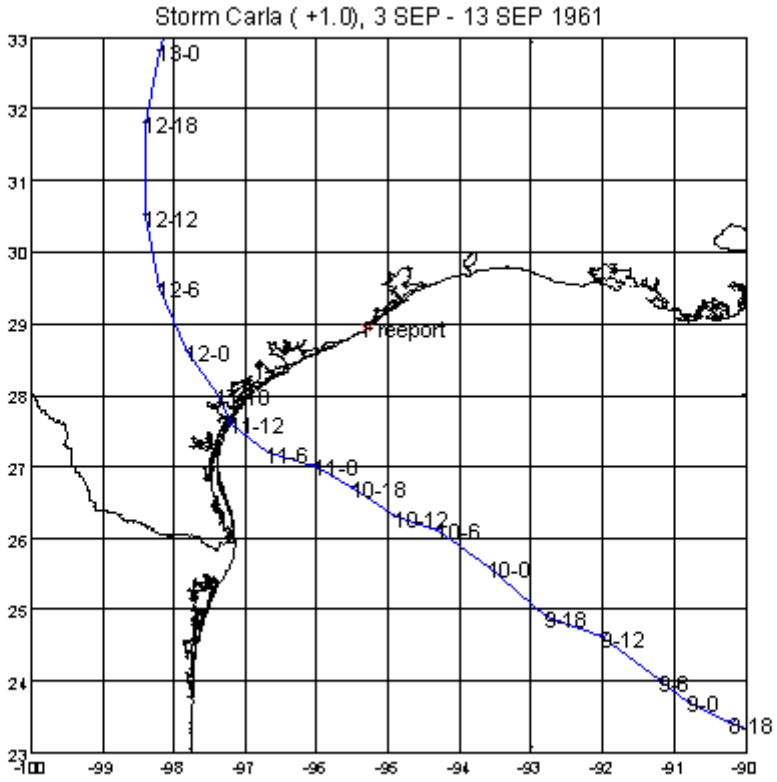
Storm Carla (+1.0), 3 SEP - 13 SEP 1961
13-0
12-18
12-12
12-6
12-0
11-12
11-6
11-0
10-18
10-12
10-6
10-0
9-18
9-12
9-6
9-0
8-18
Freeport

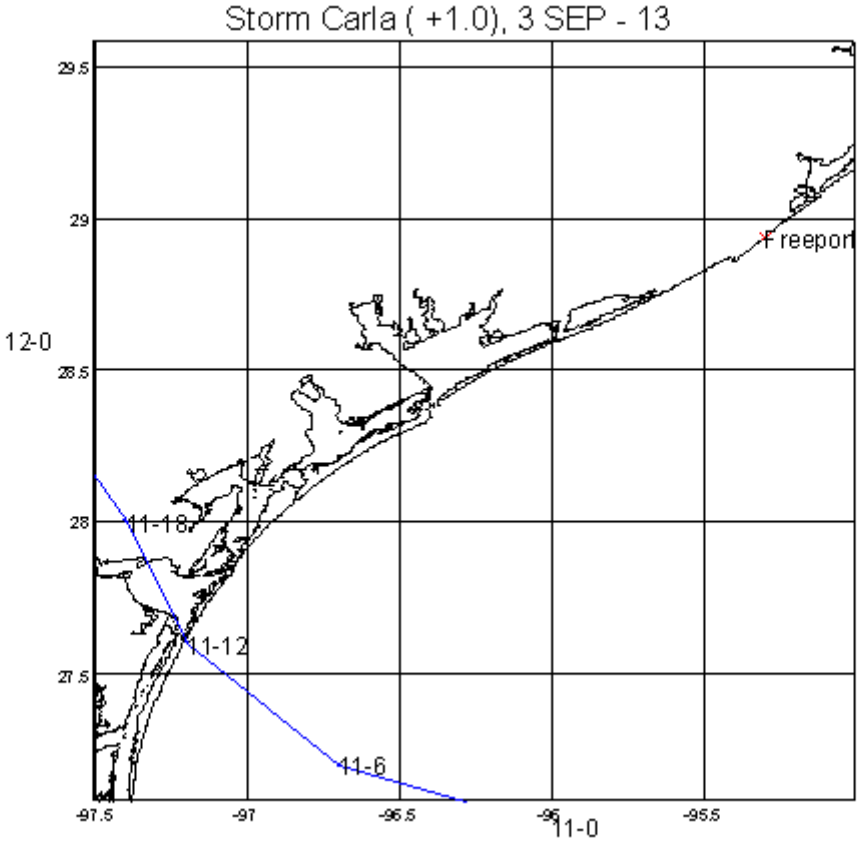
Storm Carla (+1.0), 3 SEP - 13
12-0
11-18
11-12
11-6
11-0
Freeport

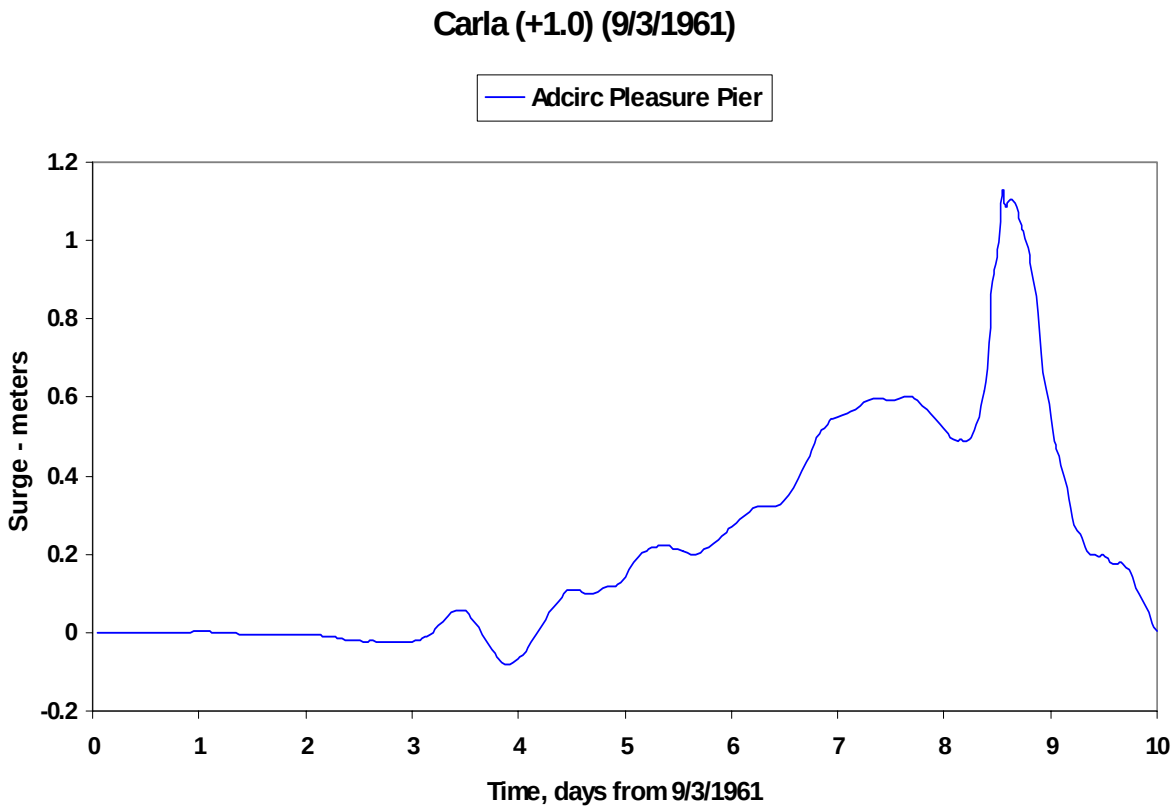
Carla (+1.0) (9/3/1961)
Adcirc Pleasure Pier
Surge - meters
1.2
1
0.8
0.6
0.4
0.2
0
-0.2
0
1
2
3
4
5
6
7
8
9
10
Time, days from 9/3/1961

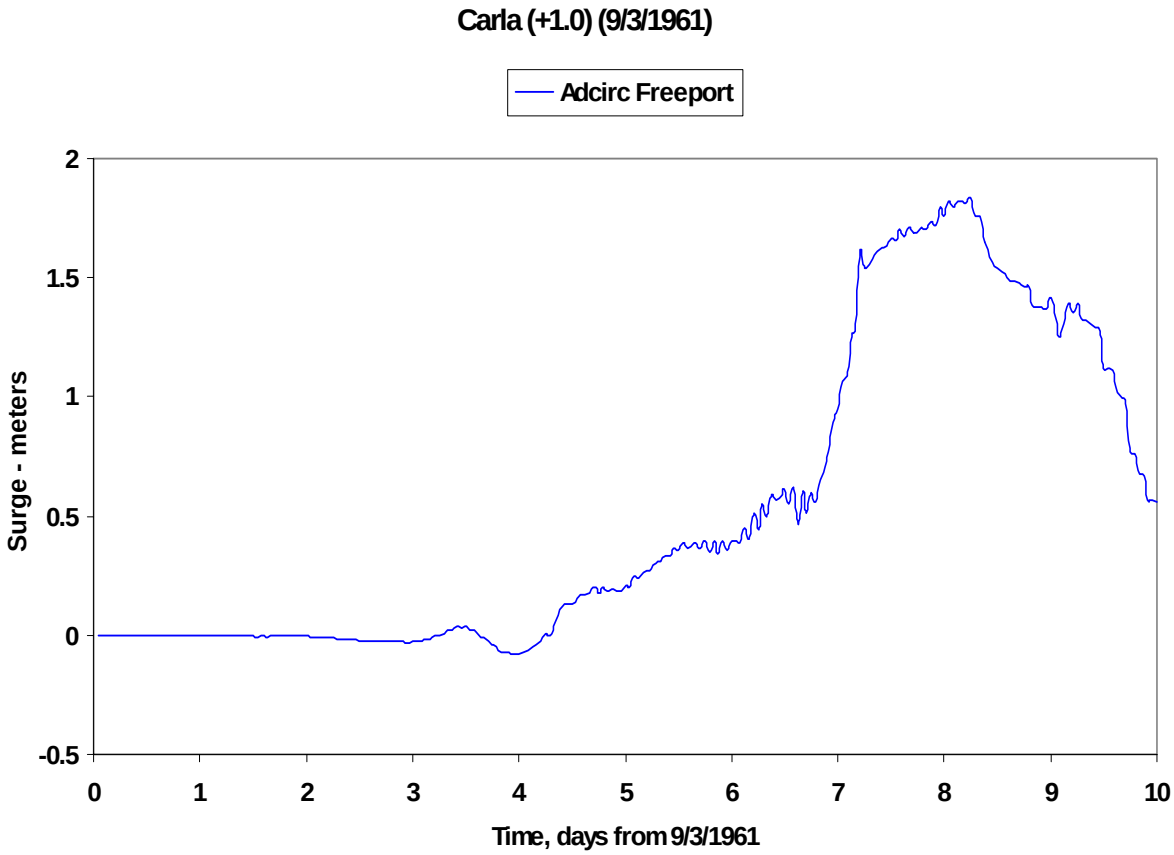
Carla (+1.0) (9/3/1961)
Adcirc Freeport
Surge - meters
2
1.5
1
0.5
0
-0.5
0
1
2
3
4
5
6
7
8
9
10
Time, days from 9/3/1961

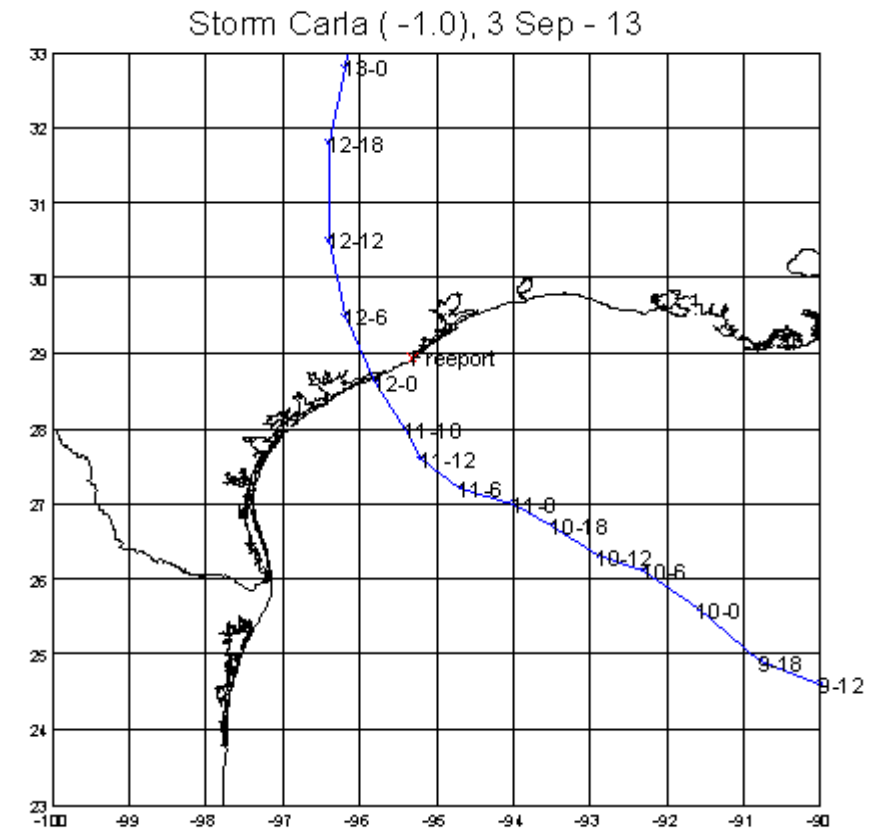
Storm Carla (-1.0), 3 Sep - 13
18-0
12-18
12-12
12-6
Freeport
12-0
11-10
11-12
11-6
11-0
10-18
10-12
10-6
10-0
9-18
9-12
33
32
31
30
29
28
27
26
25
24
23
-100
-99
-98
-97
-96
-95
-94
-93
-92
-91
-90

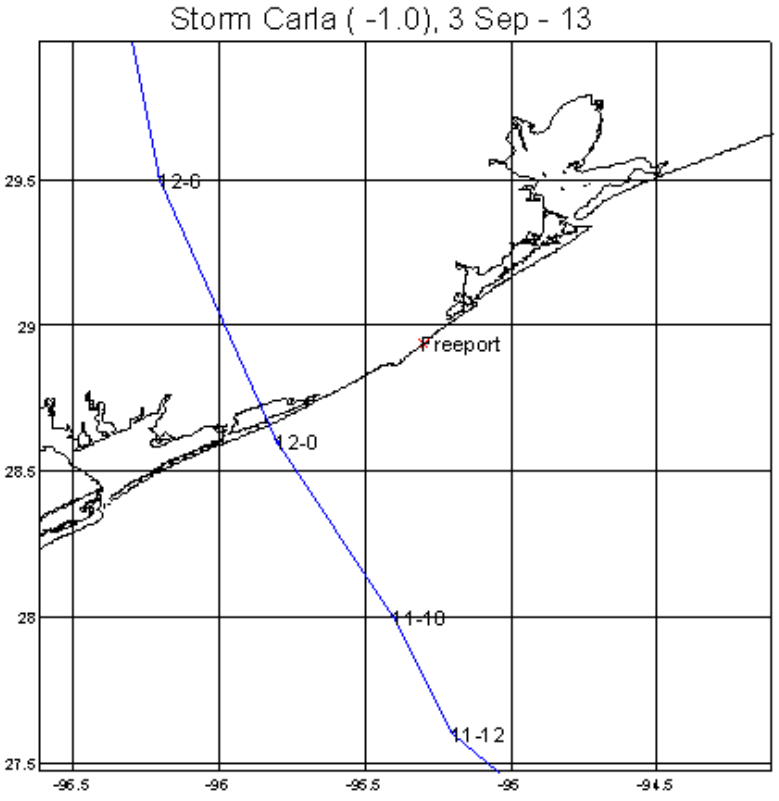
Storm Carla (-1.0), 3 Sep - 13
12-6
Freeport
12-0
11-10
11-12
29.5
29
28.5
28
27.5
-96.5
-96
-95.5
-95
-94.5

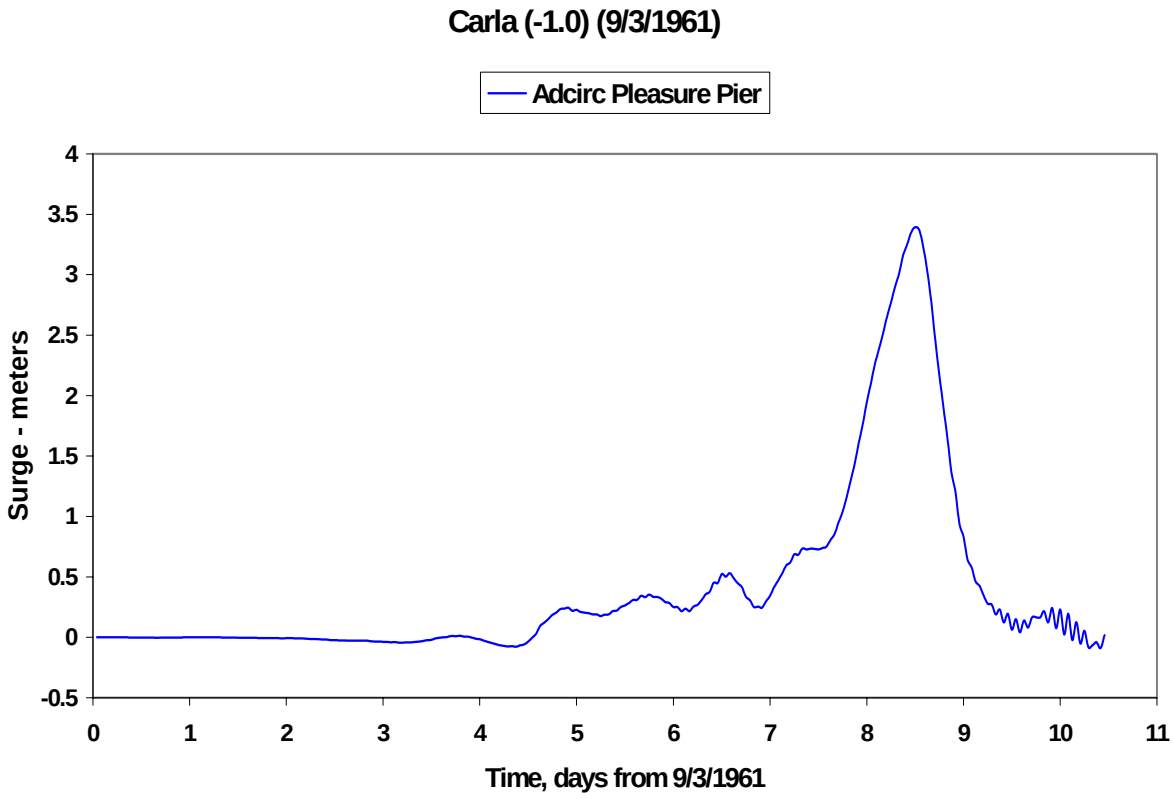
Carla (-1.0) (9/3/1961)
Adcirc Pleasure Pier
Surge - meters
4
3.5
3
2.5
2
1.5
1
0.5
0
-0.5
0
1
2
3
4
5
6
7
8
9
10
11
Time, days from 9/3/1961

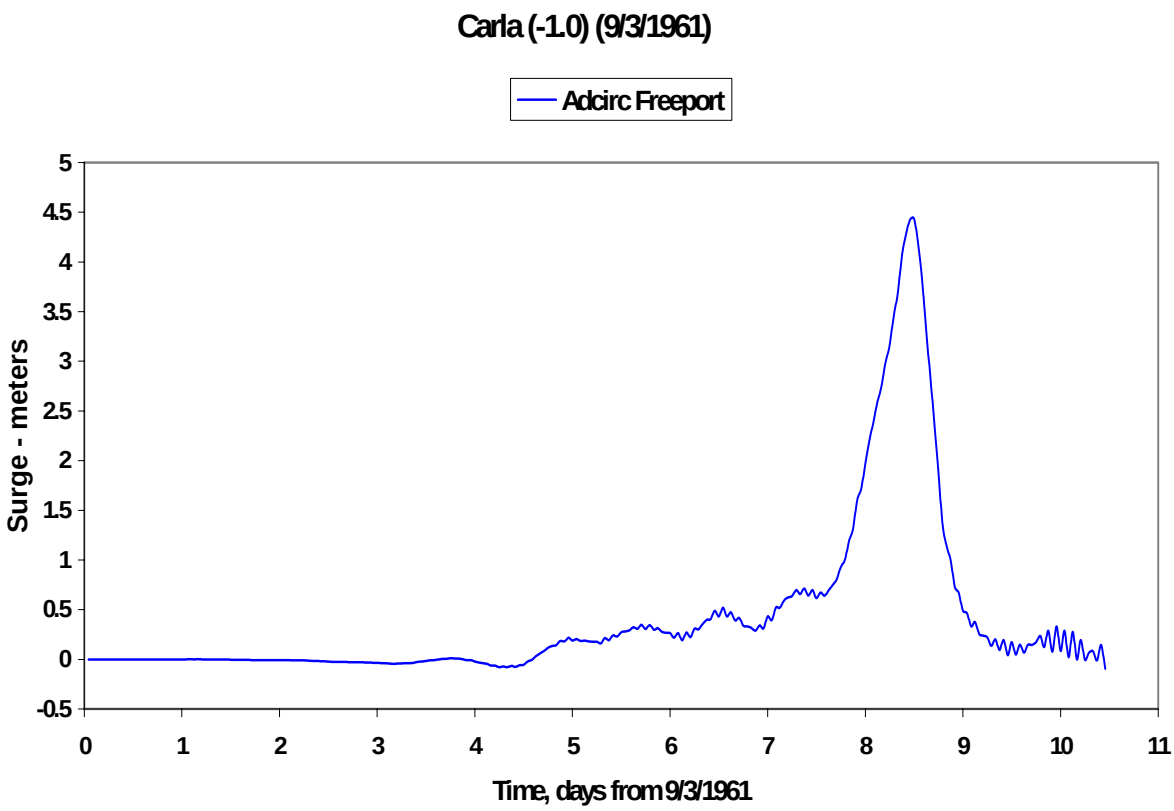
Carla (-1.0) (9/3/1961)
Adcirc Freeport
Surge - meters
5
4.5
4
3.5
3
2.5
2
1.5
1
0.5
0
-0.5
0
1
2
3
4
5
6
7
8
9
10
11
Time, days from 9/3/1961

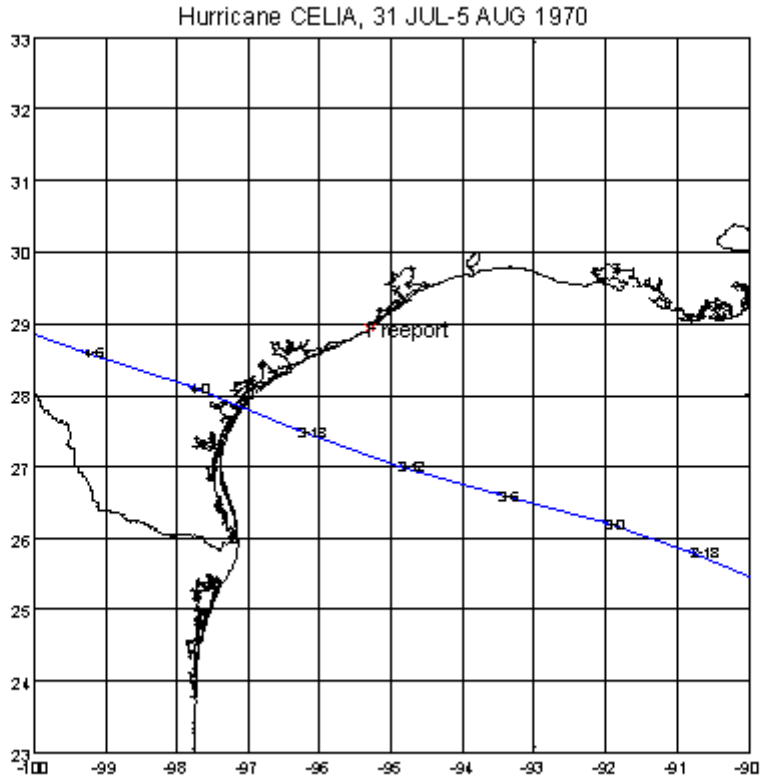
Hurricane CELIA, 31 JUL-5 AUG 1970
Freeport
3-18
33
32
31
30
29
28
27
26
25
24
23
-100
-99
-98
-97
-96
-95
-94
-93
-92
-91
-90

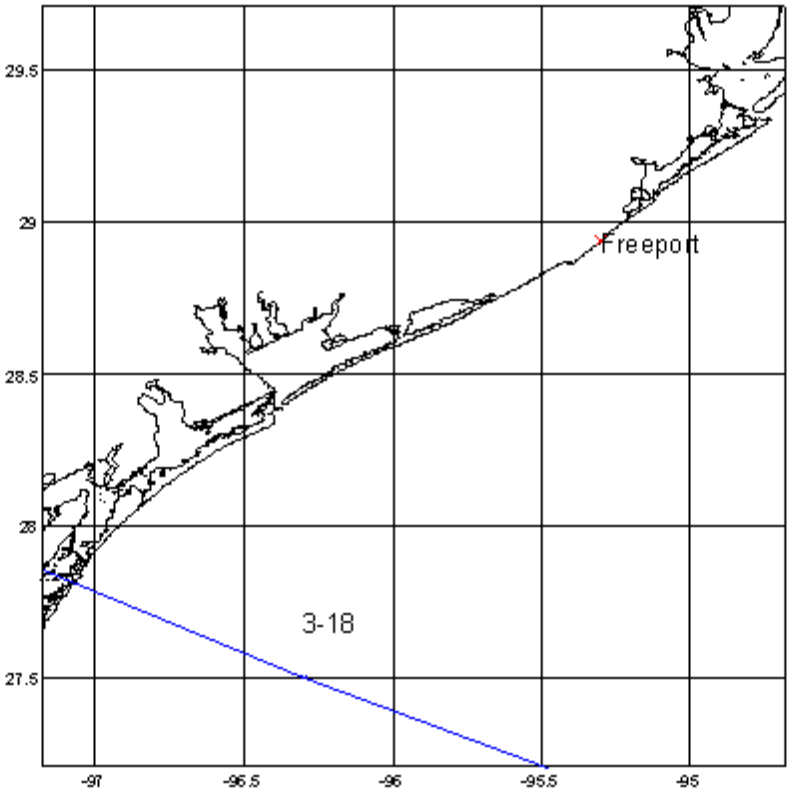
Freeport
3-18
29.5
29
28.5
28
27.5
-97
-96.5
-96
-95.5
-95

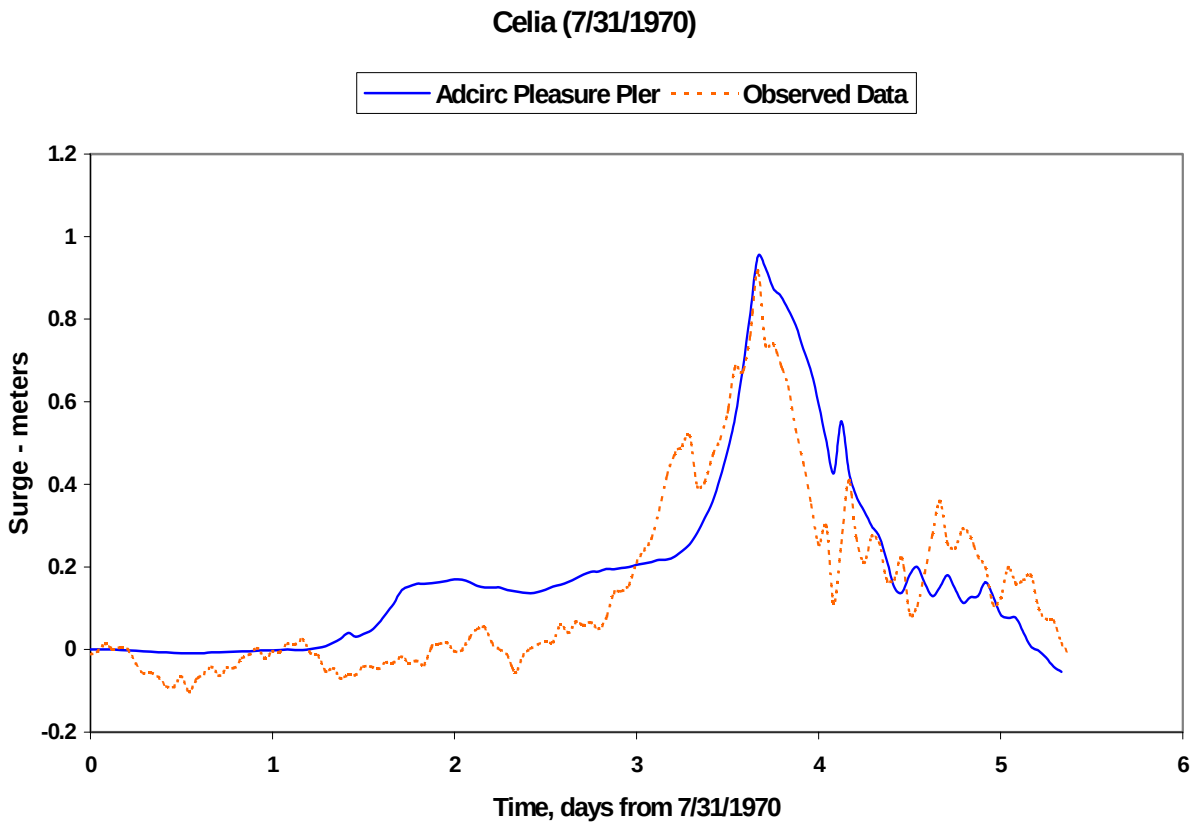
Celia (7/31/1970)
Adcirc Pleasure Pier
Observed Data
Surge - meters
1.2
1
0.8
0.6
0.4
0.2
0
-0.2
0
1
2
3
4
5
6
Time, days from 7/31/1970

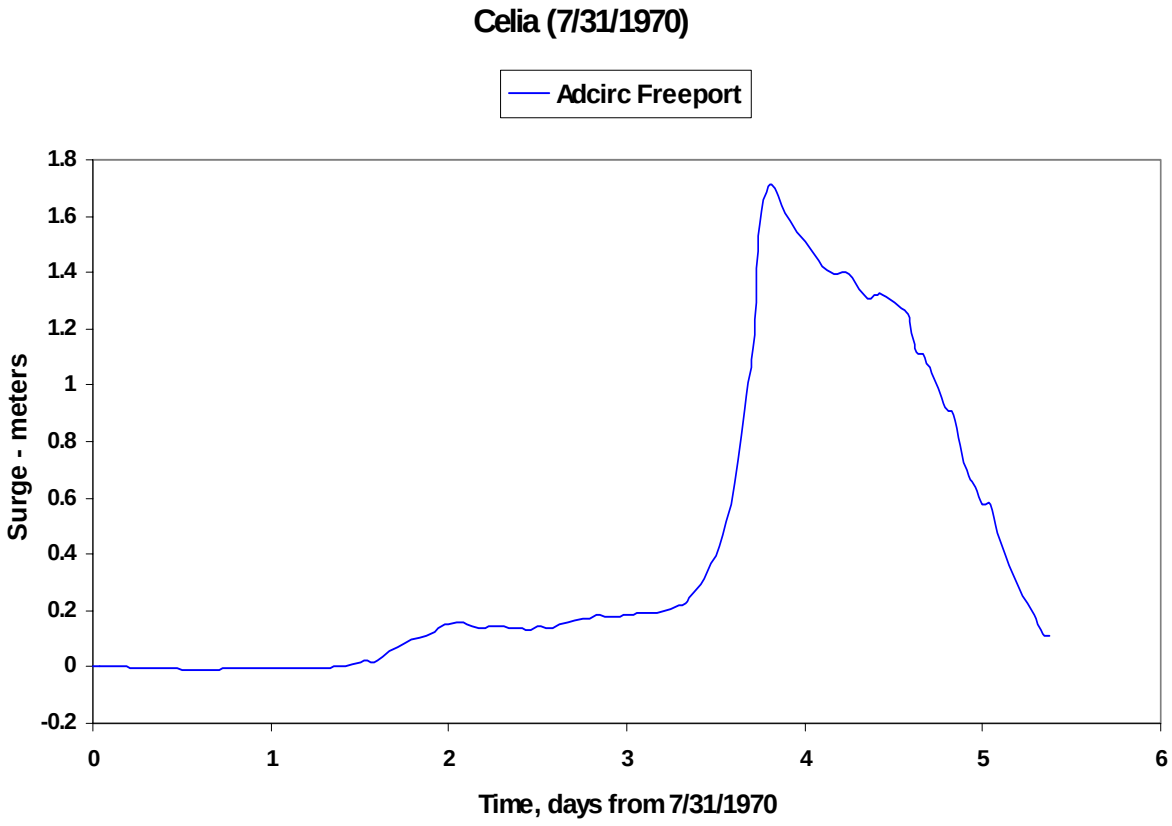
Celia (7/31/1970)
Adcirc Freeport
Surge - meters
1.8
1.6
1.4
1.2
1
0.8
0.6
0.4
0.2
0
-0.2
0
1
2
3
4
5
6
Time, days from 7/31/1970

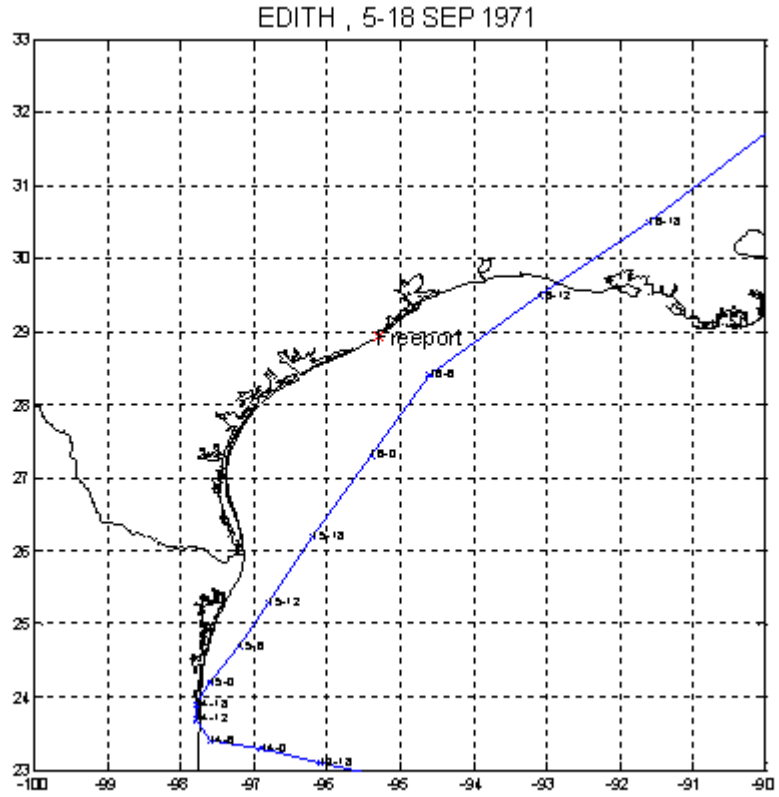
EDITH , 5-18 SEP 1971
Freeport

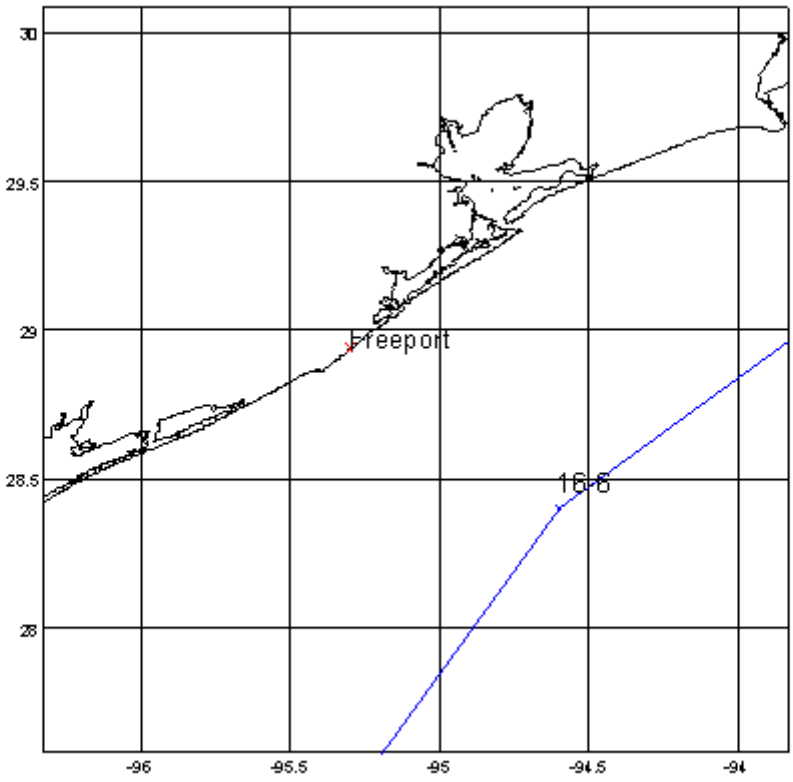
Freeport
16-6

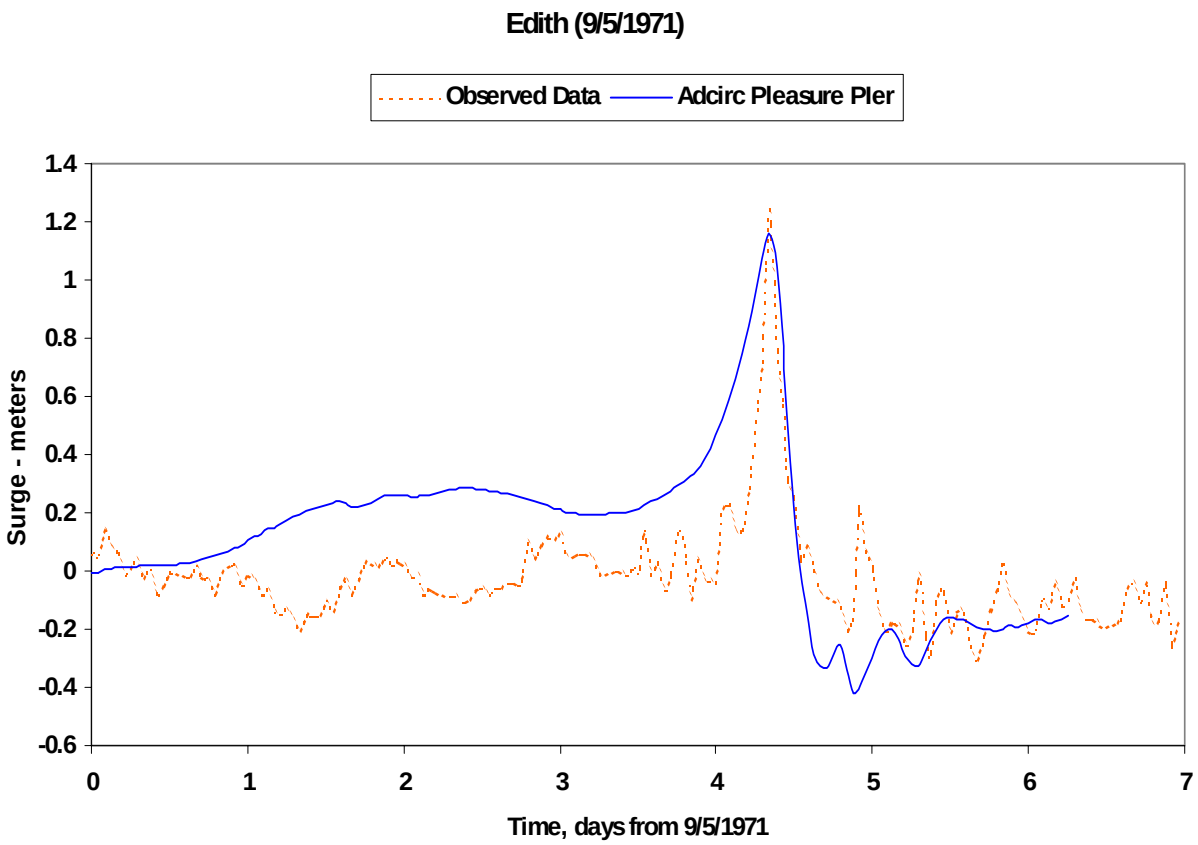
Edith (9/5/1971)
Observed Data
Adcirc Pleasure Pier
Surge - meters
1.4
1.2
1
0.8
0.6
0.4
0.2
0
-0.2
-0.4
-0.6
0
1
2
3
4
5
6
7
Time, days from 9/5/1971

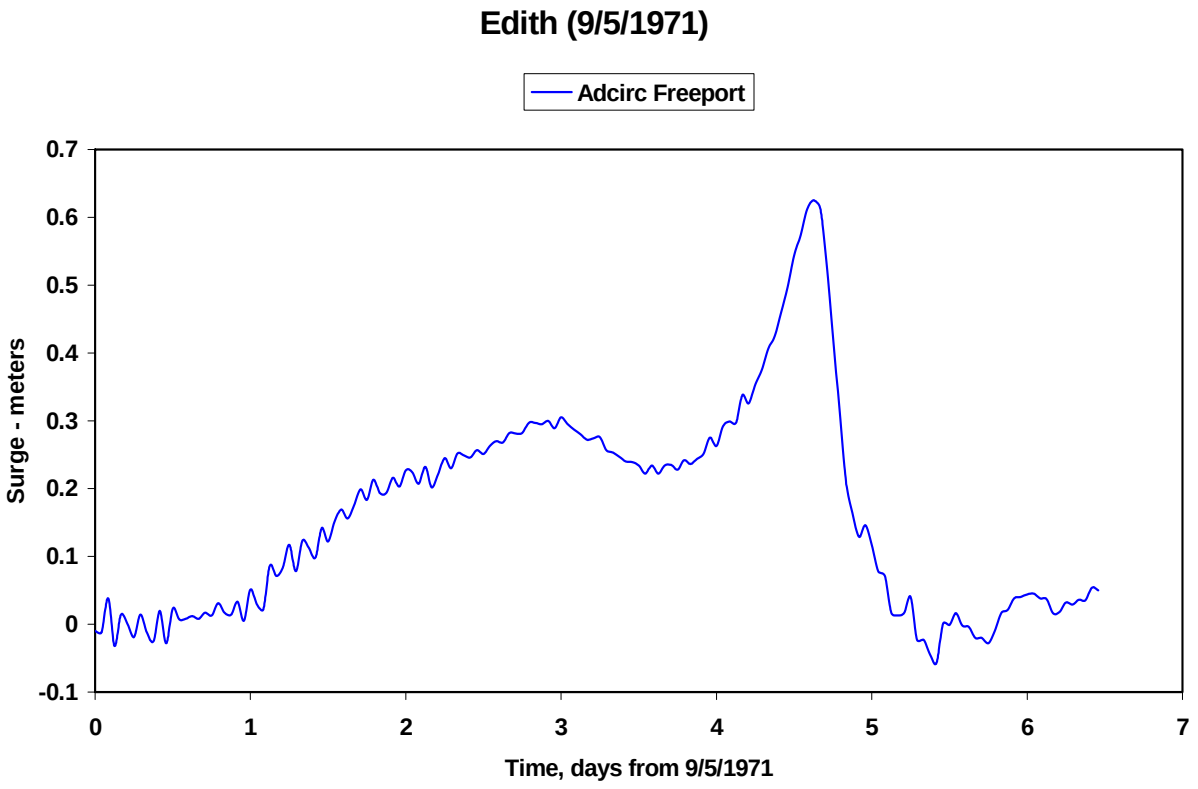
Edith (9/5/1971)
Adcirc Freeport
Surge - meters
0.7
0.6
0.5
0.4
0.3
0.2
0.1
0
-0.1
0
1
2
3
4
5
6
7
Time, days from 9/5/1971

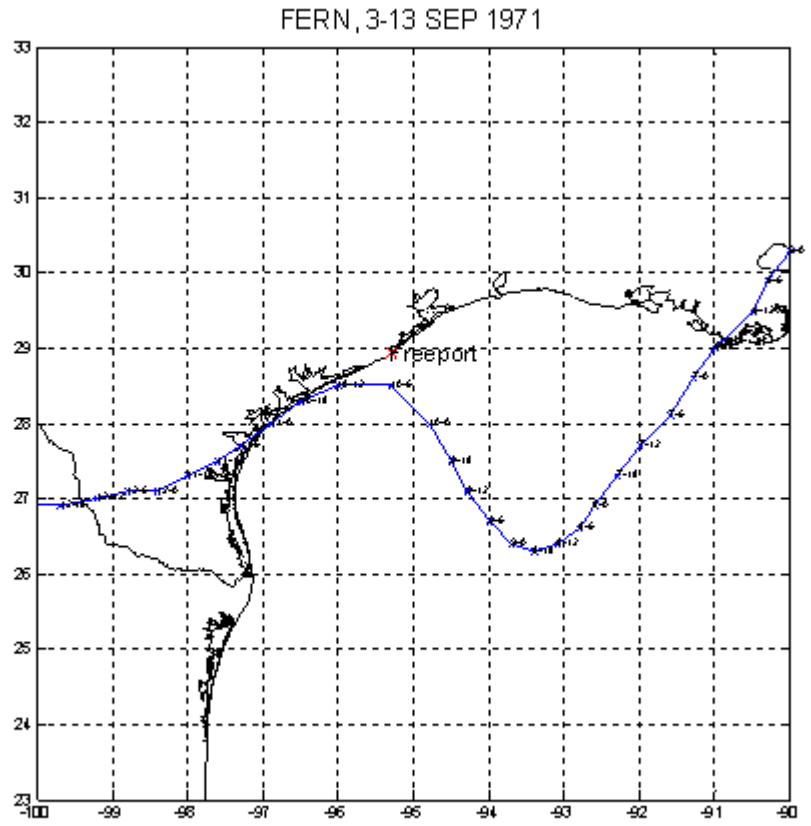
FERN, 3-13 SEP 1971
Freeport

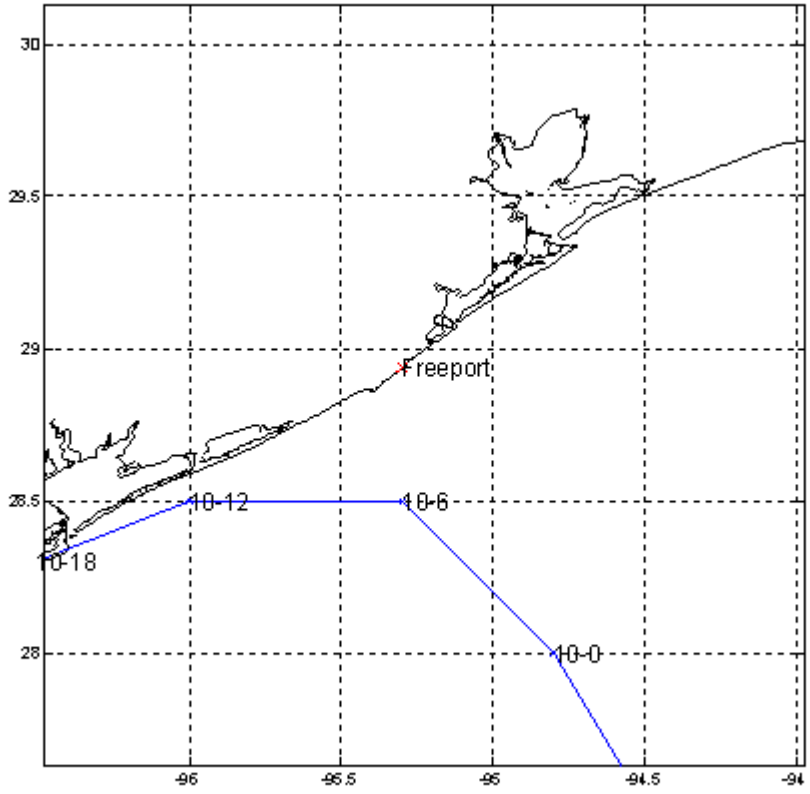
Freeport
10-12
10-6
10-18
10-0

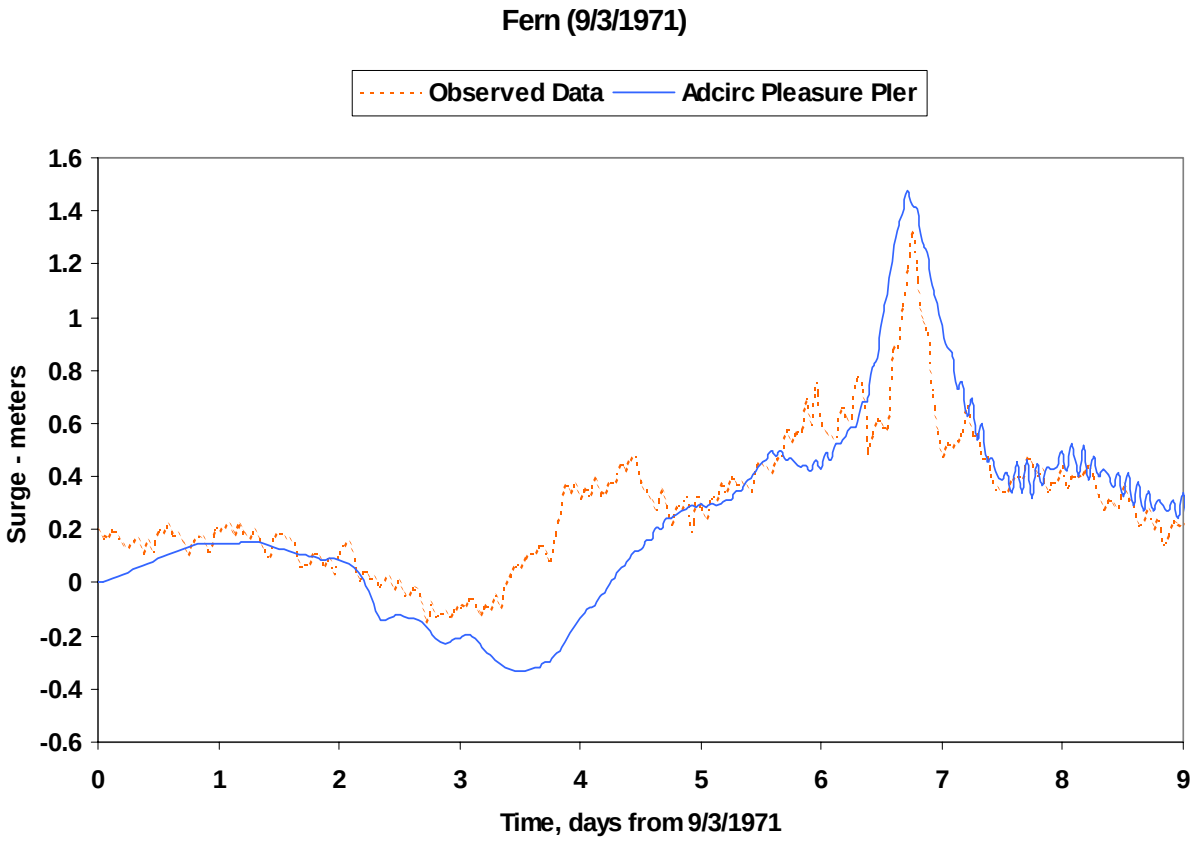
Fern (9/3/1971)
Observed Data
Adcirc Pleasure Pier
Surge - meters
1.6
1.4
1.2
1
0.8
0.6
0.4
0.2
0
-0.2
-0.4
-0.6
0
1
2
3
4
5
6
7
8
9
Time, days from 9/3/1971

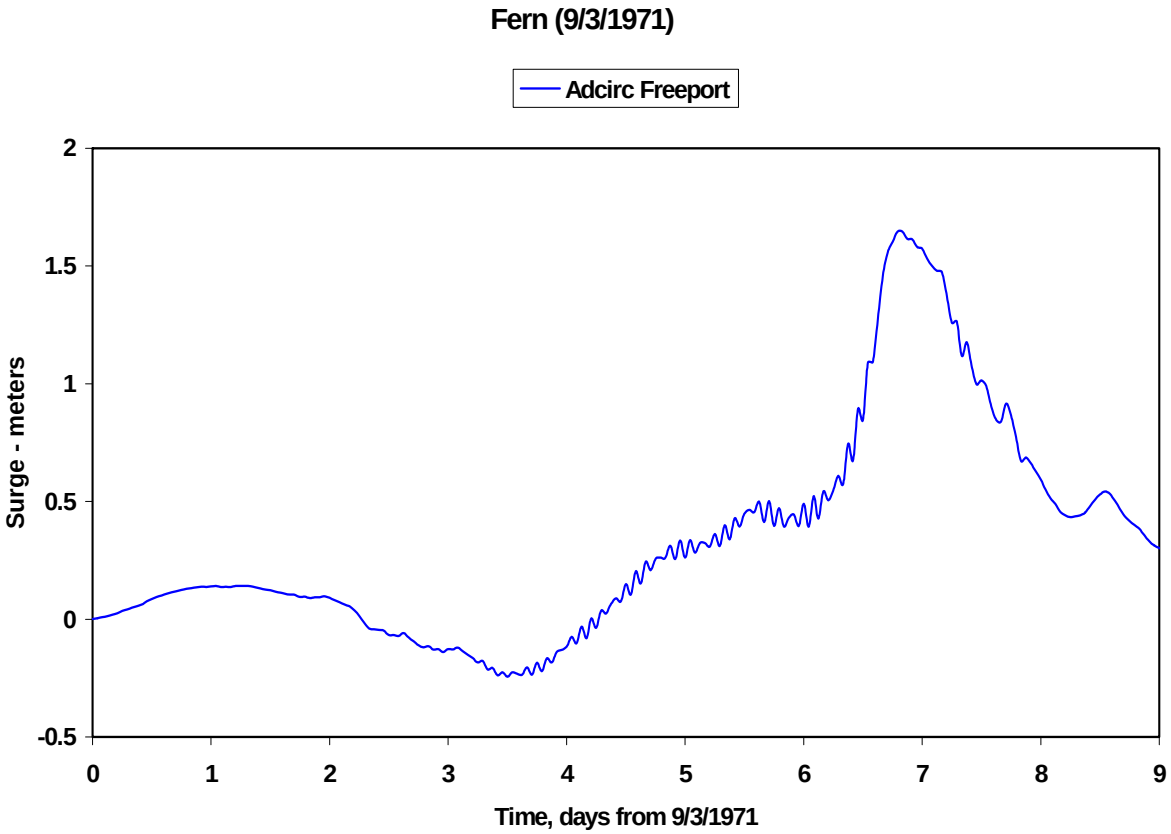
Fern (9/3/1971)
Adcirc Freeport
Surge - meters
2
1.5
1
0.5
0
-0.5
0
1
2
3
4
5
6
7
8
9
Time, days from 9/3/1971

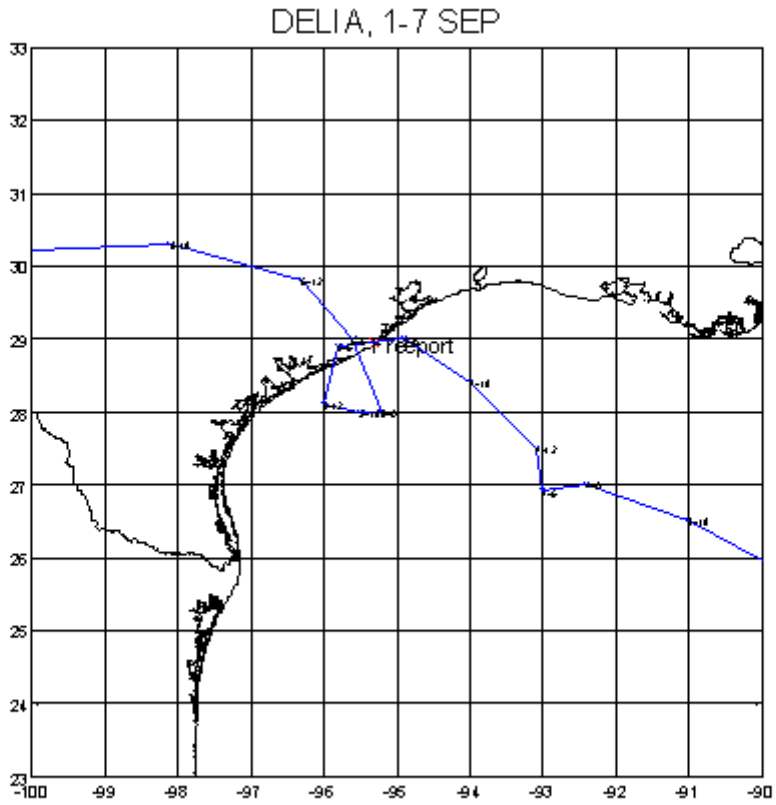
DELIA, 1-7 SEP
Freeport
33
32
31
30
29
28
27
26
25
24
23
-100
-99
-98
-97
-96
-95
-94
-93
-92
-91
-90

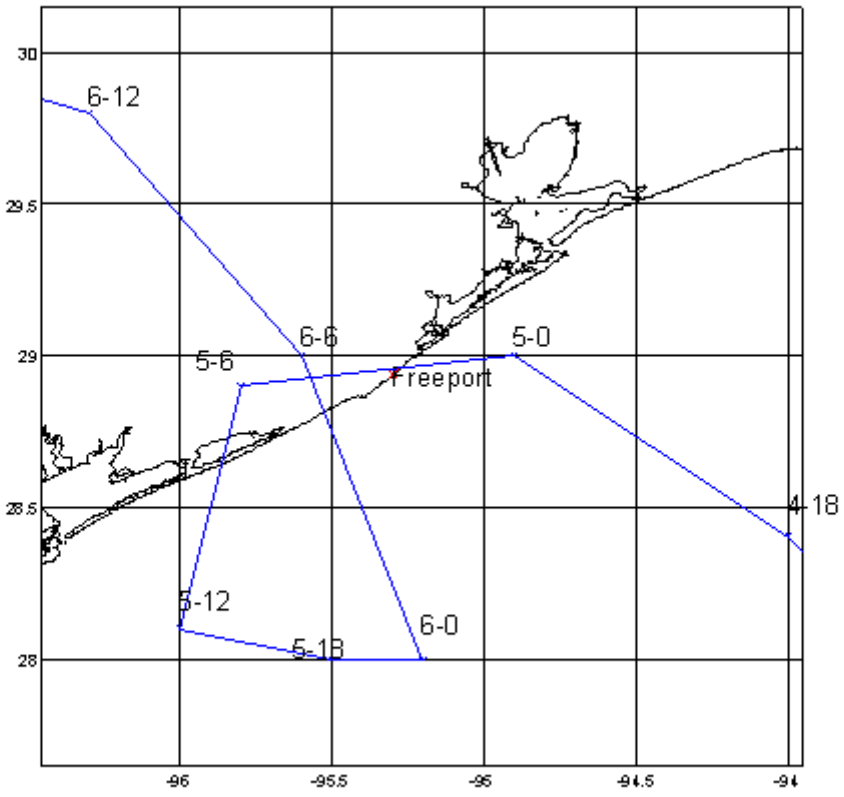
6-12
6-6
5-6
5-0
Freeport
4-18
5-12
6-0
5-18
30
29.5
29
28.5
28
-96
-95.5
-95
-94.5
-94

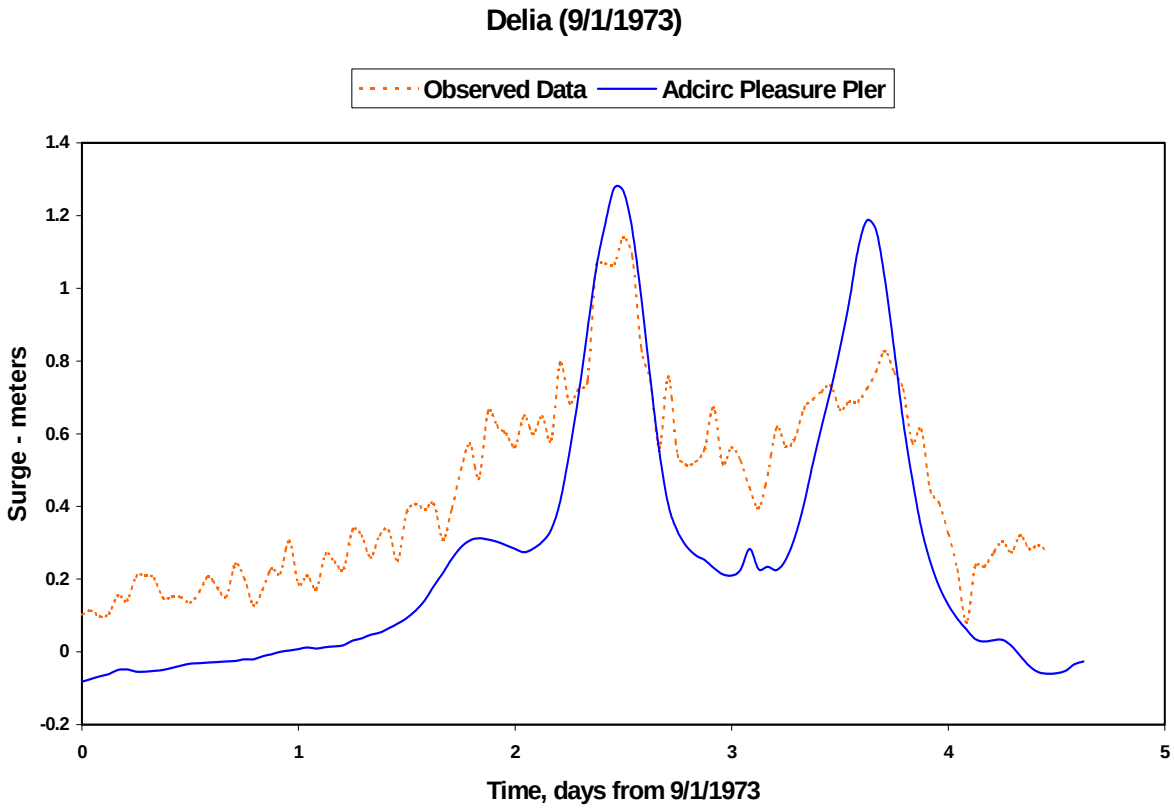
Delia (9/1/1973)
Observed Data
Adcirc Pleasure Pier
Surge - meters
1.4
1.2
1
0.8
0.6
0.4
0.2
0
-0.2
0
1
2
3
4
5
Time, days from 9/1/1973

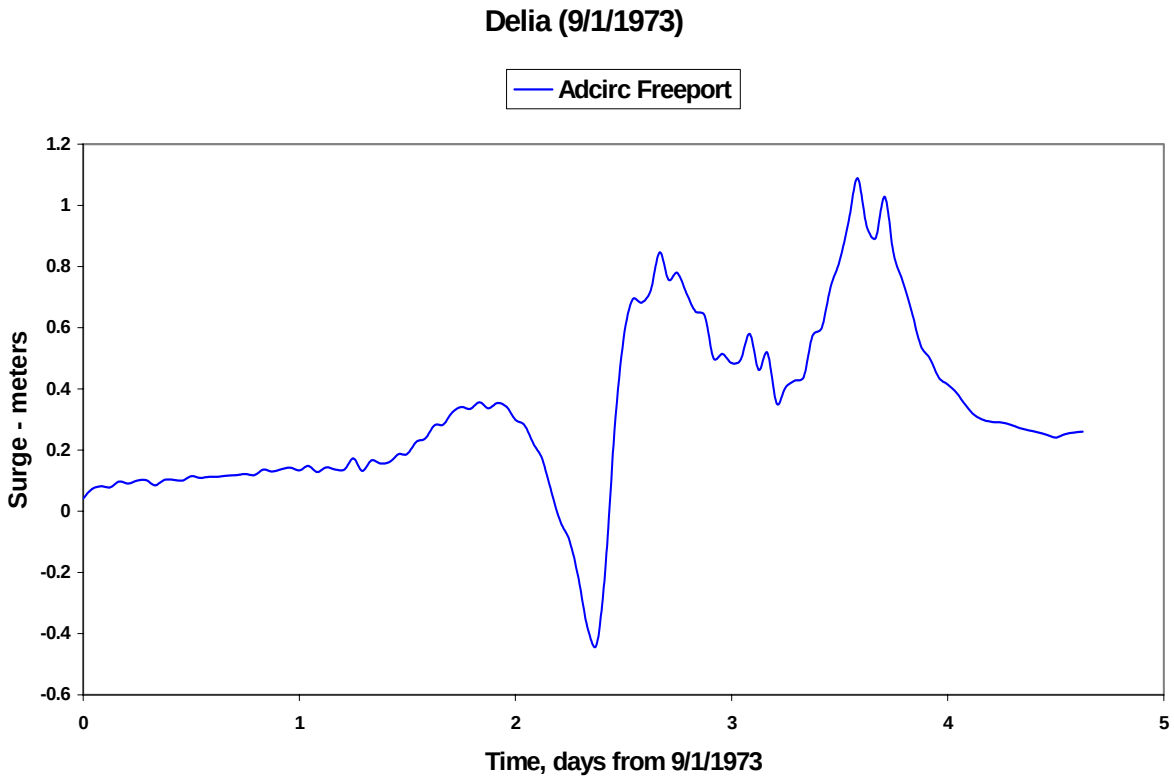
Delia (9/1/1973)
Adcirc Freeport
Surge - meters
1.2
1
0.8
0.6
0.4
0.2
0
-0.2
-0.4
-0.6
0
1
2
3
4
5
Time, days from 9/1/1973

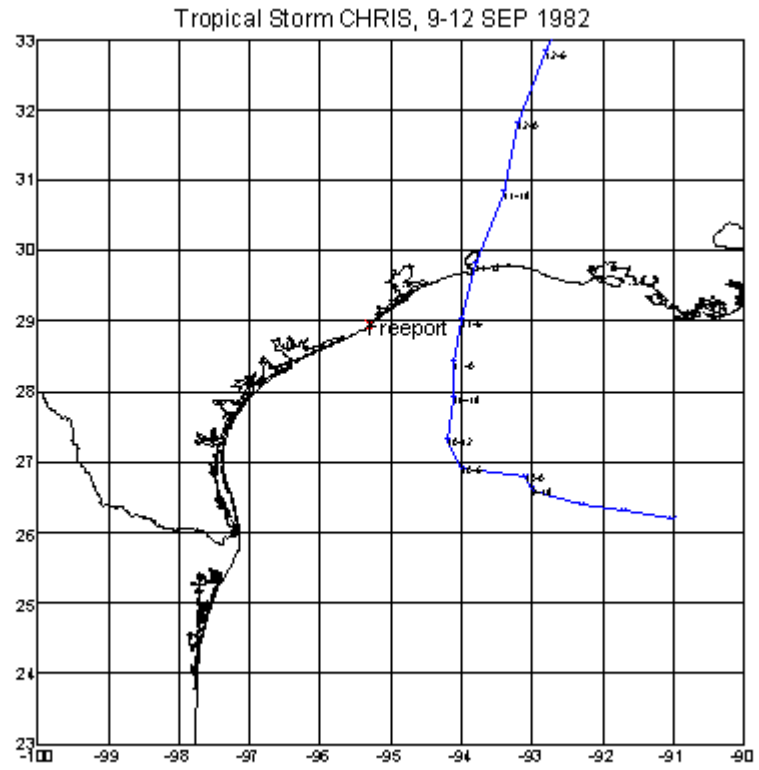
Tropical Storm CHRIS, 9-12 SEP 1982
Freeport
33
32
31
30
29
28
27
26
25
24
23
-100
-99
-98
-97
-96
-95
-94
-93
-92
-91
-90

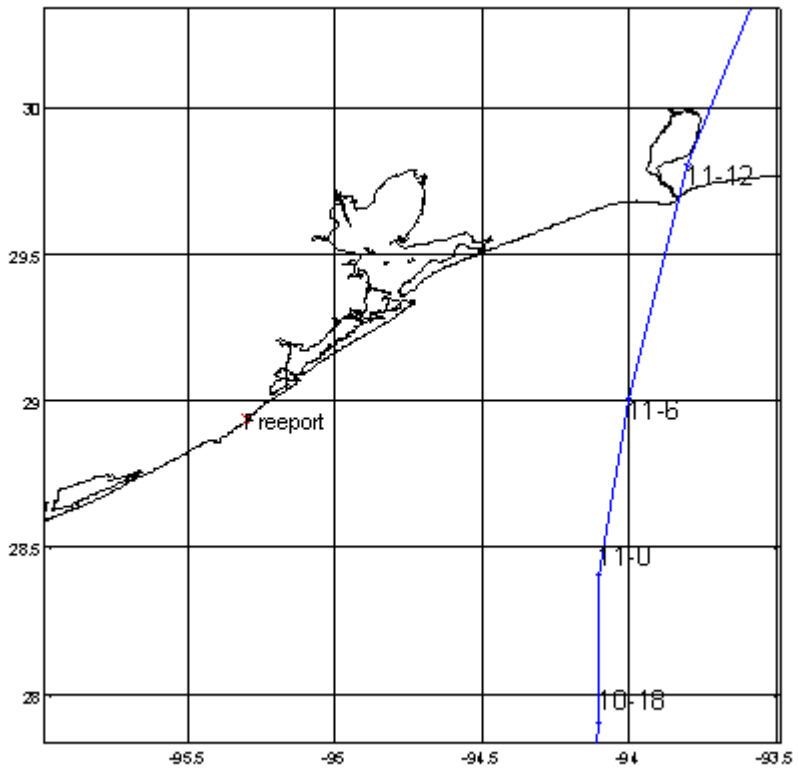
Freeport
11-12
11-6
11-0
10-18
30
29.5
29
28.5
28
-95.5
-95
-94.5
-94
-93.5

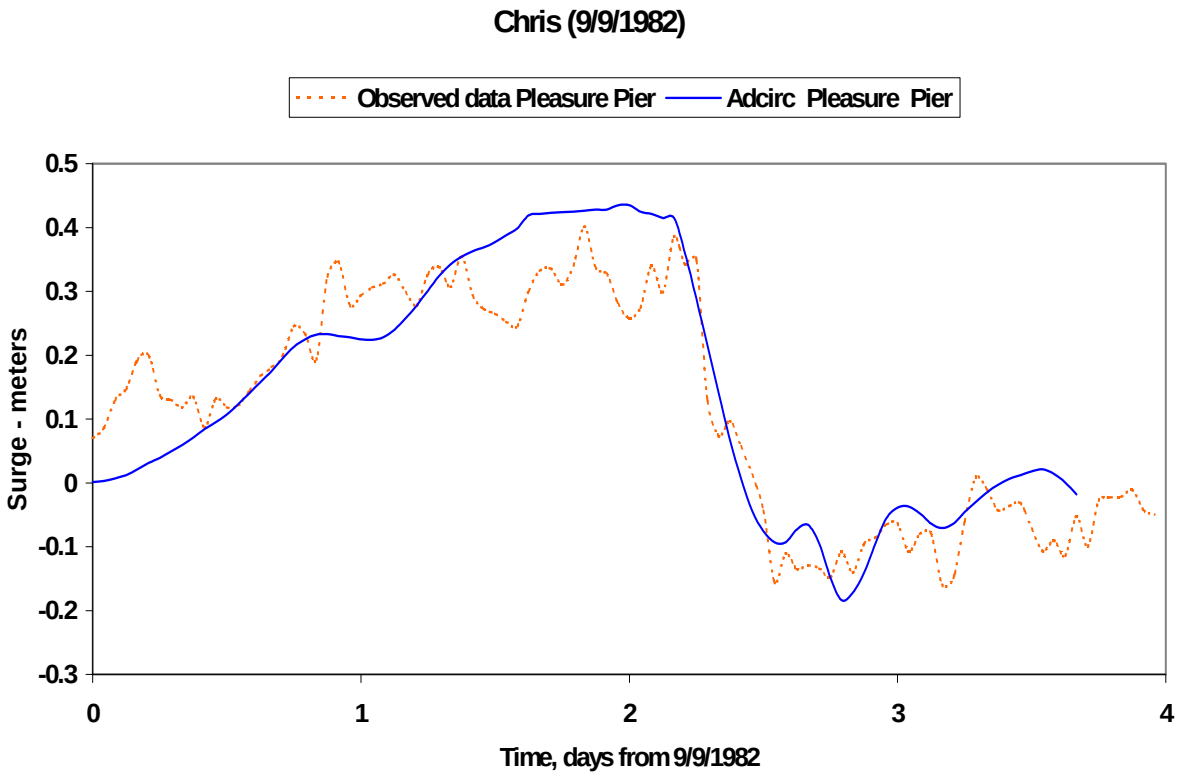
Chris (9/9/1982)
Observed data Pleasure Pier
Adcirc Pleasure Pier
0.5
0.4
0.3
0.2
0.1
0
-0.1
-0.2
-0.3
Surge - meters
0
1
2
3
4
Time, days from 9/9/1982

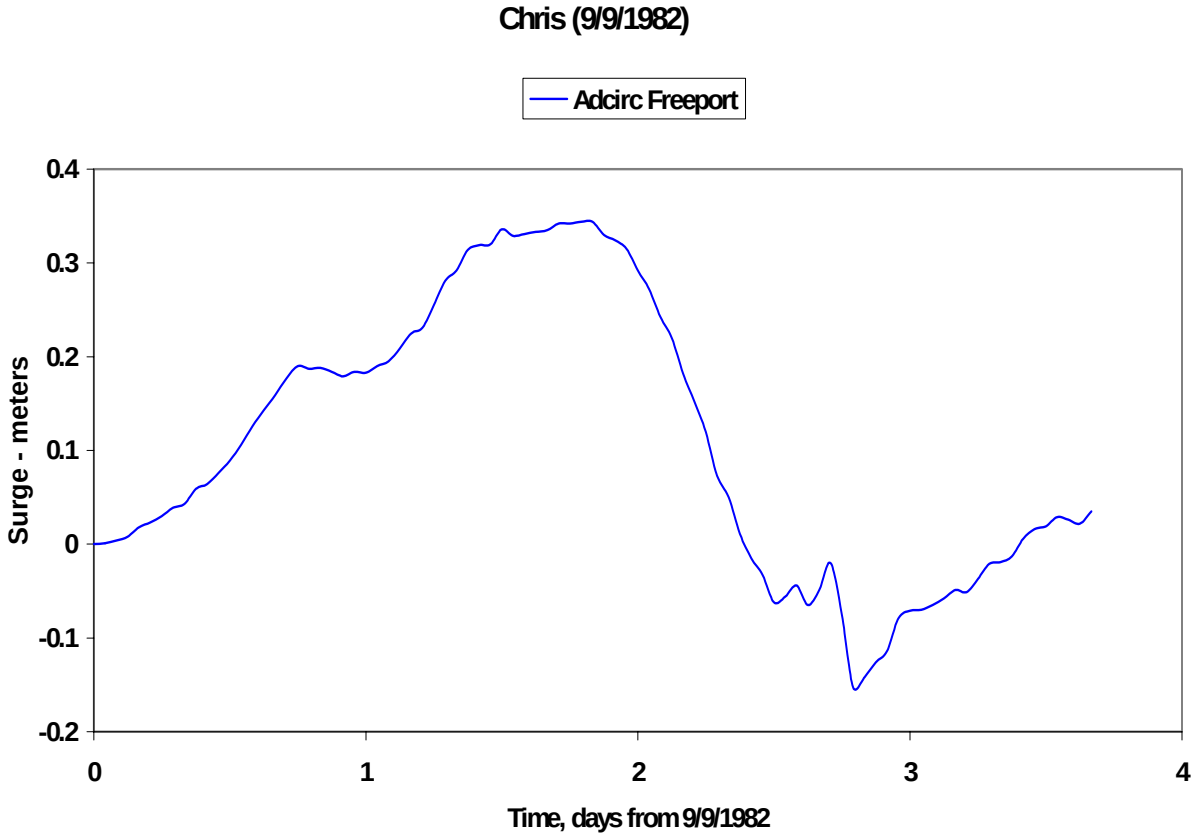
Chris (9/9/1982)
Adcirc Freeport
0.4
0.3
0.2
0.1
0
-0.1
-0.2
Surge - meters
0
1
2
3
4
Time, days from 9/9/1982

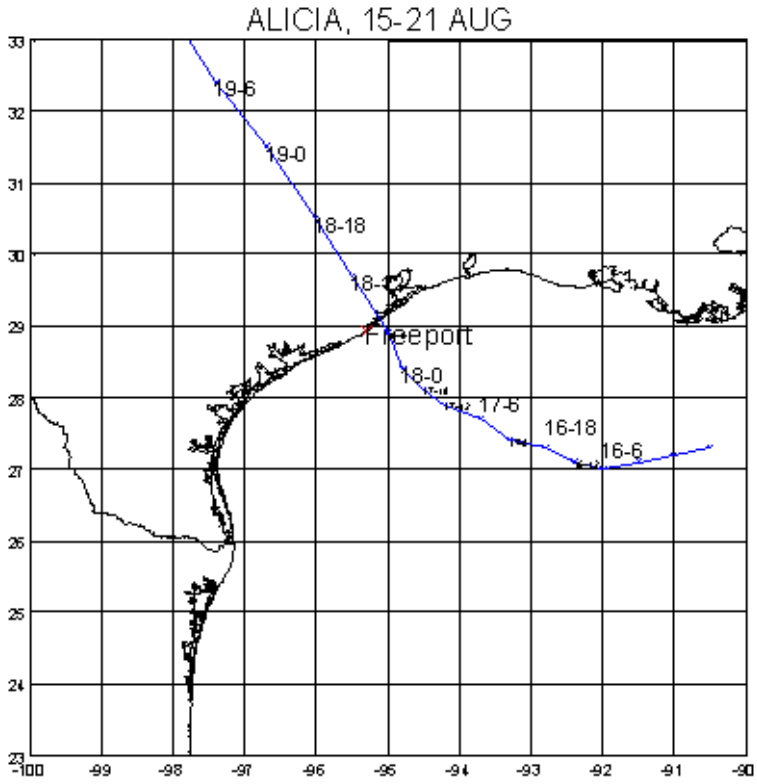
ALICIA, 15-21 AUG
19-6
19-0
18-18
18-12
Freeport
18-0
17-6
16-18
16-6
33
32
31
30
29
28
27
26
25
24
23
-100
-99
-98
-97
-96
-95
-94
-93
-92
-91
-90

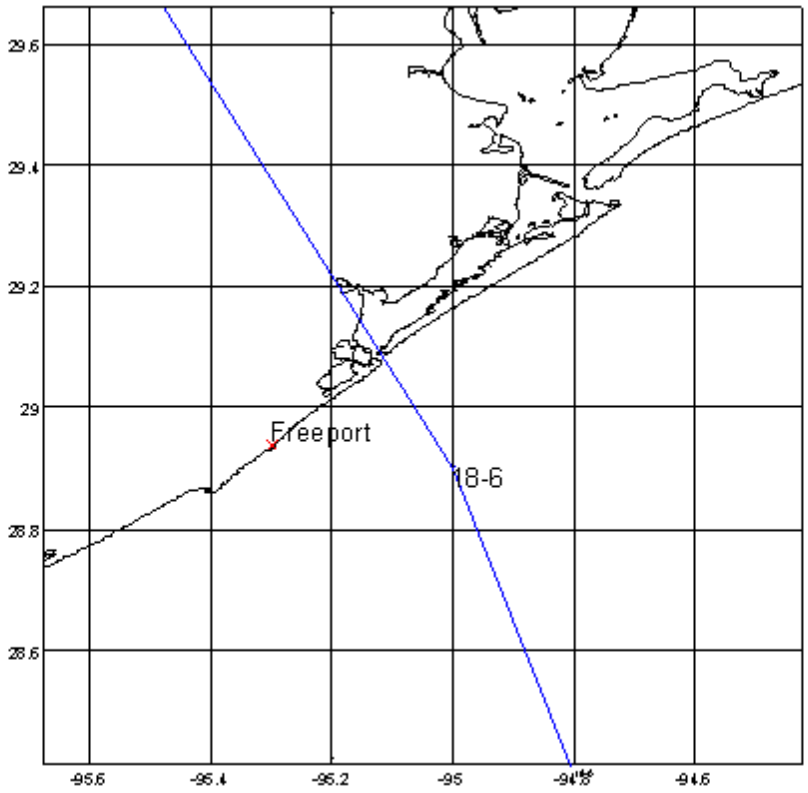
Freeport
18-6
29.6
29.4
29.2
29
28.8
28.6
-95.6
-95.4
-95.2
-95
-94.8
-94.6

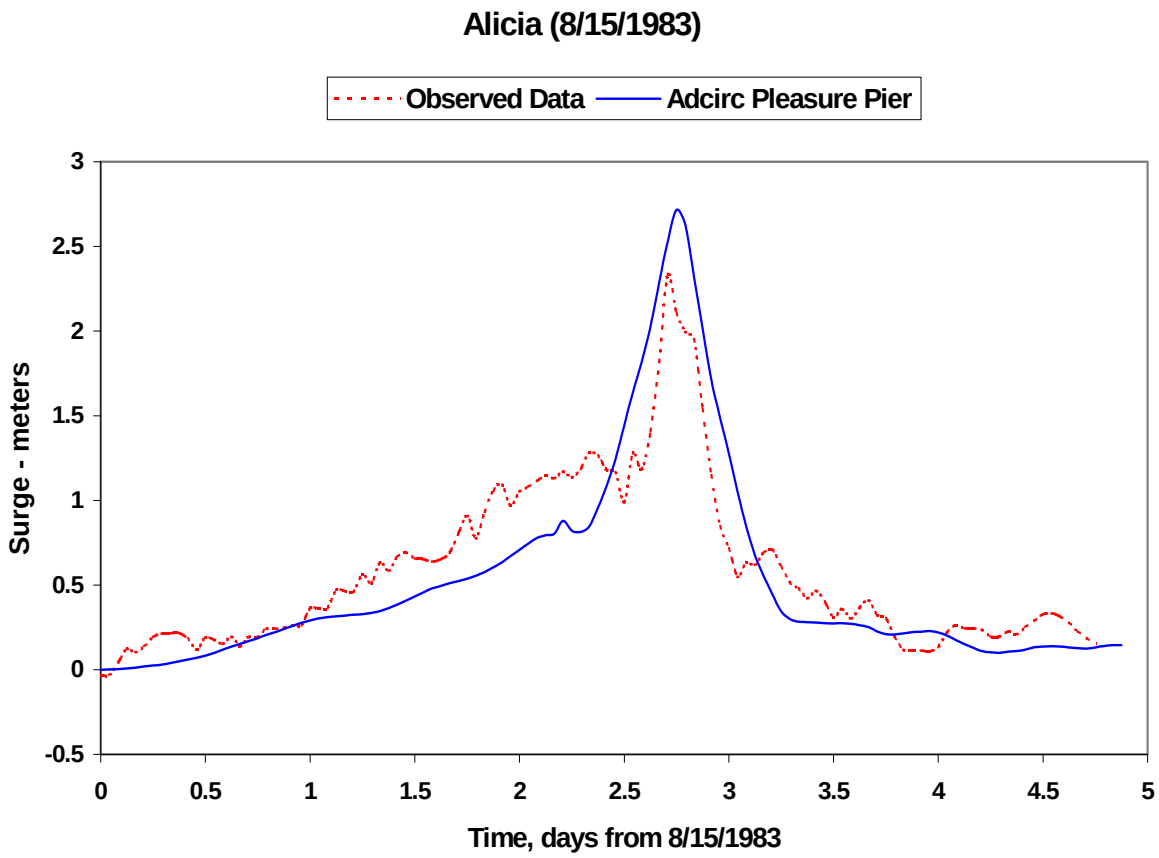
Alicia (8/15/1983)
Observed Data
Adcirc Pleasure Pier
Surge - meters
Time, days from 8/15/1983
3
2.5
2
1.5
1
0.5
0
-0.5
0
0.5
1
1.5
2
2.5
3
3.5
4
4.5
5

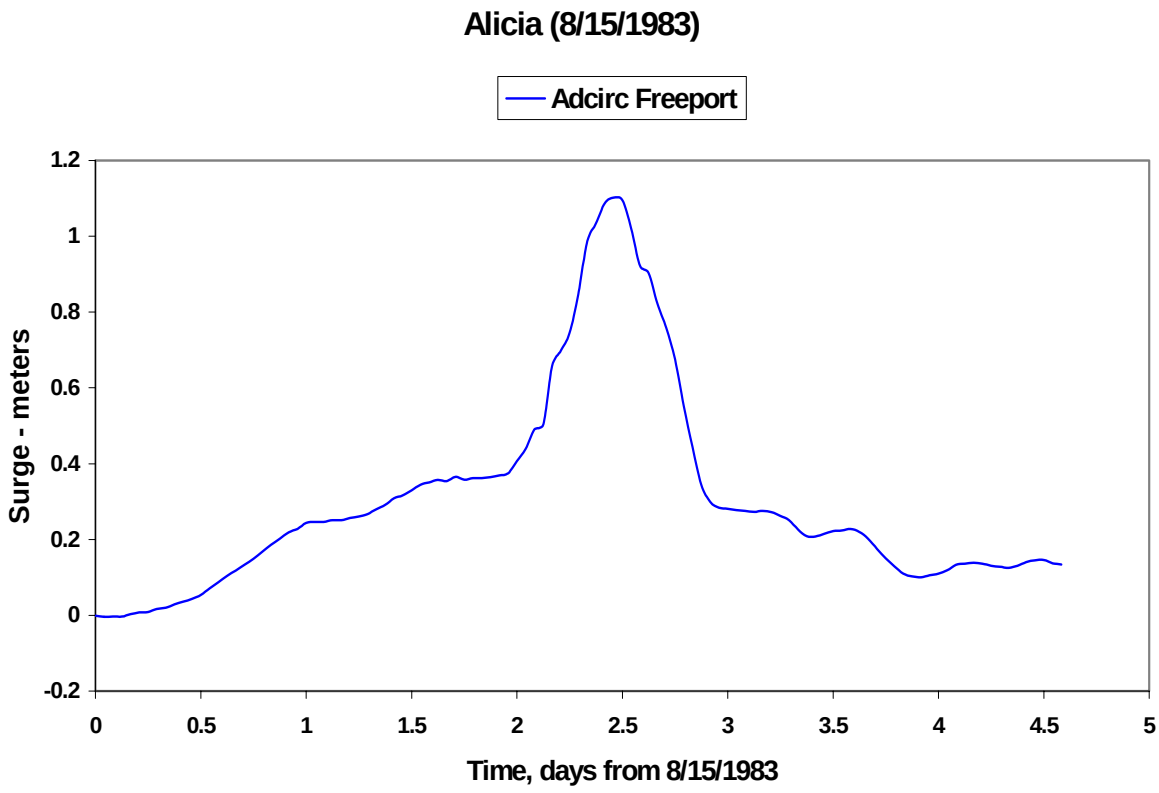
Alicia (8/15/1983)
Adcirc Freeport
Surge - meters
Time, days from 8/15/1983
1.2
1
0.8
0.6
0.4
0.2
0
-0.2
0
0.5
1
1.5
2
2.5
3
3.5
4
4.5
5

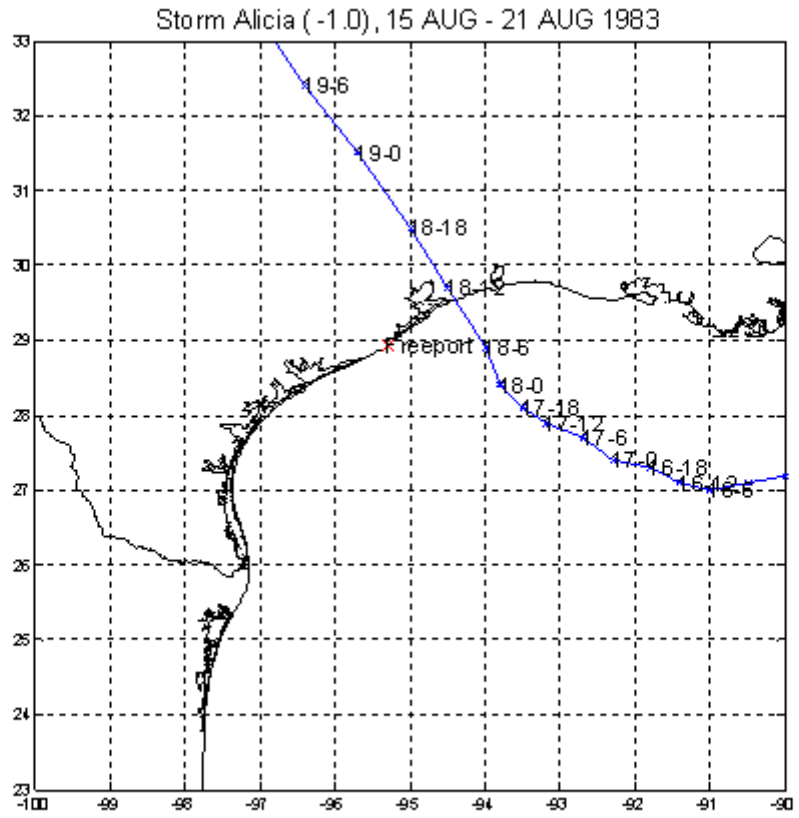
Storm Alicia (-1.0), 15 AUG - 21 AUG 1983
19-6
19-0
18-18
18-12
Freeport
18-6
18-0
17-18
17-12
17-6
17-0
16-18
16-12
16-6
33
32
31
30
29
28
27
26
25
24
23
-100
-99
-98
-97
-96
-95
-94
-93
-92
-91
-90

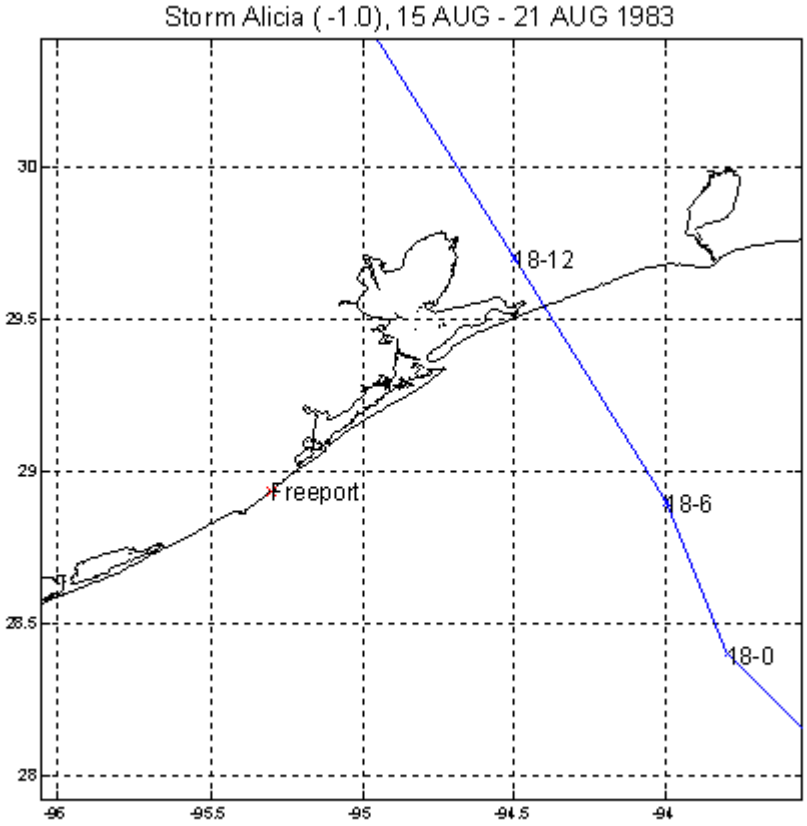
Storm Alicia (-1.0), 15 AUG - 21 AUG 1983
18-12
Freeport
18-6
18-0
30
29.5
29
28.5
28
-96
-95.5
-95
-94.5
-94

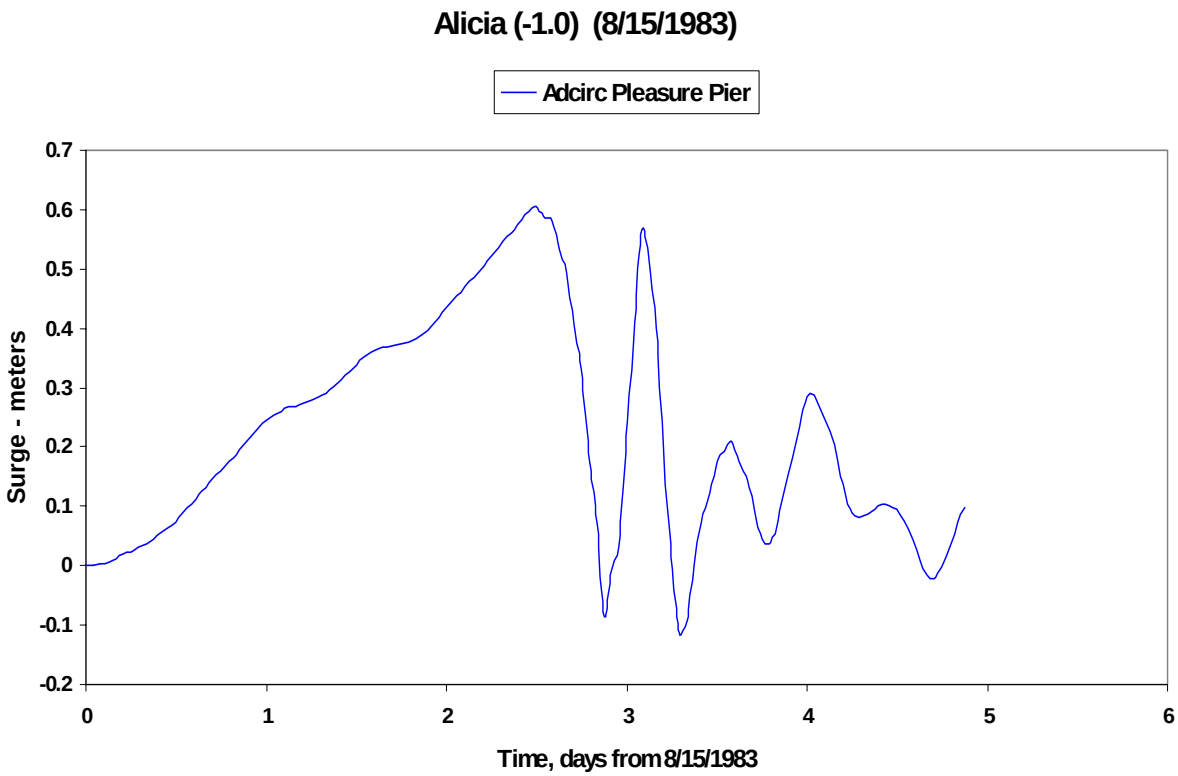
Alicia (-1.0) (8/15/1983)
Adcirc Pleasure Pier
Surge - meters
0.7
0.6
0.5
0.4
0.3
0.2
0.1
0
-0.1
-0.2
0
1
2
3
4
5
6
Time, days from 8/15/1983

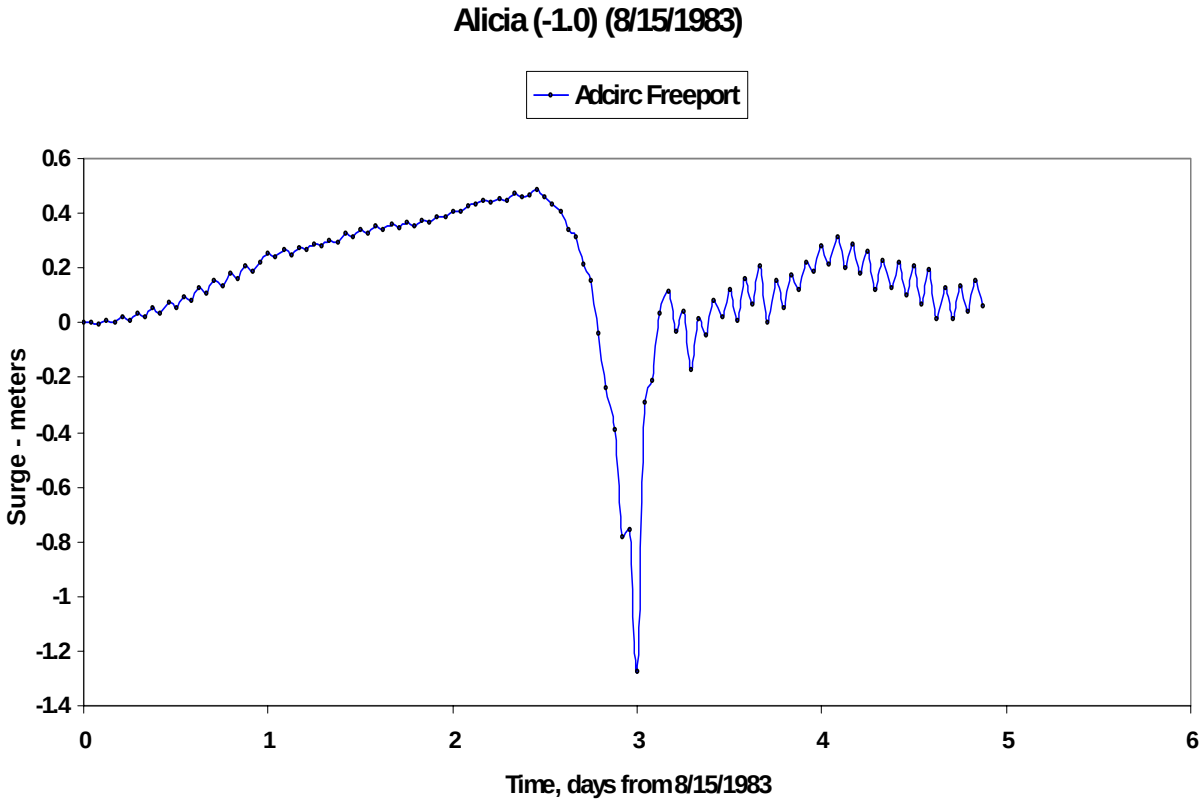
Alicia (-1.0) (8/15/1983)
Adcirc Freeport
Surge - meters
0.6
0.4
0.2
0
-0.2
-0.4
-0.6
-0.8
-1
-1.2
-1.4
0
1
2
3
4
5
6
Time, days from 8/15/1983

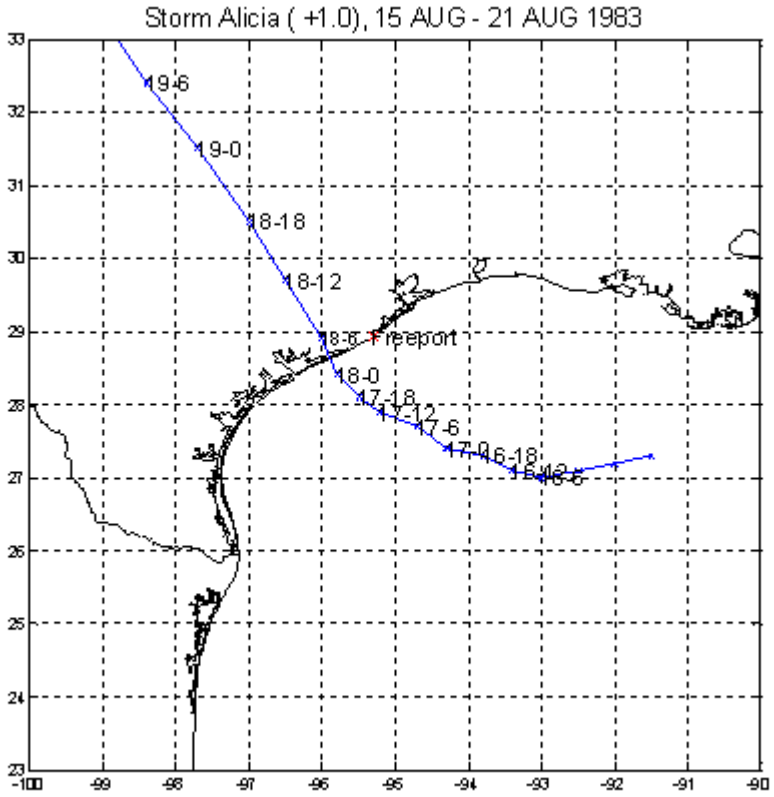
Storm Alicia (+1.0), 15 AUG - 21 AUG 1983
19-6
19-0
18-18
18-12
18-6
Freeport
18-0
17-18
17-12
17-6
17-0
16-18
16-12
16-6
33
32
31
30
29
28
27
26
25
24
23
-100
-99
-98
-97
-96
-95
-94
-93
-92
-91
-90

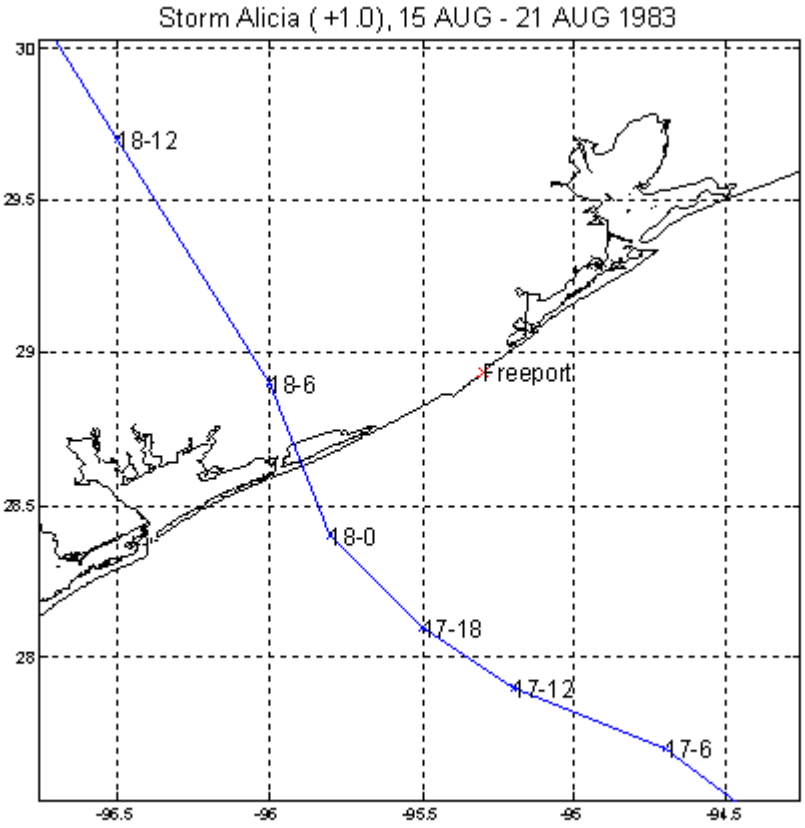
Storm Alicia (+1.0), 15 AUG - 21 AUG 1983
18-12
18-6
Freeport
18-0
17-18
17-12
17-6
30
29.5
29
28.5
28
-96.5
-96
-95.5
-95
-94.5

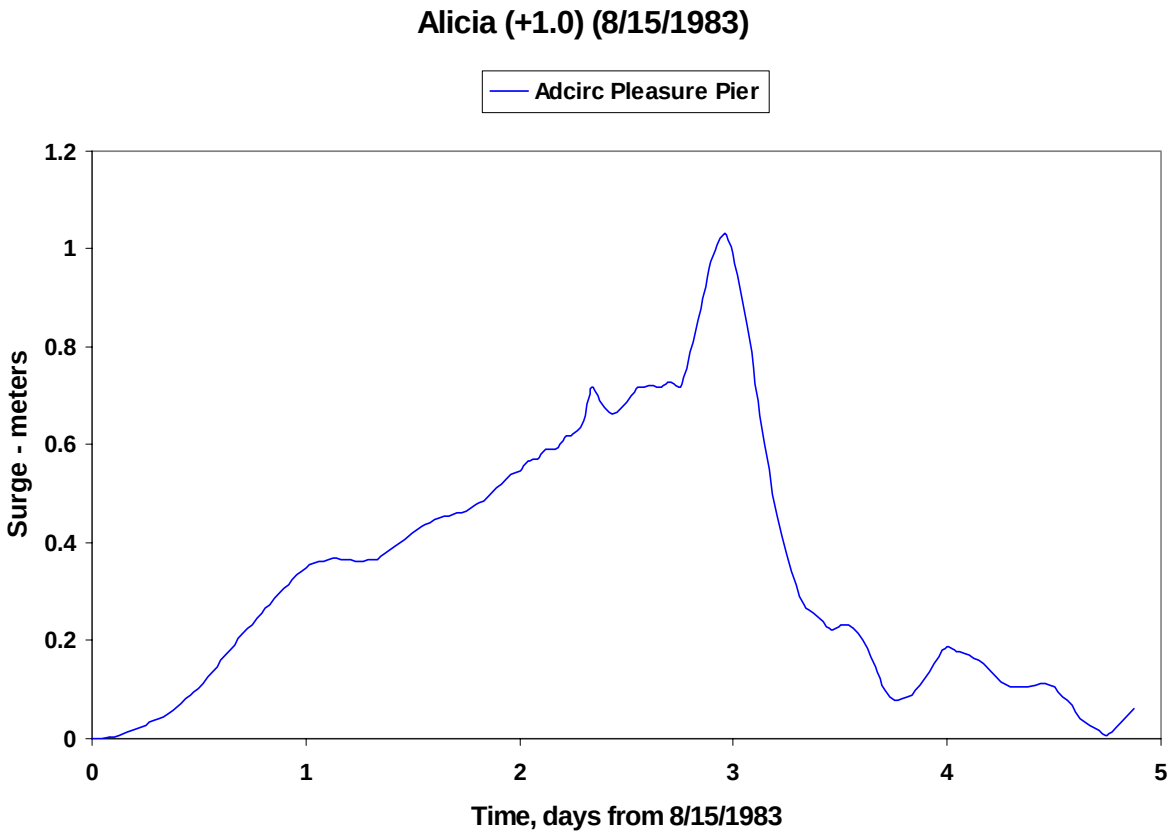
Alicia (+1.0) (8/15/1983)
Adcirc Pleasure Pier
Surge - meters
Time, days from 8/15/1983
0
0.2
0.4
0.6
0.8
1
1.2
0
1
2
3
4
5

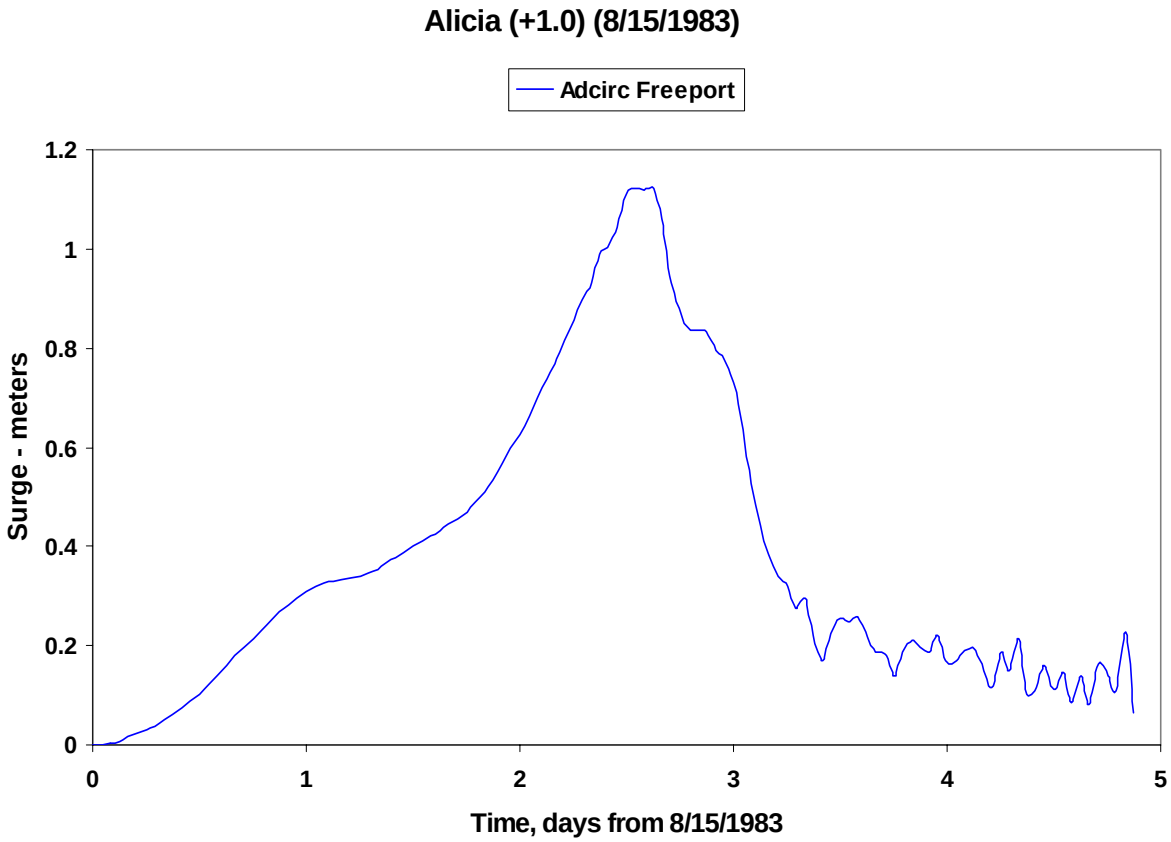
Alicia (+1.0) (8/15/1983)
Adcirc Freeport
Surge - meters
Time, days from 8/15/1983
0
0.2
0.4
0.6
0.8
1
1.2
0
1
2
3
4
5

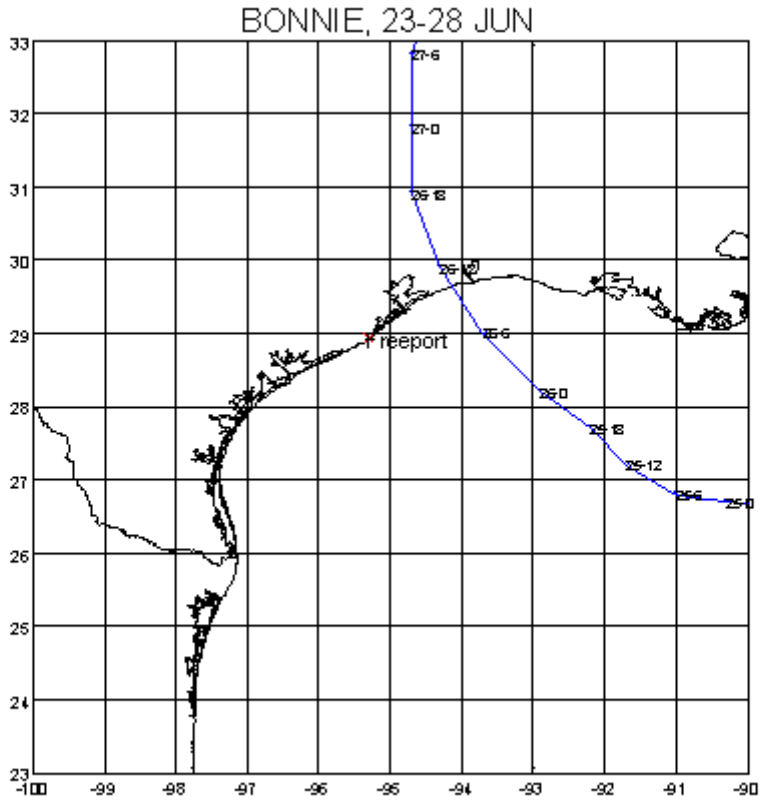
BONNIE, 23-28 JUN
Freeport
27-6
27-0
26-18
26-12
26-6
26-0
25-18
25-12
25-6
25-0
33
32
31
30
29
28
27
26
25
24
23
-100
-99
-98
-97
-96
-95
-94
-93
-92
-91
-90

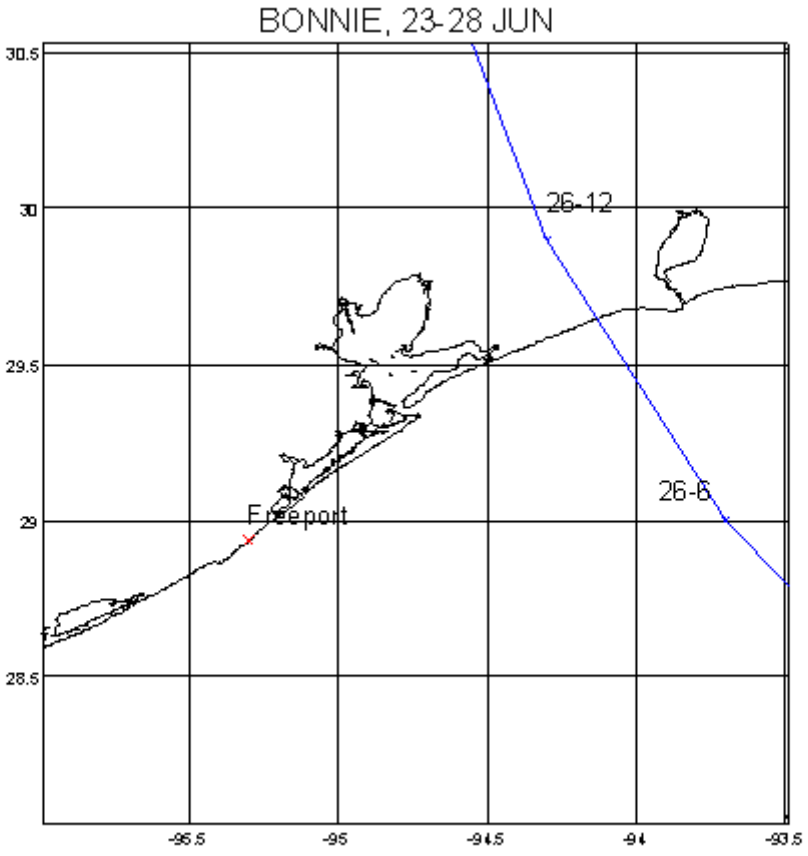
BONNIE, 23-28 JUN
26-12
26-6
Freeport
30.5
30
29.5
29
28.5
-95.5
-95
-94.5
-94
-93.5

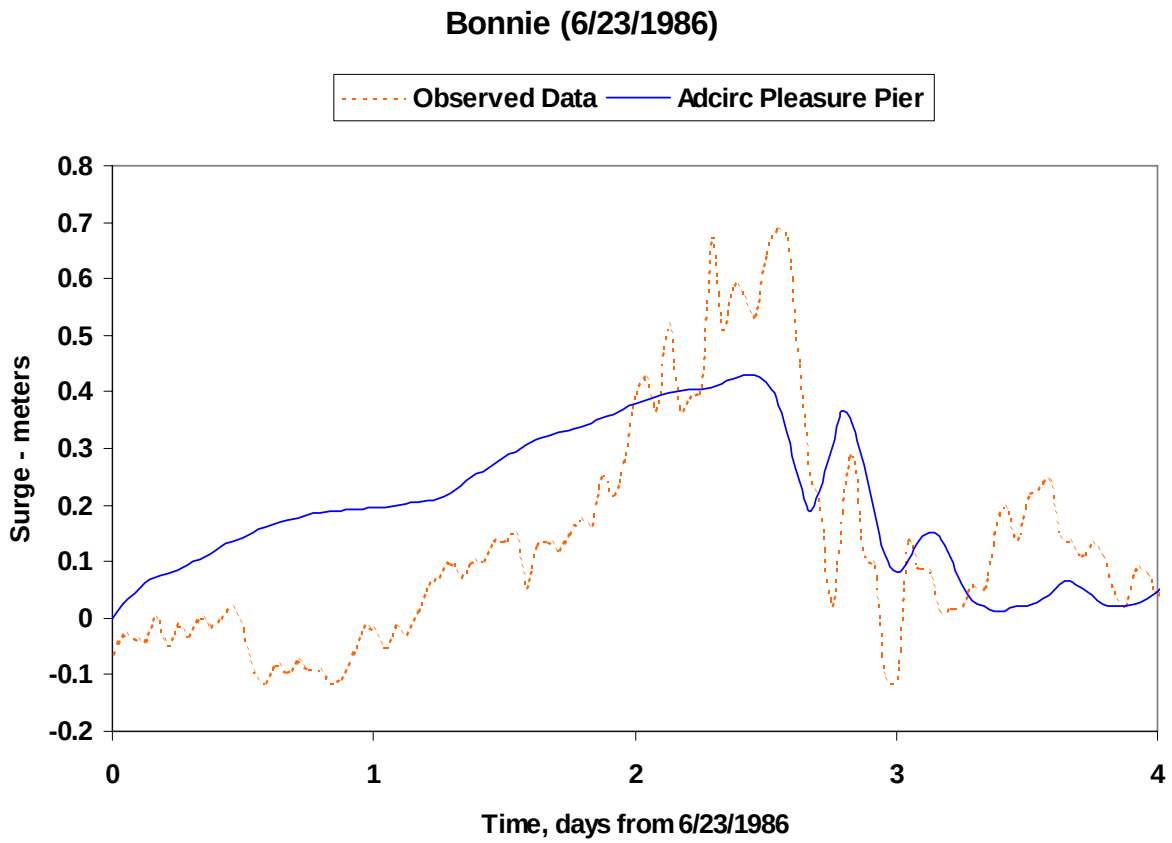
Bonnie (6/23/1986)
Observed Data
Adcirc Pleasure Pier
Surge - meters
0.8
0.7
0.6
0.5
0.4
0.3
0.2
0.1
0
-0.1
-0.2
0
1
2
3
4
Time, days from 6/23/1986

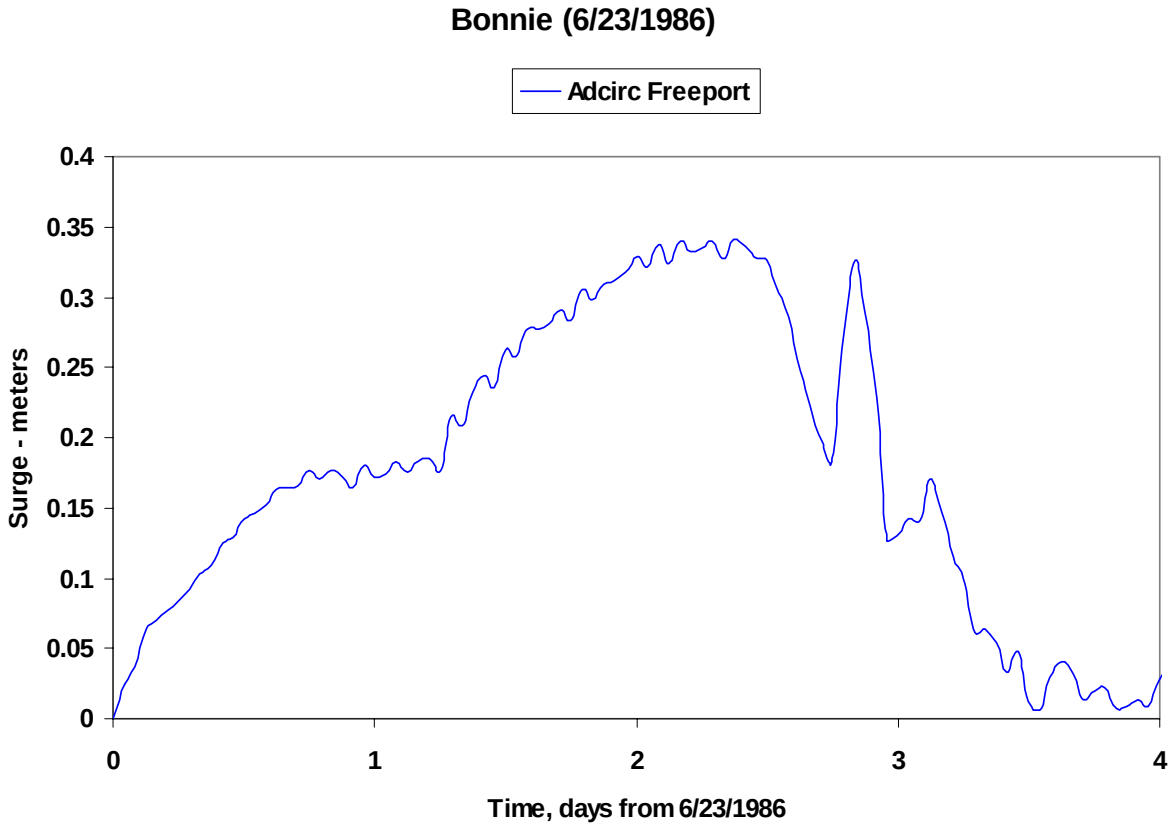
Bonnie (6/23/1986)
Adcirc Freeport
Surge - meters
0.4
0.35
0.3
0.25
0.2
0.15
0.1
0.05
0
0
1
2
3
4
Time, days from 6/23/1986

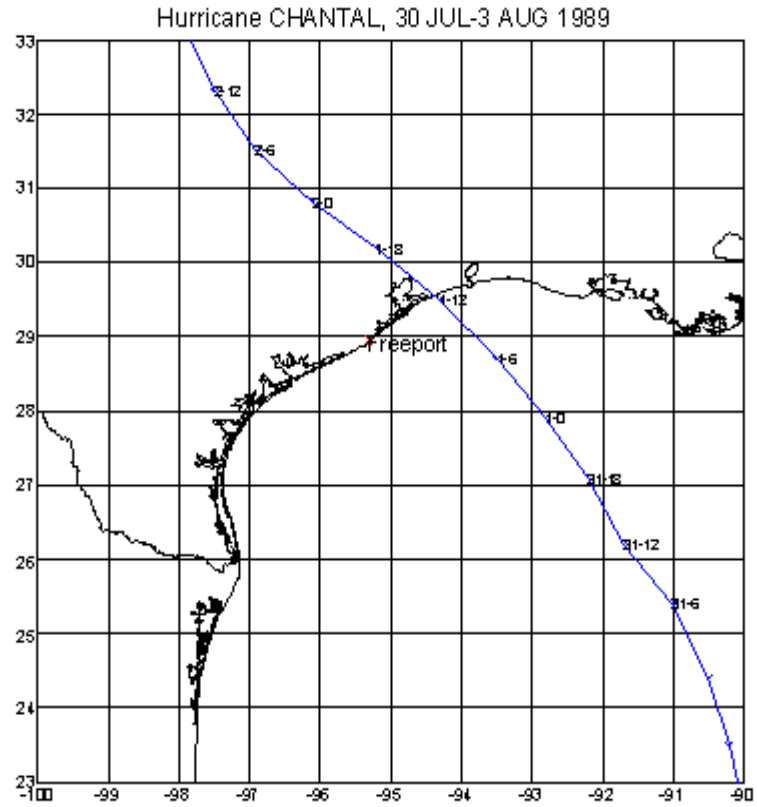
Hurricane CHANTAL, 30 JUL-3 AUG 1989
Freeport
1-18
1-12
1-6
31-18
31-12
31-6

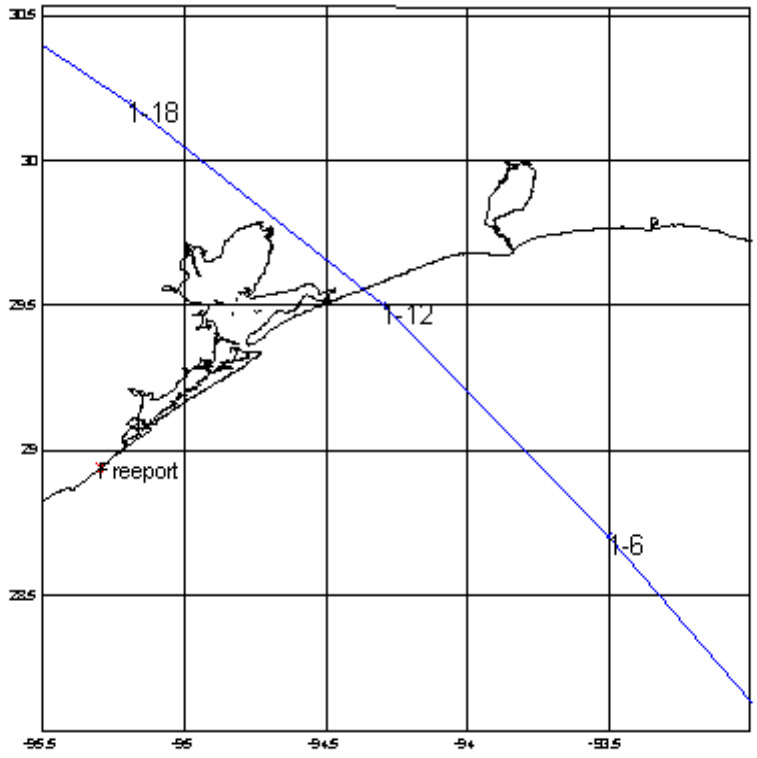
1-18
1-12
1-6
Freeport

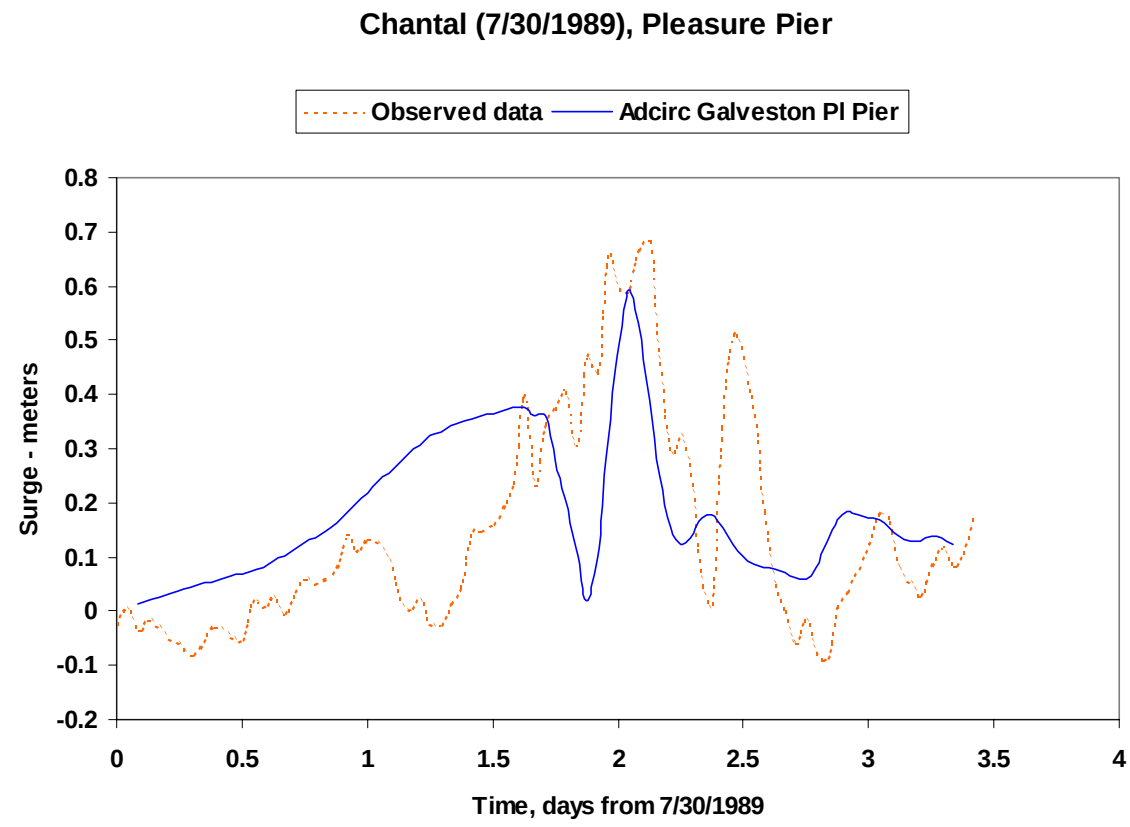
Chantal (7/30/1989), Pleasure Pier
Observed data
Adcirc Galveston Pl Pier
Surge - meters
0.8
0.7
0.6
0.5
0.4
0.3
0.2
0.1
0
-0.1
-0.2
0
0.5
1
1.5
2
2.5
3
3.5
4
Time, days from 7/30/1989

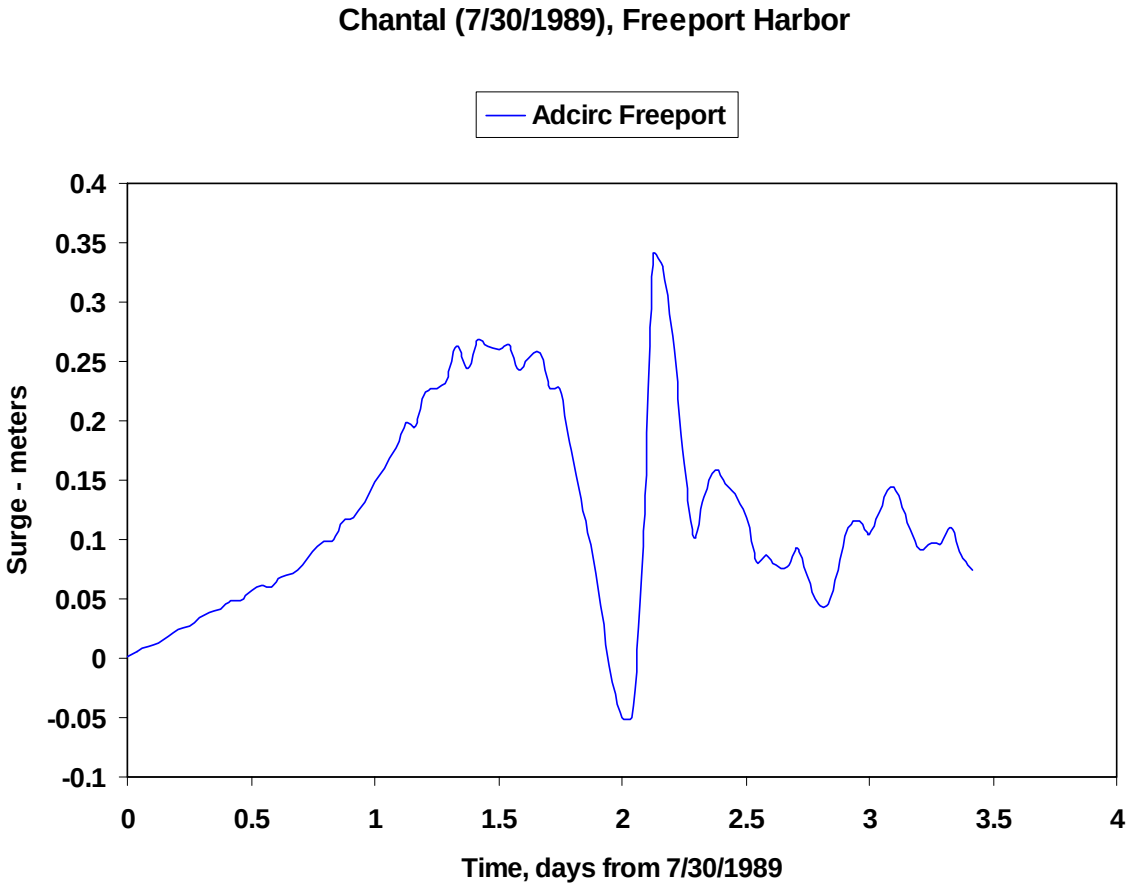
Chantal (7/30/1989), Freeport Harbor
Adcirc Freeport
Surge - meters
0.4
0.35
0.3
0.25
0.2
0.15
0.1
0.05
0
-0.05
-0.1
0
0.5
1
1.5
2
2.5
3
3.5
4
Time, days from 7/30/1989

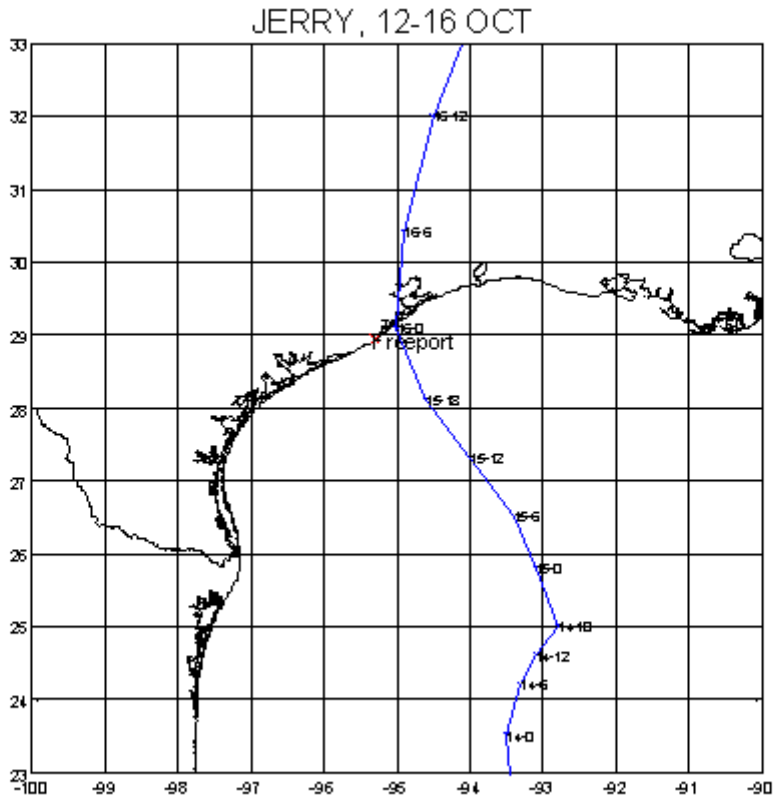
JERRY, 12-16 OCT
Freeport
16-12
16-6
16-0
15-18
15-12
15-6
15-0
14-18
14-12
14-6
14-0
33
32
31
30
29
28
27
26
25
24
23
-100
-99
-98
-97
-96
-95
-94
-93
-92
-91
-90

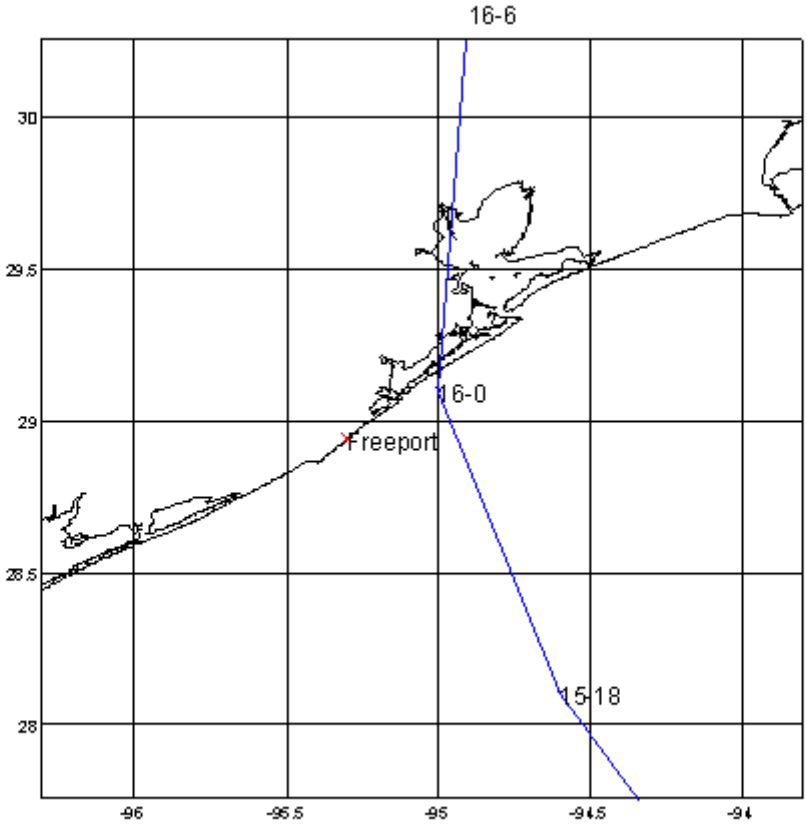
16-6
16-0
Freeport
15-18
30
29.5
29
28.5
28
-96
-95.5
-95
-94.5
-94

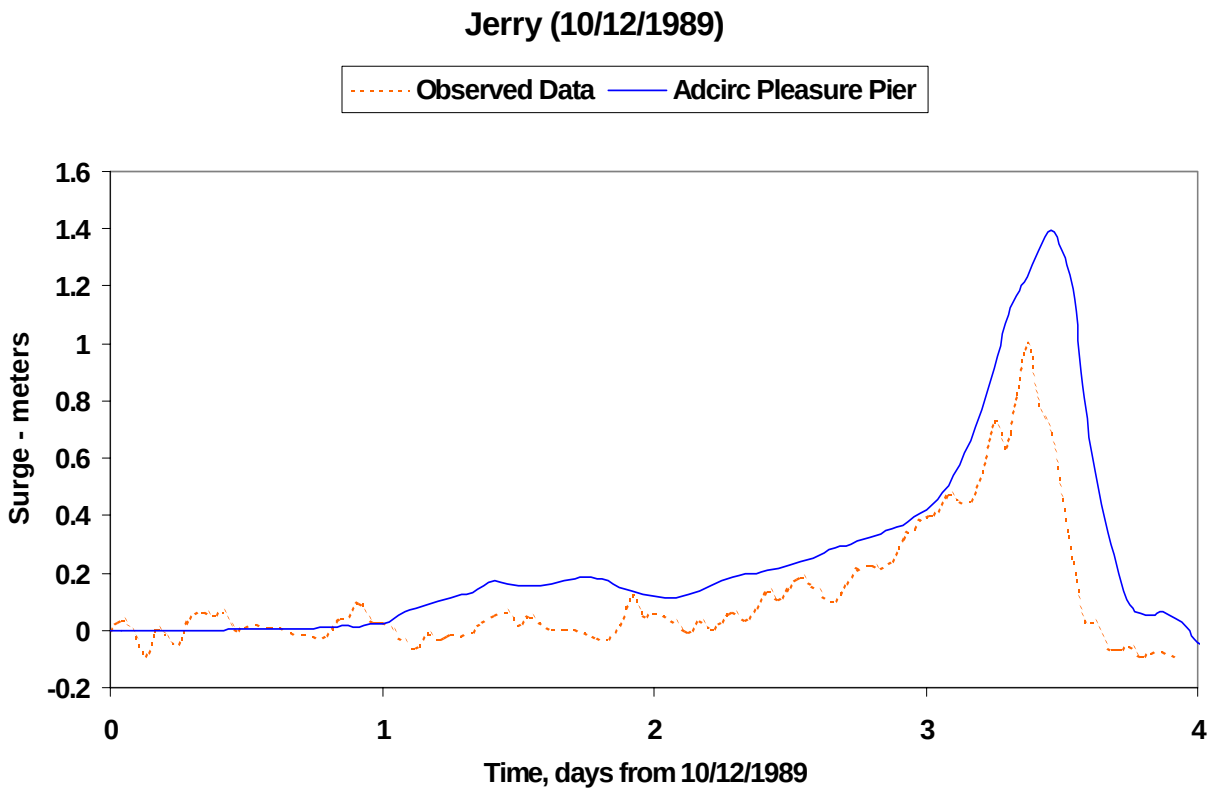
Jerry (10/12/1989)
Observed Data
Adcirc Pleasure Pier
Surge - meters
1.6
1.4
1.2
1
0.8
0.6
0.4
0.2
0
-0.2
0
1
2
3
4
Time, days from 10/12/1989

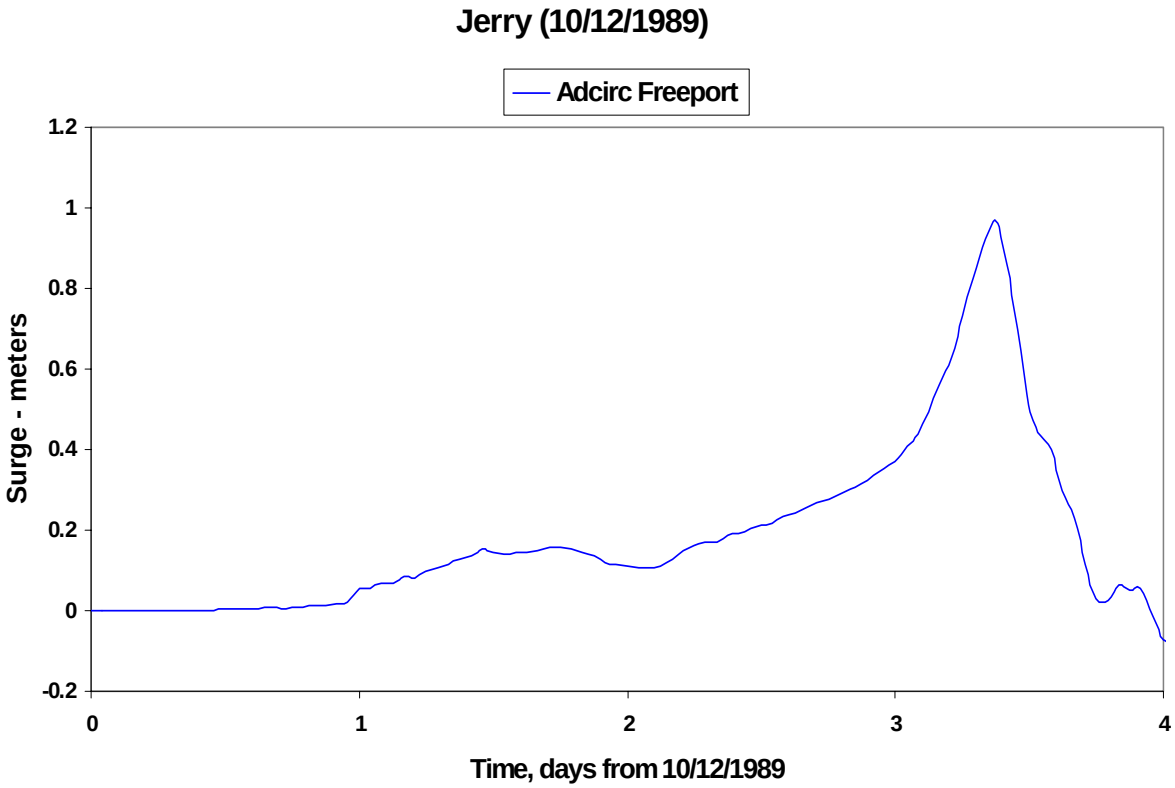
Jerry (10/12/1989)
Adcirc Freeport
Surge - meters
1.2
1
0.8
0.6
0.4
0.2
0
-0.2
0
1
2
3
4
Time, days from 10/12/1989

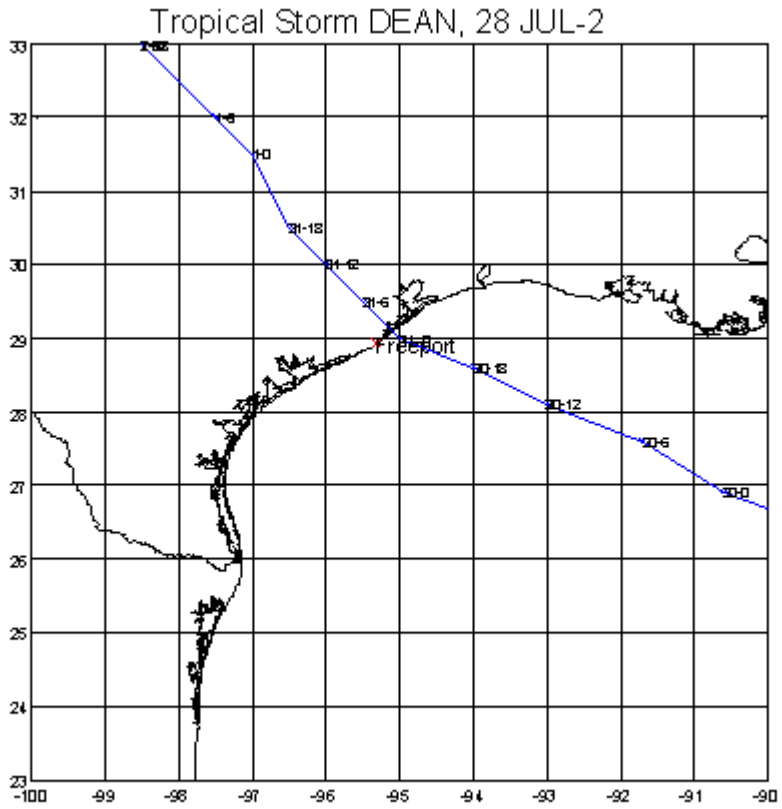
Tropical Storm DEAN, 28 JUL-2
Freeport
31-18
31-12
31-6
30-12
30-6
33
32
31
30
29
28
27
26
25
24
23
-100
-99
-98
-97
-96
-95
-94
-93
-92
-91
-90

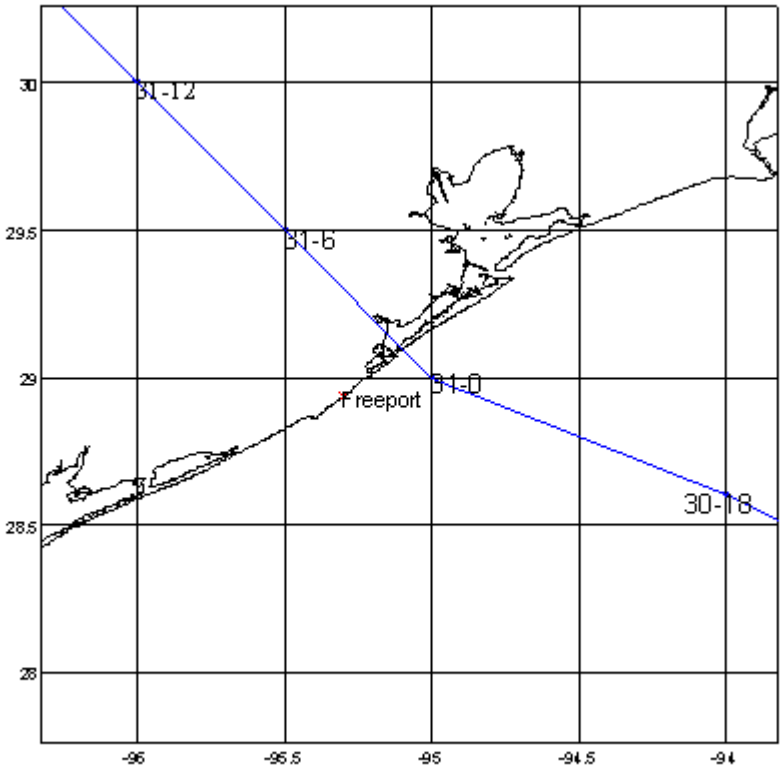
31-12
31-6
31-0
30-18
Freeport
30
29.5
29
28.5
28
-96
-95.5
-95
-94.5
-94

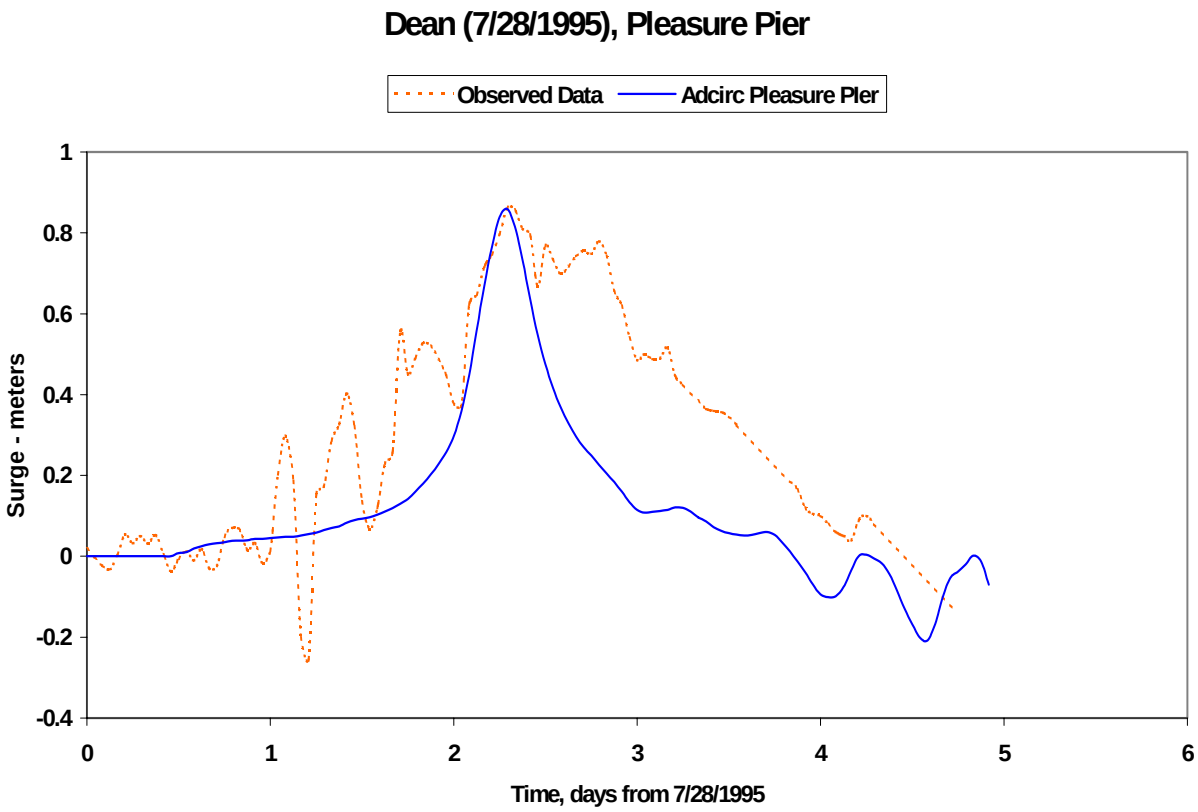
Dean (7/28/1995), Pleasure Pier
Observed Data
Adcirc Pleasure Pier
Surge - meters
1
0.8
0.6
0.4
0.2
0
-0.2
-0.4
0
1
2
3
4
5
6
Time, days from 7/28/1995

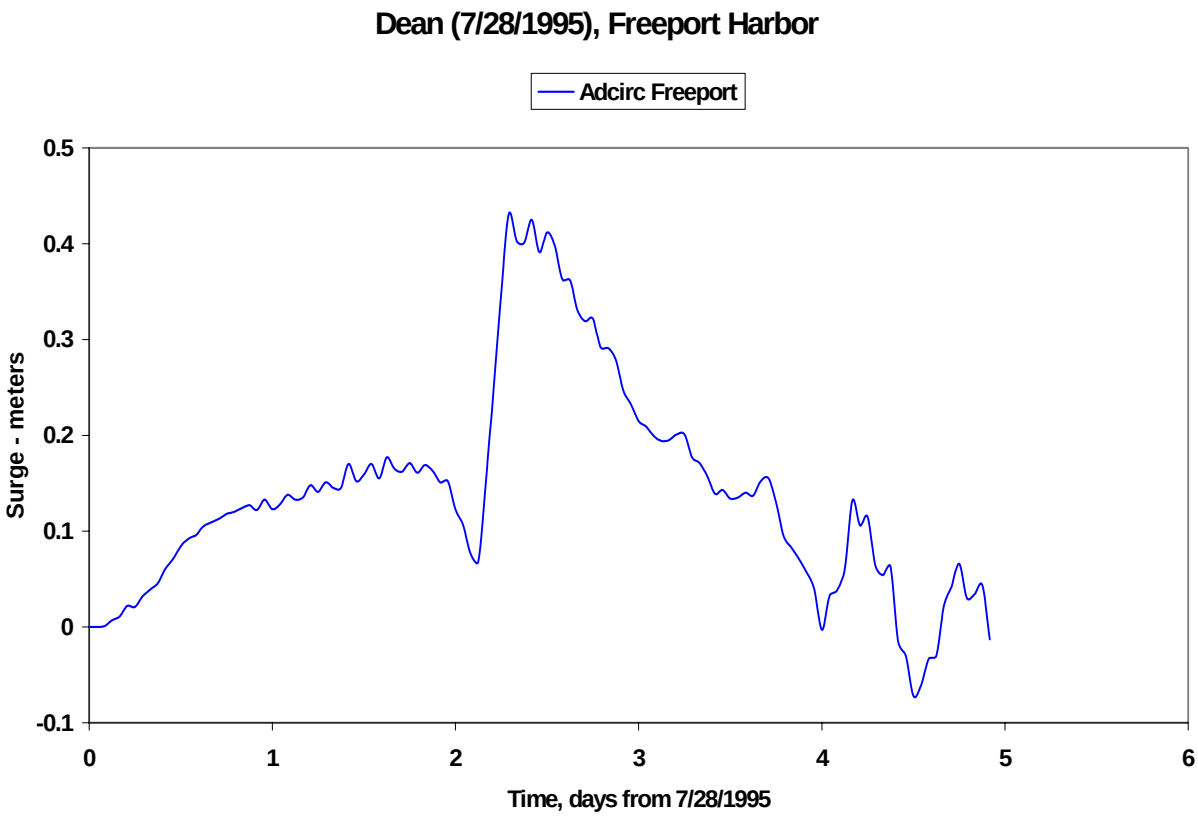
Dean (7/28/1995), Freeport Harbor
Adcirc Freeport
Surge - meters
0.5
0.4
0.3
0.2
0.1
0
-0.1
0
1
2
3
4
5
6
Time, days from 7/28/1995

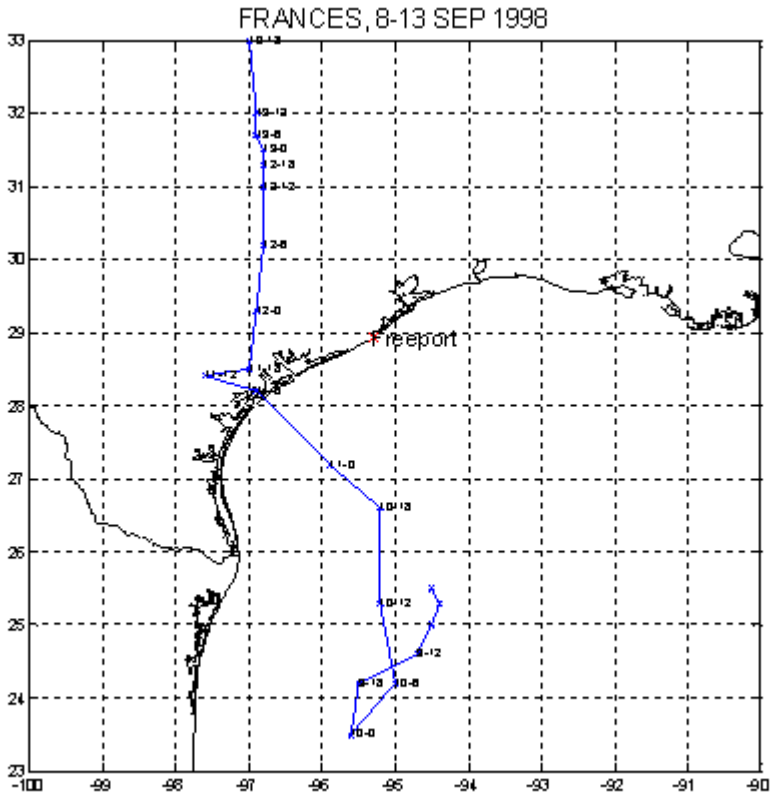
FRANCES, 8-13 SEP 1998
Freeport
33
32
31
30
29
28
27
26
25
24
23
-100
-99
-98
-97
-96
-95
-94
-93
-92
-91
-90

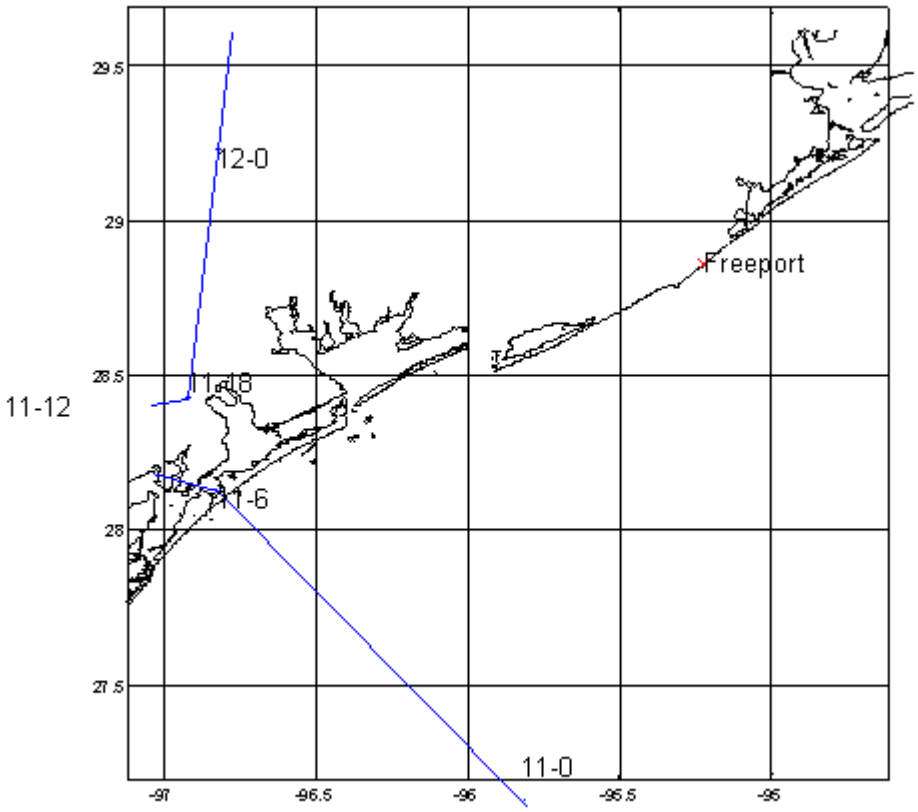
12-0
11-18
11-12
11-6
11-0
Freeport
29.5
29
28.5
28
27.5
-97
-96.5
-96
-95.5
-95

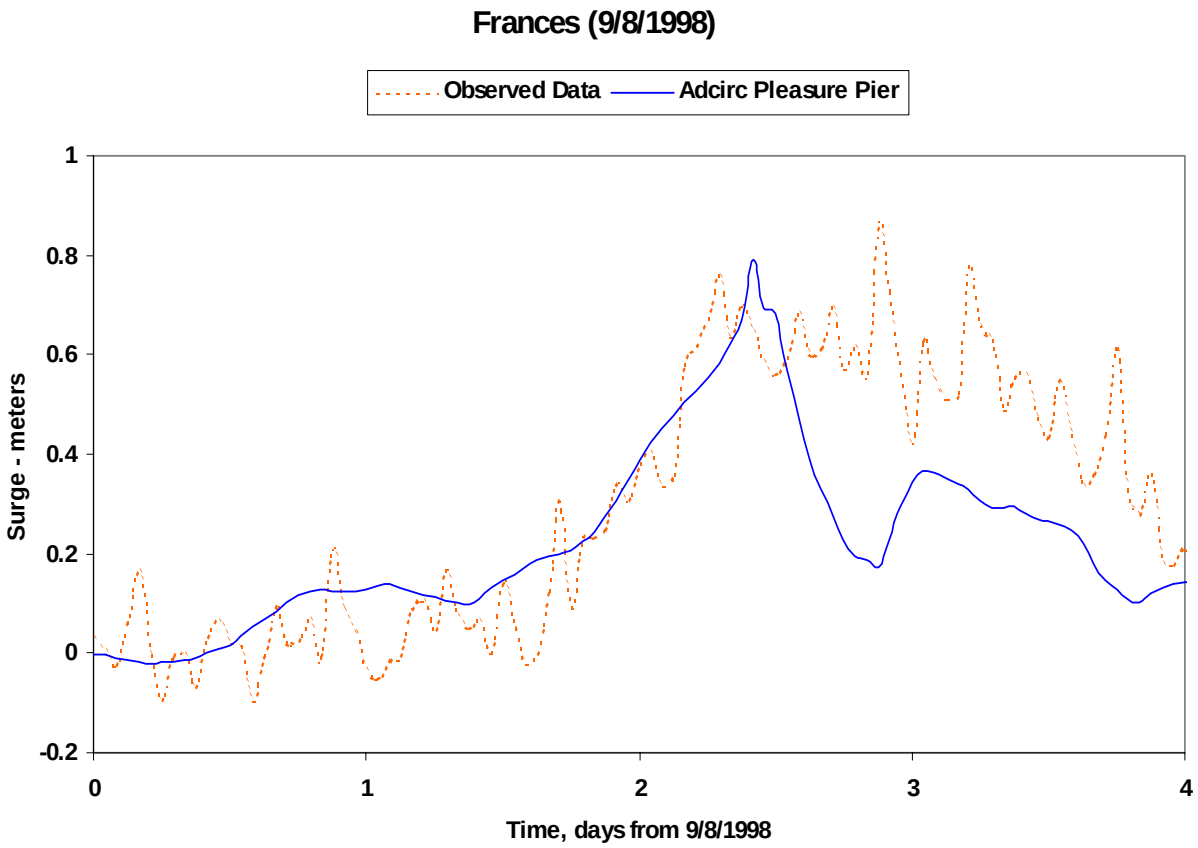
Frances (9/8/1998)
Observed Data
Adcirc Pleasure Pier
Surge - meters
1
0.8
0.6
0.4
0.2
0
-0.2
0
1
2
3
4
Time, days from 9/8/1998

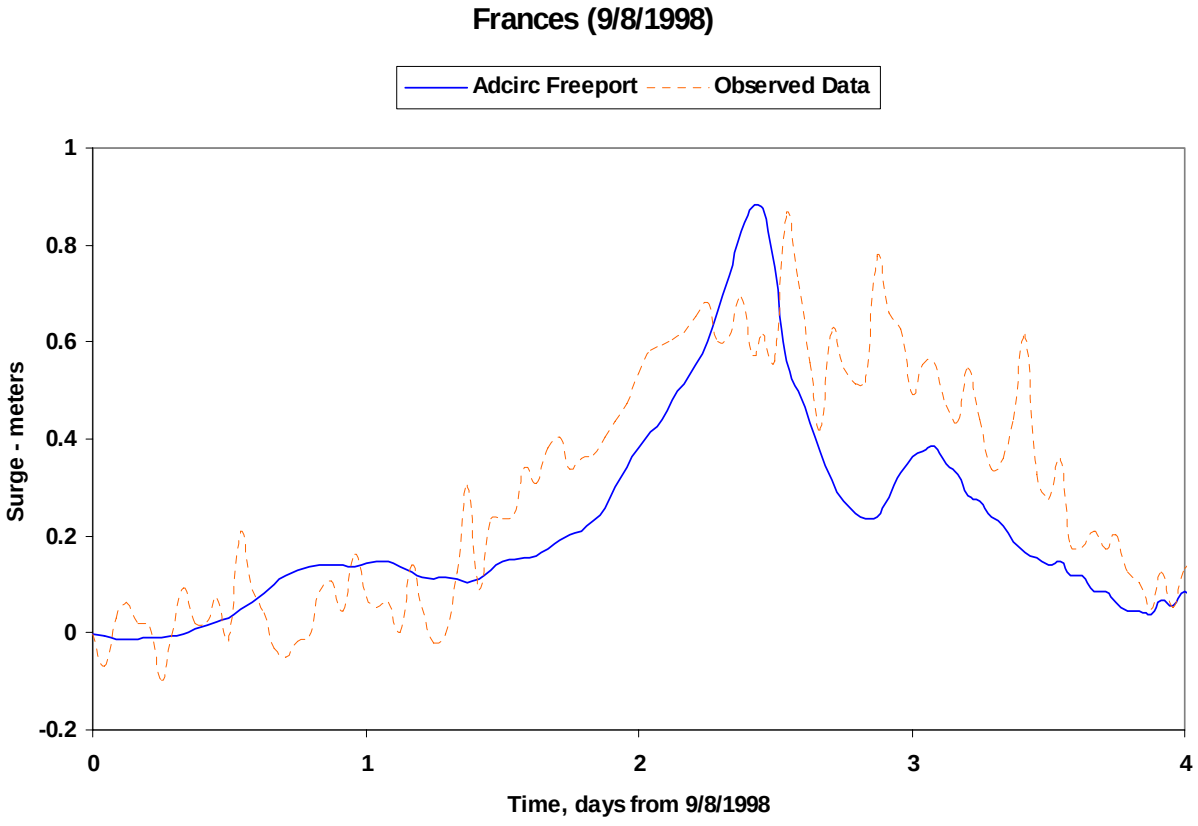
Frances (9/8/1998)
Adcirc Freeport
Observed Data
Surge - meters
1
0.8
0.6
0.4
0.2
0
-0.2
0
1
2
3
4
Time, days from 9/8/1998

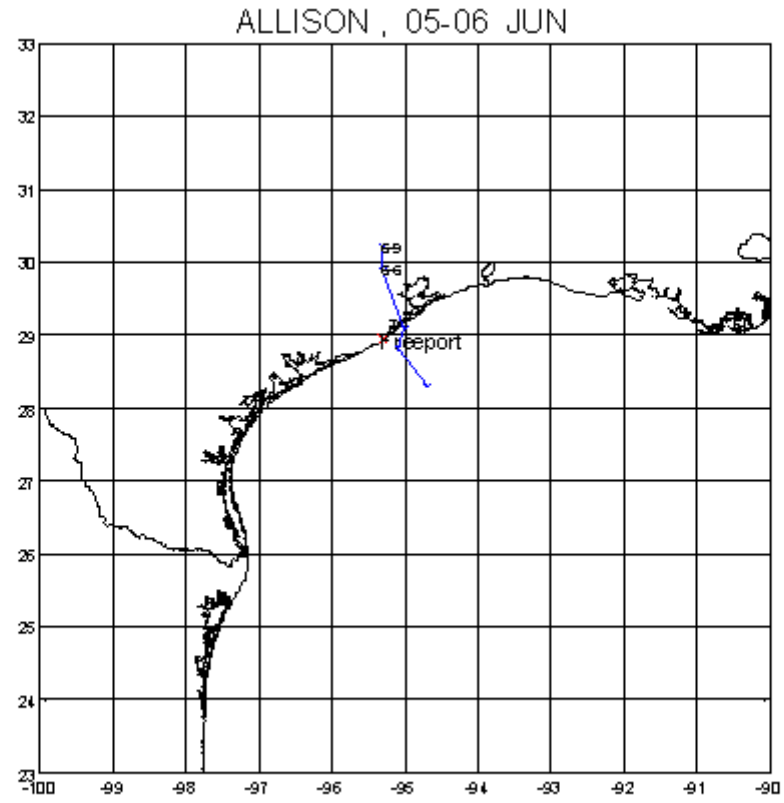
ALLISON , 05-06 JUN
Freeport

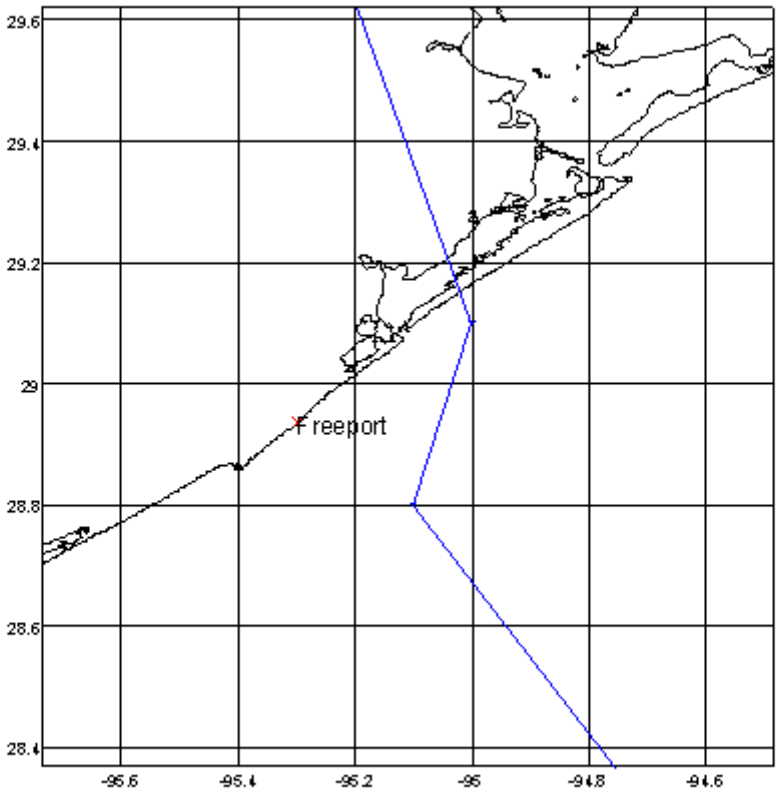
Freeport

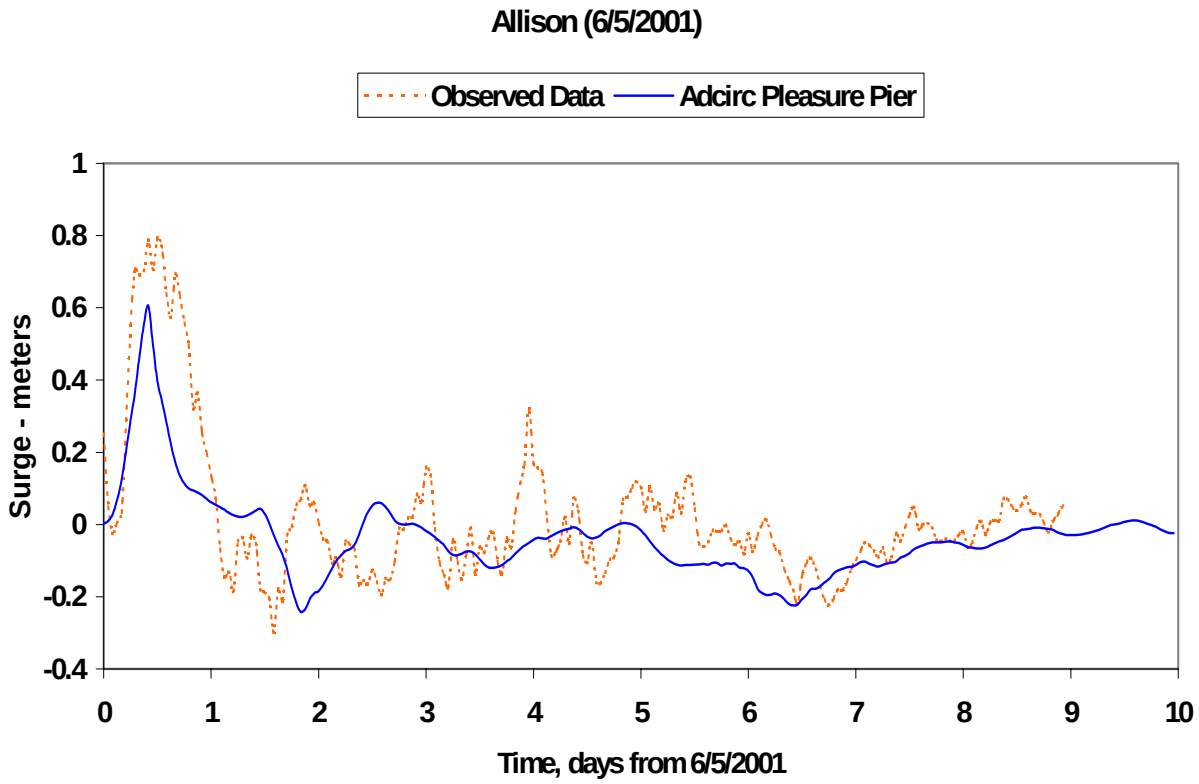
Allison (6/5/2001)
Observed Data
Adcirc Pleasure Pier
Surge - meters
1
0.8
0.6
0.4
0.2
0
-0.2
-0.4
0
1
2
3
4
5
6
7
8
9
10
Time, days from 6/5/2001

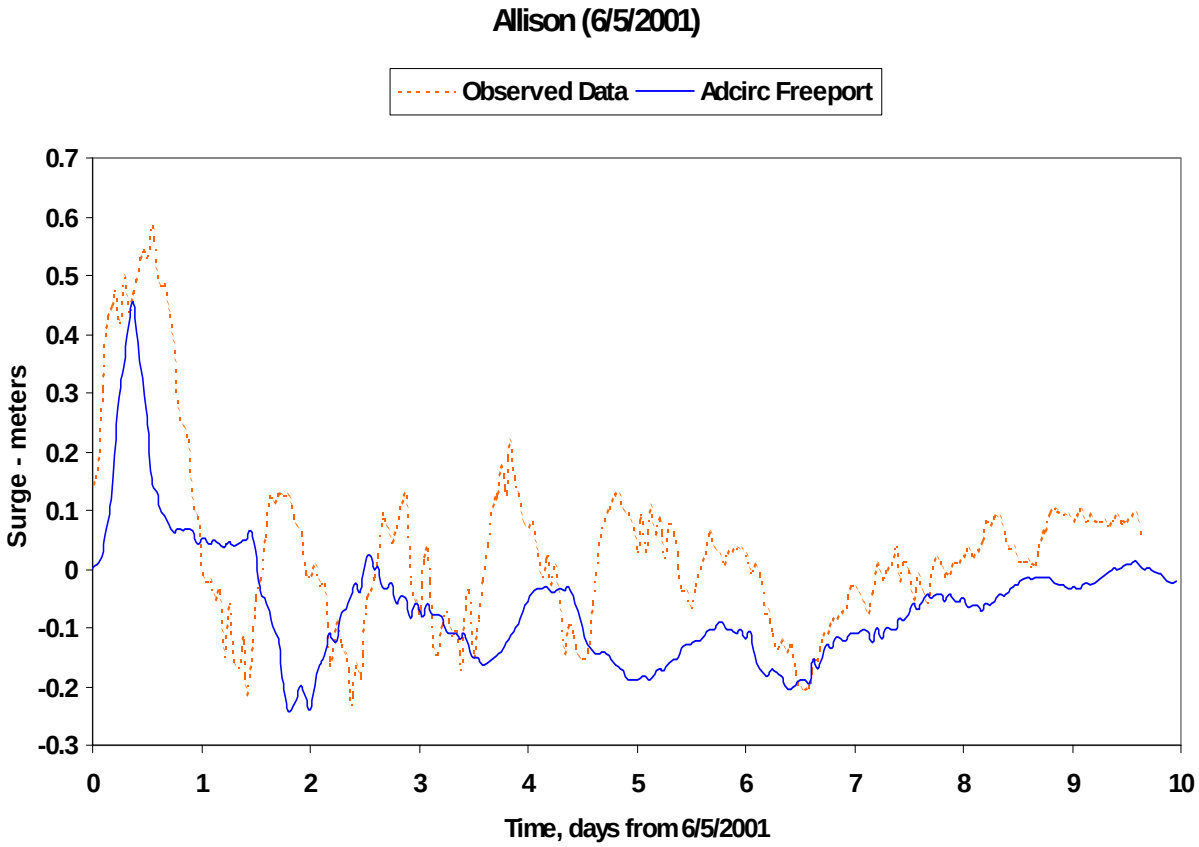
Allison (6/5/2001)
Observed Data
Adcirc Freeport
Surge - meters
0.7
0.6
0.5
0.4
0.3
0.2
0.1
0
-0.1
-0.2
-0.3
0
1
2
3
4
5
6
7
8
9
10
Time, days from 6/5/2001

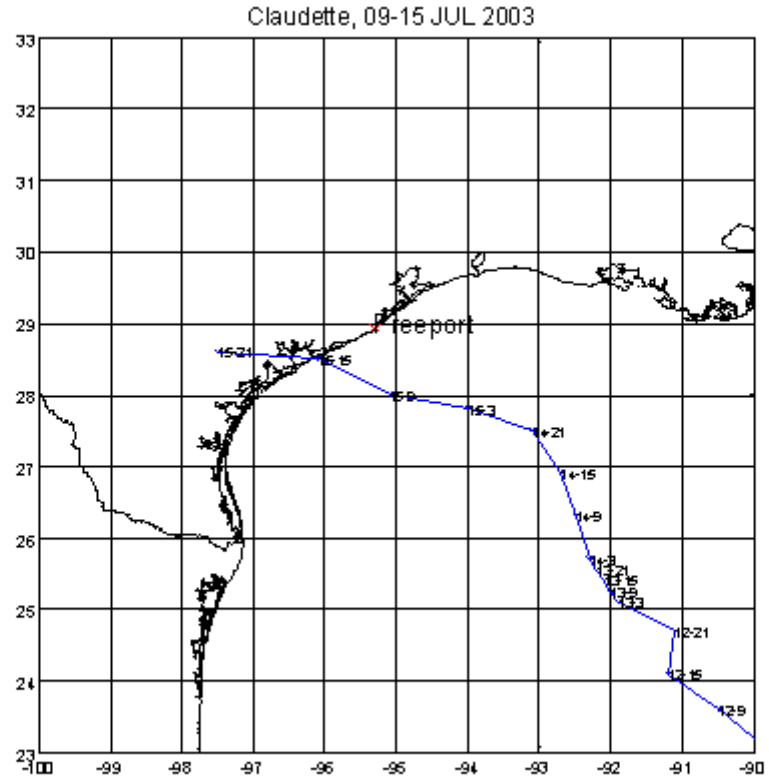
Claudette, 09-15 JUL 2003
Freeport
15-21
15-15
15-9
15-3
14-21
14-15
14-9
12-21
12-15
12-9

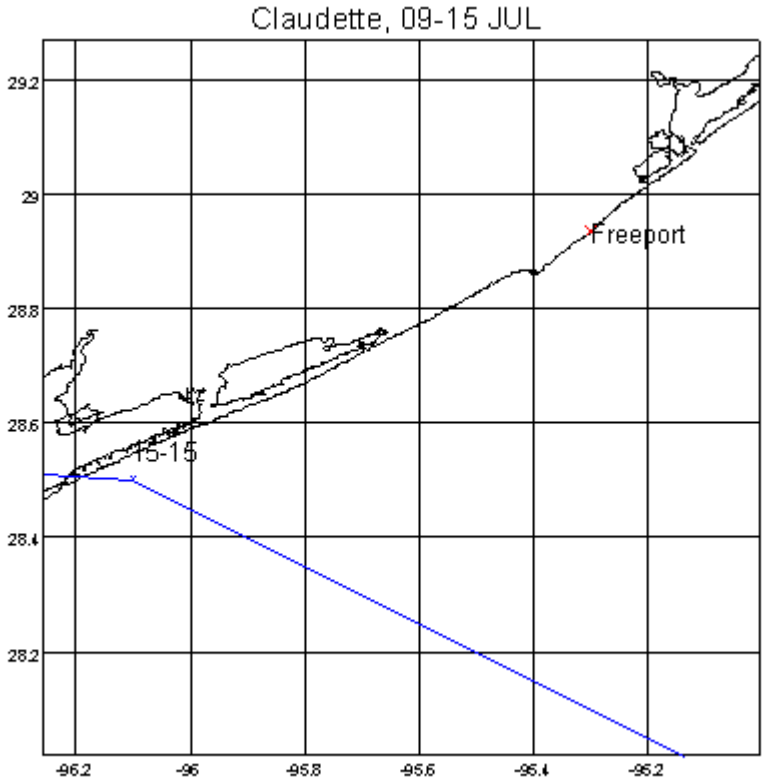
Claudette, 09-15 JUL
Freeport
15-15

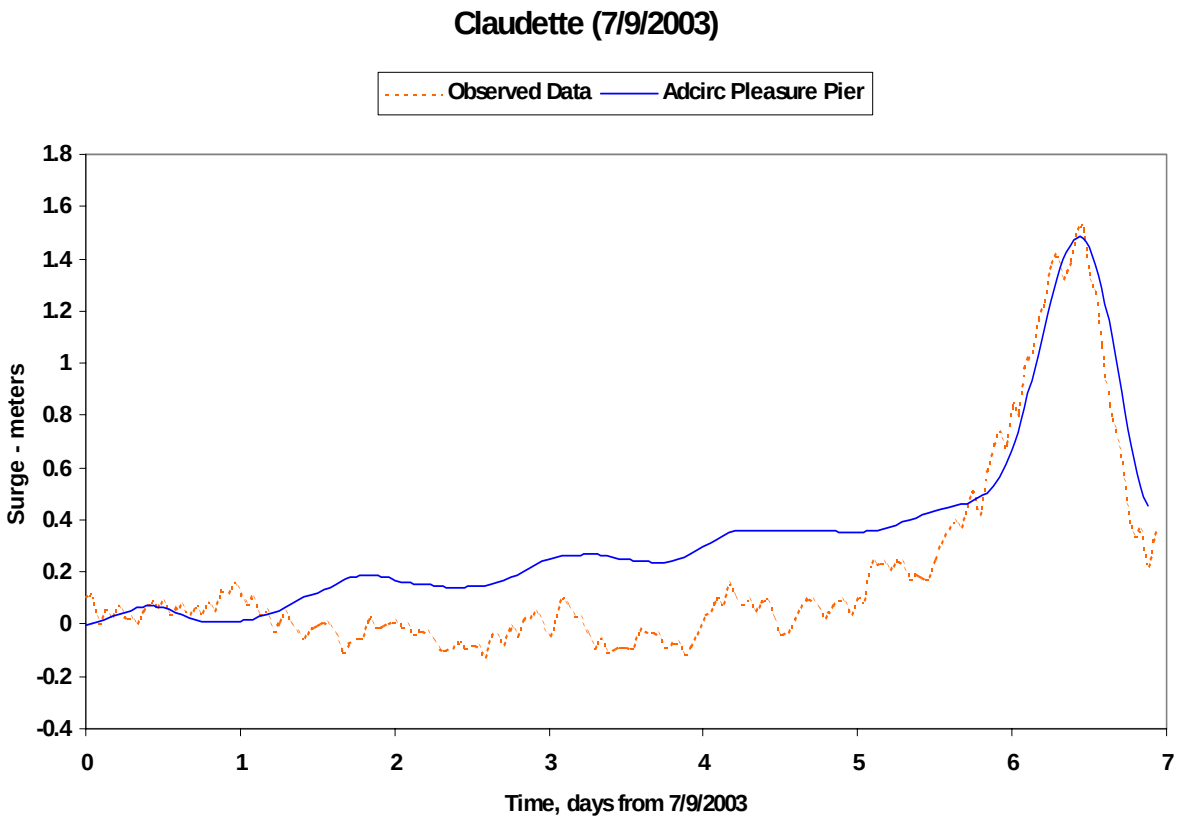
Claudette (7/9/2003)
Observed Data
Adcirc Pleasure Pier
Surge - meters
1.8
1.6
1.4
1.2
1
0.8
0.6
0.4
0.2
0
-0.2
-0.4
0
1
2
3
4
5
6
7
Time, days from 7/9/2003

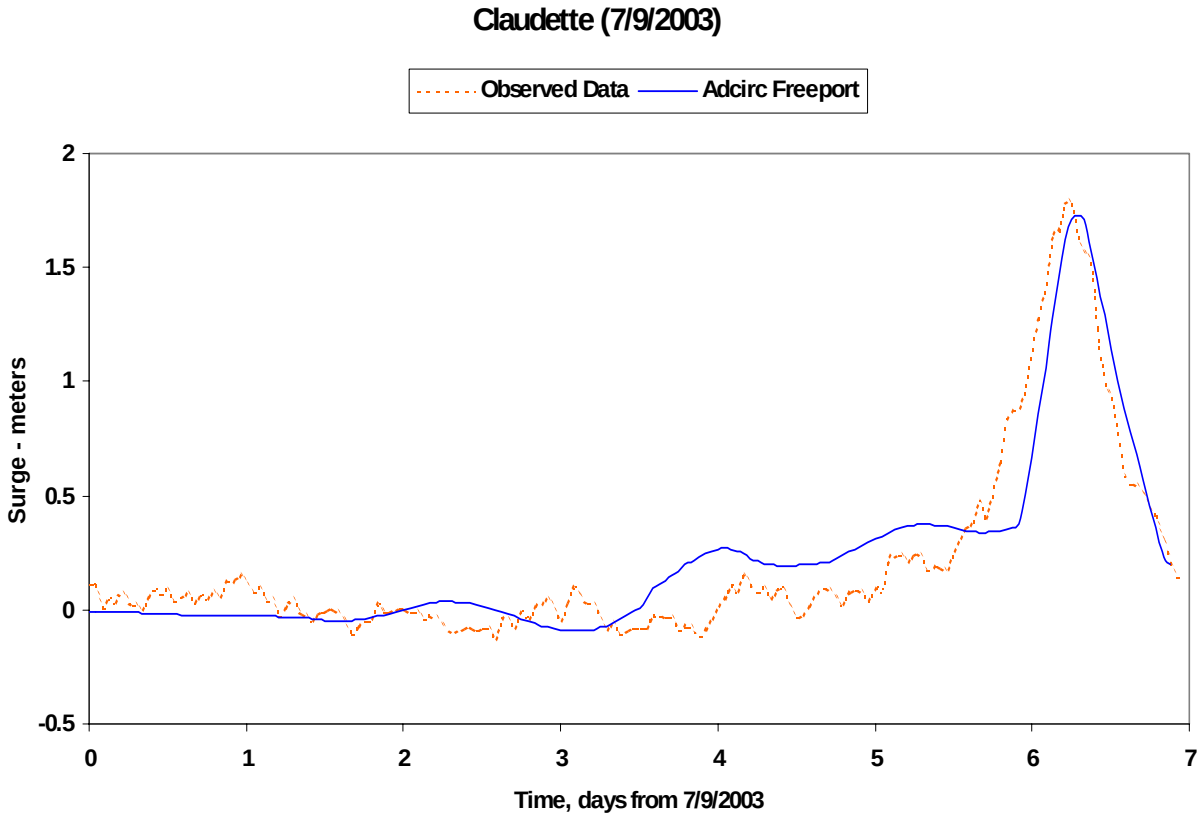
Claudette (7/9/2003)
Observed Data
Adcirc Freeport
Surge - meters
2
1.5
1
0.5
0
-0.5
0
1
2
3
4
5
6
7
Time, days from 7/9/2003

APPENDIX C

STORM SURGE FREQUENCY-OF-OCCURRENCE RELATIONSHIPS

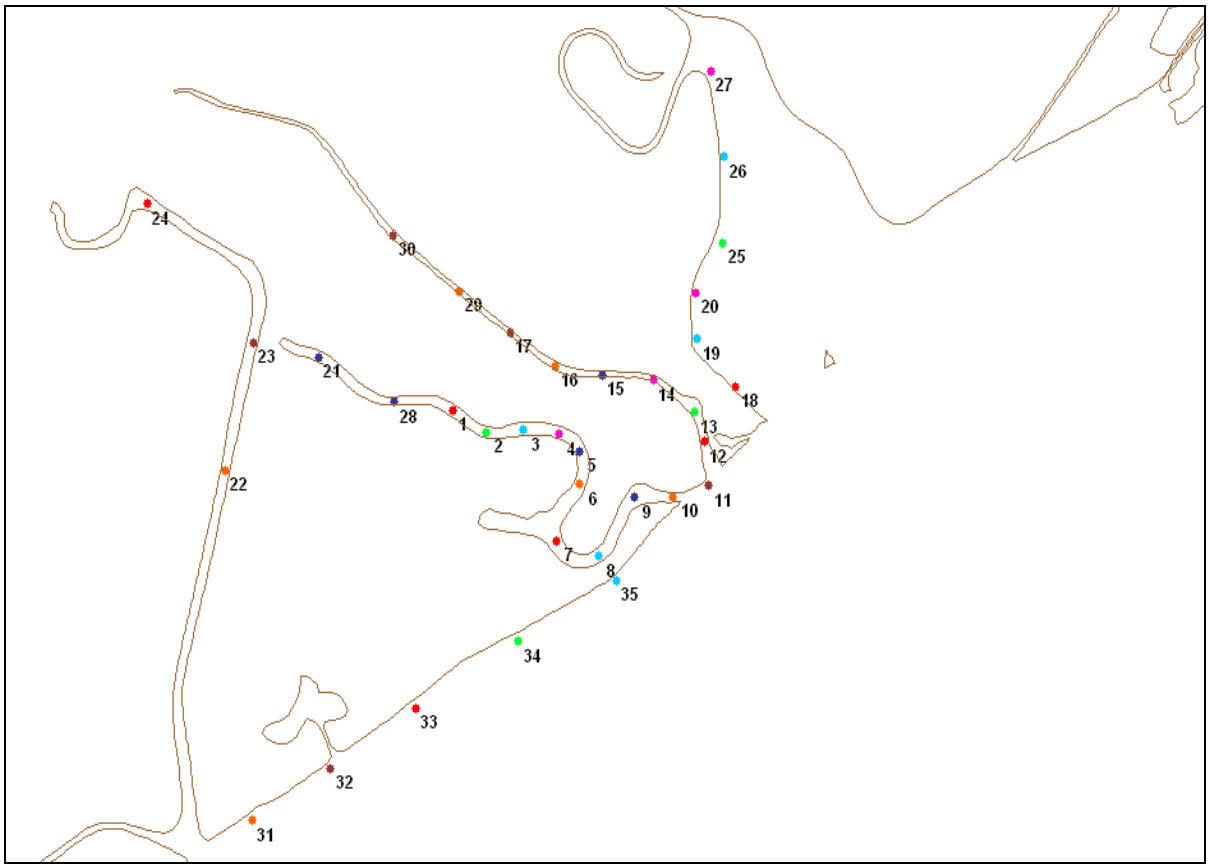

Figure: Location of points used for input to EST model

Station 1

Return Period, Yrs	Max Surge (m)	Max plus σ (m)
5	0.19	0.39
10	0.97	1.16
15	1.31	1.53
25	1.75	2.04
50	2.45	3.04
100	3.56	4.73
150	4.45	5.86
200	4.9	6.58

Station 2

Return Period, Yrs	Max Surge (m)	Max plus σ (m)
5	0.19	0.39
10	0.96	1.15
15	1.3	1.51
25	1.73	2.01
50	2.42	3
100	3.51	4.67
150	4.39	5.78
200	4.84	6.5

Station 3

Return Period, Yrs	Max Surge (m)	Max plus σ (m)
5	0.19	0.39
10	0.95	1.14
15	1.29	1.5
25	1.71	1.99
50	2.39	2.97
100	3.47	4.62
150	4.35	5.73
200	4.79	6.43

Station 4

Return Period, Yrs	Max Surge (m)	Max plus σ (m)
5	0.19	0.39
10	0.95	1.13
15	1.28	1.48
25	1.69	1.97
50	2.37	2.94
100	3.44	4.58
150	4.31	5.68
200	4.75	6.38

Station 5

Return Period, Yrs	Max Surge (m)	Max plus σ (m)
5	0.19	0.39
10	0.94	1.13
15	1.27	1.47
25	1.68	1.96
50	2.35	2.92
100	3.42	4.56
150	4.29	5.65
200	4.73	6.35

Station 6

Return Period, Yrs	Max Surge (m)	Max plus σ (m)
5	0.19	0.4
10	0.94	1.12
15	1.27	1.47
25	1.67	1.95
50	2.35	2.92
100	3.42	4.56
150	4.28	5.64
200	4.72	6.34

Station 7

Return Period, Yrs	Max Surge (m)	Max plus σ (m)
5	0.19	0.4
10	0.94	1.12
15	1.27	1.47
25	1.67	1.95
50	2.35	2.92
100	3.42	4.56
150	4.29	5.65
200	4.73	6.35

Station 8

Return Period, Yrs	Max Surge (m)	Max plus σ (m)
5	0.19	0.4
10	0.94	1.12
15	1.27	1.47
25	1.67	1.95
50	2.34	2.92
100	3.42	4.57
150	4.29	5.66
200	4.73	6.36

Station 9

Return Period, Yrs	Max Surge (m)	Max plus σ (m)
5	0.19	0.4
10	0.94	1.12
15	1.26	1.46
25	1.67	1.94
50	2.34	2.91
100	3.42	4.56
150	4.29	5.65
200	4.72	6.35

Station 10

Return Period, Yrs	Max Surge (m)	Max plus σ (m)
5	0.19	0.4
10	0.94	1.12
15	1.26	1.46
25	1.66	1.93
50	2.33	2.9
100	3.4	4.54
150	4.27	5.63
200	4.7	6.32

Station 11

Return Period, Yrs	Max Surge (m)	Max plus σ (m)
5	0.19	0.4
10	0.94	1.12
15	1.26	1.46
25	1.66	1.93
50	2.33	2.9
100	3.4	4.54
150	4.27	5.62
200	4.7	6.32

Station 12

Return Period, Yrs	Max Surge (m)	Max plus σ (m)
5	0.19	0.4
10	0.94	1.12
15	1.26	1.46
25	1.66	1.93
50	2.33	2.89
100	3.4	4.54
150	4.26	5.62
200	4.7	6.31

Station 13

Return Period, Yrs	Max Surge (m)	Max plus σ (m)
5	0.19	0.39
10	0.94	1.11
15	1.25	1.45
25	1.65	1.92
50	2.31	2.88
100	3.38	4.52
150	4.24	5.6
200	4.68	6.29

Station 14

Return Period, Yrs	Max Surge (m)	Max plus σ (m)
5	0.19	0.39
10	0.93	1.11
15	1.25	1.44
25	1.64	1.9
50	2.29	2.85
100	3.35	4.48
150	4.2	5.54
200	4.63	6.22

Station 15

Return Period, Yrs	Max Surge (m)	Max plus σ (m)
5	0.19	0.39
10	0.94	1.12
15	1.26	1.45
25	1.65	1.91
50	2.3	2.87
100	3.37	4.49
150	4.22	5.56
200	4.65	6.25

Station 16

Return Period, Yrs	Max Surge (m)	Max plus σ (m)
5	0.19	0.39
10	0.94	1.12
15	1.27	1.46
25	1.66	1.92
50	2.32	2.89
100	3.39	4.52
150	4.25	5.59
200	4.68	6.28

Station 17

Return Period, Yrs	Max Surge (m)	Max plus σ (m)
5	0.19	0.39
10	0.95	1.13
15	1.28	1.48
25	1.67	1.95
50	2.34	2.91
100	3.42	4.55
150	4.28	5.63
200	4.71	6.33

Station 18

Return Period, Yrs	Max Surge (m)	Max plus σ (m)
5	0.19	0.39
10	0.96	1.14
15	1.29	1.49
25	1.68	1.95
50	2.35	2.93
100	3.44	4.59
150	4.31	5.68
200	4.75	6.38

Station 19

Return Period, Yrs	Max Surge (m)	Max plus σ (m)
5	0.19	0.39
10	0.97	1.16
15	1.31	1.52
25	1.72	1.99
50	2.39	2.98
100	3.5	4.66
150	4.38	5.78
200	4.83	6.49

Station 20

Return Period, Yrs	Max Surge (m)	Max plus σ (m)
5	0.2	0.4
10	0.98	1.16
15	1.32	1.53
25	1.73	2.01
50	2.42	3.02
100	3.55	4.73
150	4.45	5.86
200	4.9	6.58

Station 21

Return Period, Yrs	Max Surge (m)	Max plus σ (m)
5	0.2	0.4
10	0.98	1.17
15	1.33	1.54
25	1.75	2.04
50	2.46	3.06
100	3.6	4.79
150	4.51	5.93
200	4.96	6.67

Station 22

Return Period, Yrs	Max Surge (m)	Max plus σ (m)
5	0.19	0.39
10	1.01	1.22
15	1.41	1.66
25	1.9	2.23
50	2.63	3.21
100	3.72	4.86
150	4.6	5.98
200	5.04	6.69

Station 23

Return Period, Yrs	Max Surge (m)	Max plus σ (m)
5	0.18	0.39
10	1.03	1.25
15	1.45	1.71
25	1.97	2.31
50	2.71	3.3
100	3.81	4.96
150	4.69	6.07
200	5.14	6.78

Station 24

Return Period, Yrs	Max Surge (m)	Max plus σ (m)
5	0.18	0.38
10	1.03	1.25
15	1.46	1.73
25	2.01	2.36
50	2.77	3.37
100	3.87	5.03
150	4.77	6.17
200	5.22	6.89

Station 25

Return Period, Yrs	Max Surge (m)	Max plus σ (m)
5	0.18	0.38
10	1.03	1.26
15	1.47	1.75
25	2.03	2.38
50	2.79	3.4
100	3.91	5.08
150	4.81	6.23
200	5.27	6.96

Station 26

Return Period, Yrs	Max Surge (m)	Max plus σ (m)
5	0.18	0.38
10	0.97	1.17
15	1.35	1.57
25	1.8	2.09
50	2.5	3.09
100	3.64	4.89
150	4.63	6.15
200	5.12	6.95

Station 27

Return Period, Yrs	Max Surge (m)	Max plus σ (m)
5	0.15	0.33
10	0.87	1.06
15	1.23	1.46
25	1.67	1.96
50	2.33	2.86
100	3.35	4.46
150	4.24	5.62
200	4.69	6.36

Station 28

Return Period, Yrs	Max Surge (m)	Max plus σ (m)
5	0.15	0.32
10	0.87	1.07
15	1.24	1.47
25	1.68	1.96
50	2.34	2.87
100	3.37	4.48
150	4.27	5.66
200	4.72	6.39

Station 29

Return Period, Yrs	Max Surge (m)	Max plus σ (m)
5	0.14	0.31
10	0.89	1.1
15	1.3	1.54
25	1.76	2.05
50	2.43	2.97
100	3.48	4.62
150	4.41	5.83
200	4.87	6.6

Station 30

Return Period, Yrs	Max Surge (m)	Max plus σ (m)
5	0.16	0.37
10	1.06	1.31
15	1.55	1.84
25	2.09	2.43
50	2.78	3.35
100	3.86	5.08
150	4.85	6.37
200	5.35	7.17

Station 31

Return Period, Yrs	Max Surge (m)	Max plus σ (m)
5	0.16	0.37
10	1.07	1.32
15	1.56	1.86
25	2.13	2.47
50	2.83	3.41
100	3.92	5.14
150	4.92	6.44
200	5.42	7.26

Station 32

Return Period, Yrs	Max Surge (m)	Max plus σ (m)
5	0.16	0.36
10	1.08	1.33
15	1.58	1.89
25	2.17	2.52
50	2.9	3.47
100	3.98	5.18
150	4.97	6.48
200	5.47	7.29

Station 33

Return Period, Yrs	Max Surge (m)	Max plus σ (m)
5	0.18	0.38
10	0.97	1.16
15	1.33	1.55
25	1.77	2.07
50	2.5	3.12
100	3.67	4.94
150	4.65	6.19
200	5.15	6.98

Station 34

Return Period, Yrs	Max Surge (m)	Max plus σ (m)
5	0.19	0.39
10	0.99	1.19
15	1.35	1.58
25	1.79	2.08
50	2.52	3.13
100	3.69	4.95
150	4.67	6.21
200	5.17	7.02

Station 35

Return Period, Yrs	Max Surge (m)	Max plus σ (m)
5	0.18	0.39
10	1.02	1.22
15	1.4	1.63
25	1.86	2.15
50	2.57	3.18
100	3.74	5
150	4.73	6.28
200	5.23	7.09

VITA

MANISH AGGARWAL

ADDRESS
4406 Laurel Green Court
Missouri City, TX 77459
Tel: (832) 282 7126

EDUCATION

- Master of Science in Civil Engineering, Texas A&M University, August 2004
  Major: Coastal and Ocean and Coastal Engineering.
  GPA: 3.92

- Bachelor of Engineering in Mechanical Engineering, Delhi College of Engineering, Delhi University, India.
  (July 2002)
  GPA: 3.86

EXPERIENCE

- Texas A&M University, College Station, Texas (December 2003 – August 2004)
  Graduate Research Assistant